UNIVERSITÀ DEGLI STUDI DI MILANO

DIPARTIMENTO DI CHIMICA

Scuola di Dottorato in Scienze e Tecnologie Chimiche
Corso di Dottorato in Chimica Industriale – XXVI Ciclo
Settore scientifico disciplinare: CHIM/03

"Re-discovering" an old material, Polyaniline, for modern applications

Tutor: Prof. Laura Prati
Co-tutor: Dott.ssa Cristina Della Pina
Coordinatore: Prof. Dominique Roberto

Tesi di Dottorato di:
Ermelinda FALLETTA
Matr. N° R09061

A.A. 2012-2013

TABLE OF CONTENTS

ABSTRACT……...…1

PART I: INTRODUCTION……...…2

Chapter 1: Conducting Organic Polymers…….3

1.1. Conducting Polymers……....4

1.1.1 Non-Intrinsically Conducting Polymers……4

1.1.2 Intrinsically Conducting Polymers……5

1.2. Polarons, bipolarons and solitons……..7

1.3. Conduction mechanism……10

1.4. Main synthetic techniques…….……..13

1.4.1. Chemical synthesis……13

1.4.2. Electrochemical synthesis…….....14

1.4.3. Other synthetic methods…….....15

1.4. Research and Market……...15

Chapter 2: Polyaniline……..18

2.1. History……19

2.2. Physicochemical characteristics ……19

2.3 Methods of synthesis……....22

2.3.1. Chemical synthesis……22

2.3.2. Electrochemical synthesis…….26

2.3.3. Other Conventional Methods……27

2.3.3.1 Heterophase polymerization……...27

2.3.3.1.1. Synthesis of polyaniline colloidal dispersion…….27

2.3.3.1.2. Direct and inverse emulsion polymerization ……28

2.3.3.1.3. Direct and inverse miniemulsion polymerization……..28

2.3.3.1.4. Direct and inverse microemulsion polymerization…….28

2.3.3.2. Interfacial polymerization……28

2.3.3.3. Metathesis polymerization……29

2.3.3.4. Vapor-phase deposition polymerization……...….29

2.3.3.5. Sonochemical synthesis……29

2.3.3.6. Enzymatic synthesis of polyaniline……...30

2.3.3.7. Photo-induced polymerization…….…30

2.3.3.8. Plasma polymerization……..30
2.4. Conductivity……...…….30
2.4.1. Effect of doping…….31
2.4.2. Effect of moisture……..32
2.4.3.Effect of crystallinity……..33
2.4.4. Effect of molecular weight……34
2.4.5. Conduction mechanism…….34
2.5. Techniques of characterization……36
2.5.1. FT-IR spectroscopy……...…36
2.5.2. UV-vis spectroscopy…….38
2.5.3. XRPD diffraction……..41
2.5.4. Cyclic voltammetry……...……46
2.5.5. Conductivity measurements……..51
Chapter 3: One dimensional polyaniline……..52
3.1. Importance of one-dimensional polyaniline……...….53
3.2. Synthetic methods……..…….53
3.2.1. Hard template synthesis……...…….54
3.2.2. Soft template synthesis…….54
3.2.3. Combined soft and hard template synthesis…….55
3.2.4. No-template synthesis……..…….55
3.2.4.1. Radiolytic synthesis……..…….55
3.2.4.2. Rapid mixing reaction……56
3.3. Properties…….56
Chapter 4: Composite materials……58
4.1. PANI/insulating polymers……...59
4.1.1. Techniques of preparation of PANI blends……..59
4.1.1.1. Synthetic methods to prepare PANI blends and composites……60
4.1.1.2. Blending methods……..62
4.1.2. Physicochemical properties……..63
4.1.3. PANI nanofibers by electrospinning technique……...…….65
4.2. PANI/ferrites nanocomposites…….67
4.2.1. Iron oxides nanoparticles……..67
4.2.2 Techniques of preparation of PANI/ferrites……..70
Chapter 5: Applications……72

5.1. EMI (ElectroMagnetic Interference) shielding applications……...73
5.1.1. Signal transmission……...74
5.1.2. Electromagnetic interference (EMI)……75
5.1.3. EMI shielding……...76
5.1.4. Materials for EMI shielding……..77
5.1.4.1. Metals used in EMI shielding……77
5.1.4.2. Composite materials in EMI shielding……..78
5.1.4.3. Intrinsically conducting polymers in EMI shielding……79
5.2. Biomedical applications……..81
5.2.1. Biomolecular sensing……81
5.2.2. Biomolecular actuators……83
5.2.3. Tissue engineering……84
5.2.4. Drug delivery systems……..86
5.3. Sensors applications……....87
5.3.1. Sensors based on transduction……..87
5.3.1.1. Potentiometric sensors……...87
5.3.1.2. Amperometric sensors……...87
5.3.1.3. Piezoeletric sensors……88
5.3.1.4. Calorimetric/thermal sensors……88
5.3.1.5. Optical sensors……...89
5.3.1.6. Pressure sensors……89
5.3.1.6.1. High pressure sensors……..91
5.3.1.6.2. Low pressure (touch) sensors……..92
5.3.2. Sensors based on application mode……..94
5.3.2.1. Chemical sensors……...94
5.3.2.2. Ion-selective sensors……..95
5.3.2.3. pH sensors……..96
5.3.2.4. Humidity sensors……...96
5.4. Other applications……97

PART II: EXPERIMENTAL PART……..98
Chapter 6: Synthetic methods……...……99
6.1. PANI preparation……..100
6.1.1. PANI preparation from aniline monomer……...100

6.1.2. PANI preparation from *N*-(4-amonophenyl)aniline (aniline dimer)……..100
6.1.3. PANI preparation from aniline dimer using O_2 as the oxidant……...100
6.1.4. 4-Oxo-4-(4-(phenylamino)phenylamino)butanoic acid (Aniline dimer-COOH, ADCOOH) preparation……..……101
6.2. PANI modification……101
6.2.1. PANI deprotonation (dedoping)……101
6.2.2. PANI reprotonation (redoping) with inorganic acids……101
6.2.3. PANI reprotonation (redoping) with organic acids……102
6.2.4. PANI reduction (synthesis of Leucoemeraldine)……...102
6.3. Metal oxides nanoparticles preparation……102
6.3.1 Fe_3O_4 nanoparticles (NPs) preparation……103
6.3.1.1. Fe_3O_4 nanoparticles (NPs) preparation by co-precipitation method……103
6.3.1.2. Preparation of Fe_3O_4 nanoparticles (NPs) with a mean diameter of 2.3 nm (MNP_3) by Metal Vapour Synthesis (MVS) technique……103
6.3.1.3. Fe_3O_4 nanoparticles (NPs) preparation by solvothermal method……104
6.3.1.3.1. Preparation of Fe_3O_4 NPs with a mean diameter of 10.0 nm (MNP_2)… ……..104
6.3.1.3.2. Preparation of Fe_3O_4 NPs with a mean diameter of 27.0 nm (MNP_1)…….…….……..104
6.3.2. Preparation of Fe_3O_4 nanoparticles capped with aniline dimer–COOH……104
6.3.2.1. One-step preparation of Fe_3O_4 nanoparticles capped with aniline dimer COOH…….....104
6.3.2.2. Two-step preparation of Fe_3O_4 nanoparticles capped with aniline dimer COOH……..105
6.3.3. MFe_2O_4 (M= Co, Ni, Mn, Cu, Zn and Mg) and $FeCr_2O_4$ nanoparticles preparation by co-precipitation method…….105
6.4. PANI/MFe_2O_4 (M= Fe, Co, Ni, Mn, Cu, Zn and Mg) and PANI/$FeCr_2O_4$ composites preparation……105
6.4.1. PANI/MFe_2O_4 composites preparation using H_2O_2 as the oxidant……106
6.4.2. PANI/MFe_2O_4 composites preparation using O_2 as the oxidant……106
6.5. PANI nanofibers preparation by electrospinning technique……106
6.5.1. Spun solutions preparation……106
Chapter 7: Characterization techniques……..108
7.1. Spectroscopic techniques……...109

7.1.1. Fourier Transform Infrared (FT-IR) spectroscopy……109
7.1.2. Ultraviolet-visible (UV-vis) spectroscopy……..109
7.1.3. Atomic Absorption spectroscopy (AAS)……109
7.2. Thermogravimetric technique……...110
7.3. Mass spectrometry……110
7.4. NMR spectroscopy……110
7.5. X-Rays powder diffraction ……...110
7.6. Microscopic techniques……110
7.6.1. Transmission Electron Microscopy (TEM)……....110
7.6.2. Scanning Electron Microscopy (SEM)……...111
7.7. Electrical resistivity measurements……...111
7.8. Magnetic measurements……111
7.9. Wave guide dielectric characterization……..111
7.10. Electrospinning process……...112
7.11. Direct an direct citocompatibility tests of PANI nanofibers on a SH-SY5Y human cell line……...112
7.12. Measurements of electrical conductivity as a function of force……..115
7.13. Piezoresistive measurements……...115

PART III: RISULTS AND DISCUSSION……..116
Chapter 8: Synthesis and characterization of PANI/metal oxide nanocomposites……117
8.1. New clean one-pot synthesis of polyaniline/Fe_3O_4 nanocomposites with magnetic and conductive behaviour……118
8.1.1.Catalytic polymerization……119
8.1.2. Spectroscopic characterization……..122
8.1.3. Morphological characterization……124
8.1.4. Mechanism of nanorods formation……126
8.1.5. Thermogravimetric analyses……..127
8.1.6. Magnetic measurements……....127
8.1.7.Conductivity measurements……132
8.2. The effect of nanoparticle size on the synthesis and properties of PANI/Fe_3O_4 nanocomposites……...134
8.2.1.Catalytic polymerization……134
8.2.2. Morphological characterization……138

8.2.3. Magnetic measurements……142
8.3. Synthesis and characterization of PANI/MFe_2O_4 composites: the role of the bivalent metal (M)…… ……145
8.3.1.Catalytic polymerization using $CoFe_2O_4$ NPs as the catalysts……146
8.3.2. Morphological and spectroscopic characterization……....148
8.3.3. Magnetic measurements……152
8.3.4.Catalytic polymerization using MFe_2O_4 NPs as the catalysts (M= Mn, Co, Ni, Cu, Zn, Mg) and characterization…….154
8.4. Electromagnetic characterization……..160
8.5. Microwave absorption properties……..162
8.6. Towards well-dispersed PANI–Fe_3O_4 nanomaterials……...166
8.6.1. ADCOOH characterization…….167
8.6.2. ADCOOH/Fe_3O_4 NPs composites prepared by a one-pot method and their characterization……...169
8.6.3. ADCOOH/Fe_3O_4 NPs composites prepared by a two-step method and their characterization……...172
8.6.4. Synthesis of PANI/Fe_3O_4 composites using ADCOOH/Fe_3O_4 NPs precursors prepared by a two-step method……..173
Chapter 9: Improvements in the preparation of polyaniline nanofibers by electrospinning technique and their biocompatibility. Towards pure electrospun polyaniline……..175
9.1. PANI/PEO nanofibers: effect of different raw sources……177
9.1.1. Morphological characterization……..177
9.1.2. Spectroscopic characterization……...181
9.1.3. Conductivity measurements……184
9.1.4. Tests of cytocompatibility……..187
9.2. PANI/PMMA nanofibers: effect of washing……189
9.2.1. Morphological characterization……..189
9.2.2. Spectroscopic characterization……...195
9.2.3. Tests of cytocompatibility……..196
Chapter 10: Piezoresistive properties of polyaniline: towards low cost force and strain sensors……198
10.1. Electromechanical characterization of PANI under high loading……..199
10.1.1. Electromechanical response……..200
10.1.2. Diffractometric characterization……...202

10.1.3. Electrical conductivity……..202
10.1.4. Piezoresistive effect……..203
10.2. Electromechanical characterization of PANI under low loading……206
10.3. Piezoresistive effect in polyaniline. The effect of different raw materials and doping agents……...209
10.3.1. Electrical conductivity……..213
10.3.2. Morphological characterization……214
10.3.3. Electromechanical response……..217
10.3.4. Piezoresistive effect……..219

PART IV: CONCLUSIONS……..226

REFERENCES……...230

Abstract

The chemical industry of the forthcoming years will be shaped by a number of emerging global megatrends strictly related to the growth and aging of the world population (nine billion people in 2050). This will result in demand of innovative materials able to solve new needs in different fields: health, communication, energy, environmental sustainability, etc. In this diversified context, conducting organic polymers (COPs) are expected to play an important role thanks to their polyhedric properties. Among them, polyaniline is one of the more investigated COPs owing to its peculiar properties which make it a potential substitute of conventional materials in different fields (electronics, fenestration, textile industry, sensors and many others).

However, to date many aspects related to its synthesis and application are still open. Scope of the present work is to provide alternative eco-friendly methods to the traditional synthetic routes towards PANI-based materials and enlarge their present applications in view of the novel requirements. This study has been organized in three main sections. In the first section a new green protocol will be present to prepare PANI/metal oxides nanocomposites, innovative materials in the field of EMI shielding. For the first time the double role of magnetic nanoparticles, as catalysts of the reaction and magnetic fillers of the final products, will be illustrated.

Conducting/magnetic materials are particularly tempting for their ability to reduce the electromagnetic interferences (EMI) originated by the increasing use of electronic devices and telecommunication equipment. Preliminary results in terms of their microwave absorbing properties will be shown.

The possibility to improve the health and quality of life for millions of people worldwide is, in fact, the overall goal of tissue engineering. Nanostructured PANI in form of fibers or wires could find application as novel conductive scaffolds in neuronal or cardiac stimulations. In the second section, the possibility to produce highly pure polyaniline nanofibers by electrospinning technique will be showed. These materials, characterized by high values of conductivity and cytocompatibility, could represent an alternative to traditional solutions for cardiac and neuronal stimulation.

Regarding the third section of the work, the amazing piezoresistive properties of PANI, especially in form of film, will be for the first time herein presented. Herein, the extraordinary high GF values of PANI-based films (more than 10 times higher than those of commercial piezoresistors) will be reported. The mechanical monitoring in large and small scale (buildings/touch-technology) needs of highly sensitive stress/strains sensors and PANI-based materials are particularly promising in this sector. All these characteristics contribute to make PANI and its composites innovative materials which could offer new solutions for many challenges of the future.

PART I: INTRODUCTION

Chapter 1: Conducting Organic Polymers

1.1. Conducting polymers

1.1.1. Non-Intrinsically Conducting Polymers

Most of the polymers manufactured today are insulators. When they are synthesized from olefins, as ethylene, propylene or higher ones, their backbone is made of carbon-carbon single bonds, otherwise they are made of repetitive ester, ether or amidic bonds. As there is no possibility for a charge to move along a conjugated π-bond path, these polymers show high resistivity, hence very low conductivity. The only possibility to make a conductive material is to add a second component for example metal powder or carbon black.[1] Recently, many publications show that CNTs (carbon nanotubes) are one of the best fillers (Figure 1.1). In fact, adding only 2-3 % weight of single walled carbon nanotubes (SWNT) to a polymer can improve its conductivity by several orders of magnitude (Figure 1.2). [2, 3]

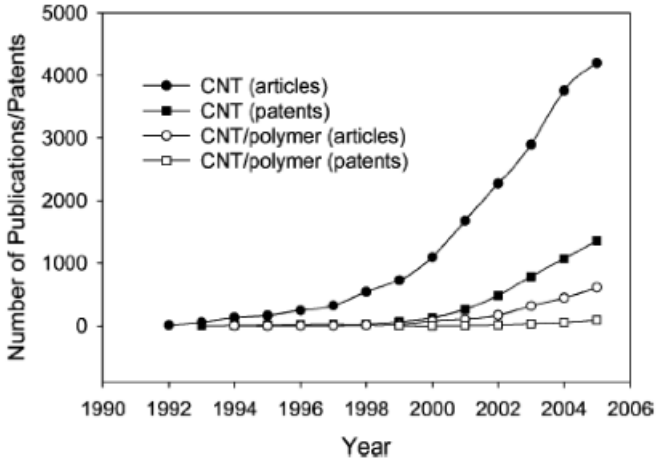

Figure 1.1.: articles and patents on carbon nanotubes (CNT) and CNT composites per year.

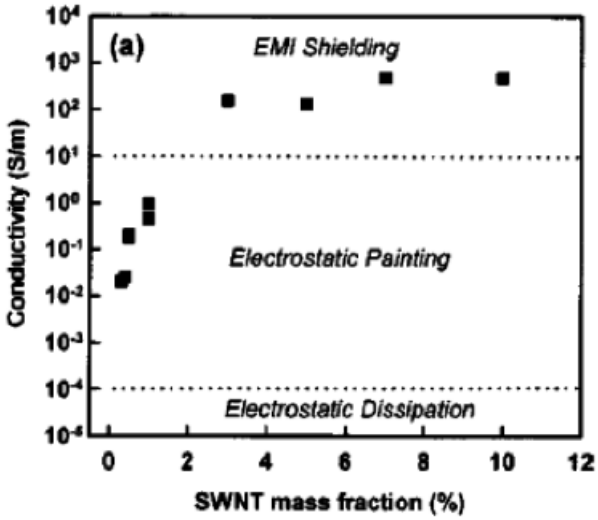

Figure 1.2.: conductivity of CNT composites as a function of its mass fraction.

1.1.2. Intrinsically Conducting Polymers

Since the discovery of the highly conducting polyacetylene (PA) in 1977,[4] the scientific community has focused its efforts on the study and optimization of a new class of materials: conductive organic polymers (COPs).

Among these innovative materials, called also "synthetic metals", polyaniline (PANI), polypyrrole (PPy) and polythiophene (PTh) are still the most studied for their peculiar characteristics, as good conductivity and high environmental stability,[5] that make them particularly attractive for applications in many fields (photovoltaic devices,[6] batteries,[7] electrodes,[8] sensors,[9] and many others).

The simplest conducting polymer is polyacetylene. Figures 1.3. a and b show its structural isomers.

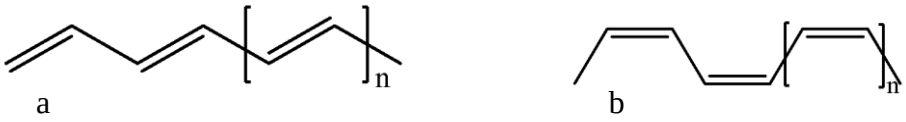

a b

Figure 1.3.: a) *trans*-PA and b) *cis*-PA

In 1958 the Italian Giulio Natta (Figure 1.4.) prepared polyacetylene with high cristallinity using a mixture of $Al(CH_2CH_3)_3$ and $Ti(OC_4H_9)_4$ as the initiator.[10]

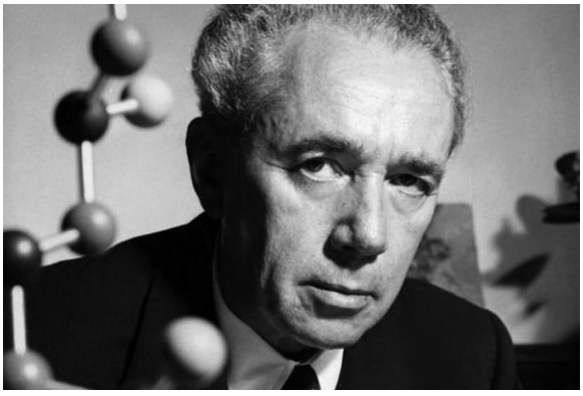

Figure 1.4.: Giulio Natta

However, the limited physicochemical characteristics of the product led to a loss of interest from the scientific community for many years.

At the beginning of 1970, the Japanese chemical Hideki Shirakawa (Figure 1.5. c) found a useful way to control the ratio of the two isomers during the synthesis of PA. The synthetic method applied was based on the use of the same Ziegler-Natta catalyst used from Natta. However, by

acting on the reaction conditions, especially temperature and catalyst amount, Shirakawa obtained a silvery film of pure *trans*-PA and a coppery film of pure *cis*-PA.

The studies on PA continued with the valuable contribution of the professors Alan J. Heeger (Figure 1.5. a) and Alan G. MacDiarmid (Figure 1.5. b). In 1977 Heeger, MacDiarmid and Shirakawa found that if treated with alogens or other compounds such as AsF_5 the conductivity of polyacetylene abruptly increased of 10^9 times, reaching the value of 10^5 S/m.[11]

In 2000 these studies on PA earned the three scientists the Nobel Prize in Chemistry *"for the discovery and development of conductive polymers"*.

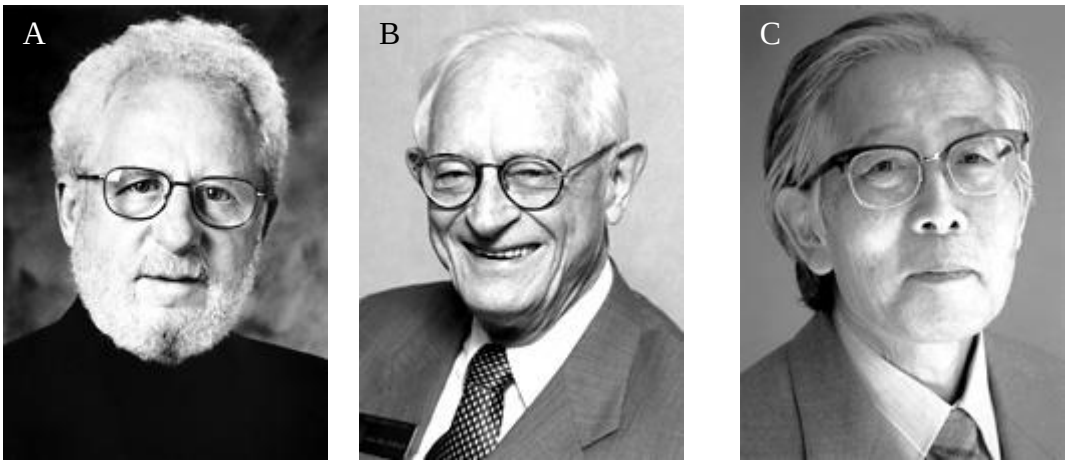

Figure 1.5.: a) Alan J. Heeger, b) Alan G. MacDiarmid, c) Hidaki Shirakawa

Among the COPs, polyacetylene is the polymer with the highest electronic conductivity. However, its high sensitivity to air and moisture makes it unusable in the common applications.

For this reason, the scientists focused their efforts on the preparation of conducting organic materials characterized by ease of synthesis, low cost but especially high stability.

The following are some of the most investigated conducting polymers and their respective starting monomers:

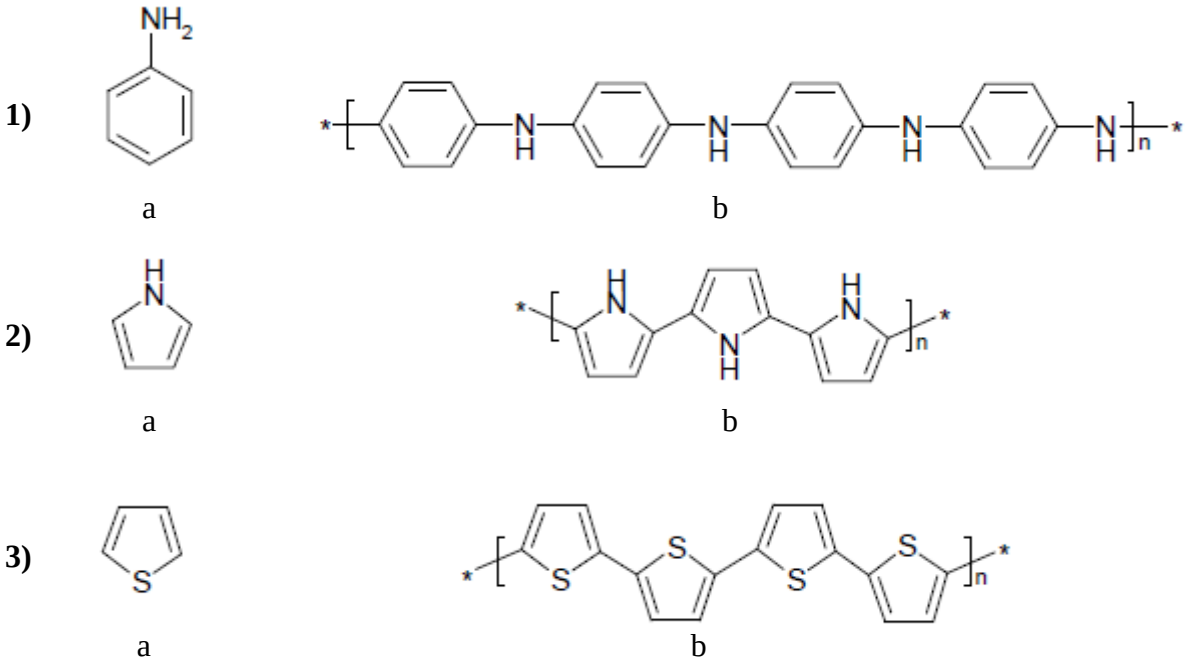

Figure 1.6.: 1a) aniline, 1b) polyaniline, 2a) pyrrole, 2b) polypyrrole, 3a) thiophene, 3b) polythiophene

1.2. Polarons, bipolarons and solitons

In the COPs the equilibrium geometry in the ionized state is different from this in the ground state. [12-14]

Figure 1.7. reports the energies involved in the ionization process of a molecule.

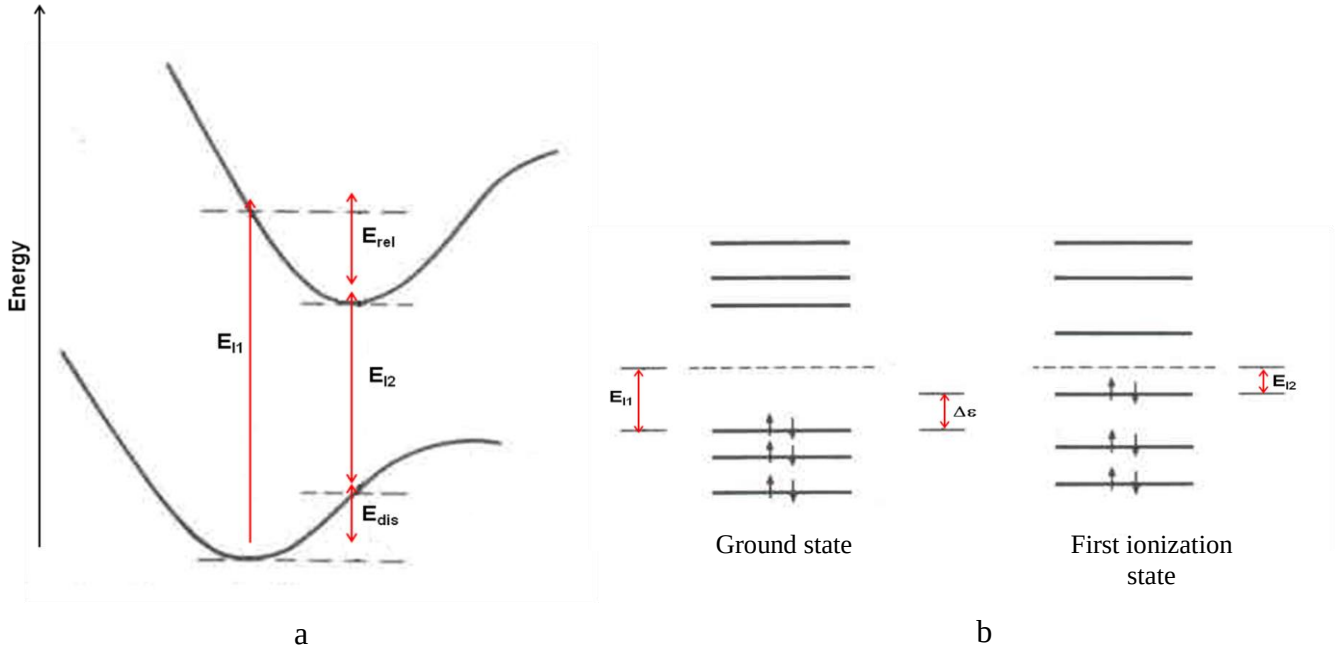

Figure 1.7.: a) Energies involved in a ionization process of a molecule, b) schematic illustration of the one-electron Energy levels for a molecule in its ground state and its first ionization state.

Following the scheme reported in Figure 1.7., when a molecule is excited it passes from the ground state to the first ionization state. The energy involved in this process is E_{I1}. However, it is possible that in the ground state the geometry of the molecule is distorted and the molecule adopts the equilibrium geometry of the ionization state. This produces a distortion energy (E_{dis} in Figure 1.7. a).

As shown in Figure 1.7. b, this distortion causes an upward shift of the highest occupied molecular orbital (HOMO) and a downward shift of the lowest unoccupied molecular orbital (LUMO).

As it can be inferred from Figure 1.7. a, the geometry relaxation in the ionized state is favoured when $E_{I1} - E_{I2} >> E_{dis}$, that is when the reduction $\Delta\varepsilon$ (Figure 1.7. b) upon distortion is larger than E_{dis} required to make the distortion.

In all materials, including polymers, an ionization process produces a hole in the valence band corresponding to a positive charge. For most of the solids this process doesn't cause lattice distortion. Moreover, the positive charge is completely delocalized and makes these materials conductive.

However, as reported above, in a conducting organic polymeric chain during the ionization process the localization of the charge is energetically favoured, because producing around the charge a local distortion (relaxation) of the lattice. This process causes the presence of localized electronic states.

For example, during an oxidation process an electron is removed from the chain, causing a lowering of the ionization energy of $\Delta\varepsilon$. If $\Delta\varepsilon$ is larger than E_{dis} necessary to distort the lattice locally around the charge, this localization process is favourable. This produces a polaron, that in chemistry is a radical anion (spin ½) associated with a lattice distortion.

When a second electron is subtracted from the chain, it can be removed from the polaron, producing a bipolar, o from another point of the chain, producing two polarons.

A bipolaron can be defined as a pair of like charges (dication or dianion) associated with a local lattice distortion.

The formation of the bipolaron is more favoured than that of two polarons, because the energy gained due to the local lattice deformation is larger than Coulomb repulsion between the two charges of same sign that are in the same location.[15]

Polaronic and bipolaronic states can be produced in polymers that have not degenerate ground states. Most of the conducting organic polymers present these conditions, because their resonant structures are not isoelectronic.

In the case of *trans*-polyacetylene the configuration of the ground state is degenerate, because the interchange of the single and double bounds doesn't involve energy variations. This means that two

geometric structures have the same energy. (Figure 1.8. A). The transition from a phase to another is described from the parameter:

$$u = d_{C=C} - d_{C-C}$$

where $d_{C=C}$ and d_{C-C} are the distance of the double and single bonds respectively.

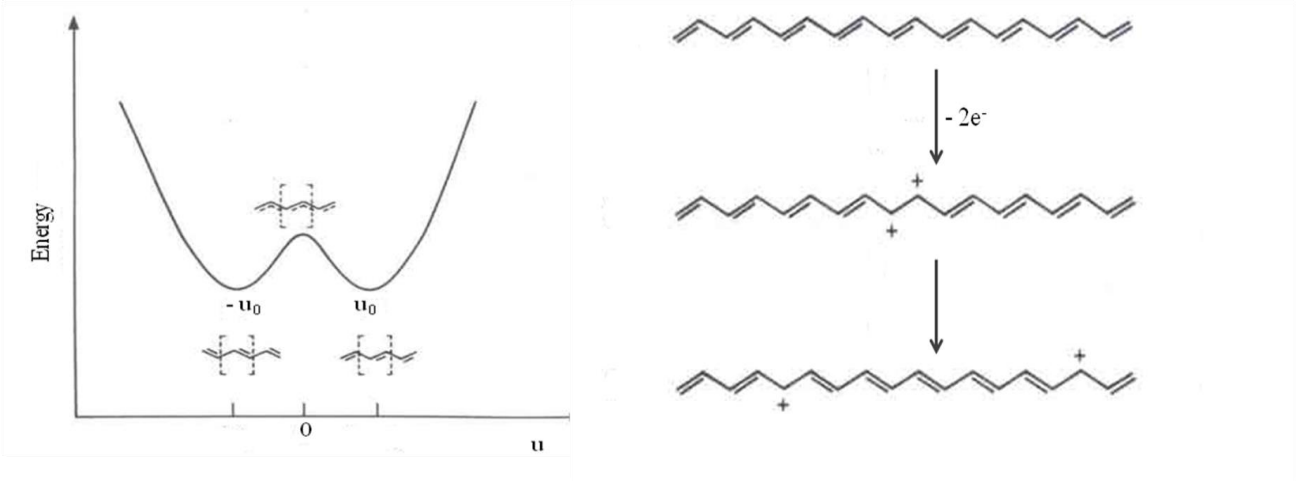

A B

Figure 1.8.: A) *Trans*-polyacetylene phases and their energetic diagrams, B) illustration of the formation of two charged solitons on a chain of *trans*-polyacetylene

As a result of this degeneracy, when a bipolaron is formed in a *trans*-polyacetylene the two charges can be separated (Figure 1.8. B) forming two single charges, named solitons. This process of charge separation is favourable because doesn't increase the distortion energy of the system. In fact, the geometric structure that appears between the two charges has the same energy as the geometric structure on the other sides of the charges. The soliton corresponds to a zero value of u (Figure 1.8. A). Solitons are defects of conjugation that sign the transition from one phase to another, as reported in Figure 1.8. A.

In the case of *trans*-PA a neutral soliton occurs when a chain contains an odd number of conjugated carbons, a radical (Figure 1.9.).

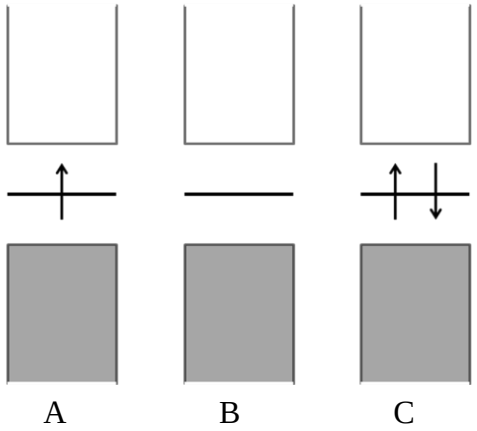

Figure 1.9.: Band structure for a *trans*-PA chain containing a A) neutral soliton, B) positively charged soliton, C) negatively charged soliton

In a long chain, the spin density in a neutral soliton is not localized on a carbon atom but delocalized on several carbons.[16-18]

The energy level associated to a neutral soliton is occupied only by n electron (Figure 1.9. A); as a result its spin is ½ and zero charge. On the contrary, positive and negative solitons (Figures 1.9. B and C) have zero spin values but are positively or negatively charged. When subjected to an electric field, charged solitons can move longitudinally along the polymeric chain thus generating current transport.

1.3. Conduction mechanism

Generally, the backbone of the common polymers mainly consists of σ bands and the hybridization of each atom of carbon is sp^3. The high energy gap ($E_{gap} > 6$ eV) between the bonding band (σ) and antibonding band (σ*) makes these materials insulating.

Differently, in the COPs the backbone consists of atoms of carbon hybridized sp^2, that form three σ bonds, and a p_z orbital that allows a π overlapping with the p_z orbital of the adjacent carbon.

The presence along the backbone of these conjugated double bonds, π delocalized system, is responsible for the electronic properties of the conducting polymers.

The presence of these conjugated double bonds produces two bands, that similarly to the metals can be called “valence band” and “conduction band” (Scheme 1.1.).[12]

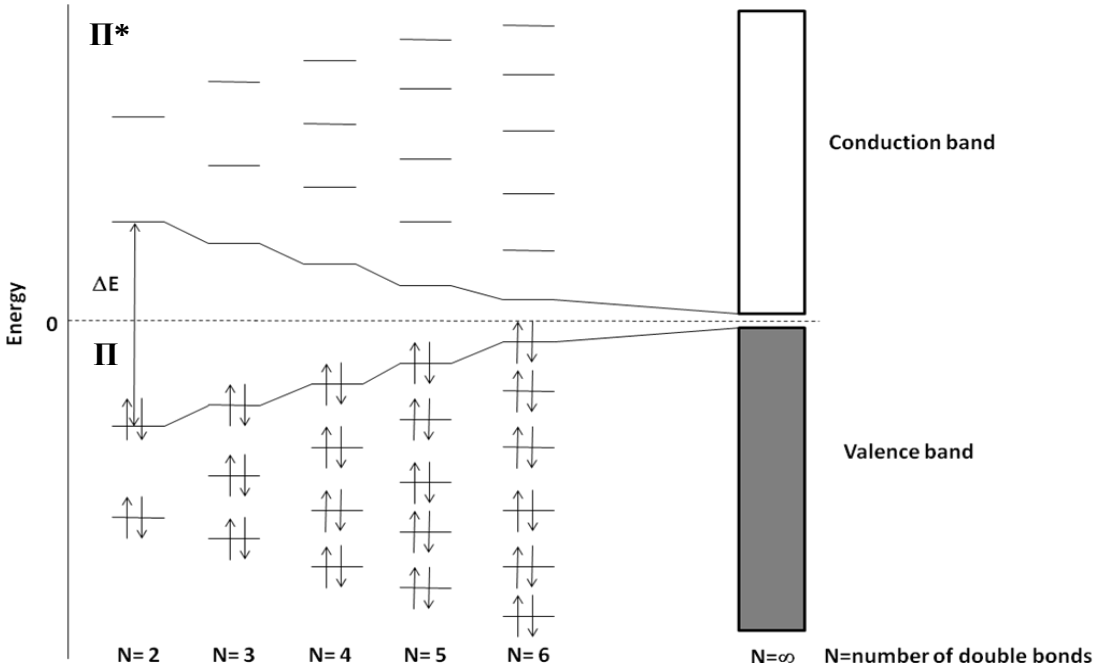

Scheme1.1.: Energy variation vs number of double bonds

Roughly, as for the inorganic materials also for the organic polymers the band model can be applied to explain their conductivity.

In COPs the electric conductivity is due to the low value of the E_{gap} (~ 1- 4 eV), that allows the electrons in the valence band (π) to access the conduction band (π*).[13]

Figure 1.9. reports a comparison between the conductivity of COPs and those of other common materials.

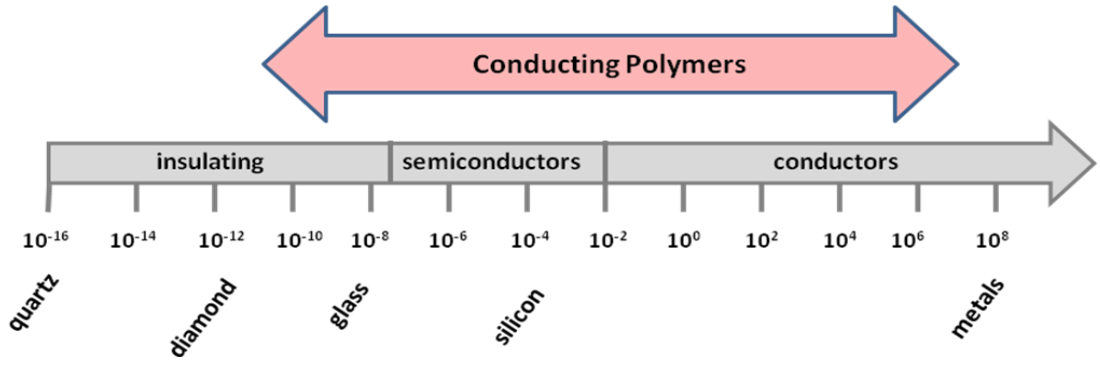

Figure 1.9.: Comparison between the conductivity of COPs and those of other common materials

In the inorganic semiconductor the removal or addition of electrons can be realized in different ways, for example by photoexcitation or by the introduction of impurities (dopants).

If the impurity provides an electron to the conduction band (CB), the doping process is called *n*-type doping. On the contrary, if the impurity subtracts an electron to the valence band (VB), producing a hole, the doping process is called *p*-type doping (Figure 1.10.). Electrons and holes are the charge carriers responsible to the electric conductivity of these materials.

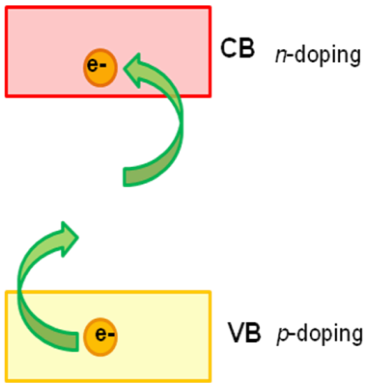

Figure 1.10.: *n*-doping and *p*-doping in the inorganic semiconductors.

However, this model doesn't explain why in the COPs the conductivity is associated with unpaired electrons but rather with spinless charge carriers.

Starting from the band model, it is possible to define two quantities: the ionization energy (IE) and the electronic affinity (EA).

The ionization energy is the energy required to remove an electron from the valence band.

The electron affinity is the energy required to capture an electron in the conduction band.

Generally, conducting organic polymers are characterized by small IE and large EA, that easily allow to oxidize (*n*-type doping) or reduce (*p*-type doping) the system.[14]

Since the inorganic semiconductors are strict, they maintain their structure also the addition of removal of electrons.

Conducting organic polymers, instead, are characterized by low coordination and high flexibility and ability to structural distortions. For these reasons, the removal or introduction of charges cause a distortion (relaxation) around them. This kind of distortions are energetically favoured because they allow the stabilization of the charges.

The distortion of the backbone, due to the addition or removal of electrons, can lead to excited states, called solitons, polarons and bipolarons, that are defects responsible for the electronic conductions. Three methods were used to generate additional solitons: chemical doping, photogeneration and charge injection. An electron will be accepted by the dopant anion to form a

carbocation (positive charge) and a free radical during the chemical doping (oxidation) of the polymer chain, known to organic chemists as radical cation or polaron to physicists.

Both the soliton and polaron can be neutral or charged (positively or negatively) as shown in Figure 1.11.

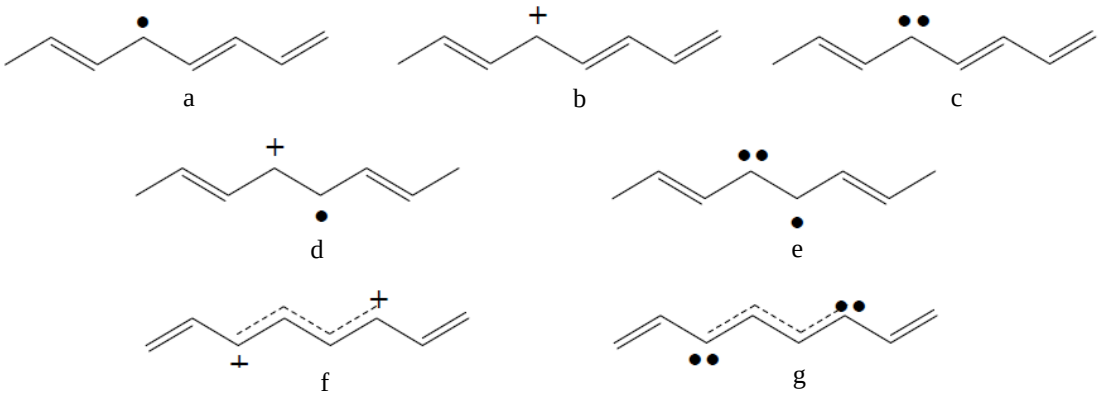

Figure 1.11.: defects in conducting organic polymers. a) neutral soliton, b) positive soliton, c) negative soliton, d) positive polaron, e) negative polaron, f) positive bipolaron, g) negative bipolaron

1.4. Main synthetic techniques

Typically COPs are prepare by traditional polymerization reactions, such as condensation and addition reactions. However, more accurately the synthetic methods of COPs can be categorized in three main groups: chemical, electrochemical and photochemical syntheses.[20]

1.4.1. Chemical synthesis

Among all the synthetic methods developed to produce COPs, the oldest and still the most popular route for the preparation of these materials in bulk is the chemical oxidative polymerization reaction. This approach remains the most used and also investigated especially for large scale production level. Stoichiometric oxidants, such as $KMnO_4$, $K_2Cr_2O_7$, $(NH_4)_2S_2O_8$ but also metals in high oxidation state,[21-24] are used at low pH values. Even though chemical synthesis is the most applied in academic and industrial fields, the control of the morphology and conductive characteristics of the products is harder than in the case of electrochemical approach. In fact, small changes of some parameters (such as temperature, concentration, etc…) cause big changes in the characteristics of the products. Moreover, the large production of waste, such as MnO_2, $(NH_4)_2SO_4$ and so on, makes this approach unsustainable in terms of environmental impact.

In the last years, alternative catalytic processes have been developed in order to reduce the production of waste and provide cleaner products. In this context the use of catalysts, in form of

salts of metals or nanopaticles, [25-30] or sonication [31-34] allow to speed up the polymerization reactions working in cleaner and mild conditions.

1.4.2. Electrochemical synthesis

Unlike chemical syntheses, electrochemical approach allows to control accurately morphology and conductive behaviour of COPs. It is particularly effective in the preparation of COPs in form of film and allows to tune easily the final thickness. Different techniques can be used including potentiostatic (constant potential), galvanostatic (constant current) and potentiodynamic (potential scanning, i.e. cyclic voltammetry) methods.[35] In this kind of reaction the choice of the solvent and electrolyte is crucial, because they have to be stable at the oxidation potential.

Electrochemical syntheses occur through addition polymerization reactions. They are oxidative processes and are characterized by three steps:

1) initiation step: radical monomer is produced by electrochemical oxidation;

2) chain propagation: radical reacts with a non-radical to produce a new radical species;

3) chain termination: two radicals react each other to create a non-radical species.

The electropolymerization mechanism is still a research topic of relevant interest. In this context, the contrasting interpretation of pyrrole polymerization is emblematic.

As an example the electropolymerization of pyrrole is reported below.[36]

Pioneering investigations of Funt and Diaz,[37, 38] then confirmed by Waltman and Bargon,[39, 40] have proposed that pyrrole activation occurs through electron transfer from the monomer forming a radical cation-rich solution near the electrode in several steps.

Step 1

In the first step pyrrole monomer (Py) is oxidized at the surface of the electrode producing cation radical ($Py^{\bullet+}$) stabilized by resonance by the mechanism reported in Scheme 1.2.

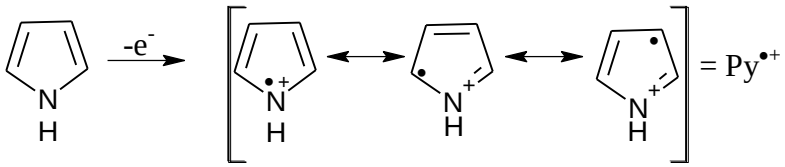

Scheme 1.2. Cation radical formation

Step 2

Thanks to their reactivity $Py^{\bullet+}$ species can react each other by coupling reaction producing dimeric cationic species, which can lose protons forming neutral dimers (Scheme 1.3.).

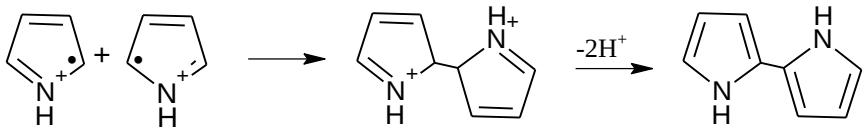

Scheme 1.3. chain propagation

Step 3

Also dimeric species can be oxidized to produce cation radicals. Moreover, since the unpaired electron is now delocalized over two rings, the potential oxidation of dimer is lower than that of corresponding monomer and it can be oxidized more easily producing trimeric cations and then neutral trimers.

Step 4

The chain propagation continues producing long polymers. It stops when two radicals react each other to create a non-radical species.

Pletcher and co-workers have suggested another mechanism in which the cation radical, formed by the loss of an electron, reacts directly with a neutral molecule giving a cation dimer [41]. The cation dimer then loses a second electron and 2 protons, thus forming the neutral dimer.

1.4.3. Other synthetic methods

In addition to two main synthetic methods reported above (chemical and electrochemical syntheses), many others have been investigated. In general, the necessity of developing new synthetic strategies is related to the possibility to obtain COPs in precise nano-sized forms, such as nanofibers, nanospheres, nanorods, etc.

Solide-state polymerization, microwave-assisted polymerization, UV light-assisted polymerization, plasma-induced polymerization and vapor phase polymerization are good examples of alternative approaches.[42]

1.5. Research and Market

From their discovery to date the scientific interest in the conducting organic polymers has grown up exponentially, as confirmed by the graph reported in Figure 1.12., which shows the number of publication per years for polyaniline.

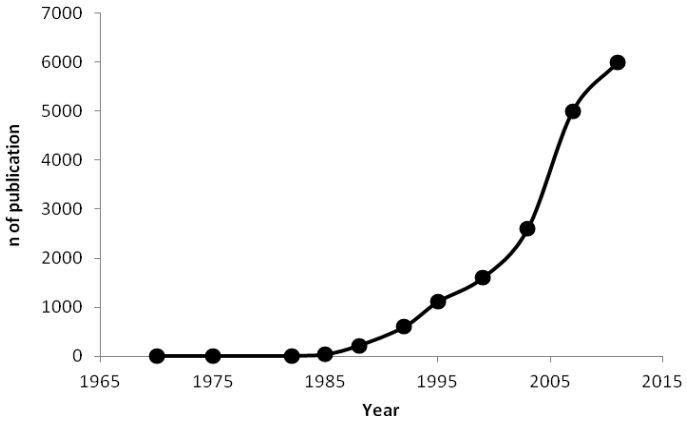

Figure 1.12.: number of publications per year for polyaniline

According to a recent market research report,[43] the total market for conducting organic polymers is expected to reach $3.4 billion by 2017.

Factors driving market of COPs are lightweight, easy fabrication, low cost and high resistance to heat that make them particularly appealing in many fields, such as electronic devices, EMI (ElectroMagnetic Interference) shielding, biomedicine, and so on. Cost is another important factor influencing the electro-active polymers market growth.

North America dominate the market for COPs. In fact, as reported in Figure 1.13, it held a 65% share of the global COPs product market, followed by Europe with a 22% share in 2011.

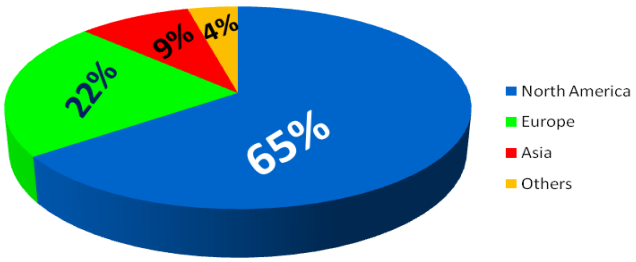

Figure 1.13.: Global production market for COPs in 2011

Recently, DuPont has signed an agreement with Ormecon Chemie of Ammersbek, Germany to commercialize their Ormecon's polyaniline-based products including anticorrosion coatings and printed circuit board, a market of $9-15 billion.

The US market for conductive polymers is forecast to reach 240.5 thousand tons by the year 2015. Conductive polymers could, in the long-term, be an alternative to silicon. Opportunities exist in display materials, chip packaging, plastic transistors, sensors, and ultracapacitors,.

However, intrinsically conducting polymers (COPs in the Figure 1.14.) production is currently small in the overall conducting polymer (CPs in Figure 1.14.) market but it is the fastest growing market in future. At present it accounts for only 12% of the total conducting polymer market, but this share is estimated to increase to 20% by 2017.

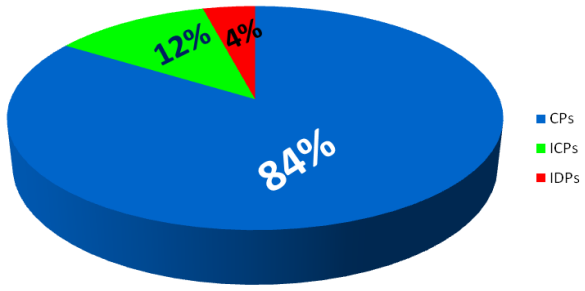

Figure 1.14.: Global market for conducting polymers in 2011. CPs= conducting polymers, COPs= intrinsically conducting organic polymers, IDPs= Inherently dissipative polymers

In any case, conductive organic polymers represent the largest submarket of the overall electro-active polymers market with an expected $2.6 billion by 2017, at a CAGR (Compound Annual Growth Rate) of 6.1% from 2012 to 2017.

Chapter 2: Polyaniline

2.1. History

Polyaniline (PANI) has the longest history among the intrinsically conducting polymers. It is one of the oldest artificial conducting polymers and its high electrical conductivity among organic compounds has attracted continuing attention.

The aniline monomer was isolated as early as 1826 when crystalline salts of aniline sulfuric and phosphoric acid were observed from the pyrolytic distillation of indigo.[44]

Although the exact date of the first reported polyaniline is unclear, aniline was oxidized early as 1834 [45] and 1840,[46] when pure aniline (observed as a colorless oil) was obtained from indigo and oxidized with chromic acid.

Observed as a black precipitate, "aniline black", in an organic form as part of melanin, a type of organic polymer, in 1934, polyaniline has been reported since 1860,[47] and some of the first accurate researches on the subject was made by Green and Woodhead.[48-50]

The terms "emeraldine" and "nigraniline" for different redox forms of aniline black, were introduced more recently (about second half of the 19th century)[51] and defined at the beginning of the 20th century, alongwith other redox forms such as leucoemeraldine, protoemeraldine and pernigraniline, as linear N–C4 coupled aniline octamers with different oxidation state, i.e., different number of *N*-phenyl-benzoquinonediimine and 4-aminodiphenylamine moieties in the backbone.[50, 52] The interest in polyaniline rose up after the demonstration by MacDiarmid that, after acidic doping, it becomes a conductor, with conductivity up to 3 S/cm.[53]

2.2. Physicochemical characteristics

Polyaniline is composed of aniline repeat units connected to form a backbone. The existence of a nitrogen atom lying between phenyl rings allows the formation of different oxidation states that can affect its physical properties.

Although leucoemeraldine, emeraldine and pernigraniline are the three most common forms, many other intermediate forms are available, depending on the degree of oxidation of the units (Figure 2.1).

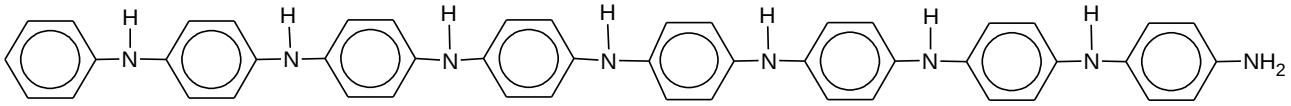

a) Leucoemeraldine

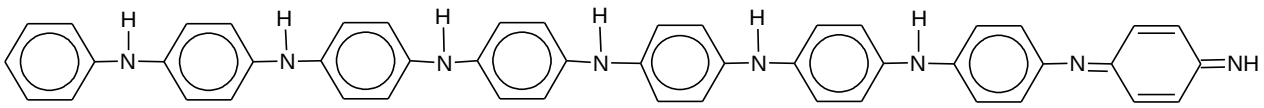

b) Protoemeraldine

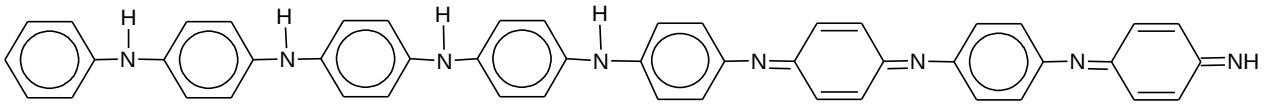

c) Emeraldine

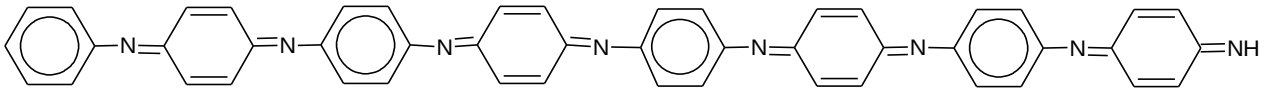

d) Nigraniline

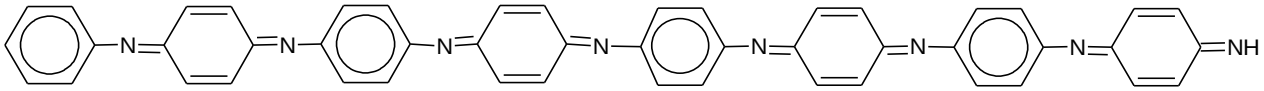

e) Pernigraniline

Figure 2.1.: Polyaniline in different oxidation states

Some properties and characteristics of polyaniline are strictly correlated to its oxidation state.

Leucoemeraldine (Figure 2.1. a) is an amorphous material, whose colour ranges from pale brown to white. This material, characterized by a high melting point, is insoluble in all solvents. In moist air it is slowly oxidized to protoemeraldine (Figure 2.1. b), more rapidly if heated.

Protoemeraldine form is characterized by a violet colour and is soluble in acetic acid. If protonated it forms yellowish-green salts.

Emeraldine (Figure 2.1. c) is the half-oxidized form. It's partially soluble in pyridine, *N*, *N*-dimethyl formamide and *N*-methylpyrrolidinone producing blue coloured solution. In the presence of organic or inorganic acids it forms a salt green coloured called emeraldine salt, which is the unique electrically conducting form of polyaniline.

In its base form nigraniline (Figure 2.1. d) it is stable and forms dark bluet coloured solutions in acetic acid, formic acid and pyridine. If heated in an acidic solution it forms green coloured salts because of its reduction to emeraldine.

In base and salt form pernigraniline (Figure 2.1. e) is not stable. In bases and acids it decomposes quickly to forms in lower oxidation state.

It is well known that polyaniline has switching, optical, conductive and solubility properties that distinguish it from other conducting polymers.[54, 55]

The ability to switch from one form to another and the optical properties of PANI are interlinked and influence each other directly. PANI is a mixed oxidation state polymer, ranging from the most reduced leucoemerladine form, which is yellow in colour, to the half oxidized emerladine which is green, and the violet fully oxidized pernigraniline[33] as illustrated in Figure 2.1. The electrochemical switching of polyaniline among the oxidation states can be readily monitored by cyclic voltammetry as illustrated in Figure 2.2.

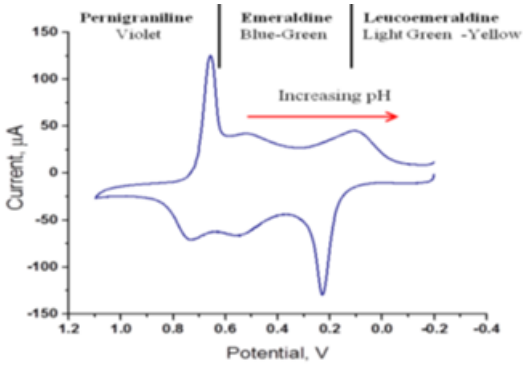

Figure 2.2.: Cyclic voltammogram of polyaniline film on a platinum electrode in 1 M HCl. Dependence of the chances in structure and colour with the potential and pH.

Moreover, the UV-visible spectrum of polyaniline is sensitive to oxidation state and transitions among the oxidation states and is accompanied by visible optical colour change.[56]

In its unique conducting form, emeraldine salt, polyaniline exhibits three characteristic bands (figure 2.3.).

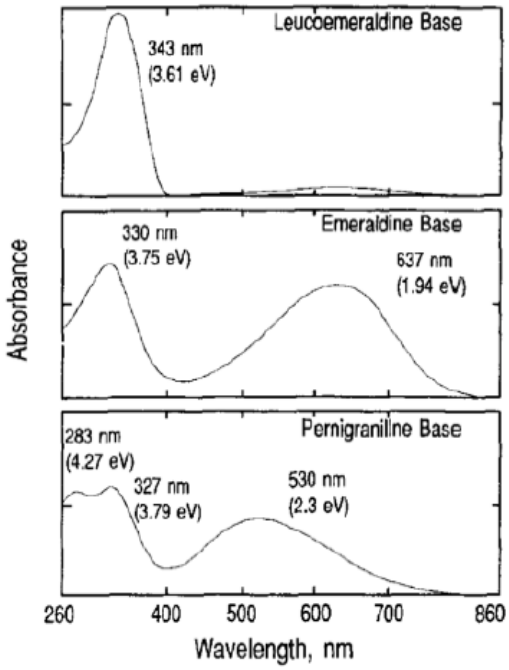

Figure 2.3.: UV-vis spectra of leucoemeraldine base, emeraldine base and pernigraniline base.

The band at *ca*. 330 nm is attributed to π-π* transition, whereas two bands at *ca*. 430 and 800 nm in the visible region are related to π-polaron and polaron-π* transitions.[57] The band at *ca*. 800 nm is shifted at lower wavelengths (*ca*. 600 nm) in emeraldine base form. The reduced leucoemeraldine

base exhibits only a band at *ca*. 320 nm due to the π-π* electronic transition, whereas pernigraniline base shows two bands at *ca*. 320 nm (π-π* band) and at *ca*. 530 nm (Peierl gap transition).[54, 58]

2.3 Methods of synthesis

Several methods can be employed to synthesize polyniline. Among them chemical synthesis, electrochemical oxidation of the monomers and polycondensation are the most popular,[52] but many other uncommon approaches, such as enzyme-catalyzed polymerisation and photochemically-initiated polymerisation are also investigated.[54] Due to its characteristics and its high air stability emeraldine base is the form of polyaniline generally obtained using any synthetic method. Pernigraniline and leucoemeraldine are usually obtained by the oxidation or the reduction of emeraldine form respectively.

2.3.1. Chemical synthesis

The chemical oxidative polymerisation represents the oldest and still the most popular way for the preparation of polyaniline. For more than twenty years many efforts have been devoted to optimizing this process. Even though the reaction is mainly carried out in aqueous medium, several papers report on the aniline polymerisation in organic solvents.[59]

However, water at low pH as the reaction solvent is still the most extensively employed. Operating in aqueous solution, generally "stoichiometric" inorganic oxidants are used, such as KIO_3, $KMnO_4$, $FeCl_3$, K_2CrO_4, $KBrO_3$, $KClO_3$, $(NH_4)_2S_2O_8$.[60-64] Although "stoichiometric" inorganic oxidants allow to produce polyaniline easily and quickly, a strong resulting drawback is represented by the formation of a large amount of by-products, that in the case of $(NH_4)_2S_2O_8$ is ammonium sulfate (*ca*. 1 kg per kg of organic polymer).

The effect of the kind of acid, its concentration and reaction temperature has been extensively investigated.[60] It has been demonstrated that temperature has a pronounced effect on the formation of branched structures and on the molecular weight of the final polymer. In particular, low reaction temperature (typically 0°C) inhibits branching. As far as the molecular weights are concerned, Adams *et al*. observed that passing from 18°C to -25°C the molecular weight of polyaniline gradually decreases, as shown in Figure 2.4.[65]

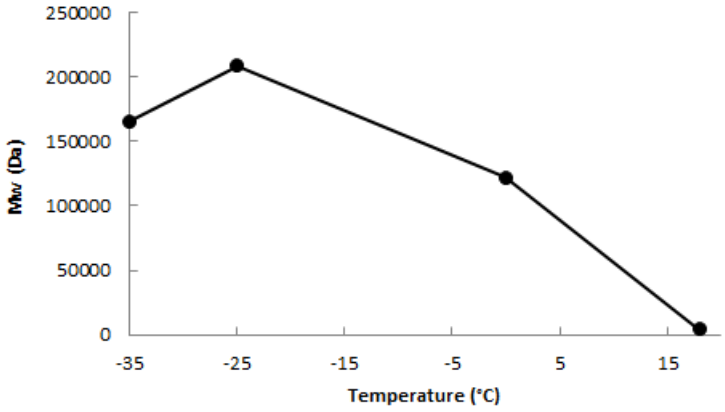

Figure 2.4.: Dependence of Mw from the temperature

However, below this temperature the molecular weight of PANI falls back.[65]

Chemical oxidative polymerization of aniline using HCl and $(NH_4)_2S_2O_8$ can be described by the following chemical equation (Equation 2.1.):

$$4x(C_6H_7N\cdot HCl) + 5x(NH_4)_2S_2O_8 \longrightarrow (C_{24}H_{18}N_4\cdot 2HCl)_x + 5x(NH_4)_2SO_4 + 2xHCl + 5x(H_2SO_4)$$

(Eq. 2.1.)

As it is possible to observe using a chemical approach PANI is obtained in form of emeraldine salt.

Starting from this reaction several modifications of the oxidative polymerization of aniline have been proposed.

In this context, an interesting alternative is represented by the interfacial polymerization or emulsion polymerization. By this approach aniline and, if required, a surfactant are dissolved in an organic solvent, whereas the oxidizing agent is in the aqueous phase. The polymerization reaction carries out at the interfacial region.[66]

A modern approach to large scale PANI production suggests the use of more environmentally friendly oxidants, such as molecular oxygen or hydrogen peroxide.[64, 67-74] This new "green" approach would open the way to novel applications.

In fact, especially for specific applications, such as medical and biomedical ones, high purity materials are required.

From a thermodynamic point of view, the reagent H_2O_2 is advantaged owing to its higher redox potential (1.77V vs SCE), which is enough for initiating and sustaining aniline polymerization.

Moreover, the formation of H_2O as the only reduction product greatly simplifies post-treatments and recycling. Often the oxidation by dioxygen and hydrogen peroxide is a slow process which can be accelerated by the use of a catalyst.[26-30, 70] A big help derives by the use of ultrasound

irradiation.[74] Many catalysts have been studied for promoting the oxidative polymerization of aniline. Among them soluble metal ions in high oxidation states or more complex heterogeneous systems have been employed.[21-31, 61-64]

As reported by Wei *et al*., the difficult step in aniline polymerization is the oxidation of the monomer to form dimeric species, that can then quickly oxidized to PANI, thanks to their lower oxidation potential.[76-79]

This means that starting from the preformed aniline dimer, *N*-4-aminophenylaniline, the oxidative polymerization can carry out more easily. Copper, copper salts, gold nanoparticles and nanosized ferrites have shown an high catalytic activity in this reaction.[26, 30, 80]

Although PANI is prepared from more than one hundred year, to date the mechanism of formation is not clear. The informations that we have essentially come from electrochemical experiments. For this reason it's assumed that chemical and electrochemical reaction mechanisms for PANI preparation are similar.

In 1960s Mohilner *et al*. [81] and Bacon and Adams[82] proposed a mechanism for the anodic oxidation of aniline to PANI in acidic media. as the first step in both chemical and electrochemical oxidative polymerization of aniline, authors suggested the formation of cation radical, called anilinium cation (Figure 2.5.)

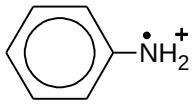

Figure 2.5.: anilinium cation

It's formation is strictly related to the pH of the solution.

The "head-to-tail" and "tail-to-tail" free-radical recombinations of aniline cation radicals lead to the formation of several dimeric species (Fig. 2.6.):

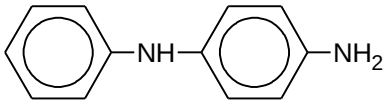

p-amminodifenilammina

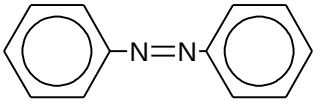

trans-azobenzene

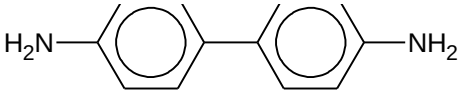

benzidine

Figure 2.6.: Dimeric species by aniline oxidation reaction

A preliminary com radical and aniline indicates that the formation of ADPA is predominant.[83]

However, the dimeric species produced during the oxidative polymerization of aniline in acidic solutions, as well as the mechanism of their formation, are still controversial.

The PANI chain-growth mechanism was investigated many times in the past and it is still open to discussion.[77, 84-89]

In 1990s Gospodinova and Terlemezyan reported a redox process between the growing chain in protonated pernigraniline form (oxidant) and aniline monomers (reductant) in acidic media (pH < 2).[84] Monomer units are gradually added to the chain reaching the emeraldine oxidation state.

To date this mechanism is still accepted, though with some modifications. Moreover, they suggested that during the growth of the chain the primary oxidant (an oxidizing specie, such as $KMnO_4$ or $(NH_4)_2S_2O_8$ in the chemical polymerization and anode in the electrochemical reaction) prefers to oxidize leucoemeraldine, proto-emeraldine, and emeraldine-like oligomers rather than aniline monomers, whereas aniline monomer is oxidized by the growing nigraniline/pernigraniline-PANI chain rather than to form new reactive species.

More in detail, during the propagation phase redox reactions among nigraniline/pernigraniline-like oligomers and aniline monomers were considered as single-electron transfer reactions leading to the formation of oligomeric cation radicals and aniline cation radicals which further undergo free-radical recombination reactions.[85, 86, 89]

It was observed that pH value of reaction medium influences branching phenomena. High levels of acidity cause branching of PANI chains.[85, 86, 89]

In the Scheme 2.1 is reported the whole mechanism of PANI formation.

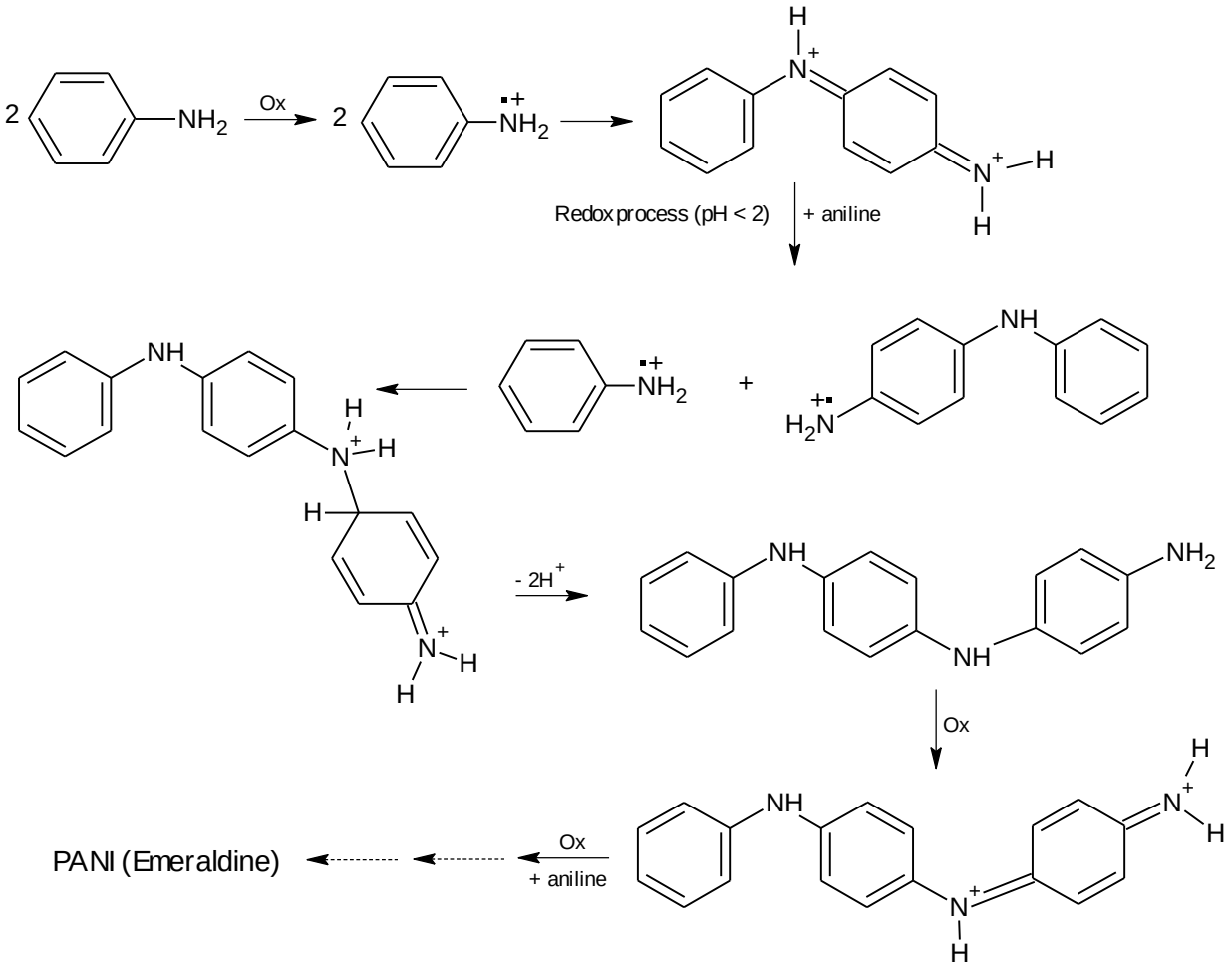

Scheme 2.1.: Redox reactions involved in the PANI formation.

2.3.2. Electrochemical synthesis

Anodic oxidation of aniline on an inert metallic electrode is the most current method for the synthesis of PANI. This method is more advantageous over classical chemical methods. The resulting product is "clean" and does not necessarily need to be extracted from the initial monomer/oxidant/solvent mixture.

In 1960s Mohilner *et al*. Reported the first electrochemical PANI preparation.[61]

Electropolymerization is generally carried out in aqueous protonic acid medium potentiostatically, galvanostatically or by potential scanning (cyclic-voltammetry polymerization). In the cyclic-voltammetry method the product is deposited layer-by layer on the anode. Using this technique homogenous polymer film of good quality was obtained using an eutectic mixture $NH_4F{\cdot}2{,}35HF$ and by the application a potential from –0,2V to 0,7 V (vs. Cu/CuF_2).[90, 91]

In the case of aniline electropolymerization, the radical cation of aniline monomer is formed on the electrode surface by oxidation of the monomer and, as in the chemical polymerization, this process is considered to be the rate-determining step.

Unfortunately, using this approach only small quantities of PANI can be produced (comparing to chemical polymerization). This limitation reduce the possibility to scale-up the production of polyaniline by electrochemical synthesis.

2.3.3. Other conventional methods

In addition to these well-established methods, many others have been developed. Some of these are modifications of the chemical and electrochemical syntheses discussed above, but many other use different approaches.

2.3.3.1. Heterophase polymerization

This method produces polyaniline of high quality. In particular, it allows to tune very accurately chemical-physical properties of the final product from a small to a large volume scale.[92-98]

The heterophase polymerization technique includes different methods of polymerization such as precipitation, suspension, microsuspension, emulsion, miniemulsion, microemulsion, dispersion, reverse micelle and inverse polymerizations.

In some of these cases (suspension, microsuspension, miniemulsion and microemulsion polymerization methods) because of its low miscibility in aqueous solution monomer forms spherical droplets whose size is controlled by a proper choice of the dispersing technique (such as stirring, ultrasonic treatment or homogenization). The addition of a stabilizer guarantees their stabilization in water. The size of the droplets varies, according to the polymerization method, in the following order: suspension >microsuspension >miniemulsion >microemulsion.

The polymerization reaction takes place inside the monomer droplets.

The emulsions are divided into two types: “direct”, oil in water (o/w); and inverse, water in oil w/o). The selection depends on the chosen emulsifier, the water to oil ratio, and the temperature of the polymerization. The microemulsion again is subdivided into general microemulsion and miniemulsion depending upon the droplet size and stability and the amount of surfactant used.

2.3.3.1.1. Synthesis of polyaniline colloidal dispersion

This method is also known as dispersion polymerization.[99, 100] In this approach a water soluble polymer, used as a steric stabilizer (i. e. poly(N-vinylpyrrolidone) (PVP)), is added to the solution, causing the formation of PANI in colloidal form. Typically, the average size of the colloidal PANI particles, obtained by using this synthetic method, range from a few tens to hundreds nanometers and the shape of the particles may be spherical, globular, granular, cylindrical or branched dendritic structures.[101, 102]

2.3.3.1.2. Direct and inverse emulsion polymerization

Aniline monomer is solubilized in an acidic aqueous solution containing the oxidizing specie. a nonpolar or weakly polar solvent (i. e. xylene, chloroform or toluene) is added forming an uniform emulsion.[103] By using this method (direct emulsion), at the end of the reaction PANI salt has to be purified by all other by-products present in the emulsion. Generally, the product is isolated by destabilizing the emulsion through the addition of acetone and washed several times.

In the inverse emulsion polymerization process an organic emulsion of aniline monomer solubilized in a nonpolar organic solvent (i. e. chloroform, isooctane, toluene or in a mixture of solvents) is added to an aqueous solution. An oil-soluble initiator, such as ammonium persulfate, benzoyl peroxide, and so on, starts the polymerization. During the course of the reaction, PANI remains as a soluble component in the organic phase. At the end of polymerization the organic phase is separated and washed repeatedly with distilled water. Acetone or other suitable solvent are used to break the emulsion and precipitate the PANI salt.[104, 105]

2.3.3.1.3. Direct and inverse miniemulsion polymerization

A miniemulsion is defined as a submicron (50-500 nm) dispersion of organic materials (oils) in water. Typically this system contains oil, water, surfactant and a co-surfactant, that usually is a low molecular weight compound poorly soluble in water but a highly soluble in monomer. These co-surfactants retard the outward diffusion of the monomer from droplets and form an intermolecular complex at the oil–water interface, thereby creating a low interfacial tension and a high resistance to droplet coalescence. For these two reasons, emulsion droplets become quite small and stable.[106, 107]

2.3.3.1.4. Direct and inverse microemulsion polymerization

A microemulsion is defined as a micro-heterogeneous system characterized by a large interfacial area and low viscous. As in the miniemulsion process, also in this case the system typically contains oil, water, surfactant and a co-surfactant. Playing with the kind and amount of components of the mixture, inverse microemulsion polymerization allow to prepare polymeric nanoparticles, hollow nanospheres and nanotubes.[108, 109]

2.3.3.2. Interfacial polymerization

This technique is particular useful to produce PANI in nanofiber form.[110] In a typical reaction ane oxidizing agent (ammonium persulfate, hydrogen peroxide and so on) and, if necessary, a polymerization catalyst are in the aqueous phase, whereas aniline monomer and in some case

surfactant in the organic phase. The polymerization reaction takes place at the interfaces of two immiscible solvents. Various products ranging from a one-dimensional radially aligned nanofiber to a spherical shaped PANI with a narrow size distribution can be obtained, setting very carefully some reaction parameters, such as temperature, concentrations of reactants, stirring speed, etc.[111, 112]

2.3.3.3. Metathesis polymerization

Metathesis polymerization is an curious method that allows to produce PANI without employing aniline monomer in the reaction mixture. In fact, heating *p*-dichlorobenzene at 220°C for 12 h in the presence of sodium amide in an organic medium (i. e. benzene) PANI is produced along with sodium chloride and ammonia.[113]

2.3.3.4. Vapor-phase deposition polymerization

This innovative technique allows to prepare PANI thin films growing directly on a substrate by polymerizing aniline monomer in a vapor-phase.[114-116] In a typical example an alcoholic solution containing the oxidizing agent (i. e. $FeCl_3$) and the acid dopant (i. e. camphor sulfonic acid) is coated on a clean polymeric substrate film, such as polyethylene terephthalate (PET), polyimide (PI), polyvinyl chloride (PVC), polystyrene (PS), and so on by dip or spin coating and then dried. Exposing the dry film to aniline vapours in a closed reaction chamber, a polymerization reaction takes place on the preformed film. At the end of the reaction a thin PANI film is produced on the substrate.

2.3.3.5. Sonochemical synthesis

Sonochemical method is a quite new technology that finds many applications in chemical syntheses. It's known that when an ultrasonic wave passes through a liquid medium a large amount of microbubbles are produced. They grow and collapse in a very short time (about a few microseconds) and this effect is called ultrasonic cavitation. It can generated local temperatures as high as 5000 K and pressures as high as 500 atm, with heating and cooling rates greater than 109 K/s.[117] Therefore, sonochemical synthesis is extensively applied in dispersion, emulsifying, crushing and particle activation. Jing et al. synthesized PANI nanofibers with high polymer yields using this technique.[118, 119]

2.3.3.6. Enzymatic synthesis of polyaniline

Horseradish peroxidase (HRP) and soybean peroxidase (SBP) are oxidoreductase enzymes able to oxidize aromatic amines, including polyaniline, in the presence of hydrogen peroxide.[120-122] The possibility to use an enzyme in combination with a "green" oxidant, such as hydrogen peroxide, makes this method particularly attracting. Unlike chemical oxidation, in enzymatic catalyzed polymerization, the oxidation rate is mainly dependent on the amount and activity of the enzyme. Although during enzymatic oxidation, no inorganic by-products are generated, the recycle of the enzyme at the end of the reaction and its stability in the reaction conditions are the biggest drawbacks of this method.

2.3.3.7. Photo-induced polymerization

The photo-induced polymerization of aniline involves the photo-excitation of aniline monomer to obtain the corresponding polymer. Wang et al. synthesized PANI by using a Nd:YAG laser to irradiate an Au electrode in a solution containing aniline under an applied external bias.[123] The morphology of the polymer produced is strictly dependent on the excitation wavelength. In fact, a more globular morphology is observed for the UV synthesis, whereas a more fibrillar morphology is detected for the visible light synthesis.[124, 125]

2.3.3.8. Plasma polymerization

Plasma polymerization (or glow discharge polymerization) uses plasma sources to generate a gas discharge that provides energy to activate or fragment aniline monomer in order to initiate the polymerization reaction. Polymers formed by this technique are generally highly branched and highly cross-linked, and adhere very well to solid surfaces. The biggest advantage to this process is that polymers can be directly attached to a desired surface while the chains are growing, which reduces steps necessary for other coating processes such as grafting. Moreover, it is a solvent-free process and a pinhole-free coating can be obtained.[126, 127]

2.4. Conductivity

Emeraldine salt is the only conductive form of polyaniline. Its conductivity is related to many factors, such as the redox and acid-base properties of the polymer, its degree of crystallinity, presence of branching, morphology, mode of synthesis and so on. As mentioned before (chapter 1, p. 9-12) the transition from insulating to conductive state in polyaniline is due to the oxidation process and to the creation on the polymer's backbone of cation radicals, either polarons or bipolarons.

2.4.1. Effect of doping

Pioneering investigations of MacDiarmid et al. demonstrated that the degree of protonation of chemically synthesized polyaniline (emeraldine oxidation state) is a function of pH solution. They observed that that the protonation degree decreased from about 50% at pH 0 to less than 10% at pH 3. Because the decreasing in protonation between pH 2 and 3 was sharp, they suggested that high degrees of protonation are a prerequisite for high conductivity values.[128]

However, this assumption is true for vacuum-dried PANI, but in wet conditions the results can be different.

In general, the protonation of PANI helps to form a polaron structure, where a current is carried by the holes. When the PANI is in a perfect EB form (50% oxidized with alternative quinoid and benzenoid rings), 50% doping will result in the protonation of the entire quinoid ring. This will lead to the formation of perfect polaron leading to a high achievable conductivity. Therefore, from an initial zero level of doping, with the increase in the degree of doping the conductivity is increased due to the formation of increasingly more polaron. Furthermore, with the increase in the degree of doping beyond 50%, the decreased conductivity may be due to the formation of bipolarons.[129, 130]

Catedral *et al*. investigated the effect of the kind of dopant on the conductivity (Figure 2.7), finding that $HClO_4$-doped sample gave the highest conductivity (109.04 S/cm), which is $2x10^5$ times greater than that of the undoped sample, while HI-doped PANI showed the lowest conductivity (0.02 S/cm).[131]

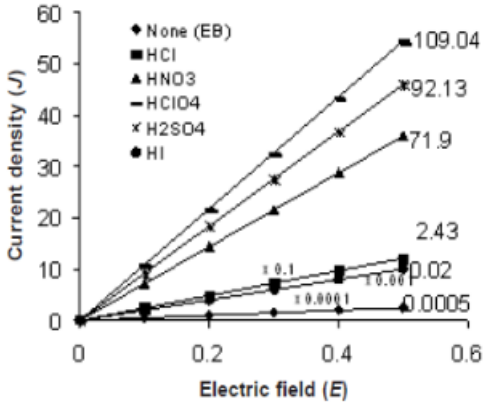

Figure 2.7.: Scaled plots of current density versus electric field for PAni-ES with different dopants showing the slopes as the conductivity in S/cm. Data from Catedral *et al*.[131]

Authors fitted conductivity values versus computed HOMO-LUMO energy gap data. They found an inverse correlation, as shown in the Figure 2.8.

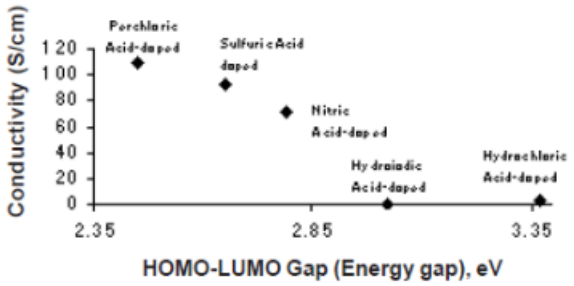

Figure 2.8.: Conductivity versus HOMO-LUMO gap plot for PANI doped with different dopants. Data from Catedral *et al*.[131]

2.4.2. Effect of moisture

The large difference between the resistivity of polyaniline in contact with electrolyte and in the vacuum-dried state implies that the moisture content of the polyaniline should be an important parameter influencing resistivity. As reported in the Figure 2.9., when PANI is exposed to moisture the resistivity increases by 1 order at pH 0.3 but by more than 2 orders at pH 3.5.[132]

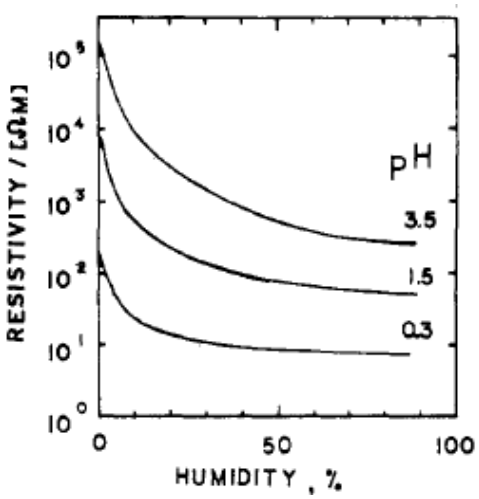

Figure 2.9.: Effect of humidity of air in equilibrium with polyaniline on resistivity. Data from Doriomedoff *et al*.[132]

The positive effect of humidity on the conductivity of polyaniline is due to the increasing in the charge transfer along the polyaniline chain. As a result, in the presence of a humid environment the polyaniline becomes more conducting.

Focke *et al*. proposed a very interesting mechanism to explain the effect of dopant and moisture on the conductivity of PANI (see paragraph 2.4.4.).[133]

2.4.3.Effect of crystallinity

The electrical properties of polyaniline are strongly influenced by the chains structure. It has been observed that with the increase in crystallinity the conductivity is increased, because the structure becomes more organized.

In fact, it is known that the *inter*-chain electron mobility in a given polymer is significantly increased with ordered solid state structure, such as crystalline domains.[133]

As reported in the previous paragraph (2.4.1.), high level of conductivity in PANI can be obtained by doping polymer with aqueous HCl. Moreover, each conducting polymer particle can be considered as a conducting crystal grain. Particles can polymerize in various sized spaces displaying different crystallinities.

Therefore, the size of crystal grain and the degree of crystallinity dramatically affect the conductivity.

X-Ray diffraction is used to investigate the chain ordering and crystallinity in polymeric materials. In general, no distinctive crystal structure is observed in undoped PANI. In this case an amorphous peak appears at a 2θ of ~ 20° (Figure 2.10 a). Studying the morphology of conducting polymer, Warren *et al*. found that the ratio of half-width to height (HW/H) of the X-ray diffraction peak reflects ordering in the polymer backbone. At small HW/H value corresponds high crystalline order.[134] After doping, a small sharp peak appears in 2θ of ~ 9.0°, which can be attributed to the crystallinity, and the peak at 2θ of ~ 20° is shifted to higher angle , corresponding to a decreased d-spacing between polymer backbones (Figure 2.10 b).[135]

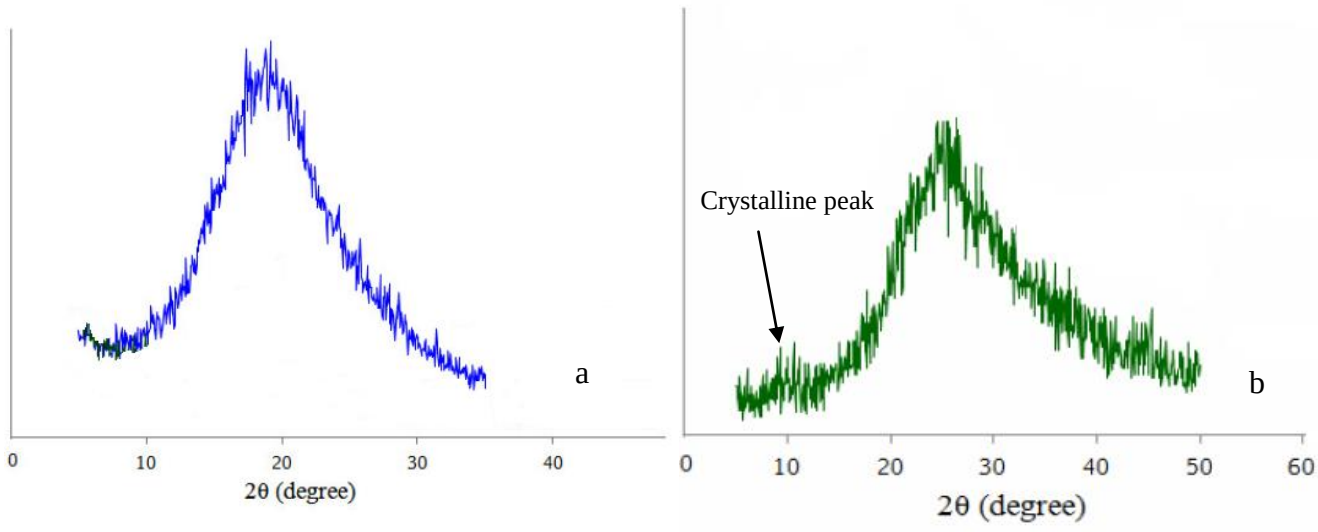

Figure 2.10.: XRPD patterns of undoped (a) and doped (b) PANI.

This indicates that the doping process leads not only to a more compact chain structure but also to enhance crystallinity of PANI.

2.4.4. Effect of molecular weight

It has been demonstrated that the molecular weight of PANI does not affect its electrical conductivity.[136-139] The observed independence of the electrical conductivity on molecular weight is in agreement with the theoretically predicted weak dependence of electronic properties on chain length of PANI.[140, 141] In fact, even though long-range delocalization of an electron cloud due to the formation of a conjugated double bond does not occur until the molecule attains a definite size, at a very high molecular weight imperfections, such as distortions, in the chain symmetry can appear producing a negative effect on the continuous charge delocalization process in a chain. This may lead to a drop in the conductivity.[142-146]

The bulk conductivity (σ_{bulk}) of PANI is the sum of three contributions: *intra*-molecular (σ_{intra}), *inter*-molecular (σ_{inter}) and *inter*-domain (σ_{domain}) conductivity (Equation 2.2.).

$$\sigma_{bulk} = \sigma_{intra} + \sigma_{inter} + \sigma_{domain} \qquad \text{(Eq. 2.2.)}$$

A good *intra*-molecular charge transfer is guaranteed by a well defined band structure of the polymers. Any type of defect in the structure may lead to the reduction in the σ_{intra}.

The σ_{domain} consists of clusters of well organized polymer chains entrapped in a relatively insulating matrix. Also in this case, a well organized structure of polymer chains can increase bulk conductivity.[147]

2.4.5. Conduction mechanism

Conductivity of polyaniline is much more complicated than that of other conducting polymers. In fact, it is the sum of two contributions: the ability of the charge carriers to move along the polymer backbone and the ability of the charge carriers to hop between the polymer chains. This second contribution becomes particularly important when the material is subjected to a force or a pressure.

Although many authors investigated conduction mechanism of PANI, the most complete theory remains that reported by Focke *et al*.[148]

They proposed a speculative mechanism to explain the dependence of conductivity on the protonation level and the moisture content both for *intra* and *inter*-chain carriers transport.

It is generally assumed that for very low values of pH only imine nitrogens are protonated [128] and in this conditions polyaniline can be represented in form partially oxidized and partially protonated.

In the presence of a protic solvent a dynamic proton exchange between protonated and unprotonated sites exists, as confirmed by NMR.[149]

Owing to proton-exchange reactions the defects (barriers) are not fixed in time and space but actually fluctuate in position.

Figures 2.10 and 2.11 show how a protonation/deprotonation cycle may facilitate *intra*-molecular and *inter*-molecular charge transport.

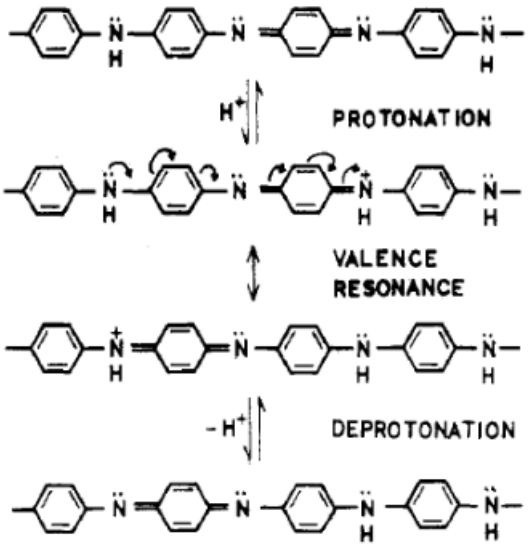

Figure 2.10: Movement of charges along the polymer backbone by proton exchange and valence resonance. Data from Focke *et al*.[148]

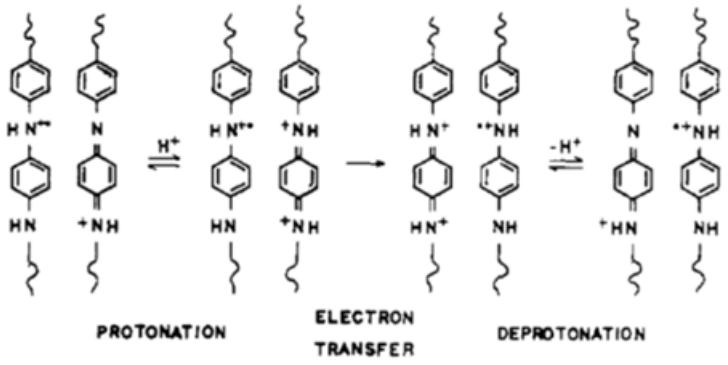

Figure 2.11: *Inter*-molecular charge transfer facilitated by proton-exchange reactions. Data from Focke *et al*.[148]

As shown in the Figure 2.10, *intra*-molecular charge transport implies a translation of imine-quinoidal structures along the polymer backbone. When the polymer is completely unprotonated, none translation is possible. However, when imine nitrogen becomes protonated, translation takes place. The long range translations (a distance of two rings) are possible by valence resonance.

However, any deprotonated imine nitrogen or protonated amine nitrogen will act as a barrier for translation along the polymer backbone. It follows that considerable mobility along the polymer chain is possible on protonation of only one of the imine nitrogens of the quinoidal structures.

Inter-chain transport is different. In fact, a double protonation is required. The first protonation is crucial because it allows the formation of radical cations. For this second type of transport authors proposed a coupling of electronic and ionic transport which increases as the degree of protonation of the imine nitrogens decreases. The dependence of the proton exchange on the presence of a source of protons explains the high increase in conductivity observed when dry PANI is exposed to humidity (Paragraph 2.4.2.). In fact, water molecules may aid in proton transport between chains by formation of hydronium ions.

2.5. Techniques of characterization

Among all techniques that can be used to characterize polyaniline, FT-IR and UV-vis spectroscopies, cyclic voltammetry and conductivity measurements are the most useful.

In fact, since its low solubility in common solvents, techniques as NMR aren't powerful instruments.

2.5.1. FT-IR spectroscopy

FT-IR spectroscopy is probably the most useful technique to characterize polyaniline. One of the most important data that could be obtained, even at a first glance, is the oxidation degree of the polymer. Figures 2.12 (A-C) show characteristic Fourier-transform IR spectra of leucoemeraldine, emeradine and pernigraniline respectively.

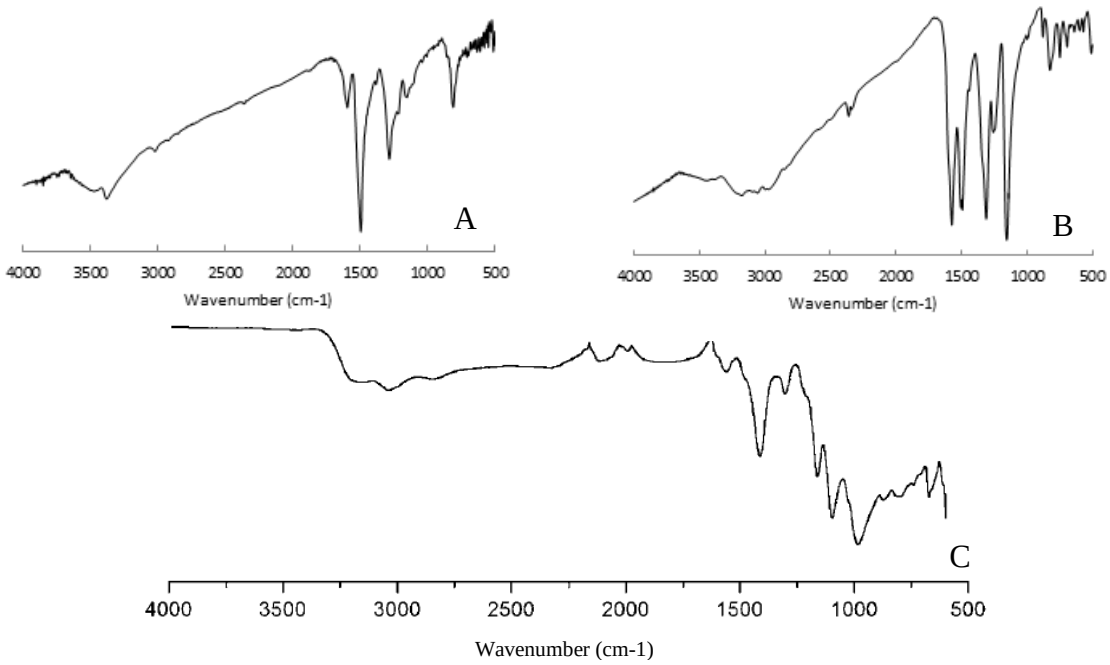

Figure 2.12: FT-IR spectra of leucoemeraldine (A), emeraldine (B) and pernigraniline (C)

The Fourier-transform IR spectrum of emeraldine (Figure 2.12 B) shows a characteristic band at 1570 cm^{-1}, assigned to the C=C stretching of the quinoid rings (N=Q=N) and two peaks at 1498 cm^{-1} and 1484 cm^{-1}, assigned to the C=C stretching vibration mode for the benzenoid rings (N-B-N). The peaks at 1311 cm^{-1} and 1246 cm^{-1} are related to the C-N and C=N stretching modes and those at 1027 cm^{-1} and 889 cm^{-1} to the in-plane and out-of-plane bending of C-N. The peaks at 754 cm^{-1} and 692 cm^{-1} correspond at deformation vibration modes for the aromatic rings, while the peak at 573 cm^{-1} is characteristic for the 1, 4 di-substituted benzene.[150] The ratio between the two bands at 1498 cm^{-1} and 1484 cm^{-1} is diagnostic to estimate the ratio between quinoid and aromatic groups and consequently the oxidation degree of the polymer. In fact, when polyaniline is in its totally reduced form (leucoemeraldine), this ratio is minor than one. In fact, leucoemeraldine is characterized by amino-benzenoid units. In its emeraldine form polyaniline contains about the same amount of amino-benzenoid and imino-quinoid units. For this reason, as reported in the Figure 2.12 B, for polyaniline in its emeraldine form is about 1. When polyaniline is in its totally oxidized form (pernigraniline) only imino-quinoid units are present in the backbone and the ratio is higher than 1.
It is interesting to note the effect of the conjugation of the polymer on the spectrum, i.e. the broad band from 2000 cm^{-1} to 4000 cm^{-1}, that covers half the instrumental range. It arises from the overlapping of many vibrational modes, especially the ones of NH and phenilene diamine groups. Moreover, some of the aminic nitrogen becomes protoned upon addition of an acid, thus becoming vastly hydrogen bonded and thus widening the band at high wavenumbers.[150]

2.5.2. UV-vis spectroscopy

One of the major limitations of conducting polymers, in particular polyaniline and polypyrrole, is that they are characterized by a very low solubility. In particular polyaniline is poorly soluble in a few solvents, as pyrrolidones and amides. A typyical UV-Vis specimen is prepared dissolving a minimal amount of PANI in 2-pyrrolidone or *N*,*N*-dimethylformamide obtaining a blue to green solution. The typical spectrum of polyaniline is reported in Figures 2.3. and 2.13.

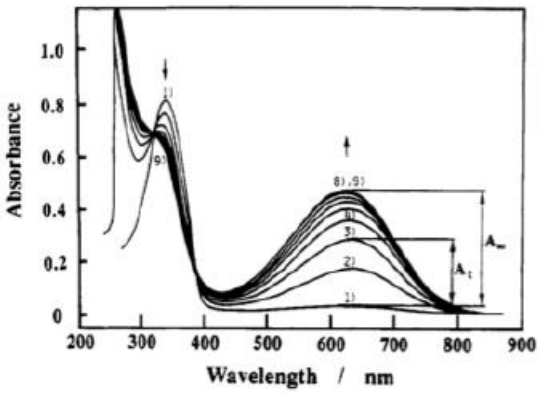

Figure 2.13. Change in the UV-Vis spectrum during the oxidation of leucoemeraldine to emeradine base with oxygen in *N*-methylpyrrolydinone. Data from Kang *et al*., ref. 151.

The band at 320 nm corresponds to the $\pi \rightarrow \pi^*$ transition of the benzenoid rings. The peak at 410 nm corresponds to the polarone-bipolarone transition and the broad peak at 800 nm to the $\pi \rightarrow \pi^*$ transition of the imine-quinoid group. UV-vis spectroscopy allows to investigate how spectrum of polyaniline varies when leucoemeraldine is oxidized to emeraldine (Figure 2.13.). In fact, the peak at 800 nm increases with the oxidation of the polymer.[151] By the use of this technique is possible also to investigate the behaviour leucoemeraldine and emeraldine when an acid as $HClO_4$ is added into the organic solution in air and in N_2. Recording spectra at different times it has been observed that leucoemeraldine and emeraldine in their protonated forms are metastable in *N*-methylpyrrolydinone.

In fact, Figure 2.14a shows that the aminic nitrogen atoms of leucoemeraldine are deprotoned and oxidised by the atmospheric oxygen at the same time, with an increment of the 650 nm band. This does not happen when the specimen is kept under nitrogen. Figure 2.14.c shows how the aminic groups of leucoemeraldine are deprotonated but not oxidised when no oxidant is present. Emeraldine shows a different behaviour. In fact, in air (Figure 2.14.b) PANI undergoes deprotonation without any further oxidation. However, in the absence of any oxidant the oxidation state decreases as the deprotonation goes on.[151]

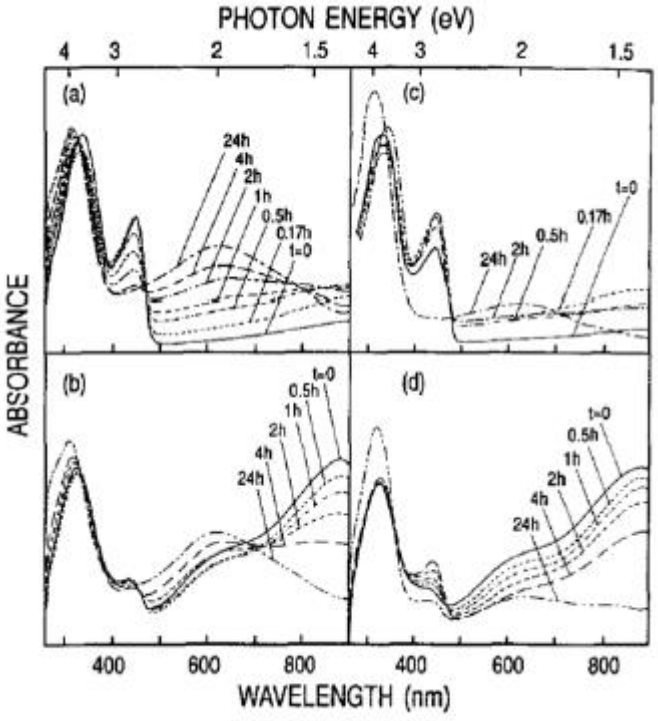

Figure 2.14.: Spectra of leucoemeraldine base in air (a) and in N_2 (c) and emeraldine base in air (b) and in N_2 (d) upon addition of $HClO_4$. Data from ref. 151.

Moreover, by the use of this powerful technique MacDiarmid *et al*. could demonstrate that the oxidation of polyanilines can range anywhere from y = 0 to y = 1, according to the general structure of PANI reported in the Figure 2.15.

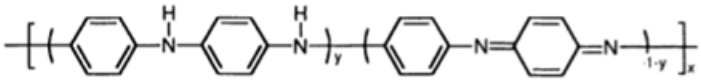

Figure 2.15.: general formula for PANI

In the range from y = 0:5 to y = 1 (from leucoemeraldine to emeraldine form) on a molecular level and in *N*-methyl-2-pyrrolidinone solution only two chromophores are present, characteristic for y = 1 and y = 0:5 species. At the molecular level all intermediate oxidation states consist only of mixtures of these characteristic chromophores.[152, 153]

UV–vis–NIR spectroscopy brings, moreover, clear information on the conformations of the molecules both in the solution and solid state. Although in base-form PANI shows a typical structure coil-like (Figure 2.16 A), into PANI chains the protonation process is accompanied by

creation of positive charges on the nitrogen atoms that, because their repulsions, can cause straightening of the chain (structure rod-like, Figure 2.16 B).

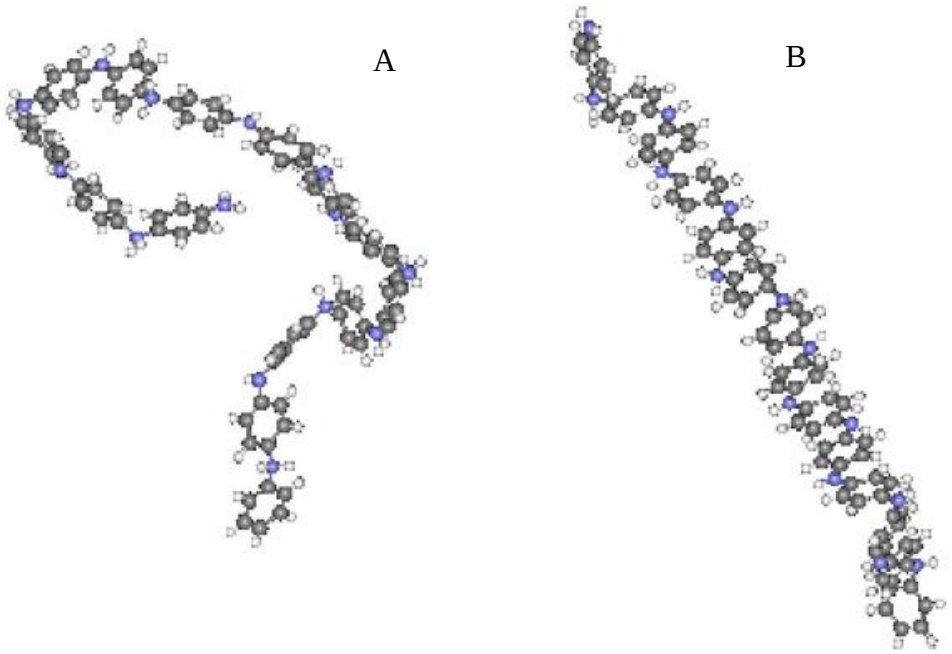

Figure 2.16.: Coil-like (A) and rod-like conformations of PANI. Data from ref. 155.

This is extremely beneficial for delocalization of the electrons (charges) along the chain, and creation energetically most favourable polaronic structure. The polymer conformation can be strongly influenced by a dopant, as well as a solvent used during the sample preparation. For example, bulky anionic dopants cannot quickly diffuse in between the chains following the delocalizing positive charges; in this case the chain expansion will be hindered.[154] Xia *et al*. investigated the effect of solvent in the conformation of PANI-HCSA (camphorsulfonic acid) demonstrating that coil-like conformation is predominant in *m*-cresol, *p*-cresol, 2-chlorophenol, 2-fluorophenol and 3-ethylphenol, whereas rod-like conformation in chloroform, NMP (N-methylpyrolidinone), DMF (*N*, *N*-dimethylformamide), and benzyl alcohol.[155]

The conformation of polyaniline chains can be determined on the basis of its UV–vis–NIR spectra, as reported in the Figure 2.17.

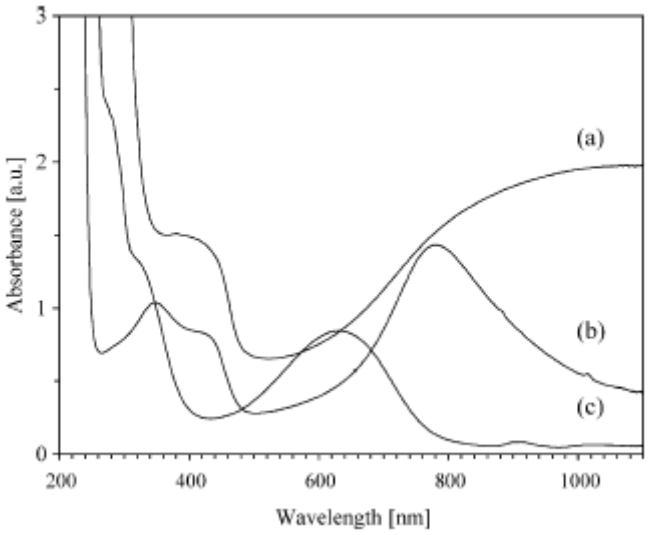

Figure 2.17.: UV-vis spectra of (a) protonated PANI in rod-like conformation and (b) protonated PANI in coil-like conformation and (c) base emeraldine. Data from ref. 154.

The band extending from 800 nm toward the near infrared region, shown in Figure 2.17. a, is called free-carrier tail and is characteristic for PANI in rod-like conformation highly conductive. Otherwise, when protonated PANI is in coil-like conformation this effect disappear (Figure 2.17. b).

2.5.3. XRPD diffraction

X-Ray Powder Diffraction (XRPD) is one of the most important analysis used to investigate the structure of a solid. In fact, several information are contained in an XRPD spectrum. These include: lattice constants, existing of different phases and, through the application of the Scherrer equation (Equation 2.3.), average crystallite size.

$$\tau = \frac{K\lambda}{\beta\cos\theta} \qquad \text{Eq. 2.3.}$$

where τ is the mean size of the ordered (crystalline) domains, K is a dimensionless shape factor, with a value close to unity. The shape factor has a typical value of about 0.9, but varies with the actual shape of the crystallite; λ is the X-ray wavelength, β is the line broadening at half the maximum intensity (FWHM) in radians and θ is the Bragg angle.

In the last thirty years the intense study of many researchers clarified the structure of polyaniline.[156-158] However, the structural characteristics were investigated more in detail by Pouget *et al*. [159, 160] They reported two distinct classes of emeraldine characterized by two different structures.

For this kind of investigation emeraldine was prepared by two different methods. Class I meraldine was prepared by chemical synthesis or by electrochemical deposition obtaining ES-I in powder or film form respectively. These materials were converted in emeraldine base (EB-I) in alkaline conditions. By another approach EB in powder form was dissolved in *N*-methyl-2-pyrrolidone (NMP) and then directly casted on substrates producing EB-II films. Alternatively, EB-I could be converted to EB-II by washing with tetrahydrofurane (THF), then with NMP, and then vacuum dried. Protonation was accomplished through treatment with aqueous HCl of pH varying from 4 to 0. As reported in the Figure 2. 18., ES-I a new crystalline structure appears, which grows in intensity with lattice parameters varying as the protonation level is increased.

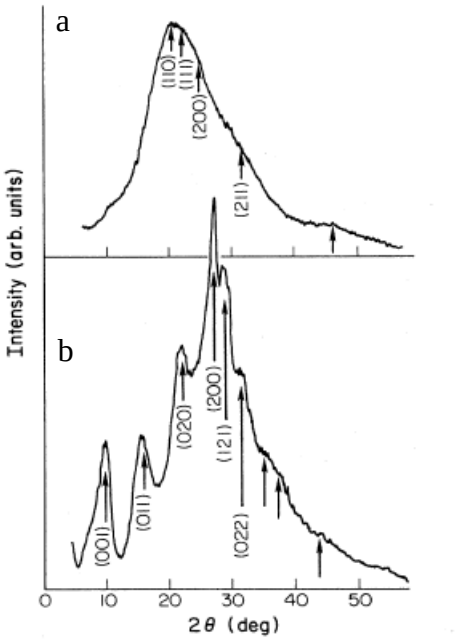

Figure 2.18.:XRPD patterns of emeraldine base (EB-I, a), and emeraldine salt (ES-I, b). Data from ref. 160.

Class I emeraldine is that for which the base form is essentially amorphous EB-I and the HCl salt exhibits ES-I structure. In general, class I materials form when the polymer is obtained from solution in protonated form.

In Figure 2.19. is reported the increase in crystallinity from EB-I to ES-I upon gradual protonation.

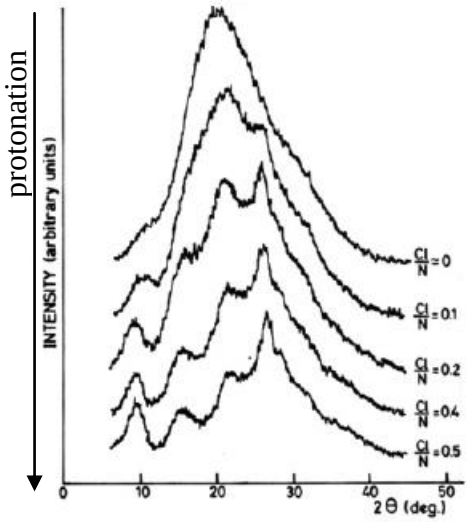

Figure 2.19.: XRPD spectra of PANI increasing the protonation level from EB-I to ES-I. Data from ref. 159.

EB-I is characterized by an amorphous structure. The d spacings measured from ES-I "low-temperature" powder are reported in Table 2.1. and the evolution of some d spacings with the [Cl]/[N] ratio is shown on Figure 2.19.

d, Å	*L*, Å	intensity	(*hkl*)[a]
9.57	45	s	(001)
5.94	35	s	(010)
4.26	35	s	(100)
3.51	70	vs	|(110)|
3.28	45	m	|(111)|
2.98	30	w	(020)
2.85		vw	|(112)|, |(021)|
2.47		w	|(120)|
2.34		vw	|(121)|, |(113)|
~2.10		vw and v broad	
~1.72		vw and v broad	

Table 2.1.: Emeraldine "Low-Temperature" HCl salt ES-I ([Cl]/[N] ~ 0.5): d= Spacing, L= Domain Length and hkl= Pseudoorthorhombic Indexation. Data from ref. 159.

Comparing Figure 2.18. with 2.20., a markedly different diffraction pattern for EB-II is shown.

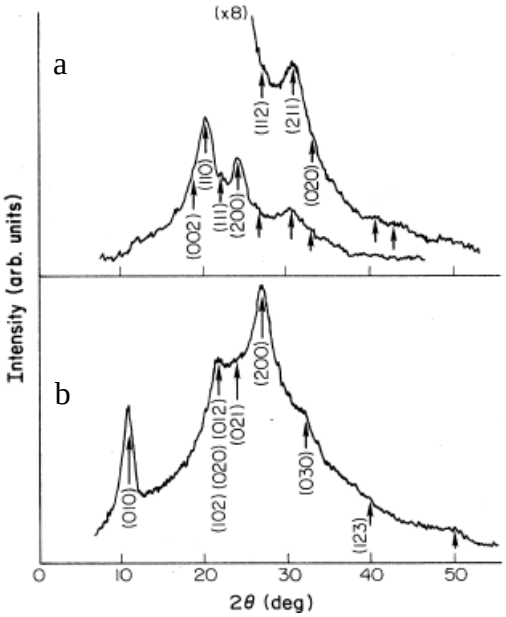

Figure 2.20.: XRPD patterns of emeraldine base (EB-II, a), and emeraldine salt (ES-II, b). Data from ref. 160.

Class II emeraldine is that for which the base exhibits partially crystalline EB-II structure and the HCl salt the ES-II structure. The d spacings of the Bragg reflections observed from EB-I1 X-ray diffraction patterns are compatible with an orthorhombic lattice symmetry. Table 2.2. presents an indexation of the reflections of longest d spacing for this lattice symmetry.

emeraldine base powder								
part insoluble in THF (from Figure 9b)	part soluble in THF (from Figure 9a)		THF/NMP-extracted powder (from Figure 8a)		NMP-cast stretched film (from Figure 7A)			
d, Å	*d*, Å	*L*, Å	*d*, Å	*L*, Å	*d*, Å	*L*, Å	intensity	(*hkl*)
					5.00	150	w	(002)
~4.57	4.56	100	4.57	50	4.60		vs	(110)
~4.25			4.20		4.27		vw	(111)
~3.82	3.83	100	3.82	50	3.91	50	s	(200)
~3.57	3.41		3.41				vw	(112)
~3.03	3.02	70	3.03	35	3.06		m	(211)
	2.82		~2.84		2.88		w	(020)
	~2.70		2.62				vw	(212)
	~2.48						vw	(121)
	2.33		~2.32				w	(213), (310)
~2.14	2.19		~2.21				w	(114), (221)
	1.95		~1.90				w	(024)
	1.84		~1.85				w	(321), (115), (130)

Table 2.2.: Emeraldine Base EB-11: d= Spacing, L=Domain Length, Intensity and bkl= Indexation. Data from ref. 159.

A schematic drawing of the EB-II structure in accord with the orthorhombic symmetry elements is reported in the Figure 2.21.

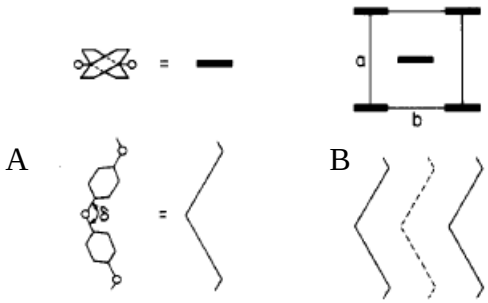

Figure 2.21.: Projection along the chain axis and side view of the average structure of (A) the polyaniline chain and (B) EB-II. The dashed line represents a chain *a/2* below or above the plane of the paper. Data from ref. 159.

Figure 2.22.shows a schematic drawing of the ES-II structure.

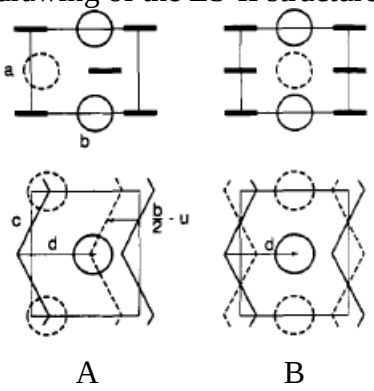

Figure 2.22.: Projection along the chain axis and side view of the two orthorhombic structures considered for ES-II. Data from ref. 159.

According to the data reported in the Table 2.1., Figure 2.23 shows a schematic drawing of ES-I structure.

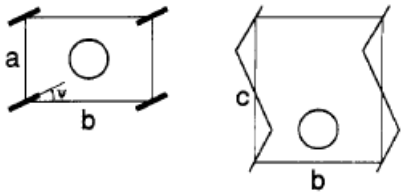

Figure 2.23.: Projection along the chain axis and side view of ES-I. Data from ref. 159.

All these differences in structure have subtle effects on the electronic properties of doped polyaniline. Judging by the similarity of the Debye-Schemer patterns, polyaniline prepared as salt and redoped with other anions such as ClO_4^- or HSO_4^- adopts structures similar to the ES-I structure. Authors noted also that the details of the crystal structure are dependent upon counterion used during the process of protonation.

2.5.4. Cyclic voltammetry

Figure 2.24. shows typical cyclic voltammograms (CVs) of PANI/$HClO_4$ films, recorded at different sweep rate (from 10 to 200 mV s^{-1}), in an aqueous solution of $HClO_4$ 1 M.[161]

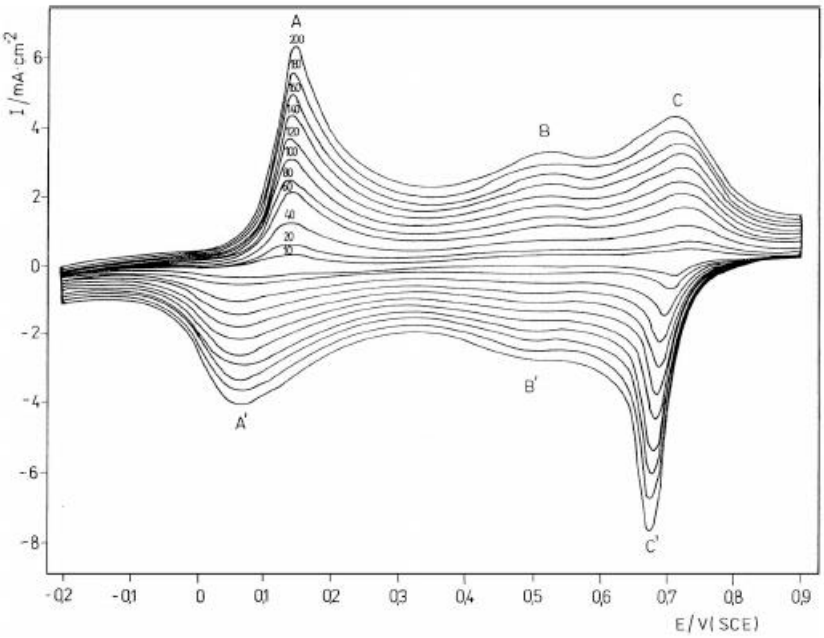

Figure 2.24.: Cyclic voltammograms of PANI-$HClO_4$ film, recorded at different sweep rate (from 10 to 200 mV s−1), in an aqueous solution of $HClO_4$ 1 M. Data from ref. 161.

There are three redox pairs, with oxidation peaks at 0.125 V (A), 0.5 V (B) and 0.7 V/SCE (C). For the first redox pair AA', the increase of the sweep rate does not influence the position of the two peak potentials. Instead, for the third redox pair CC', the anodic and cathodic peak potential are shifted towards lower potential, by increasing the sweep rate. Also, the peak potential separation increases from 30 mV (*V* D10 mV s^{-1}) up to 40 mV (*V* D200 mV s^{-1}). The second redox pair BB' is almost undistinguishable at low sweep rate (*V* D10 mV s^{-1}), but gradually increases with it. According to the literature, the oxidation peaks A and C correspond to the changes in the oxidation state of the PANI films. Snauwaert *et al.*[162] have evidenced, by X-ray photoelectron spectroscopy, that the ratio between the amine and imine content is function of the electrochemical potential. At 0.15 V/SCE the imine concentration is about 25% (protoemeraldine) and gradually increases to 50% (emeraldine) at 0.6 V/SCE and then up to 80% (nigraniline) at 0.8 V/SCE. The amine concentration is higher at low potential (75% at 0.15 V/SCE) and decreases to 20%, at 0.8 V/SCE.

So, the first peak A corresponds to the first step of oxidation of neutral PANI, and the third peak C

corresponds to the further oxidation of PANI, from emeraldine to nigraniline. The middle pairBB0 has been attributed either to the presence of ortho-coupled polymers [163] or to the degradation of PANI (soluble species such as benzoquinone and hydroquinone).[164]

In Figure 2.25. are shown voltammograms of PANI in 1 M trichloroacetic acid, recorded at different sweep rates, from 10 to 200 mV s^{-1}.

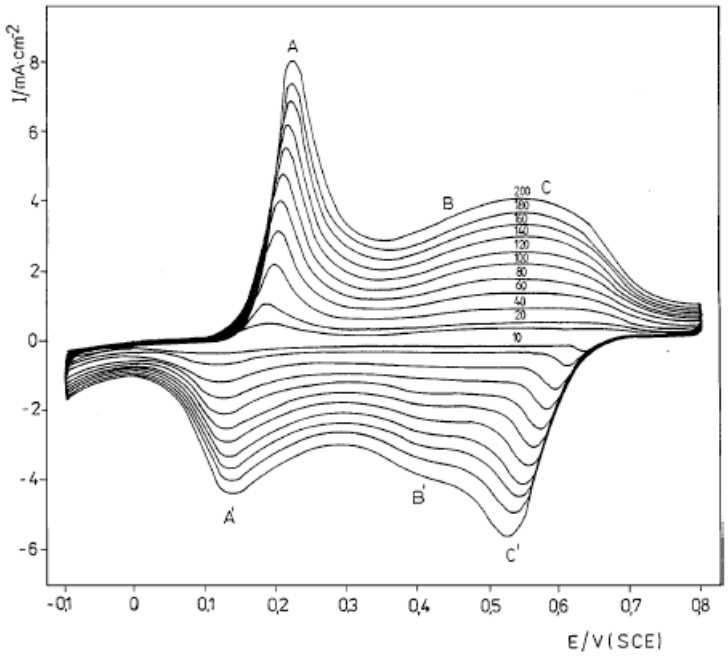

Figure 2.25.: Cyclic voltammograms of PANI-$C_2HCl_3O_2$ film, recorded at different sweep rate (from 10 to 200 mV s^{-1}), in an aqueous solution of $C_2HCl_3O_2$ 1 M. Data from ref. 161.

The first oxidation peak (A) appears at about 0.18 V/SCE and the third oxidation peak (C) appears at about 0.55 V/SCE. The middle peak B is not distinct on the oxidation wave, only on the reduction wave (B'). For the first redox pairAA0, the increase of the sweep rate shifts the position of the two peak potentials towards higher potentials. The third redox pair CC' is characterized by a constant value for the anodic peak potential and by a gradually shift of the cathodic peak potential towards lower potentials, with the sweep rate. The third peak C exhibits a very broad oxidation wave comparing with the first peak, A. This indicates that the charge transfer takes place more difficult for the second step of oxidation of PANI than for the first step of oxidation.

Figure 2.26. shows CVs of PANI in chloroacetic acid 1M, recorded at different sweep rates.

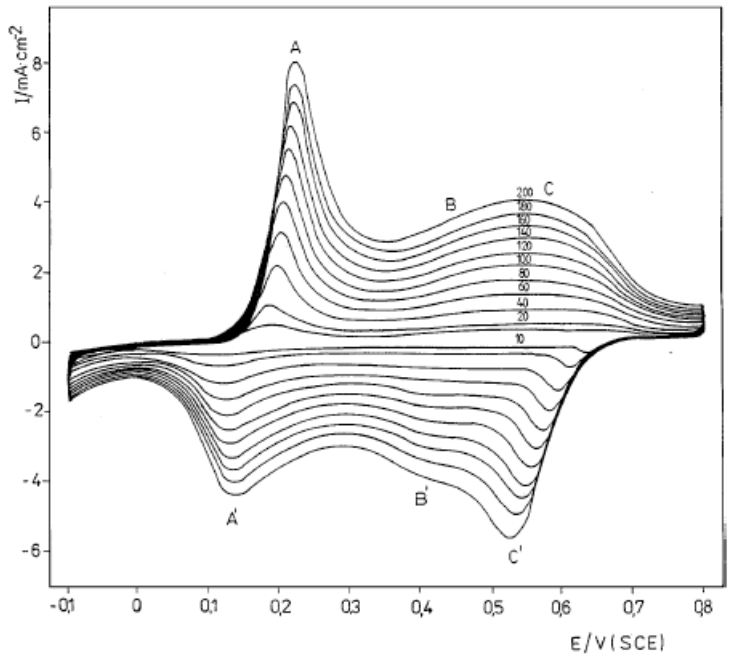

Figure 2.26.: Cyclic voltammograms of PANI-$C_2HCl_3O_2$ film, recorded at different sweep rate (from 10 to 200 mV s^{-1}), in an aqueous solution of $C_2HCl_3O_2$ 1 M. Data from ref. 161.

All voltammograms are characterized by a single redox pair AA', with broad anodic and cathodic waves. The anodic peak potentials shifts towards higher potentials while the cathodic peak potentials shifts towards lower potentials, with the sweep rate.

From the cyclic voltammograms represented in Figures 2.24–6 it is possible to observe that the oxidation and reduction potentials are different for each dopant acid. This fact was attributed to the electrostatic interaction of the dopant with the chemically flexible -NH- group of the polymer.[165]

The kinetic of the electron transfer process depends on the exchange current density ($I0$) and the anodic and cathodic transfer coefficients (αA, αC). The values of these parameters can be obtained from Tafel Equations 2.4. and 2.5.: [166]

$$\log(I) = \log(I_0) + \frac{\alpha_A n F}{2.3 n F}(E - E_e) \quad \text{anodic process} \qquad \text{Eq. 2.4.}$$

$$\log(-I) = \log(I_0) - \frac{\alpha_C n F}{2.3 R T}(E - E_e) \quad \text{cathodic process} \qquad \text{Eq. 2.5.}$$

where $E - E_e$ is the overpotential and n is the number of electrons involved in the redox process, in our case n =1.

The Tafel approximation is generally used for $|E - E_e| \geq 100/n$ mV. The exchange current density's

value, I_0, is obtained from the intercept of log|I| versus $E - E_e$ plots, while the values of α_A, α_C are obtained from the slopes of these plots. Tafel curves for PANI/$HClO_4$ films are shown in Figure 2.27.

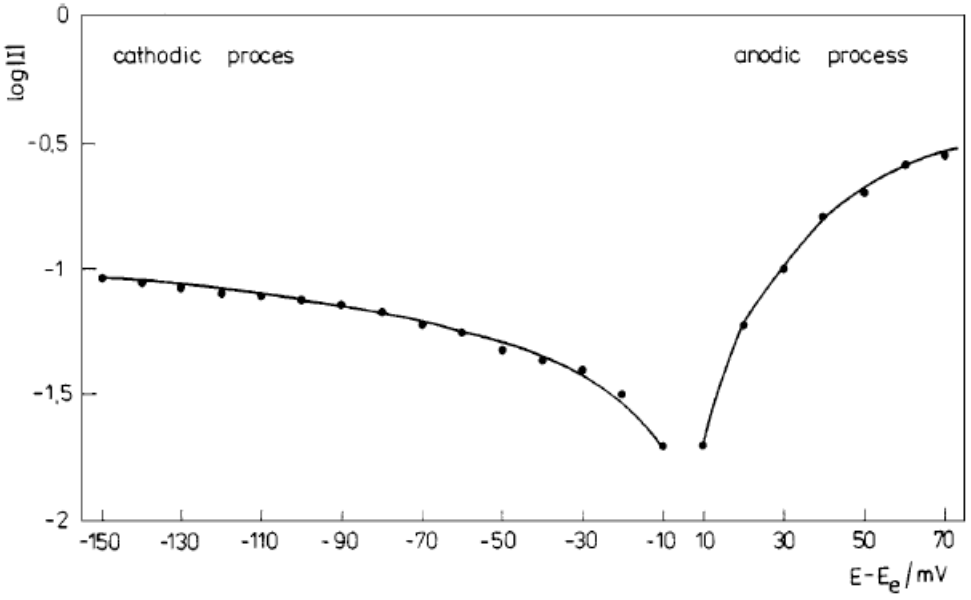

Figure 2.27.: Tafel curves for PANI/$HClO_4$ film. Data from ref. 161.

Pruneau *et al*. observed that for the anodic process, Tafel plot rises abruptly and then reaches a plateau (in the range of 60 mV to 80 mV/SCE). This fact indicates that the first step of oxidation of PANI is very fast and takes place very close to the equilibrium potential ($|E - E_e|$=60 mV). For the cathodic process, Tafel plot rises slowly and also reaches a plateau (for $|E - E_e|$>80 mV).

Since Tafel equations apply for $|E - E_e| \geq 100/n$ mV, Pruneau *et al*. determined the kinetic parameters for the cathodic process (Table 2.3.).[161]

Sample	I_0 (mA/cm^2)	α_C
PANI-$HClO_4$	0.048	0.09
PANI-$C_2H_3ClO_2$	0.036	0.1
PANI-$C_2HCl_3O_2$	0.03	0.29

Table 2.3.: Kinetic parameters derived from Tafel equations, for PANI films prepared with various acids. Data from ref. 161.

Tafel curves for PANI/$C_2HCl_3O_2$ films are represented in Figure 2.28.

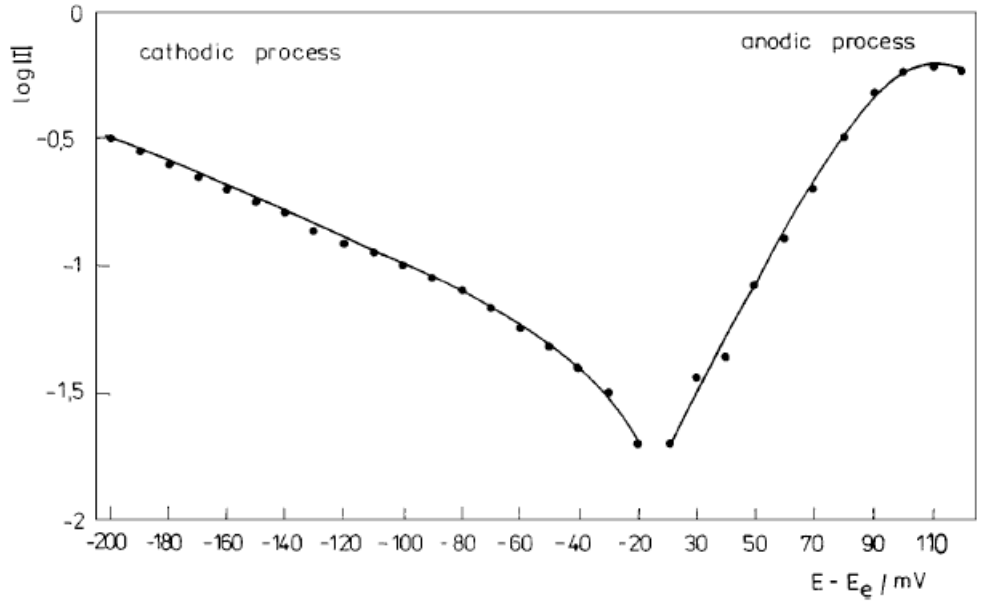

Figure 2.28.: Tafel curves for PANI/$C_2HCl_3O_2$ film. Data from ref. 161.

They are similar with those show in Figure 2.27., for PANI/$HClO_4$. The anodic plot rises abruptly (in the range of 20 to 90 mV/SCE) while the cathodic plot rises slowly. So, the first step of oxidation of PANI/$C_2HCl_3O_2$ also takes place very quickly. The kinetic parameters obtained for the cathodic process are listed in Table 2.3.

Tafel curves for PANI/$C_2H_3ClO_2$ (Figure 2.29.) are different comparing with those represented in Figures 2.27. and 2.28.

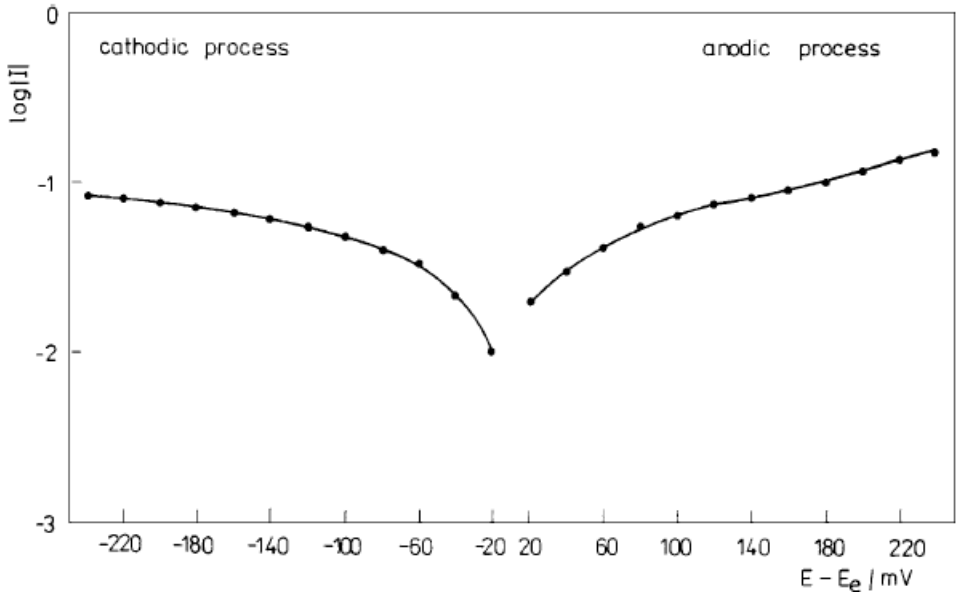

Figure 2.29.: Tafel curves for PANI/$C_2H_3ClO_2$ film. Data from ref. 161.

Both the anodic and cathodic plots rise slowly and reach a plateau, for $|E - E_e|$>80 mV. In Table 2.3. are listed the values of the kinetic parameters I_0, α_C for PANI films prepared with three different acids: perchloric, $HClO_4$, trichloroacetic, $C_2HCl_3O_2$ and chloroacetic, $C_2H_3ClO_2$.

The highest value of I_0 was obtained for PANI/$HClO_4$ and the lowest value for PANI/$C_2HCl_3O_2$. Since the cation was the same for all the electrolytes used (H^+), these differences arise from the different structure and molecular weight of the anions. The higher the molecular weight of the anions, the smaller the value of I_0.[161]

2.5.5. Conductivity measurements

Conductivity is usually measured on compressed powder or films. The two most important techniques are the two-points probe and the four-points probe. In the first one a potential and a current are measured between the two probes. The resistance is thus easily calculated. As resistivity, or its reciprocal conductivity, is an important parameter, as it does not depend on the geometrical shape of the sample, the two probe conductivity measurement is useful only when area and thickness can be measured.

The four-points probe measurement is more accurate when the sample is irregular, and its results is a resistivity. This means that the measurement does not depend on the shape of the sample. It is mostly used to measure film resistivity. The principle on which it is based is the Kelvin bridge. Basically, the two outer probes force a current passing into the sample and the inner ones measure a potential. Resistivity could be obtained using the following equations (Equation 2.6. and 2.7.).

$$\rho(\Omega * cm) = \frac{2\pi sV}{I} \qquad \text{Eq. 2.6.}$$

They can be used when the instrument has the four probes equally spaced.

Where s=distance between the sensing points, V=potential, I=current. When the thickness t is much bigger than the distance between the sensing points s.

$$\rho(\Omega * cm) = \frac{\pi tV}{ln2I} \qquad \text{Eq. 2.7.}$$

When the thickness t is much smaller than the distance between the sensing points s, i.e. in films.

Chapter 3: One dimensional polyaniline

3.1. Importance of one-dimensional polyaniline

The possibility to dispose of one-dimensional nanostructured polyaniline (1D nano-PANI) improved significantly its performances in many fields, i. e. gas sensing. The great interest is confirmed by the growing numbers of publications in this area (Figure 3.1.)

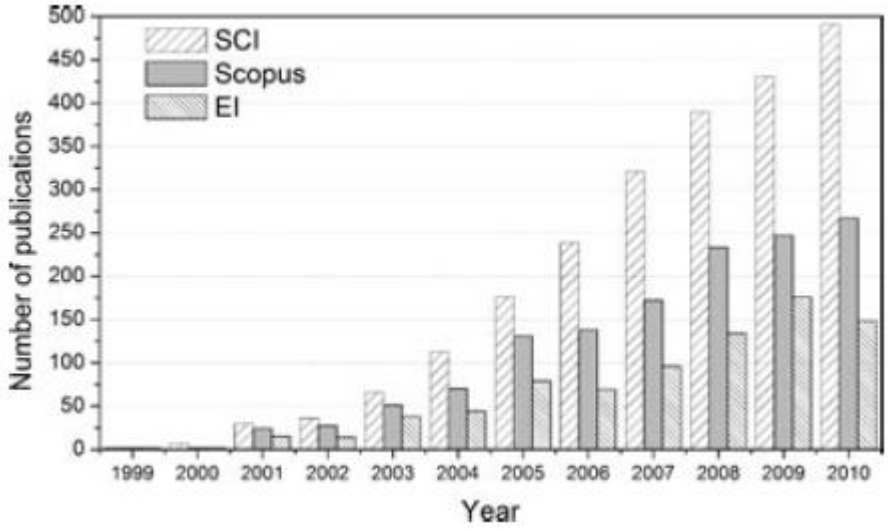

Figure 3. 1.: Results of a research realized in Jan. 6, 2012 from Web of Science, Scopus, and Engineering Village using as key words: polyaniline, nanofiber, nanowire, nanobelt, nanotube, nanorod, nanoneedle, nanostick. Data from ref. 42.

Concerning 1D nano-PANI, research works can be roughly split into the following four aspects: investigating new and efficient methods for their production, especially new template-free procedures, and clarifying the mechanism of the nanostructures formation, improving the quality of the nanostructures, finding new properties and their applications.

3.2. Synthetic methods

The simplest methods to prepare 1D nano-PANI are physical routes, such as electrospinning [167-170] and mechanical stretching,[171] and the doping induced solution route.[172] Also for 1D nanostructured-PANI the main syntheses can be categorized into chemical and electrochemical oxidative approaches, just as that occurred for the synthesis of the conventional PANI powders. This approaches can be further split into template and template-free methods. The former is subdivided into hard template (physical template [173]) synthesis and soft template (chemical template [173]) synthesis approach according to the solubility of the templates in the reacting media, while the latter is subdivided into interfacial polymerization,[32, 174] radiolytic synthesis,

[175] rapid mixing reaction method,[176] and sonochemical synthesis.[118, 119] Here the main synthetic approaches will be discussed: hard template synthesis, soft template synthesis, combined soft and hard template synthesis and no-template synthesis.

3.2.1. Hard template synthesis

Martin *et al*. proposed for the first time the hard template synthesis to prepare conducting organic polymers, such as polyaniline and polypyrrole.[177-181] 1D nanostructured-materials with controllable diameter, length and orientation can be synthesized in the pores, channels of hard templates such as membranes,[179-181] zeolites,[182] anodic aluminum oxide (AAO),[183–185] and so on. Hexagonal channels of mesoporous aluminosilicate can be used as templates to prepare PANI filaments with diameters of 3 nm.[182] Although this technique is attracting and elegant, the removal of the template at the end of the reaction is the biggest drawback. In fact, it is tedious and can compromise th morphology of the product. Typically, the polymerization reaction takes place in the channels of template after addition of stoichiometric oxidants at a mixture of monomer and template. However, in addition to the chemical oxidative polymerization, PANI nanofibers, nanotubules and nanoribbons can be also prepared by electrochemical oxidative polymerization using PTM (track-etched membrane),[186] AAO [184] and nanochannels [187] as hard templates.
Using this technique Cao *et al*. prepared PANI nanotubules encapsulated nickel nanowires using alumina membrane as the hard-template.[188]

3.2.2. Soft template synthesis

The soft template synthesis method, always called the template-free method [189–192] or self-assembly method [193] in the literatures in that no hard templates is used, entails synthesizing PANI, as well as polypyrrole,[190,194] in the presence of structure-directing molecules such as surfactants,[195, 196] deoxyribonucleic acid (DNA),[197,198] polyelectrolytes,[199] thiolated cyclodextrins,[200] sulfonated porphyrin,[201] liquid crystalline,[202] and ethanol,[203, 204] which act as templates for the production of one-dimensional nanomaterials. The surfactants are often complex acids with bulky side groups, such as the naphthalenesulfonic acid (NSA),[191, 205, 206] camphorsulfonic acid (CSA),[207-210] azobenzenesulfonic acid (ABSA),[211] chiral 2-pyrrolidone-5-carboxylic acid (PCA),[212] 4-(3-(4-((4-nitrophenyl)azo)phenyloxy)propyl)aminobenzene sulfonic acid (C3-ABSA),[213] 2-acrylamido-2-methyl-1-propanesulfonic acid (AMPSA),[214] 5-aminonaphthalene-2-sulfonic acid (ANSA),[192] etc. The polyelectrolytes include poly(acrylic acid), poly(styrenesulphonic acid), etc.[199, 215] Compared to the hard template method, this approach is simpler and cheaper because the use of soft

templates omits the tedious post-synthesis process. The formation of the one-dimensional nano-structured PANI depended on the reaction conditions, such as the concentration of aniline, the molar ratio of aniline to oxidant or the soft template. Hypotheses were proposed for the formation mechanisms of the nanostructures, although not confirmed. Because of the hydrophobic property of aniline and the hydrophilic property of the surfactants, the latter form nano- or microstructured precursors by self-assembling processes.[205, 211, 216, 217] The precursors play a template role in forming of the 1D nano-PANI.[185, 189, 193, 218, 219] The diameters and lengths of the one-dimensional nano-structured polymer are strictly related to many factors, such as the soft templates, molar ratio of surfactant to aniline, reacting temperature and time and other synthetic conditions.

3.2.3. Combined soft and hard template synthesis

Qiu et al. proposed a new technique that combines soft and hard template to produce highly oriented PANI nanostructures.[213] Typically, aniline and a surfactant (soft template) are dissolved in deionized water to form a homogenous emulsion and ultrasonicated. Afterwards the hard template is added in the emulsion and ultrasonicated for another while. Then, a stoichiometric oxidant is added rapidly into the solution and the polymerization takes place.

By the use of this technique well-oriented PANI nanotubes and nanofibers are produced within the pores of the hard template. In the absence of templates, both soft and hard, neither nanofibers nor nanotubes are obtained. This indicates that both the soft and hard template affected the formation of the nanofibers or nanotubes.

3.2.4. No-template synthesis

This method allows to synthesize one-dimensional nano-structured PANI without any templates, hard or soft. Interfacial polymerization, radiolytic synthesis, rapid mixing reaction, sonochemical synthesis, electrochemical approach are good examples of no-template synthesis of 1D nano-PANI.

Interfacial polymerization, sonochemical synthesis and electrochemical approach were already discussed in the paragraph 2.3.3.2., 2.3.3.5. and 2.3.2. respectively. Below radiolytic synthesis and rapid mixing reaction will be treated in more detail.

3.2.4.1. Radiolytic synthesis

In this method, an acidic aqueous solution of aniline and a stoichiometric oxidant is irradiated with gamma rays without any template.[175] Setting accurately some parameters, such as concentration of reagents, is possible to produce nanofibers or rod-like structures. Although no complete explanation for the formation mechanism of the nanofibers was provided up to date, however, the

authors concluded that PANI self-assembled when the polymerization is carried out with gamma irradiation. PANI nanofibers decorated with metal nanoparticles were also prepared with the same gamma irradiation procedure.[175] At the same time, thin films of PANI nanofibers were synthesized by the same group by ultraviolet irradiation of a spin coated mixture of aniline nitric acid and APS on the surface of a siliconwafer.[220] The nanofibers demonstrate typical diameters of 20–150 nm and lengths of microns.

3.2.4.2. Rapid mixing reaction

Mixing rapidly aniline with a solution of a stoichiometric oxidant, rather than the conventional slow addition of the solution of oxidant to that of aniline, PANI nanofibers with comparable shapes and sizes to those of interfacial polymerization method are obtained, rendering this method the simplest one in producing PANI nanofibers.[176] Owing to the even distribution of aniline and APS molecules in the solution, all the initiator molecules were consumed rapidly after the start of the polymerization and the secondary growth of PANI was suppressed, resulting in exclusive nanofibers in the product. The growth of the PANI nanofibers was related with the polarity of the solvents.

For example, in aqueous systems, pure nanofibers were produced, while in ethanol and isopropanol, mixture of short nanofibers attached with irregular particles and agglomerates of 100–300 nm particulates were obtained, respectively. However, according to Zhang *et al*., [193] the formation of nano-structured PANI, which was synthesized in presence of H_3PO_4 without any other template, soft or hard, was expected to originate from the micelles formed by anilinium cations, which acted as the templates in forming the nanostructures. Chiou and Epstein [221, 222] prepared PANI nanofibers by dilute polymerization, in which a small portion of acid solution containing aniline was carefully transferred to the solution of APS in acid and then leave the mixture to react without any disturbance. The diameters of the fibers can be roughly tuned by appropriate selection of the acids. The formation of the nanofibers was, as explained, owing to the reduced numbers of nucleation sites on the surface of the nanofibers in a dilute condition, which allowed PANI to grow directionally, differing from that of the competition between the directional growth and the formation of additional nucleation centers in the case of high aniline concentration, which resulted irregular PANI product.

3.3. Properties

Conductivity measurement of the hard-template synthesized PANI nanotubules [186, 223] showed that the conductivities decreased with the increasing of the diameters, and finally reaches the

conductivity of the conventional PANI powder. This was resulted from the decreasing proportion of the highly ordered layer in the materials with increasing of diameters and from the higher conductivity of the highly ordered layer than that of the disordered inner part of the fibers/tubes.[224] The analogous conductivity decrease was also observed for electrochemically template-synthesized PANI nanoribbons.[187]

The four-probe conductivity of the PANI pellet consisting of both granular particles and nanofibers,[109] or the PANI nanofibers pellet [225, 196, 226] was similar to their counterpart synthesized by the conventional procedure, and was affected by the doping acid and doping degree, and so on. The directly measured electrical conductivity of a single PANI nanotube, which was synthesized by the soft template method, is *ca*.30 S/cm,[208, 209] far more higher than the 10^{-2} S/cm order of magnitude [208, 209, 211] for the nanotube pellet due to the large intertubular contact resistance.[208, 209] Brunauer–Emmett–Teller (BET) surface area of the PANI nanofibers decreased with increasing of the fiber diameters.[33] For example, BET surface area of dedoped PANI nanofibers with diameters of 30, 50, and 120 nm are 54.6, 49.3, and 37.2 m^2/g, respectively. In addition, the BET surface area of doped PANI nanofibers was lower than that of the dedoped ones, which is in consistent with the results of the conventional PANI.

Chapter 4: Composite materials

4.1. PANI/insulating polymers

Blends of conducting polymers with conventional insulating polymers have received great attention over the last decade, especially in form of nanofibers and nanowires, because of their unique and useful properties, which are important for several potential applications such as electronic devices in optics and electronic and biomedical materials,[227-229] protective clothing,[230] filtration media,[231] charge storage devices,[232-233] and sensors and actuators.[234-236] PANI blended with some polymers have been employed for this purpose, including poly(ethylene oxide),[237] nylon-6,[238] polystyrene[235, 239] and polylactic acid (PLA).[240] In particular PLA and its copolymers are biodegradable and biocompatible, present good thermoplastic processability, and have potential applications as commodity plastics to be used in agricultural products and disposable materials.[241] Because of its biocompatibility, PLA is often used as the base material for implant devices, such as suture fibers and scaffolds for tissue engineering.[242] Recently, it has been employed in nanofiber preparation with the electrospinning technique.[243–245] Therefore, PLA is a promising candidate for the preparation of conducting nanofibers in combination with PANI for sensors and other applications.

4.1.1. Techniques of preparation of PANI blends

Although PANI blends are particularly attracting materials, the choice of the best method to produce them with specified characteristics remains an unresolved problem. The problem arises because the processing method may significantly determine the properties of the manufactured composite materials. All the synthetic methodologies can be essentially reduced to two distinct groups: synthetic methods based on aniline polymerization in the presence of or inside a matrix polymer, and blending methods to mix a previously prepared PANI with a matrix polymer. Roughly, synthetic methods include: dispersion polymerization of aniline in the presence of a matrix polymer in a disperse or continuous phase of a dispersion, chemical in situ polymerization of aniline in a matrix or in a solution with a matrix polymer, electrochemical polymerization of aniline in a matrix covering an anode, polymer grafting to a PANI surface, copolymerization of aniline with other monomers resulting in the formation of soluble aniline copolymers, which can be considered as a composite polymer. Blending methods consist of: solution blending soluble matrix polymers and substituted polyanilines, solution blending soluble matrix polymers and PANI doped by functionalized protonic acids (counterion-induced processability), solution blending undoped PANI with polymers soluble in amide or acidic solvents, dry blending followed by melt processing (MP) (mechanical mixing of doped PANI with thermoplastic polymer, then molded in a hot press or extruder).

Naturally, each of these methods has its own advantages and limitations. Specifically, the synthetic direction is probably preferable if it is necessary to produce inexpensive conducting composites, due to use of inexpensive aniline instead of more expensive PANI, or when there is a need to form composites which have conductivity only in a thin surface layer. Good homogeneity and a low percolation threshold characterize these composites. On the other hand, blending methods sometimes seem to be more technologically desirable from the standpoint of large scale production, particularly in the case of melt processing techniques. Blending methods will probably become very practicable when techniques to produce inexpensive, nanosized PANI will be well developed.

4.1.1.1. Synthetic methods to prepare PANI blends and composites

PANI composites can be produced by polymerization of aniline in dispersion systems. This kind of synthesis is carried out at low temperature by the use of a stoichiometric oxidant in the presence of water soluble polymers (used as a surfactant) or tailor-made reactive copolymers,[246] such as poly(2-vinylpyridine-co-p-aminostyrene),[247] PVA,[248, 249], poly(N-vinylpyrrolidone),[250, 251] PEO,[252] cellulose derivatives,[253, 254] poly(methylvinylether),[255] etc.

Other methods of chemical polymerization of aniline exist that are carried out in the presence of polymer matrix which does not demand the presence of surfactants in the reaction mixture.

All these methods can differ for many aspects. For example, aniline can be polymerized at lower temperatures (0–10°C), but changing the sequence of the addition of reagents to the reaction mixture. In fact, in some cases aniline is added to an acidified solution of a matrix polymer (PVA, chlorinated copolymer latex Haloflex) and oxidant APS, followed by precipitation and filtration of a conducting composite [256, 257]. In another sequence, an acidified solution of the oxidant can be added to a previously cooled solution of aniline and polymers. In particular, Gangopadhyay *et al*.[258] and Stejskal *et al*.[251] used the last approach to prepare a PANI/PVA composite that exhibits significant EMI shielding capacity, and potential for sensing moisture and methanol vapor [258, 259].

Polyaniline can be produced also by chemical aniline polymerization in/on solid polymer matrix. Unlike aniline polymerization in a solution, this method produces modified polymer matrixes with a PANI layer at their surface or inside a thin subsurface layer. Naturally, the thickness and conductivity of the layers depend on the method of modification and on the time of contact of the solid matrix with the reaction medium. These methods produce composites with a wide surface conductivity range, from semiconductor up to the conductivity of pure PANI.

Apparently, this method is not technological suitable for sheet materials, both because it requires the use of polymer matrixes with a good adhesion to PANI, and because it produces pure PANI at the matrix surface, having poor mechanical properties. At the same time, for fiber and textile materials with a well developed reactive surface, it may lead to the production of conducting fibers and fabrics with grafted PANI at the surface and inside of pores. This approach resulted in suitable materials for EMI shielding, sensors, static electricity dissipation, etc.[260-262].

Two methods to obtain electrically conductive fabrics by in situ polymerization of aniline were compared by Oh *et al*.[263]. These materials were prepared by immersing the Nylon 6 fabrics in pure aniline or an aqueous hydrochloride solution of aniline followed by initiating the successive direct polymerization in a separate bath (DPSB) or in a mixed bath (DPMB) of oxidant and dopant solution with aniline. Polymerization of aniline on porous materials has also been used to prepare conducting membrane materials whose permeability and other properties could be maintained by the porosity of the final material and conducting polymer layers formed inside pores.[264, 265] Specifically, Tishchenko *et al*.[264] elaborated composite systems based on a microporous polyethylene membrane modified in situ during the oxidative polymerization of pyrrole from the gas phase or by the polymerization of aniline in an aqueous medium. The composite membranes displayed a low resistance in electrolyte solutions owing to the coating of polypyrrole or PANI inside the pores. Another diffusion-oxidation method [260] is aniline (or other monomer) polymerization in polymer matrixes impregnated with an oxidant that also allows preparation of PANI (polypyrrole) conducting composites, but this seems not to be very practical. Specifically, it can be realized through exposing the matrix polymer (e.g. poly(acrylamide)) impregnated with an oxidizing agent to hydrochloric acid vapor, and then to the monomer vapor [266] or solution.[267]

By an electrochemical approach polymerization at an electrode (anode) surface coated by a non-conducting polymer film at the aniline oxidation potential results in the formation of a PANI/polymer composite.[268, 269] The necessary condition here is penetration (diffusion) of aniline, solvent and electrolyte through the coating to its interface with the anode,[268] to create the electrochemical prerequisites to oxidize molecules of aniline (in reality anilinium cations), and growing PANI macromolecules. This condition can be realized in two ways: through pores and by swelling the polymer coating in the reaction medium (solution), separately or in parallel, dependent on the coating porosity and swellability. Under appropriate condition, the polymerization starts at the interface between the anode surface and the coating,[268] and the resultant PANI grows from this interface into the coating bulk, forming a new electrically conducting alloy film, as shown for different matrixes in the polypyrrole case.[270–273]

4.1.1.2. Blending methods

The low solubility of PANI in common organic solvent is strictly related to its aromatic structure, *inter*-chain hydrogen bonds and effective charge delocalization in its structure.[274] Many methods have been developed to prepare PANI soluble in different solvents and facilitate the preparation of PANI conducting composites with polymers soluble in the same solvents. Some of these synthetic methods are summarized below:

1. PANI soluble in organic solvents can be prepared from aniline monomer modified with alkyl,[275, 276] alkoxy [277] and other substituents.
2. The introduction of sulfonic groups on PANI benzene rings produces water soluble sulfonated self-acid-doped PANI (SPAN) [278, 279] or highly sulfonated SPAN.[280]
3. Aniline can be polymerized with other monomers to form soluble aniline copolymers.[281]
4. The use of functionalized protonic acids as the dopants (e. g. CSA (canphorsulfonic acid), DBSA (dodecylbenzenesulfonic acid), phosphoric acid diesters, etc.), increases the solubility in non-polar or weakly polar organic solvents.[282–285]
5. The use of amide solvents such as NMP and DMF, in which PANI base is soluble.[286].

Obviously, the nature of the solvent influences the properties and ease of preparation of blends of alkoxy substituted PANI. For example, Gonçalves *et al*.[287] investigated the suitability of different solvents to prepare PU–POMA [PU= polyurethane, POMA= poly(*o*-methoxyaniline)] blend films by casting, comparing DMF, NMP and *m*-cresol. DMF was the best solvent for two reasons: suppressed deprotonation during the preparation of a predoped POMA solution in DMF as compared with NMP, due to a lower basicity of DMF as against NMP; convenience in the use of DMF owing to its lower boiling point (153°C) than NMP (202°C) or *m*-cresol (202°C).

Flexible conducting free standing films were obtained by Gonçalves *et al*. using PU–POMA solutions in DMF at different weight ratios and their flexibility is very similar to films of pure PU.[287]

Concerning composites of PANI with alkyl substituents, Anand et al. developed and studied soluble POT [poly(*o*-toluidine)] and PMT [poly (*m*-toluidine)] blends with PVC (polyvinylchloride).[288]

POT doped PANI in its base forms was soluble in THF, which is also a solvent for PVC. The authors found that POT and PMT bases produced as salts of HNO_3 were the most soluble among other bases.[288]

Sevil *et al*.[289] demonstrated that chlorine substituted PANI had enhanced solubility in comparison with pure PANI. Specifically, they prepared 2-chloro-polyaniline (2-Cl-PANI) in its non-conducting EB form, and dissolved it with PVC in THF for casting into thin composite films.

Chen and Hwang prepared water-soluble PVA/SPAN (self-acid-doped polyaniline) and PVA/PAPSAH [poly(aniline-co-*N*-propanesulfonic acid aniline)] blends.[290] They supposed that the strong interaction of these polyanilines with PVA through hydrogen bonding between hydroxyl groups (of PVA) and positively charged amine and imine sites (of SPAN and PAPSAH) led to a decrease in hydrogen bonding among PVA chains and to a partial miscibility.

By a typical amine-epoxide reaction Yamaguchi *et al*. produced blends of LEB (leucoemeraldine base) with phenylglycidylether (PGE) more soluble in acetone and chloroform than LEB.[291]

More recently, Adams *et al*.[292, 293] developed a new acid-solution processing route for preparation of highly conductive PANI films and fibers soluble in chloroform, diethylketone, hexafluoro-2-propanol, m-cresol and dichloroacetic acid. It comprises the use of AMPSA as both the protonating acid and the solvating group and dichloroacetic acid (DCAA) as the solvent. However, also other dopants such as DEHEPSA and PMMA, in DCAA or difluorochloroacetic acid can be used.[294, 295]

Moon and Park prepared blends of PANI with copolymeric acids such as poly(methylmethacrylate-co-*p*-styrenesulfonic acid) (PMMA-co-SSA), poly(styrene-co-*p*-styrenesulfonic acid) (PS-co-SSA), and poly(methylmethacrylate-co-2-acrylamido-2-methyl-1-propanesulfonic acid) (PMMA-co-AMPSA) soluble in NMP.[296]

Among copolymers used for the preparation of PANI blends polyethylene oxide (PEO), poly(methyl-methacrylate) (PMMA) and polystyrene (PS) are the most common. These copolymers are particular useful to prepare nanofibers and nanowires of PANI blends by electrospining technique, increasing the viscosity of the PANI solution.

4.1.2. Physicochemical properties

The interaction of PANI with copolymer affects not only the solubility of the blend but also other physicochemical properties, such as thermal stability, mechanical properties and conductivity.

Generally, adding an insulating copolymer into PANI its conductivity decreases,[168] but characteristic mechanical properties improve. Instead, thermal properties are strictly related to the kind of copolymer used.

However, sometimes the interaction among the blend components can cause an increase of conductivity. In fact, Jeon *et al*. observed that composites of PANI-DBSA/PC (PC= polycarbonate) prepared by an inverted emulsion polymerization method show values of electrical conductivity three times higher than pristine PANI.[297-300] FT-IR spectroscopy on the composite showed the existence of hydrogen bonding between PANI and PC, which increased the glass transition temperature with increasing PANI content.

Moreover, the comparison of DSC and conductivity data showed that the electrical conductivity increased around the glass transition temperature. The authors explained this by the fact that the PANI chains contacted more frequently and facilitated electron transfer through the hydrogen bonding between PANI and PC. In addition, the tensile strength of the composite decreased with PANI content below the percolation threshold (13 wt%) of PANI. This interaction may also be displayed by improved thermal stability of PANI/PC blends compared to pure PANI.[301] Aside from the physical–chemical interactions between PANI and copolymer used, the kind of dopant and its size should affect the properties of the PANI conducting composites. A decrease of electrical conductivity can be also due to the presence of solvent into the material. For example, cast films of doped PANI and its blends can retain solvent. This is important, especially in the case of high boiling solvents, which are very difficult to completely remove. In turn, this may affect several material properties. For example, Jousseaume *et al*.[302] revealed a decrease of the conductivity by electrical conductivity measurements during heating–cooling cycles, as the residual solvent (*m*-cresol) and moisture evaporation of. This phenomenon was explained by the existence of a frontier sensitive to the solvent at the periphery of conducting clusters.

Specifically, for PANI-DiOHP/PS films, the temperature dependence of conductivity before and after the partial evaporation of the solvent was well described by a model of a tunnel effect limited by the charging energy of conducting clusters. Changes in crystallinity, due to the presence of copolymer host, can strongly affect other important properties, such as tenacity. For example, a significant drop in crystallinity with increasing PANI fraction from 0 to 9 wt% was reported by Zhang *et al*.[303] for PANI-CSA/PA blends. In the case of blend fibers of PANI-DBSA and UHMW-PE (ultra high molecular weight polyethylene) prepared by Andreatta and Smith [304] through solution blending in decalin with various ratios of PANI to UHMW-PE, the modulus and the tenacity of the fibers ranged from 40 to 0.5 GPa, and from 2 to 0.02 GPa, respectively. Conductivity was $3 * 10^{-4}$ S/cm for blends containing 5 wt% of PANI.

It is known that PANI doped with a binary mixture of sulfonic acids possesses peculiar thermostability, conductivity and other characteristic features as compared to the polymer doped separately by sulfonic acids such as DBSA, TSA (toluene-sulfonic acid) or naphtalenedisulfonic acid.[305] Koul *et al*.[306] have shown enhanced electrical and optical properties, along with higher solubility in all common organic solvents, for PANI doped with a mixture of DBSA/TSA (1:1). Using this double doped PANI, they prepared composite films with ABS (acrylonitrile–butadiene–styrene copolymer) by casting from the chloroform solution. The surface resistance of these composites changed from 300 MΩ/cm to 1.302 kΩ/cm, dependent on the PANI doped content and the method of mixing the system components. The importance of physical–chemical interaction of

the matrix polymer and doped PANI for conducting blend properties was also demonstrated by Wang *et al*.[307] for PANI/PEO blends cast from aqueous solution. They used an acidic phosphate ester dopant prepared through reaction of $POCl_3$ with poly(ethyleneglycol) monomethylether (PEGME, M_w= 350). The DSC curves of the blends with different doped PANI loadings showed a shift of the single endothermic peak (at 67°C in pure PEO) corresponding to a suppressed melting temperature for the PEO crystallites. This effect was explained by compatibilization of the rigid conjugated polymer with the matrix polymer, achieved due to the ability of the ester dopant to form hydrogen bonds with PEO, reducing the interfacial energy of the two incompatible blend components.[307] This phenomenon may be considered to be a kind of plasticizing effect caused by the long poly(ethyleneglycol) tail of the dopant.

4.1.3. PANI nanofibers by electrospinning technique

In recent years, many processing techniques have been used to prepare polymer nanofibers. Among them, drawing,[308] template synthesis,[309, 181] phase separation,[310] self-assembly,[311, 312] electrospinning,[313, 314] etc. are the most investigated. The template synthesis allows to produce nanometer tubules and fibrils of various raw materials, such as electronically conducting polymers, metals, semiconductors and carbons. However, the removal of the template at the end of the reaction is a big drawback, because it adds steps to the final work-up of the reaction and, moreover, can compromise the final morphology of the products. The phase separation consists of dissolution, gelation, extraction using a different solvent, freezing, and drying resulting in a nanoscale porous foam. The process takes relatively long period of time to transfer the solid polymer into the nano-porous foam. The self-assembly is a process in which individual, pre-existing components organize themselves into desired patterns and functions. However, similarly to the phase separation the self-assembly is time-consuming in processing continuous polymer nanofibers. All these methods are useful in lab scale, but cannot be employed to produce nanofibers and nanowires in industrial scale. For this purpose, electrospinning technique seems to be much more appropriate.

A schematic diagram of the electrospinning setup is shown in Figure 4.1.

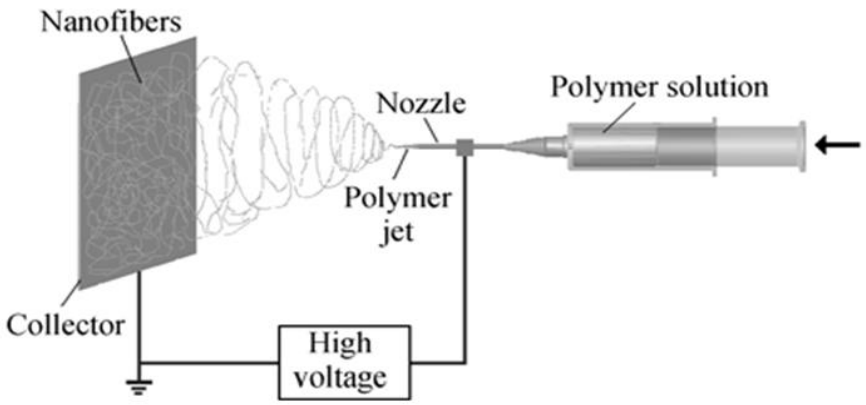

Figure 4.1.: Diagram of electrospinning setup.

There are basically three components to fulfill the process: a high voltage supplier, a capillary tube with a pipette or needle of small diameter, and a metal collecting screen. In the electrospinning process a high voltage is used to create an electrically charged jet of polymer solution or melt out of the pipette. Before reaching the collecting screen, the solution jet evaporates or solidifies, and is collected as an interconnected web of small fibers.[313, 314] One electrode is placed into the spinning solution/melt and the other attached to the collector. In most cases, the collector is simply grounded, as indicated in Figure 4.1. The electric field is subjected to the end of the capillary tube that contains the solution fluid held by its surface tension. This induces a charge on the surface of the liquid. Mutual charge repulsion and the contraction of the surface charges to the counter electrode cause a force directly opposite to the surface tension.[315] As the intensity of the electric field is increased, the hemispherical surface of the fluid at the tip of the capillary tube elongates to form a conical shape known as the Taylor cone.[316] Further increasing the electric field, a critical value is attained with which the repulsive electrostatic force overcomes the surface tension and the charged jet of the fluid is ejected from the tip of the Taylor cone. The discharged polymer solution jet undergoes an instability and elongation process, which allows the jet to become very long and thin. Meanwhile, the solvent evaporates, leaving behind a charged polymer fiber. In the case of the melt the discharged jet solidifies when it travels in the air.

Many parameters can influence the transformation of polymer solutions into nanofibers through electrospinning.

These parameters include (a) the solution properties such as viscosity, elasticity, conductivity, and surface tension, (b) governing variables such as hydrostatic pressure in the capillary tube, electric potential at the capillary tip, and the gap (distance between the tip and the collecting screen), and (c) ambient parameters such as solution temperature, humidity, and air velocity in the electrospinning chamber.[317]

In order to prepare nanofibers or nanowires of a polymer, it has to be dissolved in a solvent or melted to be introduced in the pipet or syringe. However, it is known that some COPs, especially PANI and PPY, are characterized by very low solubility and decompose before to melt.

For this reason, it is necessary to add a co-polymer into the solution in order to increase the viscosity of the solution and facilitate the electrospinning process. However, typically, co-polymers employed for this purpose are insulating and reduce the conductivity of the products.

Electrospinning technology has been successfully employed to prepare PANI-based conducting nanofibers. Many co-polymers have been employed for this purpose, including poly(ethylene oxide),[237] nylon-6,[318] polystyrene,[235, 239] poly(lactic acid) (PLA),[240] and many others.

4.2. PANI/ferrites nanocomposites

Organic–inorganic nanocomposites with an organized structure has been extensively studied because they combine the advantages of the inorganic materials (mechanical strength, electrical and magnetic properties and thermal stability) and the organic polymers (flexibility, dielectric, ductility and processability), which are difficult to obtain from individual components.[311-322]

PANI composites characterized by magnetic and conducting properties have been intensively studied. For example, Wan *et al*. prepared materials with very low coercive force (Hc ~ 0) and relatively high saturation magnetization (Ms~72 emu/g).[323, 324] The soft magnetic spinel ferrites with formula $A^{2+}B^{3+}{}_2O_4$, such as Fe_3O_4, $CoFe_2O_4$, $NiFe_2O_4$, $MnFe_2O_4$ and $ZnFe_2O_4$, have widely used in many fields, such as microwave devices due to their high saturation magnetization, high permeability, high electrical resistivity and low eddy current losses,[313-326] but also electromagnetic interference shielding (EMI) and many others.

4.2.1. Iron oxides nanoparticles

Iron oxides are common materials very widespread in nature (see Figure 4.2.).

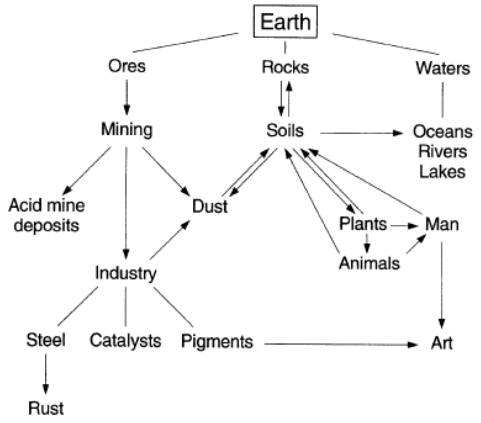

Figure 4.2.: Diffusion of iron oxides in the earth. Data from ref. 316.

They are also prepared in laboratory in different sizes and morphology.

Oxide-hydroxides and hydroxides	Oxides
α-FeOOH (Goethite)	α-Fe_2O_3 (Hematite)
γ-FeOOH (Lepidocrocite)	Fe_3O_4 (Magnetite)
β-FeOOH (Akaganéite)	γ-Fe_2O_3 (Maghemite)
$Fe_{16}O_{16}(OH)_x(SO_4)_y \cdot nH_2O$ (Schwertmannite)	β-Fe_2O_3 (Maghemite)
δ-FeOOH (Ferroxyhite)	ε-Fe_2O_3 (Maghemite)
$Fe_5HO_8 \cdot 4H_2O$ (Ferrihydrite)	FeO (Wüstite)
$Fe(OH)_3$ (Bernalite)	
$Fe(OH)_2$(Ferrous hydroxide)	
$Fe_x^{3+}Fe_y^{2+}(OH)_{3x+2y-z}(A^-)$; A= Cl^-, $1/2SO_4^{2-}$ (Green Rusts)	

Table 4.1.: Main iron oxides present on the Earth.

Iron oxides are composed of Fe and O and/or OH. In most of them iron is in trivalent state. Concerning their structure, iron oxides consist of close packed arrays of anions [usually in hexagonal (hcp) or cubic close packing (ccp)] in which the interstices are partly filled with divalent or trivalent Fe predominately in octahedral, $Fe(O,OH)_6$ but in some cases in tetrahedral, FeO_4, coordination. The various oxides differ in the way in which the basic structural units (octahedral or tetrahedral) are arranged in the space.

Materials where Fe^{3+} is the main cationic component are called spinels. There are three main families of ferrites: spinel ferrites, garnet ferrites and hexaferrites, that differ for properties and characteristics.

Concerning the structure of ferrites, the oxygens form a fcc sublattice with the cations occupying 16 octahedral (B-sites) and 8 tetrahedral (A-sites) positions. The distribution of the metal ions is very important to understand the properties of these materials.

Figure 4.3. shows the unit cell corresponding to magnetite and maghemite, typical inverse spinel ferrites.

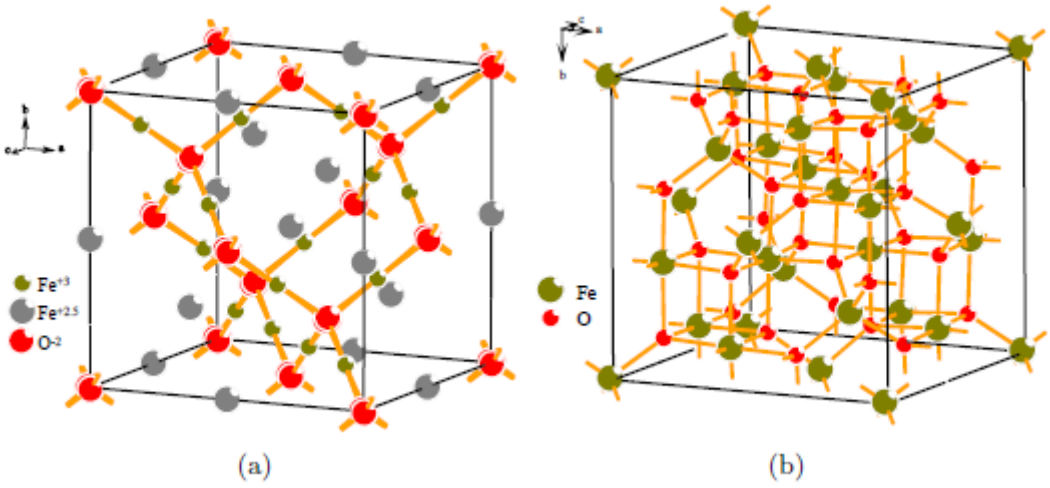

Figure 4.3.: representation of unit cell for magnetite (a) and maghmetite (b).

Spinels are characterized by direct and inverse structure. More in particular, in a structure of normal (or direct) spinels (AB_2O_4) divalent A(II) ions occupy the tetrahedral voids, whereas the trivalent B(III) ions occupy the octahedral voids in the close packed arrangement of oxide ions.

A normal spinel can be represented as: $(A^{II})^{tet}(B^{III})_2{}^{oct}O_4$.

$MgAl_2O_4$ (known as spinel), Mn_3O_4, $ZnFe_2O_4$, $FeCr_2O_4$ (chromite) etc. are typical spinels with direct structure.

In structures of inverse spinels ($B(AB)O_4$) A(II) ions occupy the octahedral voids, whereas half of B(III) ions occupy the tetrahedral voids. It can be represented as: $(B^{III})^{tet}(A^{II}B^{III})^{oct}O_4$.

Fe_3O_4 (magnetite), $CoFe_2O_4$, $NiFe_2O_4$ etc. are typical spinel with inverse structure.

The above inverse spinels can also be written as:

$Fe_3O4 = Fe^{III}(Fe^{II}Fe^{III})O_4$

$CoFe_2O_4 = Fe^{III}(Co^{II}Fe^{III})O_4$

$NiFe_2O_4 = Fe^{III}(Ni^{II}Fe^{III})O^4$

The number of octahedral sites occupied may be ordered or random. The random occupation leads to defected spinels.

Nano sized particles of iron oxide have emerged as versatile materials for different applications due to their magnetic, electronic, photonic and optical properties. The structure-function relationship of these nanoparticles have been intensively studied because of the applications in magnetic storage, gas sensing, biomedical, and catalysis applications.[328-332] Iron oxides nano particles have been prepared by a variety of methods such as sonochemical reactions,[333] mechanochemical synthesis,[334] hydrolysis, thermolysis of precursors as well as co-precipitation technique.[335] Nano particles with a virtually near to monodisperse size distribution can be produced by thermal decomposition of an iron-cupferron complex in octylamine.[336]

Due to their unique properties, currently these materials are particularly investigated for their application in different areas, such as catalysis,[337] biomedicine,[338] magnetic resonance imaging,[339] data storage [340] and many others.

4.2.2. Techniques of preparation of PANI/ferrites

Recently, thanks to their innovative properties polymeric nanocomposites have attracted a growing attention from the international scientific community, opening new perspectives in the world of nanotechnologies. The synthetic methods are distinguished in two types: in situ [341] and ex situ.[342] The former method is a two steps approach. In the first step monomer is polymerized in the presence of metallic ions. Otherwise metallic ions can be added at the end of the polymerization reaction. In the second step metallic ions are reduced chemically, thermally or photochemically.

In the ex situ methods, instead, metal nanoparticles are first synthesized, then passivated and finally dispersed in the liquid monomer that is polymerize to produce a solid nanocomposite.

In both cases the synthesis of the second component is done separately from the polymerization of monomer.

Metal/polymer nanocomposite are characterized by interesting properties that make them particularly attractive for many advanced applications (e. g., microwave absorbers, optical filters, materials for photothermal solar collectors, material refractive index ultra high / low, materials for magneto-optical and electro-optical, etc.).

More in particular, PANI/metal oxides nanocomposites have been prepared according to many different methods. A template-free method was used to prepare PANI/Fe_3O_4 composites with a core–shell structure.[343, 344]

The preparation of PANI-Fe_3O_4 nanocomposites through polymerization of aniline in the presence of a ferrofluid has been reported.[345] PANI composites containing nanomagnets (e.g. Fe_3O_4, d≈14 nm) were prepared by a chemical method.[346] PANI/nano-Fe_3O_4 composites were prepared by the solid-stabilized emulsion (Pickering emulsion) route.[347] PANI–Fe_3O_4 nanocomposites were obtained through mechanical mixing of dodecyl benzene sulfonic acid doped (DBSA)–PANI powder and HCl-doped PANI–Fe_3O_4 powder.[348] Fe_3O_4/PANI /DBSA with core–shell structure were synthesized by emulsion polymerization. Aphesteguy *et al*. prepared PANI-Fe_3O_4 through polymerization of aniline in the absence of external oxidant.[349] Mixtures of iron(II) and iron(III) compounds were used as oxidants to polymerize aniline to PANI and form Fe_3O_4 particles in a single step. PANI has been prepared also using a mixture of $FeCl_2$ and $FeCl_3$ as oxidants.[350]

Composites of magnetic microtubes were obtained through in situ polymerization of aniline in the presence of Fe_3O_4 NPs in the microchannels of AAO (anodi aluminium oxide) to result in tubular

structure of PANI/Fe_3O_4 nanocomposites.[351] Hsieh *et al*. reported the preparation of PANI/γ-Fe_2O_3 nanocomposites by a reverse micelle process.[352] PANI nanotubes containing Fe_3O_4 NPs (~10 nm in diameter) and coaxial PANI/γ-Fe_2O_3 nanofibers have been synthesized via a self-assembly process.[353, 354] In addition to all the preparations here reported, scientific literature contains many other examples of preparation of PANI/metal oxides composites.

Chapter 5: Applications

Conducting polymers can be applied in a wide variety of fields. The first and the most important characteristic that makes these materials appealing is related to their electrical properties which can be modulated varying the entity of doping. Thanks to the fact that they could be dielectrics as well as semiconductor and conductors, they find applications in diodes, transistors, sensors, drug delivery systems and many other electronics device. PANI can be also used as material for gas, pH and other chemicals sensors, as a electroactive component of strain sensors, for selective permeable membranes, for LEDs, for biomedical applications (drug delivery systems, tissue regeneration, etc.), in antenna systems and many others.[355-360]

Even though the technology based on silicon is still more reliable, conducting polymers are being developed as they are more lightweight, flexible and, once the technology is well established, they will be more economic. Another important characteristic of this class of materials is that they are particularly effective in the absorption of electromagnetic radiation in the range of microwaves. In fact, they are being developed as new materials for the electromagnetic interference shielding (EMI), replacing currents technology based on polymer-metal particles or polymer-carbon composites. The upgrade that conducting polymers could add to the current technology, based on soft iron plate or magnetic iron oxides layer, is that they can provide a significant microwave or radio absorption, without adding much weight.

As regards polyaniline, a large number of potential applications arises from the presence of various oxidation states, the possibility to interchange among them and, for every oxidation state, the possibility to vary the entity of doping.

5.1. EMI (ElectroMagnetic Interference) shielding applications

The life of the modern humanity is based on the transmission of data. Many resources are invested every year for the development of existing technology and the creation of new ones. A very big portion of the western economy and finance relies on the possibility to transfer information over long distances within seconds. Information and Communication Technology (ICT) plays also a very important role in the development of large new economies, like the ones of the BRIC (Brasil, Russia, India, China). Moreover, with the increasing pervasiveness of cell phones and wireless local area networks, and the current push to wirelessly connect handheld computers with local and wide area wireless networks, these devices can also interfere with medical equipment located in hospitals, clinics and similar. For all these reasons electromagnetic interference is potentially harmful and thus deserves a big consideration. Every year millions of devices are manufactured that are susceptible to EMI like for example cell phones, radio, Wi-Fi apparatus, personal computers and many more. The development of effective shields assumes therefore an enormous importance. They

should be made of either conductive or magnetic materials, or also a combination of both, as it could be seen later in this chapter. In some applications, these materials should have other features: in the manufacture of aircrafts they have to be lightweight, they have to withstand particular conditions either in the fabrication process or during their use and sometimes they should be as cheap as possible.

5.1.1. Signal transmission

The first electromagnetic transmission came with the advent of telegraph (1809). It was a digital transmission based on the use of only two values: zero and one. The first analogic transmission by mean of an electromagnetic signal was made possible by the invention of the telephone (1870s). Both these media made the signal travel along a wire. The first wireless communication was made by Guglielmo Marconi by the use of the radio (1894, he sent his first message over 2 km. 1901, first transatlantic transmission). Since the beginning of the 20th century many efforts were made to improve such an important field. Electromagnetic ways of transmitting data became since then part of everyday life of men all around the world, making communication easier and faster.

In general, four elements are the basis of communication and they must coexist together: a transmitter, that produces the signal, a receiver, that receives it, a signal, the subject of the communication and a medium.

Concerning the electromagnetic transmission of data, the transmitter consists in a device that produces a particular electromagnetic wave, characterized by a defined frequency and a particular pattern. This wave travels through a medium that could be a wire or, in the case of wireless communication, simply the air or the outer space vacuum. The electromagnetic signal can be transmitted in two different ways: as analog or digital signal.

An analog signal is a continuous signal that contains time-varying quantities (time, space etc), whereas a digital signal is a physical signal that is a representation of a sequence of discrete values. A digital signal is discrete and quantized. Discrete means that the domain of the signal, i.e. the time, has only some values because the value of the variable is measured only every second, millisecond etc. Quantized means that the values of the signal belong to a finite set. Figure 5.1. shows a comparison between analog and digital signal.

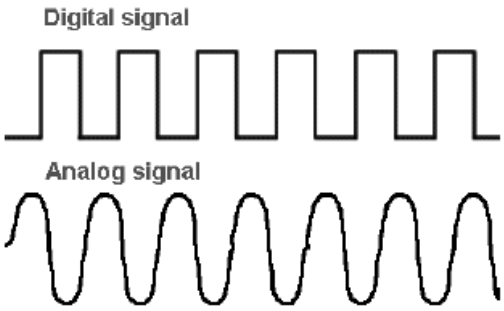

Figure 5.1.: Comparison between analog and digital signal.

5.1.2. Electromagnetic interference (EMI)

Electromagnetic Interference (EMI) is the disturbance, generated from an electromagnetic wave radiated from an external source, that affects an electrical circuit. This disturbance may interrupt or degrade the performance of the circuit or of a signal, as shown in Figure 5.2.

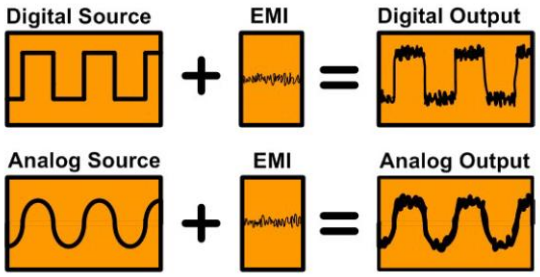

Figure 5.2.: Example of EMI on a digital and an analog signal.

The source may be any object, either artificial or natural, that carries rapidly changing electrical currents, such as an electrical circuit, a the inverter of an electrical motor. Natural but extraterrestrial source of EMI are the stars and the Sun itself.

Two types of EMI exist: narrowband or broadband. As the name suggest, a narrowband electromagnetic interference operate only on a small portion of the spectrum and it is often produced by intentional transmission like television, radio, telephones. A broadband EMI is in general created by an apparatus rapidly switching on and of an electric current. These include electric motors, like those found in industries or in washing machines, and electric power transmission lines.[361]

5.1.3. EMI shielding

Two main mechanisms exist for shielding an electromagnetic interference. The first and often primary is reflection. A fundamental characteristic that a shield should have to reflect an incoming radiation is the presence of mobile charge carriers, as the conduction electrons in a metal. For this reason metals are the most used materials for EMI shields and their method of shielding is based on the reflection. However, the weight and the stiffness of these materials make them unsuitable for application in some fields, such as aerospace industry. In this case the use of composites, made of organic polymers filled with particles, can be a smart solution.

A second mechanism for EMI shielding is absorption. An absorption shield should have electric and/or magnetic dipoles that interact with the electric and/or the magnetic field in the radiation. The presence of electric dipoles is represented by the dielectric constant.

Materials with higher ε and μ tend to be a better shield.[362] There are many methods to enhanced the magnetic permeability: reducing the number of magnetic domain walls, using small particles or creating multilayer magnetic films.[363, 364] Absorption loss is a function of ε and μ. High values of absorption loss are thus obtained from materials having high both the dielectric constant and the magnetic permeability. Absorption loss and reflection loss are also a function of the electromagnetic wave frequency: the first one increases with the frequency, the second one decreases. An important parameter that affects the loss is the shape of the material. In the presence of a large interfacial area, a third shielding mechanism happens, called multiple reflections. Examples of these materials are foams or composites. The skin depth δ at which the field drops is defined by Equation 5.1.:

$$\delta = 1/\sqrt{\pi f \mu \sigma} \qquad \text{Eq. 5.1.}$$

where *f* is the frequency of the electromagnetic wave in Hz, μ is the magnetic permeability in $H \cdot m^{-1}$ and σ is the conductivity in $S \cdot m^{-1}$.

The sum of the contributes from reflection, absorption and multiple reflection is called shielding effectiveness (SE_{dB}) and is expressed in decibel (Eq. 5.2.),

$$SE_{db} = A + R + B \qquad \text{Eq. 5.2.}$$

where A is the absorption loss, R is the reflection loss and B is a term which takes into account the loss caused by multiple-reflection inside the shield.[365, 366] A shielding effectiveness of 30dB, corresponding to 99.9% attenuation of the EMI radiation, is considered an adequate level of shielding for many applications.[367]

The mechanisms of shielding is illustrated in Figure 5.3.

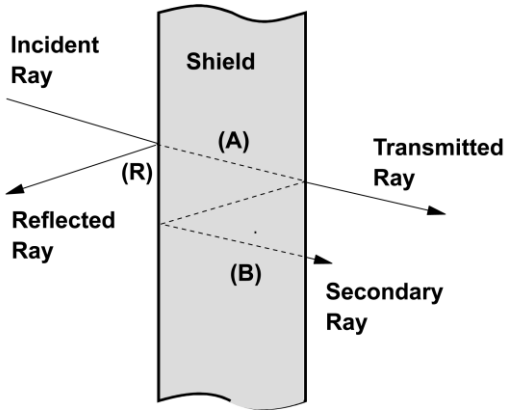

Figure 5.3.: Basic shielding mechanism.

5.1.4. Materials for EMI shielding

Over the years many different materials have been developed to obtain a good shielding power. Among them metals, conducting polymers and their composites are the most investigated.

5.1.4.1. Metals used in EMI shielding

Metals are excellent conductors of electricity and can absorb, reflect and transmit electromagnetic interference. The ability to conduct both electricity and heat make metals particularly interesting for many applications. These characteristics allow the use of metals as materials for EMI shielding. In fact, high frequency electromagnetic radiation is either prevented from escaping from the equipment or the equipment is shielded from stray radiation by metal shields and covers.[368]

The common material used for construction of enclosures for shielding is mu-metal, a high permeability alloy composed of 14% iron, 5% copper, 1.5% chromium and 79.5% nickel. The other metals/materials used as a shield are brass, aluminum, silver, nickel, stainless steel, metalized plastics and conductive carbon/graphite composites. These conductive composites have certain limitations, for example carbon/graphite suffer from brittleness, aluminum based has low impact resistance, and stainless steel has high density. The metal shield is susceptible for corrosion, which leads to Rusty Bolt Effect of nonlinearity to cause intermodulation problem especially in sea environment. The use of two different metals for shield and gasket causes galvanic corrosion which leads to nonlinearity and decrease in SE of the metallic shields.[369, 370] For shielding applications based on reflection, the weight saving benefit of magnesium enclosures extends over the full frequency spectrum. For shielding based on absorption, die cast enclosures of magnesium and aluminum provide nominally equivalent shielding effectiveness on an equal weight basis. The lower

density of magnesium offsets the higher conductivity of the aluminum. Die cast magnesium alloy enclosures for EMI shielding provide significant advantages over both plastic and alternative metal housings.[371]

5.1.4.2. Composite materials in EMI shielding

Conventional plastic materials are excellent electrical insulators having resistivity in the range of 10^{15}–10^{18} Ω · cm. For EMI shielding purpose they have to be modified by metallization processes. In particular, following methods are used for metalizing the plastic surface:[372-375]

- Foil laminates and tapes
- Ion plating
- Vacuum metallization
- Zinc flame spraying
- Zinc arc spraying
- Cathode sputtering
- Conductive paints
- Electroless plating
- Electroplating

Otherwise, plastic materials can be made conducting by incorporation of a conducting material, such as carbon black. It is known that carbon is used as a good reinforcement material in the rubber industry, as well as filler in wire and cable sheathing. Moreover, because of its graphitic nature, carbon black is a semiconductor, typically the dry resistivity is in the range of 20–0.5 Ω · cm and when used as filler in rubbers and plastics it endows the compound with antistatic/conductive properties. Calleja et al. studied the electrical conductivity of high-density polyethylene (HDPE)—Carbon fiber composites mixed with different concentrations of carbon black.[376] They found that carbon fibers provide charge transport over large distances and carbon black particles improve the inter fiber contacts. If the segmented carbon black - HDPE component lies above the percolation threshold, carbon black particle ensure the electrical interfiber contacts acting as bridges. As a result conductivity rises. Ramadin *et al*. reported the electrical properties of laminated epoxy-carbon fiber composites.[377] The electromagnetic losses as a function of frequency and specimen spacing are also studied. They observed optimum SE of the laminated epoxy composite (~ 62 dB) occurs at about 30 mm specimen spacing and frequency ~ 9 GHz. Das *et al*. reported that the EMI shielding characteristics of natural rubber and ethylene-vinyl acetate (EVA) filled with conductive carbon black (Vulcan XC-72) and short carbon fiber (SCF).[378] The EVA based composites are found to be the more effective in EMI shielding particularly when SCF is used as the conductive filler.

The SCF filled composites exhibit higher SE at lower filler loading compared to carbon black filled ones. The SE of these composites is found to be higher at X-band frequency range (8–12 GHz) compared to that at microwave frequency range (100–2000 MHz). The composites containing SCF are technically useful materials (SE ≥ 20dB) in X-band region.

Also graphite fibers found application in the EMI shielding. In fact, Simon *et al*. reported that resins containing 30% graphite fibers exhibit good shielding properties.[379] Luo and Chung reported the electromagnetic interference shielding effect of flexible graphite.[380] The SE is exceptionally high 130 dB at 1–2 GHz higher than that of solid copper. In addition to conventional shielding applications, flexible graphite can serve as a shielding gasket material, due to its flexibility.

The shielding effectiveness of stainless steel fibers filled thermoplastics is typically 36–42 dB. A number of other metal fibers such as copper, brass, aluminum and iron have been reported as fillers for EMI shielding composites, but few are used on a commercial basis. Aluminum fibers have the advantage of low specific gravity, while copper fibers offer the highest intrinsic electrical conductivity of any of the metals. Both these materials, however, are subject to surface oxidation under normal environmental conditions. For the preparation of all these composites ABS (acetylonitrile-butadiene-styrene), Nylon, PC (polycarbonate), PET (polyethylene terephthalate), PPO (Poly(p-phenylene oxide) and PS (polystyrene) are used as polymeric matrices.

5.1.4.3. Intrinsically conducting polymers in EMI shielding

Intrinsically conducting polymers are alternative materials for EMI shielding. Among all the conducting polymers, polyaniline and polypyrrole are mainly used for EMI shielding purposes. It is known that one of the inherent problems of the intrinsically conductive polymers is their low processability. In order to overcome this problem, many studies have been done. For example, Trivedi and Dhawan proposed a method to graft conducting PANI onto glass fabric, glass wool and nylon cloth to impart flexibility and mechanical strength to the PANI, which is otherwise powdery and unprocessable.[381-384]

This conducting flexible surfaces are advantageous compared with the presently popular method of preparing conductive composites by the addition of metal powder/flakes or carbon black to conventional polymer, in which uneven mixing reduces the mechanical properties, there is often compatibility between the filler and the polymer matrix, and there is a risk of surface corrosion; whereas conducting PANI grafted surfaces can withstand any level of acidic fumes and high humidity levels without any degradation. The grafted Nylon fabric affords a shielding effectiveness of 37 dB up to 50 KHz and 30 dB up to 1000 KHz, and above this frequency a sudden fall in SE is observed.

Conducting polyaniline composites are also mainly used for EMI shielding purposes. Trivedi and Dhawan 73 prepared flexible polyaniline composites with water-soluble polymers like polyvinyl alcohol/carboxymethyl cellulose and their derivatives.[385] Their resistivities lie in the range 60 Ω to 1000 Ω · cm and may prove to be useful for dissipation of electrostatic discharge. Kathirgamanathan reported that composites consisting of polyaniline coated nickel (spheres), carbon black dispersed into copoly (ethylene-propylene) matrix show SE > 20 dB in the frequency range of 10 KHz–100 MHz.[386] This kind of materials are suitable for most shielding applications. Mixtures of PANI and conducting powders such as silver, graphite and carbon black resulted to be useful for EMI shielding in the frequency range from 10 MHz to 1 GHz.[387]

Lee *et al*. observed that ES (emeraldine salt) without mixing of conductive powder shows SE of 17 dB, whereas composed with graphite or silver show SE of ~ 27 and ~ 46 dB respectively.[387]

It has been found that PANI-CSA (camphorsulfonic acid) cast film using *m*-cresol as the secondary dopant reaches a shielding efficiency of 39 dB at 1 GHz.[388, 389]

Pant *et al*. synthesized ferrofluid-conducting polyaniline composites of different concentration with a nonconducting polyvinyl alcohol matrix. They found that by increasing the ferrofluid concentration the shielding property of the material also increases.[390]

In the scientific literature the number of papers that describe new methods to produce PANI composites for EMI shielding is huge and scientists try to develop continuously materials that are more efficient and performing.

In addition to polyaniline another important conducting polymer that has received much attention in the EMI shielding is polypyrrole. However, since it is completely insoluble in any solvents and infusible, it is mainly prepared in form of composite. For example, Trivedi and Dhawan described a process for the polymerization of pyrrole on insulating surfaces like nylon, terylene and glass fabric and polymer matrix like polyvinyl alcohol (PVA) by vapor phase polymerization.[391]

The electrical resistivity of these PVA/PPy composite films is in the range 200 Ω · cm to 20 KΩ · cm. Lee and coworkers synthesized PPy and metal (Ag, Pd) compounds coated on woven polyethylene terephthalate (PET) and nonwoven polyester (PE) fabrics by electrochemical treatment.[392] PPy coated on PET or PE fabrics was electrochemically synthesized by using anthraquinone-2-sulfonic acid (AQSA) as a dopant. The results show that both conducting PPy and Ag layers contribute to the increase of EMI SE. Pomposa *et al*. developed intrinsically conducting hot melt adhesives (ICHMAS) based on PPy blends for EMI shielding applications.[393] These new materials retain the advantages of conventional hot melt adhesives (e.g., melt processibility, quick bonding, good adhesion to a wide variety of substrates etc) having a level of electrical conductivity appropriate to be used at room temperature as EMI shields in electronic, computing

and telecommunication applications (i.e., form-in-place EMI gaskets, thin film EMI shields, isolation of internal EMI-generating circuits etc.).

5.2. Biomedical applications

After the discovery in the 1980s of their compatibility with many biological molecules, research on conducting polymers for biomedical applications grew significantly. Studies have included: electrical stimulation, use in cell adhesion and migration, application in DNA synthesis and protein secretion [394–397]. Specifically, many of these studies involved nerve, bone, muscle, and cardiac cells, which respond to electrical impulses. COPs present a number of important advantages for biomedical applications, including biocompatibility, ability to entrap and controllably release biological molecules (i.e., reversible doping), ability to transfer charge from a biochemical reaction, and the potential to easily alter the electrical, chemical, physical, and other properties of the COPs to better suit the nature of the specific application. These unique characteristics are useful in many biomedical applications, such as biosensors, tissue-engineering scaffolds, neural probes, drug-delivery devices, and bio-actuators. Moreover, COPs are inexpensive, easy to synthesize, and versatile because their properties can be readily modulated by the wide range of molecules that can be entrapped or used as dopants. In addition, COPs permit control over the level and duration of electrical stimulation for tissue engineering applications, a limitation of electrets. COPs can also be tailored to create substrates with high surface area, a key aspect to decreasing impedance in neural probes.

5.2.1. Biomolecular sensing

The first biosensing device was created by integrating an enzyme into an electrode,[398] and since that time, much progress has been made in monitoring and diagnosing metabolites (e.g., glucose, hormones, neurotransmitters, antibodies, antigens) for clinical purposes. A biosensor is composed of a sensing element (i.e., biomolecule) and a transducer.[399] The sensing element interacts with the analyte of interest producing a chemical signal that is transmitted to the transducer, which ultimately transforms the input into an electrical signal. COPs are extensively used as transducers that integrate the signals produced by biological sensing elements such as enzymes.

Depending on how the chemical signal is sensed and transmitted, biosensors can be distinguished in: amperometric (measures current), potentiometric (measures potential), conductometric (measures change in conductivity), optical (measures light absorbance or emission), calorimetric (measures change in enthalpy), and piezoelectric (measures mechanical stress). The most common types of transducers are amperometric and potentiometric. An amperometric biosensor measures the

current produced when a specific product is oxidized or reduced at a constant applied potential.[399] The COP mediates the electron transfer (e.g., via hydrogen peroxide) between an enzyme, such as an oxidase or dehydrogenase, and the final electrode. Potentiometric biosensors use ion-selective electrodes as physical transducers. For example, detection of urea by ureases is performed via the production of NH_3, which interacts with PPy to produce an electrical signal. This signal could be a product of a change in pH and the subsequent ion mobility in the polymer matrix triggered by an equilibration of the dopants with the free ions in solution.[400, 401]

However, for biosensor applications electroactive materials (COPs) have been modified, integrating on its surface specific biological recognition components (bioactive macromolecules). Many different techniques have been developed for the immobilization of biologically active molecules on COPs, but in general they can distinguished in Two main classes: non-covalent and covalent modifications. Non-covalent modifications include adsorption, physical entrapment, and affinity binding. Covalent immobilization includes all techniques that create a covalent bond between the conducting substrate and the biomolecule via functional moieties.[402, 403]

Physical adsorption is the simplest method of immobilization and one of the first approaches used for biosensors. Although adsorption is simple, controlling the concentration of the immobilized compound is difficult and immobilization is not stable because of the weak non-covalent forces involved, which decrease the lifetime of the biosensor.[403] Another drawback is that compound adsorption occurs as a monolayer, which limits the quantity of sensing element. An alternative to adsorption is physical entrapment of the desired biomolecule during electropolymerization, which is one of the most extensively used techniques. During this process monomer, dopant, and biomolecules are mixed in a single solution used for electrochemical polymerization. This process is usually performed under mild conditions (i.e., neutral pH, aqueous, low oxidation potentials) without chemical reactions that could alter the activity of proteins, and only requires a single step for both polymerization and molecule immobilization. Although entrapment is a popular immobilization technique, it has some important limitations. For example, the hydrophobic nature of the polymer compromises the quaternary structure of proteins, decreasing their biological activity. To overcome this limitation, new alternatives have focused on creating more hydrophilic polymers using modified monomers, such as pyrrole rings with long hydrophilic chains.[404, 405]. Also, entrapment methods require a high concentration of the biomolecule (~0.2–3.5 mg/mL), which is not always available and increases the cost of the process. Finally, the entrapment procedure diminishes the accessibility of analytes to the sensing element and thus affects affinity complex formation (e.g., antibody–antigen, hybridization of nucleotides). As a result, other immobilization techniques, such as affinity binding and covalent modification, have been explored

to overcome these limitations. Affinity binding methods are based on immobilizing molecules on the surface of COPs via strong non-covalent interactions. An attractive alternative to affinity binding for biomolecule attachment involves the introduction of appropriate functional groups into COPs backbones or the surface modification of the polymers, followed by covalent bonding (i.e., grafting) of bioactive macromolecules to the surfaces. In comparison to adsorption, entrapment, and affinity binding immobilization, this approach is typically more robust and stable to external environmental factors, allows high loading, and increases biosensor lifetime; however, it is usually more complex and sometimes requires reaction conditions not suitable for biomolecules. Compared to the entrapment methods, surface chemical conjugation increases the accessibility of the analytes and enhances the formation of affinity interactions. Another conjugation method is chemical grafting after polymerization of unmodified COPs.

5.2.2. Biomolecular actuators

Bioactuators are devices that are used to create mechanical force, which in turn can be used as artificial muscles. COP scaffold subject to an electrical stimulation shows a change in the volume. This property can be exploited for the construction of bioactuators. Artificial muscles consist of a three-layers system, where two outer layers are made of COP and the middle layer comprises a non-conductive material.[406, 407] When current is applied across the two COP films, one of the films is oxidized and the other is reduced. The oxidized film expands owing to the inflow of dopant ions, whereas the reduced film expels the dopant ions and in the process shrinks, as shown in Scheme 5.1.

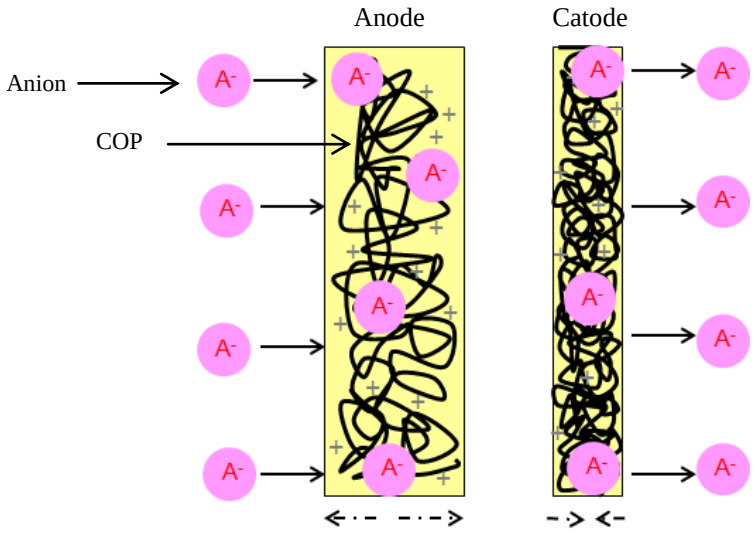

Scheme 5.1.: volume change as a consequence in an oxidation/reduction process for a bioactuator.

Ions can enter the polymer either in the oxidized state as shown in Equation (5.3.) or in the reduced state as in Equation (5.4.):[408]

$$P^+A^- + e^- \Longleftrightarrow P^0 + A^- \qquad \text{Eq. 5.3.}$$

$$P^+A^- + C^+ + e^- \Longleftrightarrow P^0 + (AC) \qquad \text{Eq. 5.4.}$$

where P^+ represents the polymer in doped oxidized state and P^0 the polymer in undoped reduced state. P^+A^- indicates that an anion A^- is incorporated in the polymer as the dopant ion and $P^0(AC)$ indicates that a cation is inserted during reduction. The combined effect of simultaneous expansion and contraction is translated into a mechanical force that bends the polymer, which mimics the effect of muscles in biological systems.[409]

5.2.3. Tissue engineering

In order to employ a material for tissue engineering applications this has to show good conductivity, reversible oxidation, redox stability, biocompatibility, hydrophobicity (40–70°C water contact angle promotes cell adhesion), three-dimensional geometry and surface topography. These are typical characteristics of COPs and for this reason they are widely used in this field.

Polypyrrole was one of the first materials investigated for this purpose. Several studies have demonstrated cell and tissue compatibility of PPy *in vitro* and *in vivo*. To date, it has been demonstrated that PPy can be used to support cell adhesion and growth of a number of different cell types, including endothelial cells,[396, 410, 411] rat pheochromocytoma (PC12) cells,[412, 413] neurons and support cells (i.e., glia, fibroblasts) associated with dorsal root ganglia (DRG),[414, 415] primary neurons,[416, 417] keratinocytes,[418] and mesenchymal stem cells.[419] Besides studies on its biocompatibility PPy doped with *p*-toluene sulfonate (TS) was investigated as material for electrical stimulation of cells and it was observed that it can modulate cellular response. Electrical stimulation of PPy in its oxidized form can also be used to modulate cell function.[413] For example, PC12 cells seeded on electrochemically synthesized PSS (polystyrenesulphonate)-doped PPy films having a resistivity of ~1kΩ were found to exhibit a ~91% increase in median neurite length when a positive potential of 100mV was passed through the PPy for 2 h.[413] These studies demonstrate that cell growth and function can be drastically enhanced at the interface of PPy undergoing electrical stimulation. However, the oxidation/reduction processes of the COPs can affect the cell activities in different ways. For example, bioactive molecules can be adsorbed, entrapped or expelled during the electrochemical processes. These phenomena can have positive or

negative effects on the cells depending on the type of bioactive molecule involved. Sometimes, in fact, this approach is used to entrap biomolecules, such as adenosine 5'-triphosphate (ATP) [420–422] and nerve growth factor (NGF) [412] in PPy and other COPs for both drug delivery and tissue engineering applications. In addition to its surprising electrical conductivity, another important characteristic of PPy that has be taken into account is its mechanical properties. As reported earlier, COPs, such as PPy and PANI, are crystalline and brittle and for this reason cannot be considered ideal candidate for tissue scaffold materials.

In order to overcome this limitation PPy was modified in form of composite (e. g., PPy/polystyrene [423]) or by covalent modification (e. g., PPy functionalized at the β position with either a methyl ester or a carboxylic acid side chain [424]). However, polypyrrole modified with polystyrene suffers from low biodegradability. For this reason other copolymers were investigated. Among them polylactic acid (PLA) seems to be the most performing so PPy nanoparticle–PLA composites were created and shown to be both degradable and conductive (resistivity ranging from $2 \cdot 10^7$–15 Ω · cm).[425] Both parameters could be modulated by varying the amount of PPy in the blend.

Unlike that for PPy, the interest in PANI for this kind of applications has been slower. However, more recently the investigations on this polymer for tissue regeneration have risen. It has been proven that biocompatibility of PANI is specific to particular cells. Many efforts have been directed to improve biocompatibility, conductivity, and mechanical properties of polyaniline. Most of these strategies involve noncovalent and covalent techniques, as previously reported for PPy-based materials. Cell biocompatibility of doped PANI (with HCl) has been observed in vitro.[426] However, an initial lag in cell (cardiac myoblast) growth rate was found in the presence of doped PANI. It can be attributed to the acid leaching from doped polymer in the cell medium that causes a decrease in conductivity. For this reason other methods have been investigated to modify PANI to render it biocompatible maintaining at the same time the desirable electroconductivity. For example, composites of PANI-PEO-PPO (PEO= polyethylene oxide, PPO= polypropylene oxide), where PPO is entrapped within PANI while PEO is exposed at the surface, show higher hydrophilicity and conductivity (~0.6 S/cm).[427] Similarly, PANI–chitosan nanocomposites are characterized by biocompatibility and good surface characteristics.[428] Moreover, PANI–gelatin composites have been demonstrated to have good biocompatibility in vivo and enhanced mechanical properties that allow it to be electrically spun into fibers to generate three-dimensional scaffolds.[228] Concerning covalent modification, direct modification of the aniline monomer to create a functional group (methyl chloride) allows to link PANI with other species, for example aminoacids.[429] This kind of modification results in good PC12 cell attachment, proliferation, and response to NGF.

5.2.4. Drug delivery systems

Current drug-delivery systems are effective at the controlled release of drugs, even though the application is still narrowed to targeting cell clusters rather than the individual cells. The possibility of having more specific novel drug-delivery systems opens the way to new formulations alternative to the traditional ones. COPs, properly electrostimulated, are able to release a number of therapeutic proteins and drugs, such as NGF,[412] dexamethasone,[430, 431] and heparin.[432] In fact, the change in volume of COPs upon electrical stimulation, discussed in the previous paragraph 5.2.3., has also been exploited for the development of actuators to create drug delivery devices.[433]

The scheme below (Scheme 5.2.) reports how polypyrrole works in drug release.

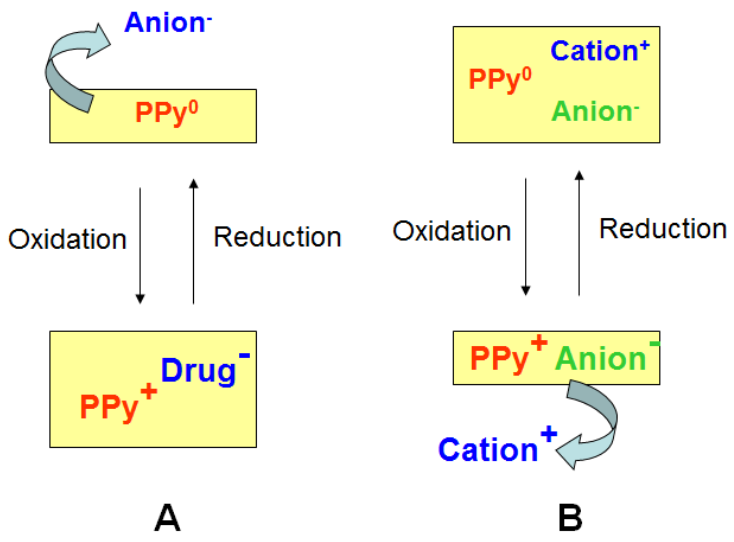

Scheme 5.2.: PPY drug release mechanism

PPY prepared with mobile anions (generally small anions) is able to release anionic drugs on reduction with a consequent contraction (A). On the contrary, PPY prepared with immobilised anions (generally big anions) incorporates cationic drugs on reduction with a consequent swelling and expels them on oxidation while contracting (B).[434]

More in detail, Hodgson *et al*. reported the release of bovine serum albumin and NGF entrapped within PPy doped with polyelectrolytes (e.g., dextran sulfate) under electrical stimulation.[412] Polyelectrolytes improve the release of the entrapped protein. For this release, PPy was reduced with negative potential, producing a rapid expulsion of anions with a mechanism similar to that reported in Scheme 5.2.

Using PPy as electroactive material and biotin as a co-dopant NGF was released under electrical stimulation.[435] For this application COPs provide great flexibility in the number and types of drugs that could be delivered.

5.3. Sensors applications

Polyaniline, as well as other conducting organic polymers,[436, 437] when exposed to specific conditions, such as acidic or basic vapors and liquids, such as HCl, ammonia gas,[438, 439] or ammonia water,[440, 306] CO_2,[441] as well as some neutral gases including chloroform,[442] alcohols,[443] etc., changes its electrical conductivity. This modification makes it a novel promising material for sensor applications. However, conventional PANI shows poor sensitivity because of the poor diffusion of analyte molecules into the polymer and its composites films.[444-446] On the contrary, one-dimensional nano-structured PANI exhibits the best performances, thanks to its significantly enhanced exposure area and penetration depth for gas molecule.[174, 446, 447]

Sensors can be classified depending on the mode of trasduction and the kind of application.

5.3.1. Sensors based on transduction

Sensors based on transduction are called transducers. They are devices that convert a signal in one form of energy to another form of energy. A sensor is used to detect a parameter in one form and reports it in another form of energy, often an electrical signal.

5.3.1.1. Potentiometric sensors

Potentiometric sensors can be distinguished into symmetric and asymmetric. A potentiometric sensor either symmetric [448] or asymmetric [449] depends on the homogeneous and heterogeneous interface between the dipolar layers of charges. Symmetrical potentiometric sensors are classical electrodes in which the ion-selective membrane is placed between two solutions. In an asymmetrical ion selective electrode, one side of the membrane is in contact with a solid phase while the other one is exposed to the measured solution. A potentiometric sensor measures the change in potential caused by a chemical reaction that separates electric charge.

Potentiometric sensors based on the combination of electropolymerized materials and neutral ionophores offer attractive advantages in food analysis.[450] More in detail, PANI was successfully used in potentiometric sensors for pH measurement,[451, 452] and the determination of different species, such as ammonia,[453] metal ions,[454–456] sulfite,[457] antioxidants and many other compounds.[458–464].

5.3.1.2. Amperometric sensors

An amperometric sensor is a detection and quantitative measurement device in which redox events associated with the selective recognition of an analyte of interest are processed by an

electrochemical transducer to produce signal in form of current, whose magnitude is proportional to the quantity of analyte present. The recognition component of an amperometric sensor usually consists of an electroactive redox substance (e. g., COPs) or composite of chemical or biological origin intimately connected to the transducer's electronics. Amperometric sensors measure the current generated at the surface of the electrode as a result of electron transfer from the oxidation or reduction reaction of the electroactive species, typically at a constant applied potential. Umana & Waller proposed a new amperometric sensor based on an enzyme (glucose oxidase) immobilized on a film of PPy during the electropolymerization of the corresponding monomer.[395] This electrode is useful to detect glucose in aqueous solutions for a period of up to 7 days.

5.3.1.3. Piezoeletric sensors

Piezoelectric sensors measure the electrical potential caused by applying a mechanical force (pressure, acceleration, strain or force) to a piezoelectric material, that is a material that produces an electric field when exposed to a change in dimension caused by an imposed mechanical force (piezoelectric or generator effect) or, conversely, produces a mechanical stress when subjected to an applied electric field (electrostrictive or motor effect). The effect of an applied pressure on the electrical properties of conducting composites has been studied under static [465] and dynamic [466, 467] conditions. Some materials exhibit a decrease of the electrical resistivity when a compressive force is applied on their surface, as a result of the reduction of the inter-particulate distance and the subsequent formation of conducting networks inside the insulating matrix.[465, 468–470] In contrast, other systems present the opposite behavior; the electrical resistivity increases while the material is being pressed due to the disconnection of the conducting particle contacts caused by the shear stress components and the ensuing rupture of the paths of charge carriers.[466] These contradictory results indicate that a specific piezo-resistive response of a conducting composite should be related to the microstructure of the material and, also, to the experimental conditions in which the study was performed.

5.3.1.4. Calorimetric/thermal sensors

A thermistor is a type of resistor whose resistance varies significantly with temperature. This kind of materials can be used as cheap and sensitive temperature sensors. Conducting organic polymers in combination with enzymes have been used for this purpose.[471]

5.3.1.5. Optical sensors

An optical sensor is a device that converts light rays into electronic signals. More in particular, it measures light absorbed or emitted as a consequence of a biochemical reaction. Optical sensors have been used in new technologies for detecting small amounts of chemical, gaseous species. In this context, polyaniline and polypyrrole have been strongly investigated thanks to their amazing optical properties that make them powerful materials for the determination of chemicals in vapour and liquid state. Polymer nanofibers, such as polyaniline nanofibers, with uniform diameters less than 500 nm can be made in bulk quantities through a facile aqueous and organic interfacial polymerization method at ambient conditions. The nanofibers have lengths varying from 500 nm to 10 μm and form interconnected networks in a thin film. Thin film nanofiber sensors can be made of the polyaniline nanofibers having superior performance in both sensitivity and time response to a variety of gas vapors including acids, bases, redox active vapors, alcohols and volatile organic chemicals.[472]

5.3.1.6. Pressure sensors

A pressure sensor measures pressure, typically of gases or liquids. Pressure is an expression of the force required to stop a fluid from expanding, and it is usually stated in terms of force per unit area. A pressure sensor usually acts as a transducer; it generates a signal as a function of the pressure imposed.

Pressure sensors can be used to indirectly measure other variables such as fluid/gas flow, speed, water level, and altitude. Pressure sensors can alternatively be called pressure transducers, pressure transmitters, pressure senders, pressure indicators and piezometers, manometers, among other names.

Pressure sensors can vary drastically in technology, design, performance, application suitability and cost and can be classified in terms of pressure ranges they measure, temperature ranges of operation, and most importantly the type of pressure they measure. Pressure sensors are variously named according to their purpose, but the same technology may be used under different names.

Generally it is possible to distinguish:

Absolute pressure sensor: it measures the pressure relative to perfect vacuum;

Gauge pressure sensor: it measures the pressure relative to atmospheric pressure. A tire pressure gauge is an example of gauge pressure measurement; when it indicates zero, then the pressure that it is measuring is the same as the ambient pressure.

Vacuum pressure sensor: it is a sensor that measures pressures below atmospheric pressure, showing the difference between that low pressure and atmospheric pressure (i.e., negative gauge

pressure), but it may also be used to describe a sensor that measures low pressure relative to perfect vacuum (i.e. absolute pressure).

Differential pressure sensor: it measures the difference between two pressures, one connected to each side of the sensor. Differential pressure sensors are used to measure many properties, such as pressure drops across oil filters or air filters, fluid levels (by comparing the pressure above and below the liquid) or flow rates (by measuring the change in pressure across a restriction). Technically speaking, most pressure sensors are really differential pressure sensors; for example a gauge pressure sensor is merely a differential pressure sensor in which one side is open to the ambient atmosphere.

Sealed pressure sensor: this sensor is similar to a gauge pressure sensor except that it measures pressure relative to some fixed pressure rather than the ambient atmospheric pressure (which varies according to the location and the weather).

It is important to discuss also the characteristics which are used to quantify all sensors.

Accuracy: the accuracy of a sensor relates to its ability to measure the absolute value of a specified metric. Very accurate sensors typically require calibration to a known standard to account for drift and changes in environmental conditions. For example, a user will typically tare a microbalance before making a precise weight measurement. This characteristic is particularly relevant to polyaniline sensors because the electrochemical properties of polyaniline may vary widely with environmental characteristics such as electrolyte species/concentration and temperature, as well as material characteristics such as oxidation state, microstructure, and molecular weight.

Precision: it is a measure of a sensor's ability to produce the same output with identical inputs. Precision incorporates repeatability, when multiple measurements are taken over a short period of time, as well as reproducibility, when multiple measurements are taken over long periods of time, by different users, with different instruments, or at different locations. The key to high reproducibility in polyaniline sensors is to ensure that the pretreatment of the polymer is consistent, as the equilibrium chemical state of polyaniline depends on its oxidation history.

Resolution: the resolution, also known as discrimination, of a strain sensor is defined as the smallest deflection which produces a detectable output. While this is important characteristic in any strain sensing device, it is generally a result of noise within all the components of a strain measuring instrument, and not the sensing element alone. For this reason, examining resolution is not particularly relevant to the fundamental electrochemical properties of polyaniline.

Range: the input range will dictate the operational conditions of a sensor, and the output range will dictate the system required to interpret the signal. The input range of a polyaniline sensor is limited by the greatest strain which can be applied to the material before inducing permanent damage or

deformation. The output range will influence the type of circuitry required to interpret the signal, primarily whether amplification is necessary.

Sensitivity: it is a measure of the slope of the output with increasing input. The magnitude of the electrical output of polyaniline will depend on how efficiently work done by stretching a polyaniline film can be converted into electrical energy. This characteristic will dictate the viability of polyaniline based energy harvesting devices.

Linearity: like sensitivity, linearity takes into account the slope of the output with increasing input; however it focuses on the slope variation over the functional range of the sensor. Non-linear sensors require more complex systems to interpret the output signal, but non-linearity can be corrected with a calibration curve.

Hysteresis: it is the dependency of the output signal on the trajectory of the input. In a polyaniline sensor, hysteresis may depend on input factors such as strain rate or whether applied strain is positive or negative.

Random Error: also called noise, random error is sensor output which does not result from the input. This type of error typically affects the resolution of a sensor; as the output signal to noise ratio (S/N) approaches 1, it becomes difficult to distinguish the two. The time dependency of ion diffusion into polyaniline will reduce high frequency noise produced by ambient vibrations.

Systemic Error: it is introduced through inputs which are unintentional or out of the control of the user. These inputs can be introduced via operational/observational variation (user error), drift, attenuation or distortion of the signal in the transmission system, or environmental changes such as temperature variation. Systemic errors typically affect the accuracy of a sensor, and can be corrected using compensation methods such as internal calibration standards, filtering, and feedback. Ensuring that the test fixture is well constructed and the methodologies are consistent will help to reduce systemic variation in polyaniline sensor output. Testing polyaniline in steady state conditions will reduce drift.

5.3.1.6.1. High pressure sensors

The measurement of high pressure is indispensable in many fields for national economy development and defense industry, especially in military production, research and experiment of strategy and tactics weapon. For instance, the applications of pressure measurements such as new materials synthesis in high pressure environment, underground nuclear weapon explosion, safety protection in highway, underwater shock wave measurement and protection in accident collision all call for high pressure sensors. The pressure to be measured in these applications reaches the level of GPa or even higher. Therefore, an ultra-high pressure sensor is not only indispensable for military

departments but also has a bright application for civilian use in the future. The sensor should be capable of working in harsh environments such as high pressure and high temperature, and keeping stability and reliability. Moreover, it should meet accuracy requirements in high pressure conditions.

Conducting organic polymers integrated with transducers have been investigated as sensor pressure. In fact, it is known that when an external ultra-high pressure is exerted onto a polymeric substance, the distances between the molecular chains decrease. The amount of internal defects and free volume will decrease, and the restrictions on molecular chain motions will increase. The increase in the molecular chain interactions will change some of the materials properties drastically. For instance, the electrical resistivity of polymer will be affected differently by different types and sizes of charge carriers when an external pressure exerted on the polymer increases. If the charge carriers are particles of large sizes such as ions, the decrease in free volumes and *inter*-chain distances will obstruct the mobility of ions between molecular chains. Consequently, the electrical resistivity will increase. Conversely, if the charge carriers are small particles such as electrons, the decrease in *inter*-chain distances will cause overlaps of molecular orbitals and enhance the mobility of charge carriers between molecular chains. Thus, the electrical resistivity will decrease.[473]

Zhang *et al*. reported the effect of high pressure (35-140 MPa) applied on PANI pellets and pressure time, demonstrating that increasing pressure and pressure time, conductivity value of PANI gradually increases to a maximum value and then decreases.[474] The same behaviour was observed from many other authors when PANI pellets were subjected to more high pressure (GPa).[475]

More recently, Varma and Jayalekshmi investigated the performances of PANI/MWCNTs (multi-walls carbon nanotubs) composites as pressure sensors.[476] They demonstrated the positive effect of MWCNTs in the polymeric matrix for this kind of applications. Moreover, many authors dealt with the effect of the variation of temperature on the conductibility.[477, 478]

Similar investigation were carried out on PPy and its composites in form of pellets and films obtaining similar results.[479-481]

5.3.1.6.2. Low pressure (touch) sensors

Tactile sensors are basically arrays of force sensors that enable monitoring across a whole specific surface area, and not only discrete points pressure monitoring. They are demanded in applications where unstructured environments or uncertainty are present, like minimal invasive surgery (MIS), robotics, rehabilitation, virtual reality, telepresence, or industrial automation.

Many different approaches have been proposed to fabricate these sensors, most of them are based on piezoresistive principles [482-489] or capacitive [490-494], and a few are based on optical [495] or piezoelectrical transduction.[496] Most of these sensors are made using technologies for micro-electro-mechanical systems (MEMS) on silicon [483, 490, 497] or on polymers.[482, 486, 494] These technologies are not orientated to large area devices, and many of them are proposed for applications that demand high spatial resolution and good performance in terms of errors, like MIS.[490] Moreover, most of these realizations have ranges in the order of hundreds of mN or even μN. Especifications for the sensors to be used in robotics depends on the especific application (for instance fine manipulation or assistance in moving people). However, ranges in the order of tens of Newtons per tactel are common.[498, 499] Sensors that cover larger areas and have also wider input ranges can be obtained by arranging single force sensors on a usually flexible substrate,[484, 489, 492] but this increases costs because many instances of these force sensors are needed and because they must be assembled on the substrate. To lower the cost of the sensor it is better to obtain the whole array in the batch fabrication process minimizing further assembly of separate components. The commercial capacitive sensor reported into ref. 498 is designed for manipulative tasks in robotics and is able to cover large areas and it is stretchable, so it can be mounted on freeform surfaces. However, signal conditioning of capacitive sensors is more complex than that for piezoresistive sensors and most proposals for large area low cost sensors are based on piezoresistive materials, especially to obtain smart tactile sensors with very compact electronics that can be placed close to the raw sensor.[500-502] A new generation of large tactile sensors are being developed and commercialized, where a piezoresistive polymer film is used,[503, 504] showing a decrease in electrical resistance when a normal force is applied. However, their use for large surface applications seems unlikely due to the high cost of materials used. The electroactive materials incorporated in currently developed configurations use metallic microparticles (silver) embedded on a polymer film, metallic central films (silver) separated by a pressurable elastomeric polymer film, or a combination of both of them.[503, 504] In spite of the valuable advances that these technologies show, the use of high cost materials such as silver is an important impediment since large surface applications cannot be afforded by these types of sensors. Another large area, flexible pressure sensor was proposed by Someya *et al*.[505] In this case, a pressure-sensitive flexible layer made of polydimethylsiloxane (PDMS) containing electrically conductive graphite particles was used. But once again, the fabrication process was complicated as well as the cost of the final device increased by the deposition of gold layers (vacuum evaporated) and polyimide layers (cured at 180°C). The technology developed by CIDETEC [506] uses conducting polymers as electroactive materials for construction of pressure sensors. The spincoating of flexible plastic films of

polyethyleneterephtalate (PET) with conductive inks obtained from conductive polymers results in a flexible conductive film on flexible plastic substrates. The presence of a roughness at microscopic level leads to a resistivity decrease when different pressures are applied. This new technology shows great advantages for application on high surface area.

5.3.2. Sensors based on application mode

Depending on the use of sensors, they can also be classified into different classes. In fact, it is possible to distinguish sensors employed to measure chemicals, such as gases or liquids, ions, alcohols, pH and humidity.

5.3.2.1. Chemical sensors

A chemical sensor is a device that transforms a chemical information, ranging from the concentration of a specific sample component to total composition analysis, into an analytically useful signal. The chemical information, mentioned above, may originate from a chemical reaction of the analyte or from a physical property of the system investigated. Chemical sensors have been widely used in such applications as critical care, safety, industrial hygiene, process controls, product quality controls, human comfort controls, emissions monitoring, automotive, clinical diagnostics, home safety alarms, and, more recently, homeland security. In these applications, chemical sensors have resulted in both economic and social benefits. An application of COPs for detection of gaseous analytes belongs to the well developed field of chemosensor design. Gases interacting with COPs can be divided in two main classes: gases which chemically react with COPs and gases which physically adsorb on COPs. Chemical reactions lead to changes in the doping level of COPs and alter therefore their physical properties like resistance or optical absorption. Electron acceptors like NO_2, I_2, O_3, O_2 are able to oxidize partially reduced COPs and therefore increase their doping level. To oxidize COPs, the gas should have a higher electron affinity than the COPs. NO_2 was found to increase the number of charge carriers in PANI [507] through oxidative doping with NO_2^- ions and therefore decrease the resistance. Oppositely, an oxidation of nanofibers of emeraldine salt by NO_2 to pernigraniline base state leads to an increase in resistance.[508] SO_2 also increases the number of charge carriers in PPY thus decreasing the resistance.[509] Electron donating gases like H_2S, NH_3 and N_2H_4 reduce and therefore dedope COPs, which leads to an increase in resistance. Ammonia [600, 511] and H_2S [512] were found to decrease the conductivity of COPs. Weak physical interactions of non-reactive volatile organic compounds (chloroform, acetone, aliphatic alcohols, benzene, toluene, etc.) with the polymer may lead to modification of COPs resistance. The mechanisms were not studied in details. An adsorption of ethanol and hexanol on dipentoxy

substituted polyterthiophene was supposed to change the potential barrier at the boundaries between COPs grains.[513] Resistance increases due to adsorption of chloroform, acetone, ethanol, acetonitrile, toluene and hexane on PANI, PPY and polythiophene derivatives were explained by COP swelling leading to a higher distance between the PANI chains [174, 514, 515] or by modification of the dielectric constant of COPs.[516] Acetone was suggested to diffuse into the inter-segmental spaces in the PPY matrices and thus destroying the dispersing interactions between aromatic pyrrole rings and inducing a higher disorder.[517] For such compounds as acetone a formation of hydrogen-bonds with PPY was also suggested. These interactions hinder electron jumping and hence decrease the conductivity of PPY. Interaction of methanol with emeraldine salt of PANI increases the number of charge carriers through hydrogen bonding of methanol with reduced amine sites in the polymer. On the contrary, such interaction of methanol with emeraldine base leads to twisting of the polymer chains, resulting in a lower mobility of the charge carriers and an increase of the polymer resistance.[518] Interaction of short chain aliphatic alcohols with various PANI derivatives increases the order in the polymer films which is accompanied by expansion of polymer chains and conductivity increase.[174, 443] Adsorption of short chain aliphatic alcohols to PANI/PSS blends is assumed to enhance the charge transfer between adjacent PANI particles by reducing of the potential barrier for hopping/tunnelling processes, or by increasing of interchain and interparticle charge mobility.[519] However, an adsorption of long chain aliphatic alcohols leads to higher film resistances, in this case a prevailing effect of these non-polar compounds is their insulating properties hindering charge transfer between polymer chains.[174, 443]

5.3.2.2. Ion-selective sensors

Generally, ion sensors have been developed taking the polymer as the conductive system/component, or as a matrix for the conducting system. When such systems come in contact with analytes to be sensed, some ionic exchange/interaction occurs, which in turn is transmitted as an electronic signal for display. Ion selective electrodes (ISE) are suitable for determination of some specific ions in a solution in the presence of other ions. The quantitative analysis of ions in solutions by ISEs is a widely used analytical method, with which all chemists are familiar. Commercial potentiometric devices of varying selectivity for both cations and anions are common in most laboratories.[520] Ion sensors find wide application in medical, environmental and industrial analysis. They are also used in measuring the hardness of water. Potentiometric ISEs for copper ions have been prepared by screen-printing, with the screen-printing paste composed of methyl and butyl methacrylate copolymer, copper sulphides and graphite.[521] Ion-sensitive chemical transduction is based on ion selectivity conveyed by ionophore—ion-exchange agents,

charged carriers and neutral carriers—doped in polymeric membranes. In addition to organic salts, several macrocyclics, such as antibiotics, crown ethers and calixerenes, are used as neutral carriers, functioning by host–guest interactions.[522-525]

The polymeric membrane-based device consists of an internal electrode and reference solution, the selective membrane across which an activity-dependent potential difference develops, and an external reference electrode to which the membrane potential is compared in the potential measurement. The response and selectivity of an ion-selective device depend on the composition of the membrane. A new Ca^{2+}-selective polyaniline (PANI)-based membrane has been developed for all-solid-state sensor applications.[526] The membrane is made of electrically conducting PANI containing bis [4-(1,1,3,3-tetramethylbutyl) phenyl] phosphoric acid (DTMBP-PO4H), dioctyl phenylphosphonate (DOPP) and cationic (tridodecylmethylammonium chloride, TDMACl) or anionic (potassium tetrakis (4-chlorophenyl) borate, KTpClPB) as lipophilic additives. PANI is used as the membrane matrix, which transforms the ionic response to an electronic signal. A new potentiometric sensor electrode for sulfide based on PPY films has been introduced by Atta *et al*.[527]

5.3.2.3. pH sensors

A simple and speedy device to measure the acidity and alkalinity of a fluid. A pH meter acts as a volt meter that measures the electrical potential difference between a pH electrode and a reference electrode and displays the result in terms of the pH value of the solution in which they are immersed.

From many years polyaniline has been investigated as new organic material to pH measure in aqueous solution.[528-531] Increasing pH at a given potential, polyaniline undergoes a deprotonation process that causes a gradually decrease of conductivity of the polymeric material. Similarly at a given pH changing potential conductivity changes. This is true for PANI but also for polypyrrole. Thanks to these propeties, De Marcos and Woldeis developed a pH sensor based on a film of PPy.[532] Many studies have focused on PANI.[533-536, 53]

5.3.2.4. Humidity sensors

Humidity sensors are useful for the detection of the relative humidity (RH) in various environments. These sensors attracted a lot of attention in the medical and industrial fields. The measurement and control of humidity are important in many areas, including industry (paper, food, electronic), domestic environment (air conditioner), medical (respiratory equipment), etc. Polymer, polymer composites and modified polymers with hydrophilic properties have been used in humidity sensor

devices. Venancio *et al*. described a new simple method to fabricate cheap and "throw-away" sensors for air moisture.[537] In the first step, a 16-finger *inter*-digitated graphite pattern was introduced onto a PET (polyethylene terephthalate) film or a copy paper by a specific procedure. In the second step, either a coating of PANI nanofibers was deposited on the pattern by dipping into the aqueous dispersion of 2-acrylamido-2-methyl-1-propane-sulfonic acid doped PANI nanofibers or an HCl-doped PANI film by in situ deposition. Sensitivity to moisture, which is given as the resistance change ratio of the sensors, of the sensor with PANI nanofibers (ΔR = 93.3% ± 19%) is much higher than the one with in situ deposited PANI film (ΔR =5.05% ± 0.79%), which, as explained, resulted from the higher active surface area of PANI nanofibers than the in situ deposited PANI film. PANI nanofibers were deposited on a SAW resonator as a selective coating to enhance the sensitivity of the humidity sensor.[538] In comparison with the uncoated oscillator, which did not show an obvious frequency change on humidity changes, the PANI nanofiber coated one exhibited a larger frequency shift. The sensitivity, in terms of $\Delta f/f$, was at least 16.8 ppm/ $(\%RH)^{-1}$ at room temperature, about two times higher than the best reported for SAW humidity sensors in publications. PANI nanofiber films were fabricated onto screen printed electrodes by using the chemical deposition method and investigated for humidity sensors.[539] At a lower relative humidity (<50% RH), the electrical resistance of the sensor decreased with increasing humidity. While at a higher relative humidity, the electrical resistance of the sensor increased with humidity. The reversed behavior was attributed to the distortion of the nanostructure or change in the oxidation state of PANI with the absorption of water molecules.

5.4. Other applications

Some other applications of COPs, like support for the lipase-mediated reaction,[540] a precursor for nanocarbons,[541] a reducing agent for gold nanoparticles with controlled sizes,[542] materials for batteries, catalysts, solar cells, hydrogen storage, field-effect transistors, fuel cells, etc.[543] were also reported but are not elaborated on here.

PART II: EXPERIMENTAL PART

Chapter 6: Synthetic methods

6.1. PANI preparation

Polyaniline was prepared by different techniques, using H_2O_2 or molecular O_2 as the oxidant and aniline monomer or its dimer (*N*-(4-aminophenyl)aniline) as the reagent.

6.1.1. PANI preparation from aniline monomer

Synthesis of Emeraldine Salt 1 (ES1) from aniline monomer was carried out according to a method reported in the literature.[544] In particular, aniline (5.0 g, 54.0 mmol) was dissolved in 40 mL of HCl 5 M. The solution was stirred at low temperature (ice bath). Then, an aqueous solution of $(NH_4)_2S_2O_8$ (22.0 g, 96.5 mmol in 80 ml water) was added drop by drop keeping the temperature in the 0-5 °C range. After 6 hours the green product was filtered on a buchner funnel, washed with water and acetone (to remove organic soluble oligomers), dried at 60°C until constant weight, powdered with a mortar and stored for future characterization and use.

The yield was 69%.

6.1.2. PANI preparation from *N*-(4-amonophenyl)aniline (aniline dimer)

Emeraldine Salt 2 (ES2) was synthesized from *N*-(4-aminophenyl)aniline (AD) using a green method previously developed by Della Pina *et al*.[36] 5.0 g (27.0 mmol) of AD were dissolved in 125 mL of HCl 1 M. After the complete dissolution of AD (*ca*. 30 minutes) 25 mL of an aqueous solution of H_2O_2 35% (H_2O_2/AD molar ratio ~ 10) and 50 mg of $FeCl_3{\cdot}6H_2O$ (AD/Fe molar ratio=150) were added under stirring. After 24 hours, a green product was filtered on a buchner funnel, washed with water and acetone (to remove organic soluble oligomers) until clearness of the mother liquors, dried at 60°C until constant weight, powdered with a mortar and stored for future characterization and use.

The yield was 81%.

6.1.3. PANI preparation from *N*-(4-amonophenyl)aniline (aniline dimer) using O_2 as the oxidant

500 mg (2.7 mmmol) of AD were dissolved in 30 mL of water. 10 mL of HCl 1 M (AD/HCl= 1, molar ratio) was added to the solution and the mixture was stirred for 30 minutes until complete dissolution of AD. 5 mg of $FeCl_3{\cdot}6H_2O$ (AD/Fe molar ratio=150) were added under stirring and the mixture was stirred under pressure of oxygen (2 bars) for 3 days at 80°C.

At the end of the reaction, mixture was cooled at room temperature and filtered on a buchner funnel. A green product was filtered on a buchner funnel, washed with water and acetone (to remove organic soluble oligomers) until clearness of the mother liquors, dried at 60°C until constant

weight, powdered with a mortar and stored for future characterization and use. The yield was 71%. This product will be called ES2'.

6.1.4. Aniline dimer-COOH (ADCOOH) preparation

The synthesis of aniline dimer-COOH (ADCOOH) was carried out according to a method reported in the literature.[344] *N*-(4-amonophenyl)aniline (0.9 g , 5.0 mmol) and succinic anhydride(0.5 g, 5 mmol) were dissolved in 30ml CH_2Cl_2 and stirred at room temperature for five hours. As the reaction proceeded, a white-grey precipitate was formed. At the end of the reaction, the precipitate was filtered on a buchner funnel, washed several times with diethyl ether until clearness of the mother liquors, dried at 60°C until constant weight, powdered with a mortar and stored for future characterization and use.

The yield was 90%.

6.2. PANI modification

Modifications carried out on PANI (ES1 and ES2) prepared by the methods described above were reactions of deprotonation, reprotonation with different acid dopants and reduction.

6.2.1. PANI deprotonation (dedoping)

ES1 and ES2 were separately dispersed in a solution of NH_4OH (NH_4OH/ES= 2, molar ratio) for three hours. At the end of the reaction, a dark violet precipitate was collected on a buchner funnel, washed with water abundantly until the mother liquors were neutral, dried at 60°C until constant weight, powdered with a mortar and stored for future characterization and use. The products obtained by the deprotonation of ES1 and ES2 will be called emeraldine base 1 and 2 (EB1 and EB2) respectively.

6.2.2. PANI reprotonation (redoping) with inorganic acids

500 mg of EB1 and EB2 were separately dispersed in 20mL of water. Different inorganic acids (HCl, H_2SO_4 and H_3PO_4) were added separately (aniline/inorganic acid=2, molar ratio). After 24 hours, reprotonated PANI (ES1/HCl, ES 1/H_2SO_4, ES1/H_3PO_4, ES2/HCl, ES2/H_2SO_4, ES2/H_3PO_4) were collected by filtration on a buchner funnel, washed with water abundantly until the mother liquors were neutral, dried at 35°C until constant weight, powdered with a mortar and stored for future characterization and use.

6.2.3. PANI reprotonation (redoping) with organic acids

500 mg EB1 and EB2 were separately dispersed in 50mL of CH_2Cl_2 for two hours. Dodecylbenzenesulfonic acid (DBSA) or camphorsulfonic acid (CSA) was added (aniline/DBSA=2, molar ratio) and the reaction mixtures were stirred for 24 hours at room temperature. Then, the products were filtered on a buchner funnel, washed several times with CH_2Cl_2, dried at 35°C until constant weight, powdered with a mortar and stored for future characterization and use. Solid products will be called PANI/DBSA(or CSA)$_{solid}$, whereas liquor mothers containing the corresponding soluble polymers will be called PANI/DBSA(or CSA)$_{solution}$. PANI/DBSA(or CSA)$_{solutions}$ were evaporated under vacuum by the use of a rotary evaporator, dried at 35°C until constant weight, powdered with a mortar and stored for future characterization and use. Their values of solubility in $CHCl_3$ were calculated (Table 6.1.).

Sample	Solubility in $CHCl_3$ (mg/mL)
PANI1/DBSA$_{solution}$	8
PANI2/DBSA$_{solution}$	26
PANI1/CBSA$_{solution}$	4
PANI2/CBSA$_{solution}$	22

Table 6.1.: Solubility in $CHCl_3$ of PANI1(2)/DBSA(CSA).

6.2.4. PANI reduction (synthesis of Leucoemeradine, LE)

Leucoemeraldine (LE) was prepared following the synthesis described by Green and Woodhead.[49, 50] 1 g of EB1 and EB2 was separately dispersed in 10 mL of a hydrazine solution 35 % and the reaction was stirred for 5 hours. At the end of the reaction, the product was filtered, washed abundantly with water, dried under vacuum and stored under nitrogen.

6.3. Metal oxides nanoparticles preparation

Fe_3O_4 nanoparticles (NPs) were prepared by different techniques: chemical co-precipitation method, metal vapour synthesis (MVS) solvothermal method.

All the other metal oxides were prepared only by the chemical co-precipitation method.

6.3.1. Fe_3O_4 nanoparticles (NPs) preparation

6.3.1.1. Fe_3O_4 nanoparticles (NPs) preparation by co-precipitation method

Fe_3O_4 NPs powder-type (Fe_3O_4 NPs_p) were prepared according to the method of Deng *et al*.[545] 3.2 g of $FeSO_4 \cdot 7H_2O$ were dissolved in 70 mL of water in the presence of 70 mg of poly(ethylene glycol) (PEG) under nitrogen atmosphere. 0.6 mL of H_2O_2 30% (w/w) (Fe: H_2O_2 = 3:1, molar ratio) were slowly added and the pH was corrected to 13 by adding NaOH 8 M. The reaction mixture was stirred at 50°C for 6 h. The black product was recovered by magnetic separation, washed several time by water, dried in oven at 110°C overnight until constant weight, powdered with a mortar and stored under inert atmosphere (N_2) for future characterization and use.

The yield was 91%.

Fe_3O_4 NPs ferrofluid-type (Fe_3O_4 NPs_{ff}) were prepared according to the method of Xu et al.,[546] but with some variations.

Thus, 6.0 g of $FeCl_3 \cdot 6H_2O$ and 2.2 g $FeCl_2 \cdot 4H_2O$ were dissolved in 25 mL of water and stirred in a 200 mL beaker under nitrogen atmosphere at 80°C. Then 12.5 mL of ammonia solution were rapidly added into the solution and the mixture was kept reacting for 30 min. After adding 0.94 g of oleic acid to the black dispersion, the stirring was maintained for other 90 min. The magnetic powder was collected by a magnet at the bottom of the beaker, the supernatant liquid removed and the solid residue washed several times with water. After drying overnight in air, the solid material was transferred into 100 mL of toluene thus obtaining a stable magnetic ferrofluid solution (40% w/w).

6.3.1.2. Preparation of Fe_3O_4 nanoparticles (NPs) with a mean diameter of 2.3nm (MNP_3) by Metal Vapour Synthesis (MVS) technique

Following the metal vapour synthesis technique, 250 mg of metallic iron were evaporated in 100mL of acetone. This solution of Fe nanoparticles was maintained under inert atmosphere (Ar) at -40°C. Then, 1 mL of oleic acid was added and the solution was maintained at room temperature in air. After 24 hours Fe_3O_4 nanoparticles were separated by centrifugation. They were re-dispersed in 75 mL of *n*-hexane obtaining a stable colloidal solution. The ICP analyses showed an iron content of 187.5 mg. The TEM analyses confirmed the presence of Fe_3O_4 nanoparticles having a mean diameter of 2.3 nm with a distribution ranging from 1 to 4 nm.[547]

6.3.1.3. Fe_3O_4 nanoparticles (NPs) preparation by solvothermal method

6.3.1.3.1. Preparation of Fe_3O_4 NPs with a mean diameter of 10.0 nm (MNP_2)

In a 50 mL three-necked flask $Fe(CO)_5$ (2.13 mmol), oleic acid (8.51 mmol) and octyl ether (12 mL) was mixed under nitrogen and magnetic stirring. The molar ratio between precursor and surfactant was 1:4 and the precursor concentration was ca. 0.18 M. The solution was heated at 105°C for 10 minutes, then (with a rate of 3°C/min) until 285°C and kept at this temperature for 1h. After cooling at room temperature, the solution was washed with acetone and centrifuged at 6000 rpm for 10 minutes once and then 2 times with petroleum ether. Finally, NPs were dispersed in toluene.[548]

6.3.1.3.2. Preparation of Fe_3O_4 NPs with a mean diameter of 27.0 nm (MNP_1)

In a 50 mL three-necked flask Fe-oleate (1.52 mmol), trioctylamine (30 mmol) and oleic acid (0.76 mmol) was mixed under nitrogen and magnetic stirring. The solution was heated until to 360°C (3.3°C/min) and kept at this temperature for 30 min. The mixture was cooled at room temperature, then washed with acetone and centrifuged at 6000 rpm for 10 minutes for 5 times. At the end NPs were dispersed in toluene.[549]

6.3.2. Preparation of Fe_3O_4 nanoparticles capped with aniline dimer–COOH

Below different methods to prepare Fe_3O_4 nanoparticles capped with aniline dimer–COOH are reported. The one-step method is taken from the scientific literature,[344] the two-step technique represents an innovative approach.

6.3.2.1. One-step preparation of Fe_3O_4 nanoparticles capped with aniline dimer–COOH

The synthesis of Fe_3O_4NPs capped with ADCOOH (Fe_3O_4 $NPs_{ADCOOH)}$ was carried out according to a method reported in the literature.[344] $FeCl_2 \cdot 4H_2O$ (0.9 g) and $FeCl_3 \cdot 6H_2O$ (2.4 g) were dissolved under N_2 in demineralized Milli-Q water (20 ml) under vigorous stirring. The solution was heated to 60°C and, then, 5 ml of a solution of NH_4OH (28% w/w) was quickly added, immediately followed by addition of a solution of aniline dimer–COOH (different amount of ADCOOH in 2 ml of acetone). Mixture was stirred for 1 hour at 80°C. The reaction mixture was then cooled slowly to room temperature. A dark powder was filtered, washed sequentially with acetone and ethanol, dried at 60°C until constant weight, powdered with a mortar and stored for future characterization and use.

The yield was 65%.

6.3.2.2. Two-step preparation of Fe_3O_4 nanoparticles capped with aniline dimer–COOH

1 mL of Fe_3O_4 NPs_{ff} prepared in section 6.3.1.1. were dried by the use of a rotary evaporator. Fe_3O_4 NPs_{ff} were washed several timed (*ca*. 10) with acetone to remove oleic acid and dried.

Meanwhile, ADCOOH was dissolved in different solvents (acetone, methanol, tetrahydrofuran and 1, 4-dioxane). The concentration of these organic solutions is reported in Table 6.2.

ADCOOH (mg)	Solvent (mL)	Concentration (mg/mL)
100	5	20
"	"	"
"	"	"
50	"	10

Table 6.2.: Concentration of solutions containing ADCOOH in different solvents.

2 mL of each solution were put in contact with Fe_3O_4 NPs_{ff} , washed as described above, for 12 hours.

Fe_3O_4 NPs_{ADCOOH} were recovered by centrifugation, dried at 60°C until constant weight, powdered with a mortar and stored for future characterization and use.

6.3.3. MFe_2O_4 (M= Co, Ni, Mn, Cu, Zn and Mg) nanoparticles preparation by co-precipitation method

All the other metal oxides were prepared only as powder-type following a typical chemical co-precipitation method. Aqueous solutions of Fe^{3+} 0.3 M (solutions A) and M^{2+} 0.15 M (solutions B) were prepared dissolving the correct amounts of salts in HCl 0.4 M. 20 mL of solution A and 20 mL of solution B were mixed together and stirred for 20 minutes at 80°C under nitrogen atmosphere. Then, a solution of NaOH 1.5 M was quickly added until pH 13 under vigorous stirring. After 2 hours, the products were magnetically decanted, washed repeatedly with distilled water until neutral pH, dried in oven at 110°C overnight until constant weight, powdered with a mortar and stored for future characterization and use.

All yields were ~ 85 %.

6.4. PANI/MFe_2O_4 (M= Fe, Co, Ni, Mn, Cu, Zn and Mg) composites preparation

PANI/MFe_2O_4 were prepared by oxidative polymerization of aniline dimer, using H_2O_2 or molecular O_2 as the oxidants in the presence of the corresponding amount of MFe_2O_4.

The products obtained by these reactions will be labeled as follows: PANI/MFe_2O_4.

6.4.1. PANI/MFe_2O_4 composites preparation using H_2O_2 as the oxidant

The typical synthesis was conducted as follows: 500 mg (2.7 mmol) of AD were dispersed in 30 mL of water. 2.7 mL of HCl 1 M (AD/HCl= 1, molar ratio) were added into the solution and the mixture was stirred for 30 minutes until complete dissolution of AD. Then, 1.2 mL of an aqueous solution of hydrogen peroxide 35% (H_2O_2/AD= 5, molar ratio) were added. Finally, different amounts of MFe_2O_4 (as prepared in sections 6.3.1., 6.3.2., 6.3.3.) were added into the solution. After 24 hours, a dark product was recovered by filtration on a Buchner funnel and washed repeatedly with water and with acetone until clearness of the mother liquors. The product was dried in an oven at 60°C until it reaches a constant weight, powdered with a mortar and stored for future characterization and use.

6.4.2. PANI/MFe_2O_4 composites preparation using O_2 as the oxidant

The typical synthesis was conducted as follows: 500 mg (2,7 mmol) of AD were dispersed in 30 mL of water. 2.7 mL of HCl 1 M (AD/HCl= 1, molar ratio) was added into the solution and the mixture was stirred for 30 minutes until complete dissolution of AD. Then, different amounts of MFe_2O_4 (as prepared in sections 6.3.1., 6.3.2., 6.3.3.) were added into the solution. The dispersion was stirred under pressure of molecular oxygen (3 bars) for 3 days at 80°C. Finally, a dark product was filtered on a Buchner funnel, washed repeatedly with water and with acetone until clearness of the mother liquors, dried in an oven at 60°C until it reaches a constant weight, powdered with a mortar and stored for future characterization and use.

6.5. PANI nanofibers preparation by electrospinning technique

$PANI1/DBSA_{solution}$ and $PANI2/CSA_{solution}$ were used to produce PANI nanofibers by electrospinning process.

6.5.1. Spun solutions preparation

Poly(ethylene oxide) (PEO; Mw=600000) and Poly(methy lmetacrilate) (PMMA; Mw=1000000; 350000) were used as binder (co-polymer). Concerning PANI/PEO blends, samples ($PANI1/DBSA_{solution}$, and $PANI2/CSA_{solution}$ were dissolved in $CHCl_3$ using the values of solubility reported in Table 6.1. The amount of PEO into the organic solutions of $PANI/DBSA_{solution}$ ranged from 0 to 1% wt with respect to the amount of PANI.

Concerning PANI/PMMA blends, PANI/DBSA was dissolved in a mixture of $CHCl_3$:DMF 5:1w/w maintaining a concentration of 7-8 mg/mL.

The amount of PMMA ranged from 30 to 83% wt with respect to the amount of PANI.

Once PEO or PMMA were added into the polymeric solution, mixture was stirred for 12 hours at room temperature. In all cases homogeneous solutions were obtained. No phase separation was observed before use.

Chapter 7: Characterization techniques

7.1. Spectroscopic techniques

As far as spectroscopic techniques are concerned, FT-IR, UV-vis and AAS spectroscopies were employed, as described below.

7.1.1. Fourier Transform Infrared (FT-IR) spectroscopy

A small amount of product was mixed with KBr and finely crushed. The resulting powder was, then, compressed in 13 mm diameter pellets with a 10 ton hydrostatic press and analysed on a Jasco FT-IR 410 spectrometer. The range of the measurement was 500-4000 cm^{-1} with a resolution of 0.5 cm^{-1}.

7.1.2. Ultraviolet-visible (UV-vis) spectroscopy

A small amount of product was dissolved in few millimetres of solvent (generally, *N*, *N*-dimethyl formamide or 2-pyrrolidone).

The blank, i.e. the spectrum of the solvent, was recorded before the sample in 1 cm optical path quartz cuvette, using an HP8453 diode array UV-vis spectrophotometer. The range of the measurement was 250-1100 nm with a resolution of 1 nm.

7.1.3. Atomic Absorption spectroscopy (AAS)

About 20 mg of product were dissolved in 5 mL of sulfonitric mixture at 80°C until dissolution. Then, the excess of acid was evaporated and the solution was diluted with MilliPore water and analyzed using a Perkin Elmer3100 spectrometer. Wavelengths were set as reported in Table 7.1.

Metal	λ (nm)
Fe	248.7
Co	240.7
Ni	232.0
Cu	324.8
Zn	213.9
Mg	285.2
Mn	279.5

Table 7.1: Values of wavelength used to quantify metals in AAS.

The concentrations of metals into the solutions, and hence in the composite materials, were calculated from absorbance *via* a linear regression on the data obtained analysing 1, 5, 7.5, 10 ppm standard metals solutions.

7.2. Thermogravimetric technique

Thermograms of samples were carried out on a Perkin Elmer TAC 7/DX instrument. In each experiment, a small amount of sample (about 10 mg) was put on a platinum pan and heated under N_2 in the range of 50-1000°C with a heating rate of 1°C/min.

7.3. Mass spectrometry

Liquid secondary ion spectrometry (LSIMS) was employed. Spectra were acquired on a VG Autospec M246 double focusing mass spectrometer operating in the positive ion mode in the range of 150-500 z/m. 3-Nitrobenzyl alcohol was used as the matrix.

7.4. NMR spectroscopy

^{1}H NMR spectra were recorded in D_2O on a Bruker 300 MHz instrument.

7.5. X-Rays powder diffraction

A small amount of product was placed in a sample quartz holder and analyzed using a Rigaku D III-MAX horizontal scan powder diffractometer with Cu Kα radiation. 2Θ ranged from 10 to 80 with an increment of 0.04 (2θ)/s.

7.6. Microscopic techniques

Morphological characterizations were carried out by TEM, SEM and STEM techniques as reported below.

7.6.1. Transmission Electron Microscopy (TEM)

TEM images were recorded using a Zeiss LIBRA EFTEM FEG TEM, operating at 200 kV and equipped with an in-column omega filter for energy selective imaging and diffraction.

The samples were prepared by drop drying a toluene solution in the nanoparticle samples case or an acetonitrile dilute suspension in the case of PANI/Fe_3O_4 nanocomposite samples.

Size distribution of studied samples were determined by a statistical analysis processed by means of the PEBBLES, freely available software developed in the Laboratory of Nanotechnology, ISTM-CNR.

7.6.2. Scanning Electron Microscopy (SEM)

The SEM specimens were prepared by drop-casting the polymeric suspension onto an aluminium foil and the measurements were carried out on a SEM-LEO 1430 microscope.

7.7. Electrical resistivity measurements

Electrical resistivity was measured by different techniques.

Electrochemical impedance spectroscopy (EIS): the electrical behaviour and the specific electrical conductivity σ ($S \cdot cm^{-1}$) of the solid materials were obtained by measuring the resistance R (Ω) by electrochemical impedance spectroscopy (EIS). AC-Impedance tests were performed on a pressed pellet of polymers using an AUTOLAB PGSTAT 30 Metrohm in the frequency range from 10 mHz to 1 MHz by applying an excitation ac-voltage of 10 mV rms.

Two-wire method: the electrical resistivity of the samples was measured by the two-wire method, where the voltage was applied and the current measured by a Keithley 487 picoammeter/voltage source. All measurements were performed in direct current (DC) mode, at room temperature. On each sample, two parallel rectangular gold electrodes were deposited by magnetron sputtering on one side of the sample. Copper wires were attached to the electrodes with silver paint to ensure good electrical contact.

7.8. Magnetic measurements

Magnetic measurements were carried out by the use of a Quantum Design MPMS XL-5 SQUID magnetometer. Magnetization-demagnetization M–H curves have been measured after zero-field cooling to 5 K, increasing the field up to 50 kOe, and decreasing it to −600 Oe. The temperature dependence of the magnetization has been measured between 5 and 300 K after zero-field cooling (ZFC) or field cooling (FC, H_{cool} = 100 Oe).

7.9. Wave guide dielectric characterization

In order to obtain small 2cmx2cmx0.2cm tiles of sample a mould was set-up. Materials were prepared mixing 1 g of sample with 3 g of commercial PVAc glue (dispersion of polymer in water ca. 50%). The viscous fluid was deposited in the mould layer by layer. Between the deposition of one layer to another 20 minutes passed to let glue dry out. When the tile reaches the desired thickness it was dried in an oven at 60°C for 24 h. Then, the mould was removed and tiles were polished with sandpaper. Samples were analyzed on a Anritsu VNA (37277) Vector Network Analyzer in the range of 18 to 26 GHz.

7.10. Electrospinning process

The electrospinning setup used was supplied by Linari Engineering-Pisa, Italy. The electrospinning parameters were: temperature (21°C), injection rate (from 0.3 to 1.98 ml/h), a target-capillary distance (12 cm) and relative humidity (RH) (<40%). Concerning the way of fiber collection a static collector and a rotating collector (the rotation speed of the drum was 30 rpm) were used.

7.11. Indirect and direct cytocompatibility tests of PANI nanofibers on a SH-SY5Y human cell line

Pretreatment of samples: PANI nanofibers (NFs) were cut producing small samples with areas ranging from 4.16 to 9.67 mm^2. They were stored in a refrigerator until use.

To tests indirect cytocompatibility samples of NFs were disinfected in different manners. They were treated in ethanol 70% (v/v) for 15 min. After this time, ethanol was removed by a pipette. The treatment was repeated maintaining PANI NFs in ethanol for 48 hours. Then, ethanol was evaporated for 3 hours under a hood.

In another test PANI NFs were put I contact for 48 hours in PBS (phosphate buffer solution, pH 7.2-7.4) + 3% (v/v) of penicillin/streptomicyn.

Finally, they were exposed for 10 minutes under UV irradiation (253.7 nm).

Samples were prepared for SEM observation in a chemical hood.

SH-SY5Y cell line: culture conditions and medium: SH-SY5Y cells (human neuroblastoma cell line, ATCC® CRL-2266™) were cultured at 37°C, 5% CO_2, in Dulbecco's modified Eagle's medium (DMEM, Gibco, Invitrogen, product code 10938) supplemented with 10% (v/v) fetal bovine serum (FBS, Gibco, Invitrogen, product codes 26140 or 10270), 1% (v/v) L-glutamine (Gibco, Invitrogen, product code 25030) and 1% (v/v) penicillin/streptomycin solution (Gibco, Invitrogen, product code 15140-148). Before using, media were filtered with vacuum filter systems (Corning, product codes 431097 or 430769).

SH-SY5Y cell line, thawing out and splitting: Cryopreserved SH-SY5Y cells were kept in cryogenic vials in 80% (v/v) FBS, 10% (v/v) DMEM and 10% (v/v) dimethyl sulfoxide (DMSO, Sigma, product code D8418) within a tank (Forma Scientific Inc, 8038 model) filled with liquid nitrogen at about -190°C. After vials had been carefully opened, ice crystals were melted by gently pipetting 1ml of culture medium (previously heated at 37°C) with a Pasteur pipette (Copan, product code 201CS01). The suspension was transferred to a 50 ml centrifuge tube (BD Falcon, product code 352070) containing 10 ml of medium and centrifuged (Eppendorf AG, 5415R model) at 900 rpm for 5 min. The supernatants were discarded and the pellet was suspended with 10 ml of

medium and placed in a 75 cm^2 flask (BD Falcon, product code 137787). After checking the cell density by an inverted optical microscope (Leica, LEITZ DM IRB model), the flask was moved to the incubator. After 80%-90% of the available surface had been colonized, the medium was discarded by aspiration and cells were gently washed with 2 ml phosphate buffered saline (PBs, Gibco, Invitrogen, product code 14190) to remove serum and cell debris. 1 ml of trypsin (Gibco, Invitrogen, product code 154000) was added and the flask was moved back to the incubator for 3-5 min. After the cells had been detached, trypsin was eluted with 5 ml of medium and the suspension was transferred to a 50 ml centrifuge tube, to be centrifuged at 900 rpm for 5 min. The supernatants were discarded, while the cells were suspended with fresh medium and counted.

Cell counting: Fifty μl cell suspension was transferred to a 0.65 ml microcentrifuge tube (Corning, product code 3206) and mixed with the same volume of trypan blue (Sigma, product code T8154). Ten μl was pipetted in a haemocytometer grid (Neubauer chamber) and the viable cells were counted.

Trypan Blue (Fig. 1A) is a commonly used dye to distinguish between viable and nonviable cells: the first ones exclude the dye and they appear white, while the second ones absorb the dye and they are coloured in blue (Fig. 1B). This property relies on the negative charge of the cromophore, that may not interact with the cells unless their membrane is damaged.

Neubauer chamber (Fig. 2) is composed of two opposite identical grids, that are divided into nine squares (each one is identified with a letter from A to I in Fig. 2). A glass is placed 0.01 mm over the grids and the empty volume is filled with 10 μL cell suspension.

The number of white cells lying within the squares A, C, E, G and I was counted (the cells lying on the boundaries were skipped) and the mean value was determined. Then it was multiplied by 2 (to consider the elution with Trypan Blue) and 10^4 (because every square has a volume of 0.01 mm^3), that is:

Cell density (cell number/ml) = mean number of counted cells $\cdot$ 2 $\cdot$ 10^4 (Eq. 1).

By multiplying the cell density and the suspension volume (ml), the total number of cells may be estimated:

Cell number = mean number of counted cells $\cdot$ 2 $\cdot$ 10^4 * suspension volume (Eq. 2).

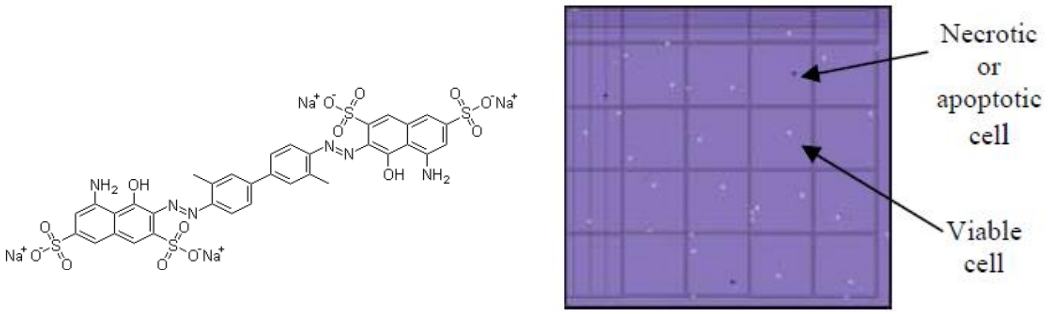

A B

Figure 1: Trypan blue: A) Trypan blue: chemical structure [www.chemblink.com], B) viable cells appearing white and unviable cells appearing blue after Trypan Blue staining [www.bme.gatech.edu].

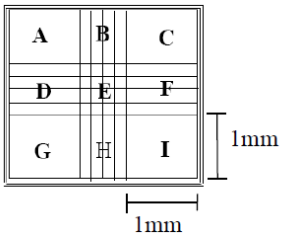

Figure 2: Neubauer chamber

Sample sterilization: Samples were dipped in PBS, moved to a 24-well cell culture plate (Corning, product code 3526), dried under laminar flow and sterilized by UV radiation (254 nm) for 30 minutes.

Indirect cytocompatibility evaluation (Cell viability assessment: MTS assay): Samples (1/group) were dipped in 1.5 ml cell culture medium and incubated at 37°C, 5% CO^2. This procedure was repeated four and six days later.
On day 6, SH-SY5Y cells were plated in 96-well cell culture plates (Corning, product code 3596). Three conditions were considered:

A. 30,000 cells/well, that is 93,750 cells/cm^2;
B. 20,000 cells/well, that is 62,500 cells/cm^2;
C. 10,000 cells/well, that is 31,250 cells/cm^2.

To assess the effect of leachable released by the nanofibers on SH-SY5Y cell viability, on day 7 culture medium was replaced with 100 µl supernatants collected from the plates where the nanofibers had been incubated with culture medium.
After 24 h for the condition A, about 72 h for the condition B and 48 h for the condition C, cell viability was assessed by 3-(4,5-dimethylthiazol-2-yl)-5-(3-carboxymethoxyphenyl)-2-(4-sulfophenyl)-2H-tetrazolium (MTS, CellTiter 96® AQueous One Solution Cell Proliferation Assay, Promega, product code G3582) assay. According to the instructions provided by the manufacturer, MTS was mixed to culture medium and 100 µl was added to each well (n=4). The samples were

incubated at 37°C for 2-4 h, then their absorbance was recorded at 490nm (Tecan spectrophotometer, Infinite® 200 PRO model).

Results were reported as mean ± standard deviation with respect to controls cultured with fresh medium.

7.12. Measurements of electrical conductivity as a function of force

Measurements of electrical conductivity as a function of force were carried out on pellets of PANI having diameter of 13 mm and thickness of 1 mm. They were prepared pressing 200 mg of each material for 30 minutes at 100 kN using a hydraulic press (Atlas Manual Hydraulic Press).

Concerning measurements at high values of force (0-100 kN), each material was tested at room temperature. A MTS Alliance RT/100 testing machine was used. The values of force were increased from 0 to 100 kN with a crosshead displacement of 0.07 mm/min.

Concerning measurements at low values of force (0-20 N), each material was tested at room temperature and after a thermal treatment for 2 hours at 50 and 100°C. Each pellet was placed on digital balance and the values of force were gradually increased and decreased by the use of a screw.

In both cases each pellet was subjected to 3 cycles of loading and unloading and electrical conductivities were obtained indirectly by the resistivity measures using an AMEL 338 multimeter.

7.13. Piezoresistive measurements

The piezoresistive effect was quantified by 4-point-bending tests. In those tests, the electrical resistance changes with strain were measured. The 4-point-bending tests were performed in a Shimadzu-AG-IS 500 N testing instrument at speeds from 0.2 to 2 mm/min and a maximum vertical (z axis) displacement of 2 mm. Each test was composed by four cycles of deformation.

Stability tests were also performed in selected samples up to 40 cycles. The electrical resistance and its variations during the deformation process were monitored by a digital multimeter Agilent 34401A.

PART III: Results and Discussion

Chapter 8: Synthesis and characterization of PANI/metal oxide nanocomposites

As reported in Chapter 4 section 4.2., conductive polymeric compounds exhibiting outstanding electric and magnetic properties, i. e. polymeric matrices incorporating Fe_3O_4 nanoparticles, are of great interest for many applications.[550–554] In the last years, many methods have been developed to synthesize this kind of nanocomposites. Some of them are based on the precipitation of magnetic nanoparticles in the presence of polymer in an organic solvent, such as *N*-methyl pyrrolidinone (NMP).[346] In other synthetic approaches magnetic nanoparticles (MNPs) are prepared in advance and then added to the solution containing aniline that will be subsequently polymerized by the use of an oxidant under acidic conditions [555] or under UV light irradiation.[556]

In this chapter a new clean one-pot synthesis of PANI/Fe_3O_4 composites will be presented using O_2 and H_2O_2 as the oxidants and Fe_3O_4 nanoparticles as the magnetic fillers and reaction catalysts under mild conditions. Because MNPs promoted catalytically the reaction of PANI preparation, the effect of nanoparticle size on the synthesis and properties of PANI/Fe_3O_4 nanocomposites was also deepened.

Preliminary results in terms of microwave absorbing properties will be presented.

Moreover, in order to clarify what is the catalytically active metallic center in the spinel structure, iron(II) was substituted with another bivalent cation (Mn, Co, Ni, Cu, Zn, Mg) and the effect of such a substitution on the catalytic performance was investigated.

Finally, an innovative synthetic approach to produce well dispersed PANI/Fe_3O_4 composites will be proposed.

8.1. New clean one-pot synthesis of polyaniline/Fe_3O_4 nanocomposites with magnetic and conductive behaviour

As reported by Wei *et al*. the most energy demanding step in the polymerization of aniline is its oxidation to produce dimeric and trimeric species.[76, 77] Once they have been produced, they evolve rapidly to produce oligomeric and polymeric materials. However, the redox potential of the couple aniline/emeraldine salt is relatively high (1.46 V). This means that, accordingly, oxygen is unable to carry out the reaction owing to its low redox potential (E°= 1.23 O_2/H_2O V). On the contrary, from a thermodynamic point of view hydrogen peroxide (E°= 1.78 H_2O_2/H_2O V) could represent a good choice. However, owing to kinetic limitations the use of a specific catalyst is necessary.[36] Another possibility to overcome this thermodynamic limitation consists in replacing the starting material (aniline) with another more reactive species, such as *N*-(4-aminophenyl)aniline (aniline dimer, AD). Previous investigations showed that copper powder or its salts are useful catalysts for this reaction.[26]

Herein, for the first time the double role (magnetic fillers and catalysts) of both pristine and oleic-acid-coated Fe_3O_4 nanoparticles in the oxidative polymerization of *N*-(4-aminophenyl)aniline is reported.[80]

8.1.1. Catalytic polymerization

Tables 8.1. and 8.2. show the polymerization yields obtained by the oxidative polymerization of AD in the presence of MNPs using molecular oxygen or hydrogen peroxides as the oxidizing agents respectively.

AD/Fe_3O_4 (molar ratio)	MNPs ferrofluid-type ($MNPs_{ff}$)		MNPs powder-type ($MNPs_p$)	
	Sample no.	Yield (%)	Sample no.	Yield (%)
Without Fe_3O_4 NPs	1	0	2	0
681	3	2	4	9
343	5	7	6	10
228	7	10	8	14
137	9	15	10	25
50	11	46	12	48
20	13	55	14	57
10	15	60	16	62
5	17	69	18	68

Table 8. 1.: Polymerization yields for the aerobic oxidative polymerization of AD in the absence and in the presence of MNPs. Reaction time= 3 days, reaction temperature= 80°C, pO_2= 3 bar.

AD/Fe_3O_4 (molar ratio)	MNPs ferrofluid-type ($MNPs_{ff}$)		MNPs powder-type ($MNPs_p$)	
	Sample no.	Yield (%)	Sample no.	Yield (%)
Without Fe_3O_4 NPs	19	40	20	40
681	21	39	22	40
343	23	42	24	41
228	25	61	26	55
137	27	60	28	54
50	29	67	30	62
20	31	88	32	87
10	33	85	34	83
5	35	87	36	91

Table 8. 2: Polymerization yields for the anaerobic oxidative polymerization of AD in the absence and in the presence of MNPs. Reaction time= 24 h, reaction temperature= 25°C, H_2O_2/AD= 5, molar ratio.

The polymerization yields were calculated by comparing the mass of all the reactants (AD, HCl, MNPs and, for $MNPs_{ff}$ also oleic acid) with that of the composite material finally collected. When oleic acid was present, it was considered completely transferred into the composite materials. The amount of MNPs embedded into the polymeric matrix was measured by atomic absorption spectroscopy (AAS) and the results, reported in Table 8.3., confirm that MNPs were completely transferred in the final composites.

Sample no.	Fe_3O_4/composite % (w/w) calculated	Fe_3O_4/composite % (w/w) measured
15	18.6	17.8
16	18.0	17.1
17	25.0	24.7
18	25.5	24.4
33	13.2	12.8
34	13.5	12.7
35	20.0	19.4
36	19.1	18.1

Table 8.3.: Fe_3O_4 content in the PANI/Fe_3O_4 composites.

These results proved that the catalytic effect of MNPs was not due to their corrosion into the solution but to their surface activity, partially according to the literature.[557, 558]

Moreover, comparing the results reported in both Table 8.1 and 8.2 it is possible to observe that the catalytic activity of both powder and ferrofluid-type MNPs was very similar.

However, their catalytic behaviour under aerobic conditions was more pronounced than in the presence of hydrogen peroxide. In fact, using molecular oxygen as the oxidizing agent yield increased from zero to 68–69% by increasing the amount of MNPs. On the contrary, using H_2O_2 as the oxidant the catalytic effect was less evident, because also in the absence of any catalysts hydrogen peroxide resulted to be able to oxidize AD producing PANI with 40% yield.[26]

Graphic 8.1. shows the catalytic yields calculated according to Equation 8.1. (Eq. 8.1.),

$$Y_c = Y_f - Y_o \qquad \text{Eq. 8.1.}$$

where Y_c is the catalytic yield reported in Graphic 8.1., Y_f is the yield of some reactions reported in Table 8.1. and 8.2. and Y_0 the yield obtained in the absence of MNPs (Sample no.: 1, 2, 19 and 20).

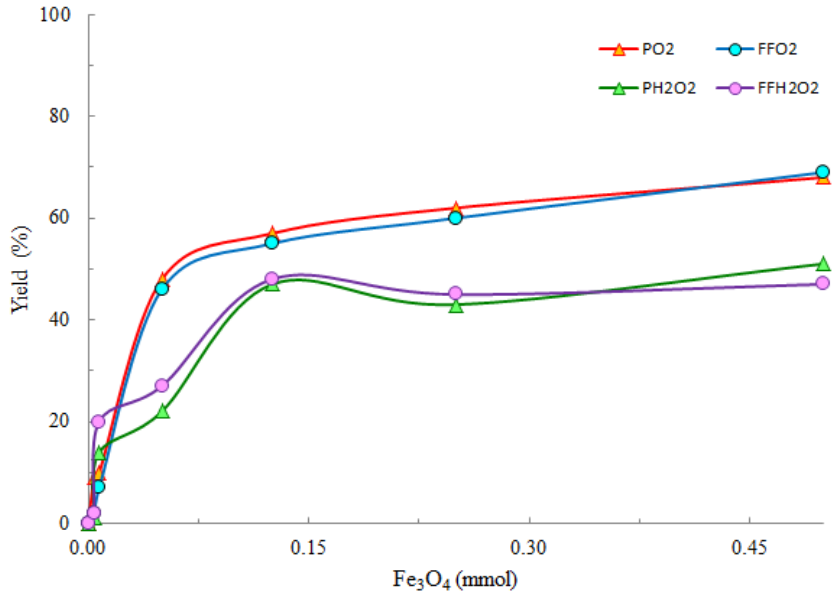

Graphic 8. 1.: Dependence of the catalytic yields of the AD oxidative polymerization on the amount of MNPs

It is worth to notice that in terms of catalytic yields better results were obtained using molecular oxygen. The different behaviour of the two oxidants was related to the intrinsic instability of H_2O_2 that can reduce its presence in the reaction mixture and consequently its oxidizing power.

8.1.2. Spectroscopic characterization

FT-IR and UV-vis spectroscopies (Figures 8.1. and 8.2.) confirmed that in all composites polyaniline was obtained in its conducting emeraldine form.

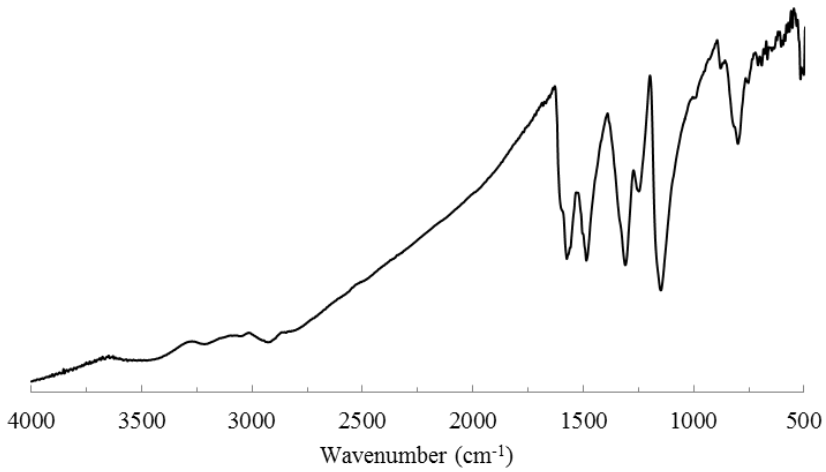

Figure 8.1.: FT-IR spectrum of a generic PANI/Fe_3O_4 composite.

In more detail, FT-IR spectrum reported in Figure 8.1. showed all the characteristic bands of PANI in its conducting form, as previously discussed (Chapter 2 section 2.5.2.).

In particular, this was confirmed by the presence of two diagnostic bands at 1498 cm^{-1} and 1570 cm^{-1} that can be assigned to the C=C stretching vibration mode for the benzenoid rings (N-B-N) and the C=C stretching of the quinoid rings (N=Q=N) respectively and by their ratio (about 1, see Chapter 2 section 2.5.1.) Moreover, the band at 1140 cm^{-1} (electronic like band) and the broad band between 2000-4000 cm^{-1} were indicative of a good electronic delocalization into the chains.[150]

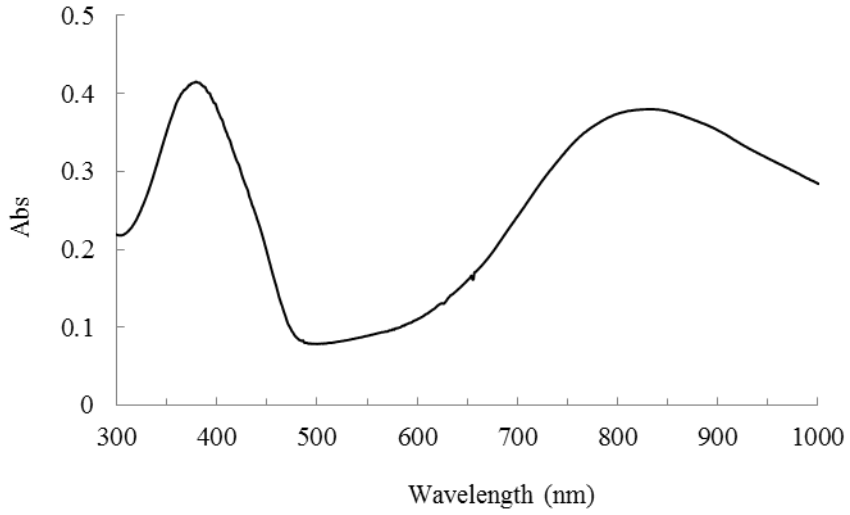

Figure 8. 2.: UV-vis spectrum of a generic PANI/Fe_3O_4 composite.

The UV-vis spectrum showed two characteristic bands at about 300 and 849 nm, due to the π-π* transition of the benzenoid ring and benzenoid/quinoid transition respectively.

The amount of MNPs into the composites was measured by atomic absorption spectroscopy, as reported above, but also confirmed by X-ray powder diffraction analyses (Figures 8.3. A and B).

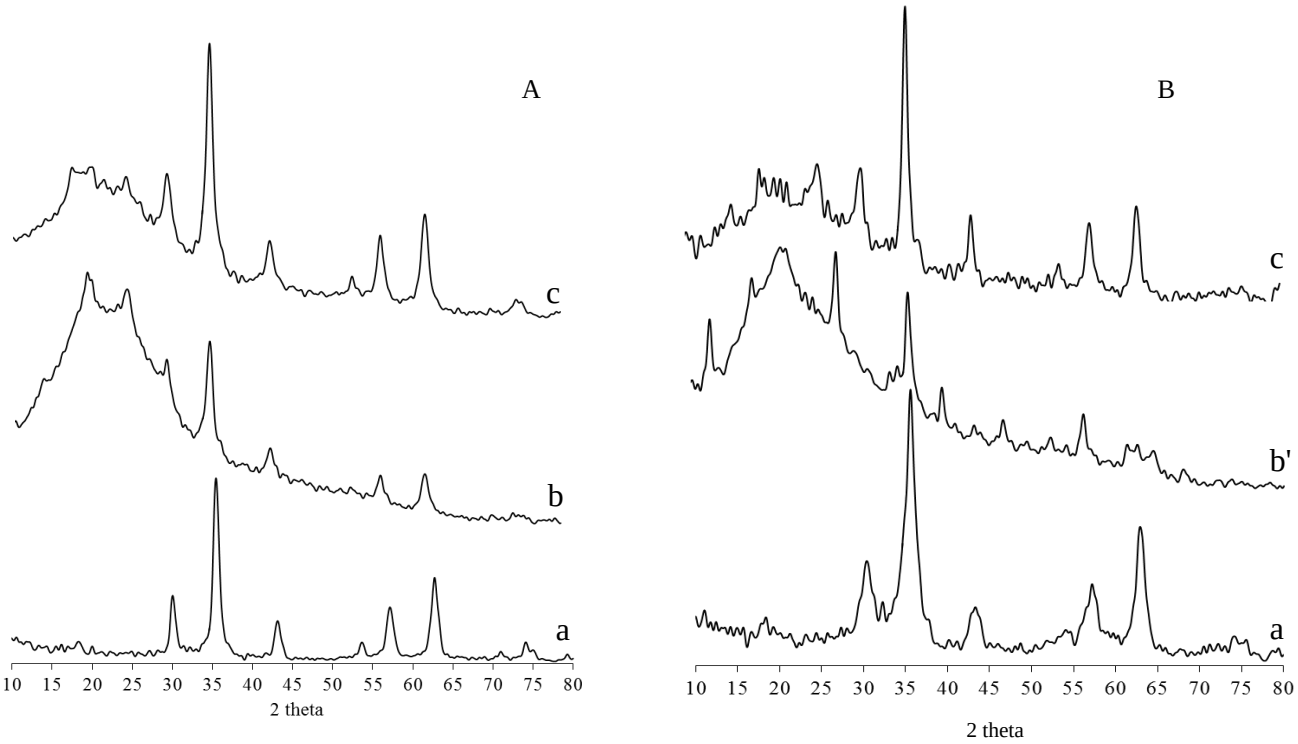

Figure 8.3.: A) XRPD patterns of $MNPs_p$ (a) and its composites with PANI (b= sample no. 16, c= sample no. 18), B) XRPD patterns of $MNPs_{ff}$ (a') and its composites with PANI (b'= sample no. 15, c'= sample no. 17)

All the diffractograms clearly showed the characteristic Bragg diffraction peaks corresponding to the Miller indices for the reflection planes (220), (311), (400), (422), (511), (440) at 2θ= 30.3, 35.6, 43.2, 53.6, 57.1 and 62.8 respectively for Fe_3O_4, while the broad peak at about 2θ ≈ 20 was assigned to PANI with very low crystallinity. Moreover, these results confirmed that Fe_3O_4 was in spinel phase [559, 560] and the purity of the products *via* the absence of other phases of iron oxide such as maghemite or hematite. Obviously, the intensity of the diffraction peaks of MNPs in the PANI/Fe_3O_4 composites (Figures 8.3. b, c, b', c') became stronger with increasing the nanoparticle loadings.

Control over the dispersion of the nanoparticles in the polymer matrix is a critical point to produce high quality composites.

However, according to the literature,[561, 562] the reduced intensity of the diffraction peaks of PANI indicated a strong interaction between PANI backbone and MNPs and, consequently, a good dispersion

The average size of nanoparticles was calculated according to the Debye-Scherrer equation (Eq. 2.2.):

$$\tau = \frac{K \cdot \lambda}{\beta \cdot \cos\theta} \qquad \text{Eq. 2.2.}$$

where *k* is the shape factor, λ is the X-ray wavelength (0.15418 nm), α is the full width at half-height and θ is the Bragg angle. The results are reported in Table 8.4.

Sample	Mean diameter (nm)
$MNPs_p$	11.0
Sample no. 15	11.1
Sample no. 17	11.0
$Fe_3O_4NPs_{ff}$	11.0
Sample no. 16	13.4
Sample no. 18	13.6

Table 8.4.: Mean diameter of the MNPs calculated by the Scherrer's equation.

8.1.3. Morphological characterization

The average size of MNPs calculated by the Debye-Scherrer equation was confirmed by TEM characterization (Figures 8.4. A and B).

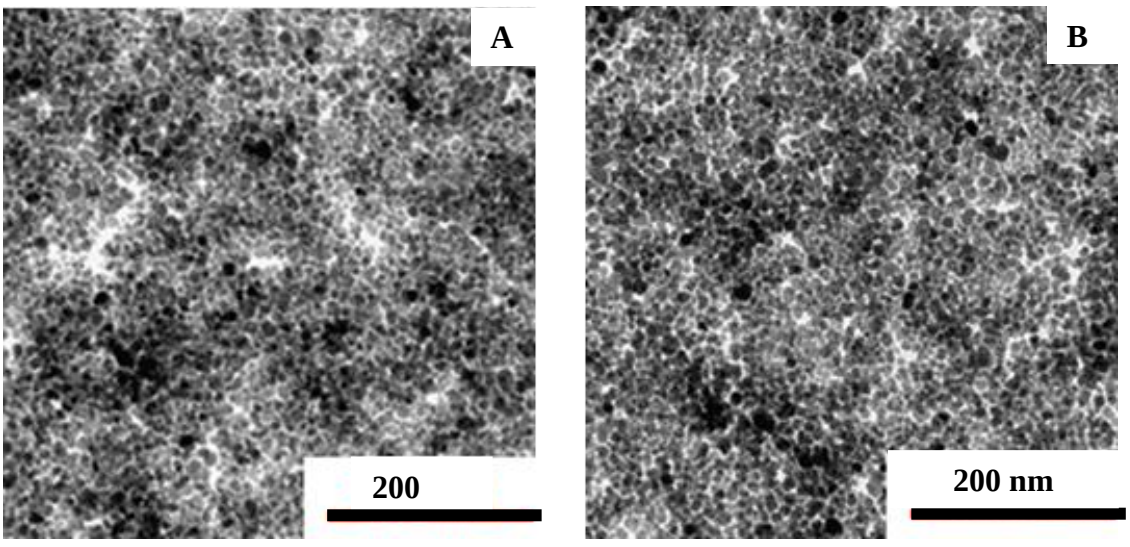

Figure 8.4.: TEM images of (A) $MNPs_p$, (B) $MNPs_{ff}$.

However, differently from the $MNPs_p$ embedded into the polymer matrix that maintained the same size, in the composites containing $MNPs_{ff}$, these latter showed a larger diameter probably due to agglomeration phenomena.

Although MNPs powder and ferrofluid-type displayed a very similar catalytic behaviour (see Tables 8.1., 8.2. and Graphic 8.1.), they influenced differently PANI/Fe_3O_4 composites morphology (Figures 8.5 and 8.6.).

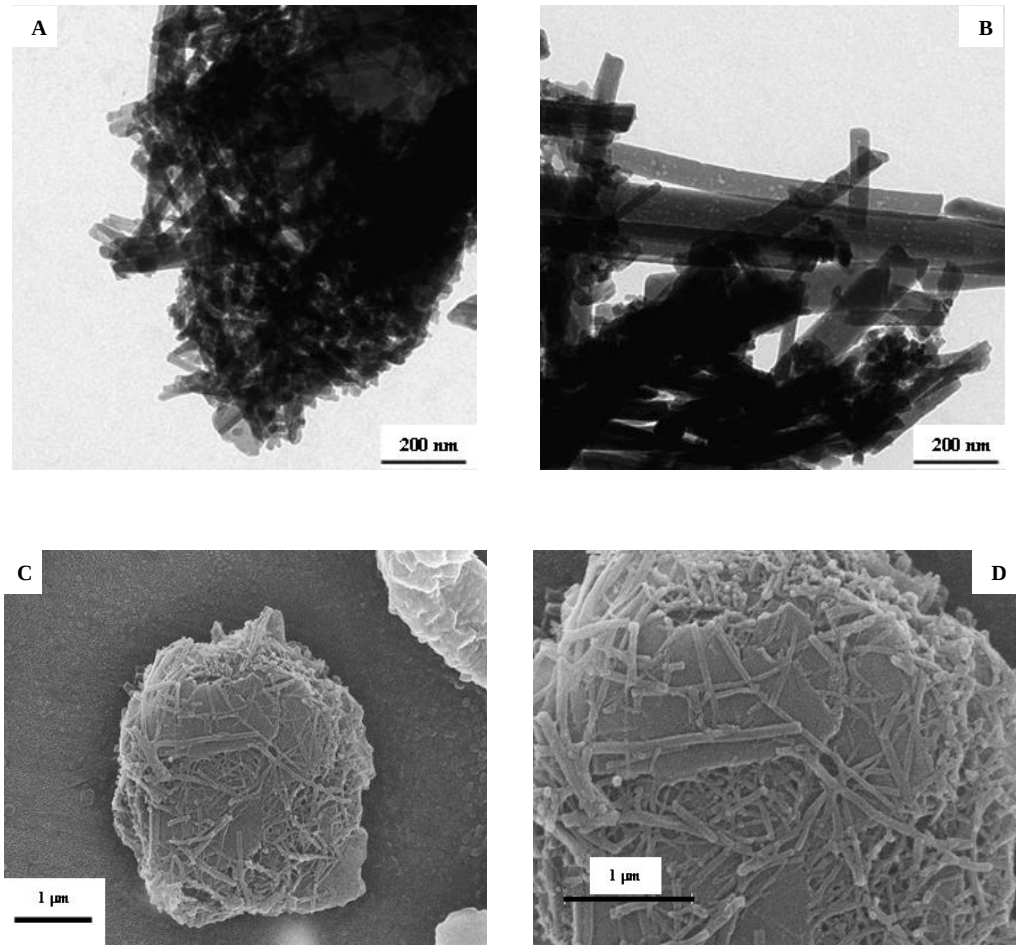

Figure 8.5.: TEM (A and B) and SEM (C and D) images of PANI/$MNPs_{ff}$ composites.

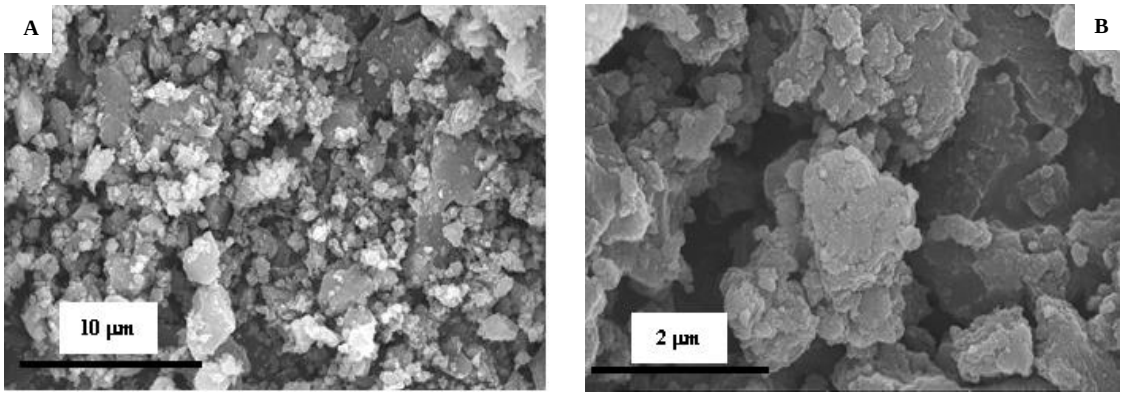

Figure 8. 6.: SEM images of PANI/$MNPs_p$ composites.

Figures 8.5 A-D show that PANI/$MNPs_{ff}$ composites exhibited rod-like morphology with diameters ranging from 30 to 110 nm. On the contrary, composites containing $MNPs_p$ presented more irregular structures.

8.1.4. Mechanism of nanorods formation

PANI/$MNPs_{ff}$ composites synthesis reported above can be considered as a kind of interfacial polymerization. In fact, in this case magnetic NPs were introduced into the reaction mixture in an organic solution. As reported in the literature,[563] interfacial polymerization is an useful template-free synthetic approach to produce polyaniline in form of nanofibers/-wires/-rods and, in this context, Zhang and many other authors reported the possibility to form pure PANI or PANI/Fe_3O_4 composites in form of nanorods and nanotubes following a self-assembly process.[193, 342]
According to the mechanism proposed by Zhang and coworkers, Scheme 8.1. reports an hypothetic mechanism of synthesis able to justify nanorods formation by the one-pot approach reported above.

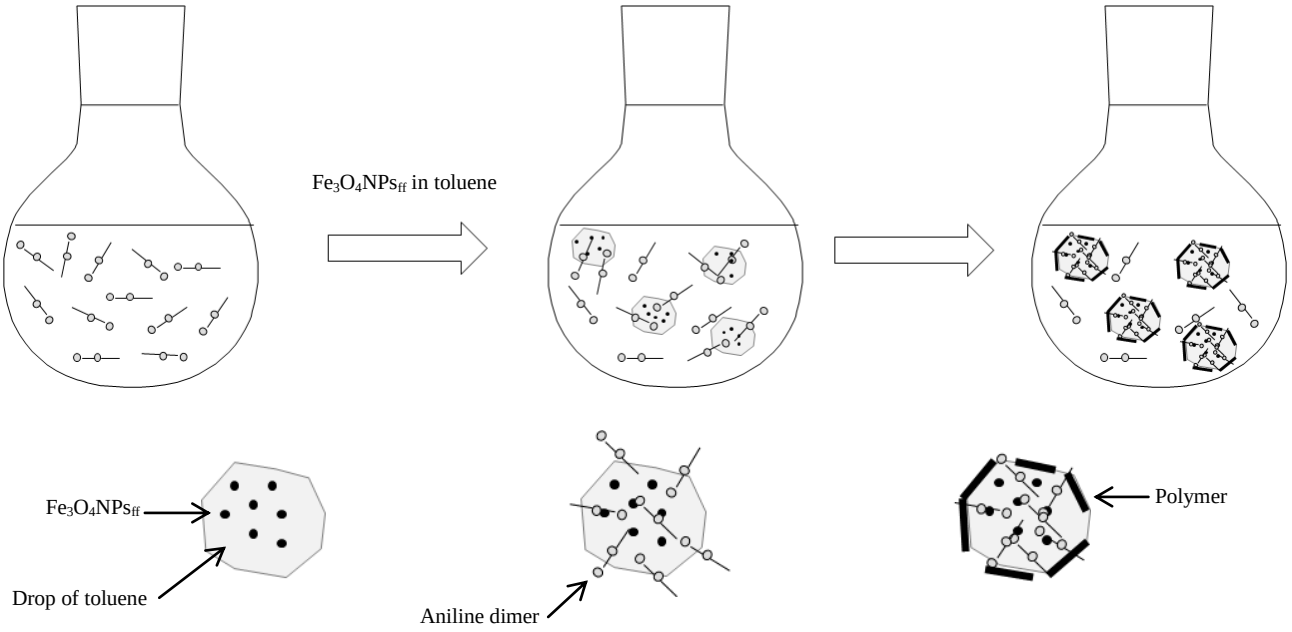

Scheme 8.1.: Hypothetic mechanism for PANI/$Fe_3O_4NPs_{ff}$ nanorods formation.

More in detail, *N*-(4-amonophenyl)aniline is soluble in acidulated water but also in organic solvent, as toluene. Therefore, when MNPs ferrofluid-type were added, AD partially diffused into the organic solvent. The reaction mixture resulted in a biphasic system constituted of aqueous phase containing the oxidant (H_2O_2 or O_2) and part of AD molecules and an organic phase containing the iron oxide NPs and the remaining part of AD. The reaction took place primarily at the water/toluene interface, where the present magnetic NPs can catalyze the first step of the polymerization reaction

among the molecules present on the surface of the organic phase, thus producing nanorods through an elongation process.

On the contrary, in the case of MNPs powder-type all the reagents were in the same phase and the polymerization reaction took place immediately. Any control of morphology wasn't allowed.

8.1.5. Thermogravimetric analyses

The TGA (thermogravimetric analyses) results of pure PANI and PANI/Fe_3O_4 composites are reported in Figure 8.7.

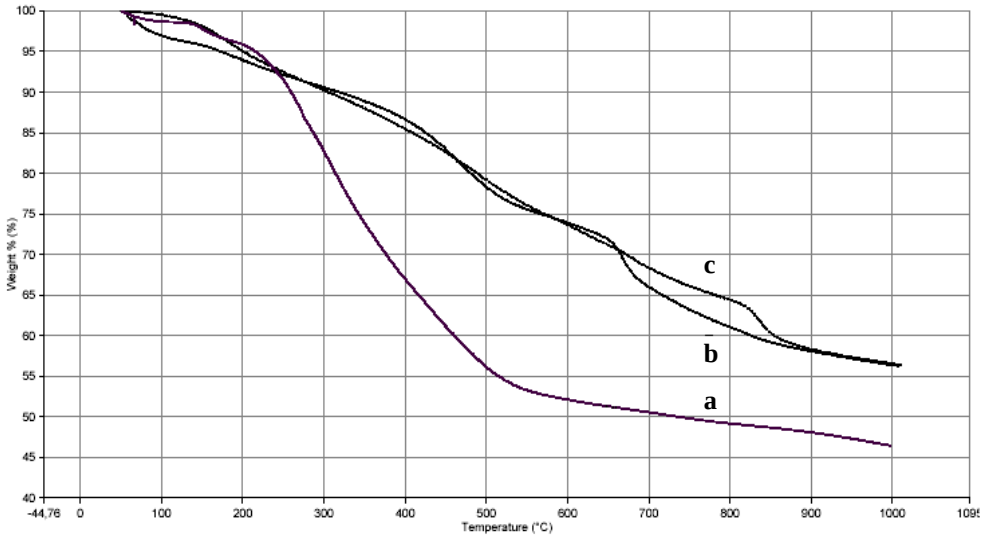

Figure 8.7.: TGA results for (a) pure PANI (Sample no. 20), (b) Sample no. 34 and (c) Sample no. 36.

The TGA curve of pure PANI (Figure 8.7. a) showed three major weight losses, the first step at around 120°C due to the expulsion of water molecules, the second step at 230-550°C due to the loss of dopant and the third at 600-1000°C due to the thermal decomposition of the polymer. MNPs embedded into the polymeric matrix improved the thermal stability of PANI, probably through the interaction between magnetic nanoparticles and PANI chains. In fact, the weight losses were much less for the composites (Figures 8.7. b and c).

8.1.6. Magnetic measurements

The magnetization-demagnetization M–H curves of MNPs powder and ferrofluid-type, Sample no. 18, 36, 17 and 35 are presented below (Figure 8.8.). The curves were recorded at 5 K after zero field cooling from 300 K. Magnetization M is referred to the Fe_3O_4 mass in each sample.

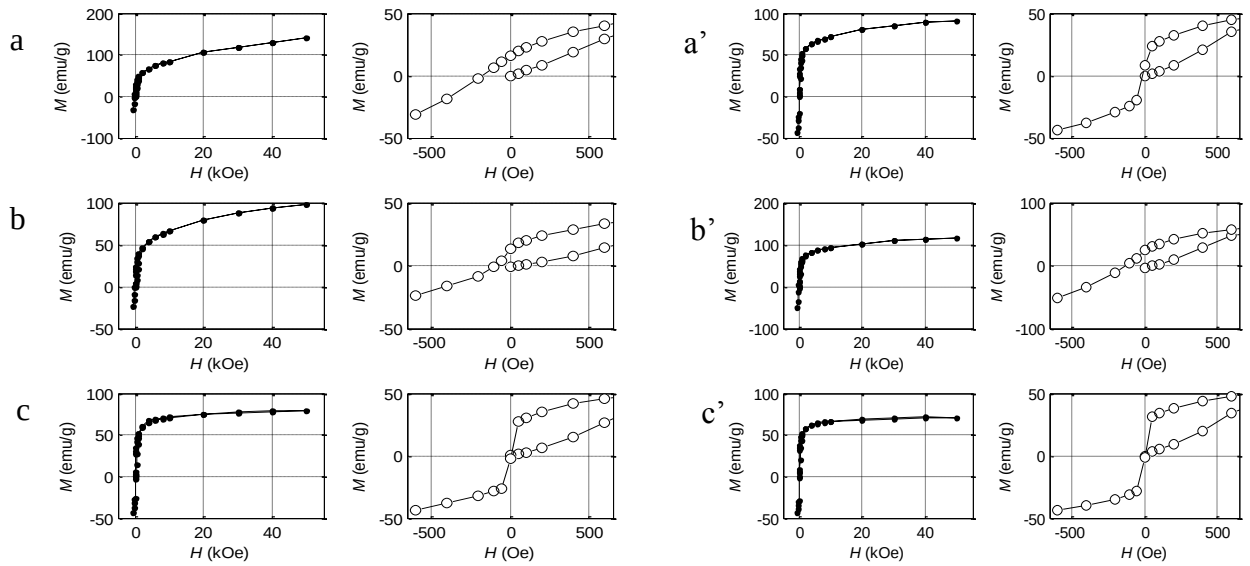

Figure 8.8.: Magnetization-demagnetization M-H curves of (a) Sample no.36, (b) Sample no. 18, (c) $MNPs_p$, (a') Sample no. 35, (b') Sample no. 17, (c') $MNPs_{ff}$.

The saturation magnetization M_s, the remanence M_r and the coercive field H_c are reported in Table 8.5.

Parameter	$MNPs_p$	Sample no. 36	Sample no. 18	$MNPs_{ff}$	Sample no. 35	Sample no. 17
M_s (emu/gFe_3O_4)	79	141	98	71	116	91
M_r (emu/gFe_3O_4)	0	16	13	0	24	8
H_c (Oe)	0	-170	-90	0	-125	-15
T_{irr} (K)	265	140	160	265	185	205
$T_{max,ZFC}$ (K)	>300	85	155	280	160	180
$T_{der,ZFC}$ (K)	80/15	5	≈ 30	70/20	≈ 25	≈ 30

Table 8.5.: Magnetic properties of MNPs powder and ferrofluid-type, Sample no. 18, 36, 17 and 35.

As shown in Figure 8.8., both MNPs in powder and ferrofluid form saturated within 50 kOe and didn't exhibit hysteresis. On the contrary, their composites didn't saturate even to kOe and exhibited remanence and coercitivity. As reported in Table 8.5. and 8.6., this effect was strictly related to the volume fraction of MNPs.

Parameter	$Fe_3O_4NPs_p$	Sample no. 36	Sample no. 18	$Fe_3O_4NPs_{ff}$	Sample no. 35	Sample no. 17
X_v		1.7%	4.0%		3.5%	8.6%
D (nm)	9.5(a)	30	22	11(b)	27	20

Table 8.6.: Magnetite volume fraction (X_V) and estimated mean distance between magnetite nanoparticles in PANI–Fe_3O_4 composites (Exp. 17, 18, 35, 36) and pristine Fe_3O_4 nanoparticle samples (ferrofluid and powder) (D), calculated assuming random distribution of the nanoparticles in the PANI matrix.; b= assumed equal to nanoparticle diameter.

In fact, increasing the volume fraction of MNPs into the composites, their magnetic parameters, such as M_s, M_r and H_c decreased.

To better understand the magnetic properties of PANI/Fe_3O_4 composites, ZFC (zero-field cooling) and FC (field cooling) magnetization were measured (Figure 8.9.). The characteristic temperatures derived from ZFC/FC data are reported in Table 8.5.

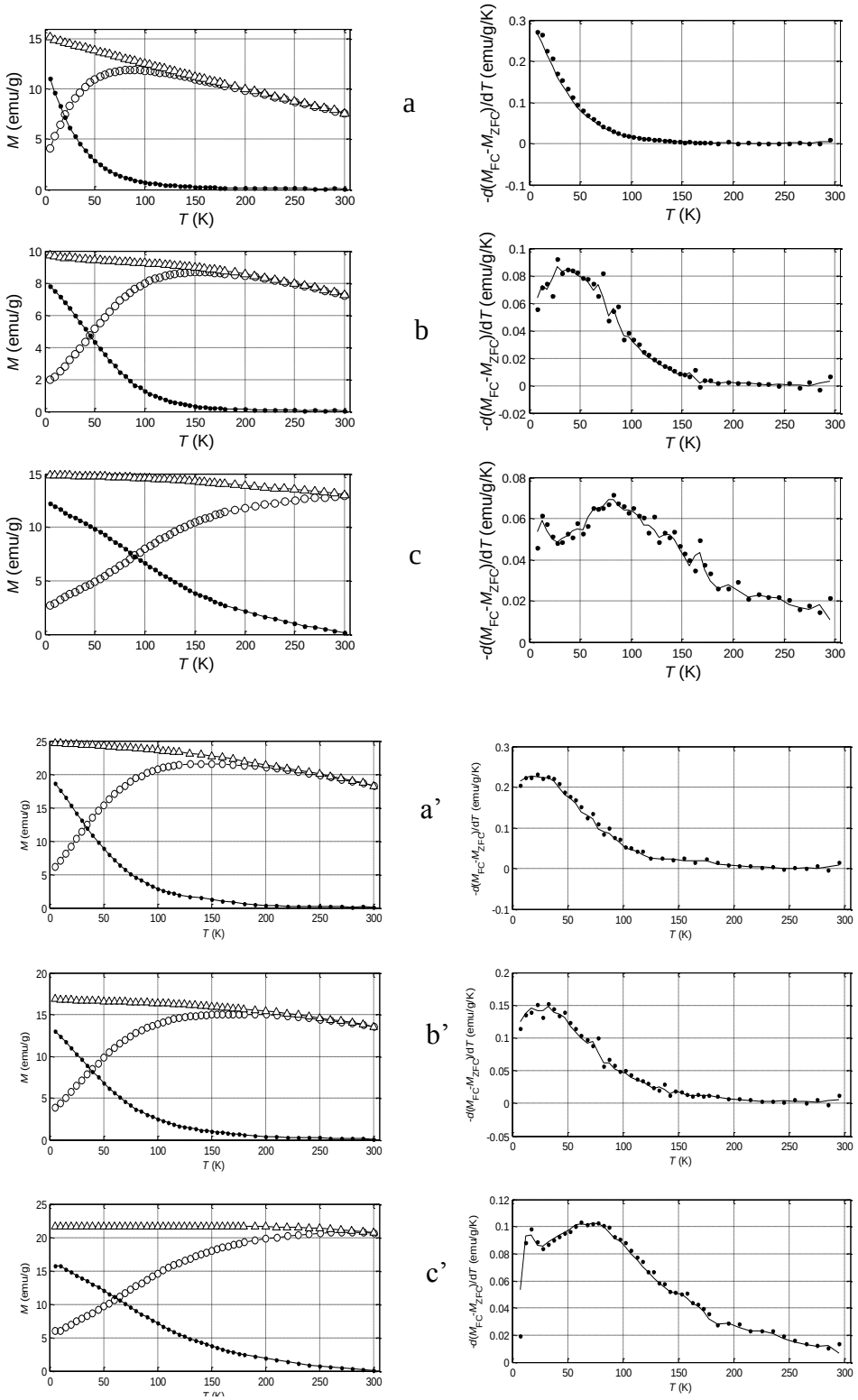

Figure 8.9.: ZFC and FC magnetization (100 Oe) of (c) MNPs powder and (c') ferrofluid-type, (b) Sample no. 18, (a) 36, (b') 17 and (a') 35. On the left, temperature dependence of M_{FC} (open triangles), M_{ZFC} (open circles) and $M_{FC}-M_{ZFC}$ (dots). On the right, derivative $-d(M_{FC}-M_{ZFC})/dT$ (dots).

The non-overlapping ZFC and FC curves indicated an irreversible behaviour at low temperature for all the samples, probably due to the presence of anisotropic magnetic interactions (AMIs), such as the magnetocrystalline anisotropy, surface anisotropy, *inter*-particle interactions, etc., which were

able to block the magnetization when temperature was low. At the temperature of maximum ZFC magnetization ($T_{max,ZFC}$), the thermal energy was comparable to the AMIs. The difference $M_{FC} - M_{ZFC}$ represents the blocking effect of the AMIs, that was parameterized by Fiorani *et al*. by T_{irr},[564] reported in Table 8.5. It indicates the temperature at which the value of this difference falls to 3% of its value at 5. Above such a temperature, the thermal energy is larger than the AMIs for most magnetic particles. As reported in Tables 8.5., $T_{max,ZFC}$ and T_{irr} showed that the temperature at which the magnetic anisotropy barrier was overcome by the thermal energy was higher for samples with larger volume fractions of Fe_3O_4.

The graphic of the derivative $-d(M_{FC} - M_{ZFC})/dT$ reported in Figure 8.9. represents the distribution of the energy barriers in the sample. Maxima in these plots ($T_{max,der}$) are reported in Table 8.5.

When the volume fraction X_V of magnetite was low (Sample no. 36), the barrier distribution decreased monotonously from 5 K upwards. At medium Fe_3O_4 fraction, the barrier distribution was wider and features a broad maximum at about 30 K. In nominally pure samples, the distribution was even wider, the broad peak shifts at 80 K and another maximum was visible at about 15 K. The interpretation of the magnetic nanoparticles behavior was complex because there are several effects that must be taken into account.[565] Magnetic nanoparticles behave differently from the corresponding bulk material due to finite-size effects, surface effects and *inter*-particle interactions. Superparamagnetism [566] is a finite-size effect whereas a typical surface effect is that the saturation magnetization of a nanoparticle is different from that in the bulk.[567] In the low magnetite content Sample no. 36, where the *inter*-particle interactions were weaker, the magnetization at 5 K was not saturated even at 50 kOe because of the peculiar behaviour of the nanoparticle surface layers. AMIs are affected by all the effect types: for instance, the magnetocrystalline anisotropy scales as the particle volume, the anisotropy of the particle surface layers is different from the core anisotropy, and the *inter*-particle interactions (e.g. dipole–dipole) introduce concentration-dependent magnetic anisotropy.

The results indicated that the magnetic behaviour of the PANI–Fe_3O_4 composites was strictly related to the *inter*-particle interactions, according to the literature.[557, 568] The dependence of the shape of the M–H curves and of the characteristic quantities M_s, M_r, and H_c on the Fe_3O_4 content was clear evidence of the presence of strong *inter*-particle interactions.[569] The ZFC and FC magnetization curves further supported this view in that the flattening of the FC curve at low T, the higher $T_{max,ZFC}$ and T_{irr},[570] and the higher peak position of the distribution of the effective magnetic anisotropy barriers observed upon increasing the Fe_3O_4 volume fraction are known signs of *inter*-particle interactions. When *inter*-particle interactions are stronger than thermal energy, they give rise to a frozen collective state where the magnetic moments of the nanoparticles are coupled

to each other.[565] This coupling is an additional source of magnetic anisotropy since the minimum-energy orientation of the individual magnetic moments depends on the spatial distribution of the other nanoparticles. The M–H curves recorded at 5 K after zero field cooling provided insight into such a frozen state. As already known,[567] a larger fraction of the magnetic component led to a decrease in coercivity and to magnetic saturation at lower fields. Saturation magnetization at low temperature larger than in the bulk was more rarely observed [571] and it probably was a surface effect.[572]

The ZFC/FC data confirmed the importance of *inter*-particle interactions in PANI/Fe_3O_4 composites. The characteristic temperatures T_{irr} and $T_{max,ZFC}$ strongly depend on the Fe_3O_4 content mirroring the increase in both maximum and median anisotropy barrier, respectively. The distribution of the effective anisotropy barriers, represented by the derivative $-d(M_{FC} - M_{ZFC})/dT$, depends on the magnetite fraction and it seemed that there are two contributions to this distribution. The first was a broad distribution of barriers peaking at a magnetite-content-dependent temperature. It was less important in the most dilute Sample no. 36 where it manifested just as a shoulder. Such a contribution can be attributed to AMI barriers arising from *inter*-particle interactions. The other contribution was independent on the magnetite content and peaks at about 15 K. It was clearly visible in the most dilute sample and in the pure samples where the *inter*-particles barrier contribution shifted to higher temperature. It can be attributed to a surface effect, that is, to the formation of a frozen state within the surface layer of each nanoparticle.[564]

It was also interesting to note that the AMI barrier distributions in Samples no. 17, 18 and 35 were more similar to each other (and more different from that of Sample no. 36) than what it can be expected on the basis of the magnetite volume fractions. This may be an indication that at Fe_3O_4 volume fraction >2% some clustering of the magnetite nanoparticles in the PANI matrix occurred.

8.1.7. Conductivity measurements

Table 8.7. reports the conductivity values of Sample no. 18, 36, 17 and 35 measurements by electrochemical impedance spectroscopy (EIS) technique.

Sample no.	Thickness (mm)	0 V ($S \cdot cm^{-1}$)	0.5 V ($S \cdot cm^{-1}$)	1 V ($S \cdot cm^{-1}$)
18	0.095	$2.76 \cdot 10^{-3}$	$6.01 \cdot 10^{-3}$	$5.12 \cdot 10^{-3}$
36	0.100	$2.50 \cdot 10^{-3}$	$1.62 \cdot 10^{-3}$	$1.48 \cdot 10^{-3}$
17	0.152	$2.00 \cdot 10^{-2}$	$2.50 \cdot 10^{-2}$	$5.40 \cdot 10^{-3}$
35	0.121	$1.60 \cdot 10^{-2}$	$1.60 \cdot 10^{-2}$	$1.60 \cdot 10^{-3}$

Table 8.7.: Conductivity values of Sample no. 18, 36, 17 and 35.

Figures 8.10. A-D display Nyquist plots of Sample no. 18, 36, 17 and 35 and reflect the various elements of a circuit model based on electronic conductivity.

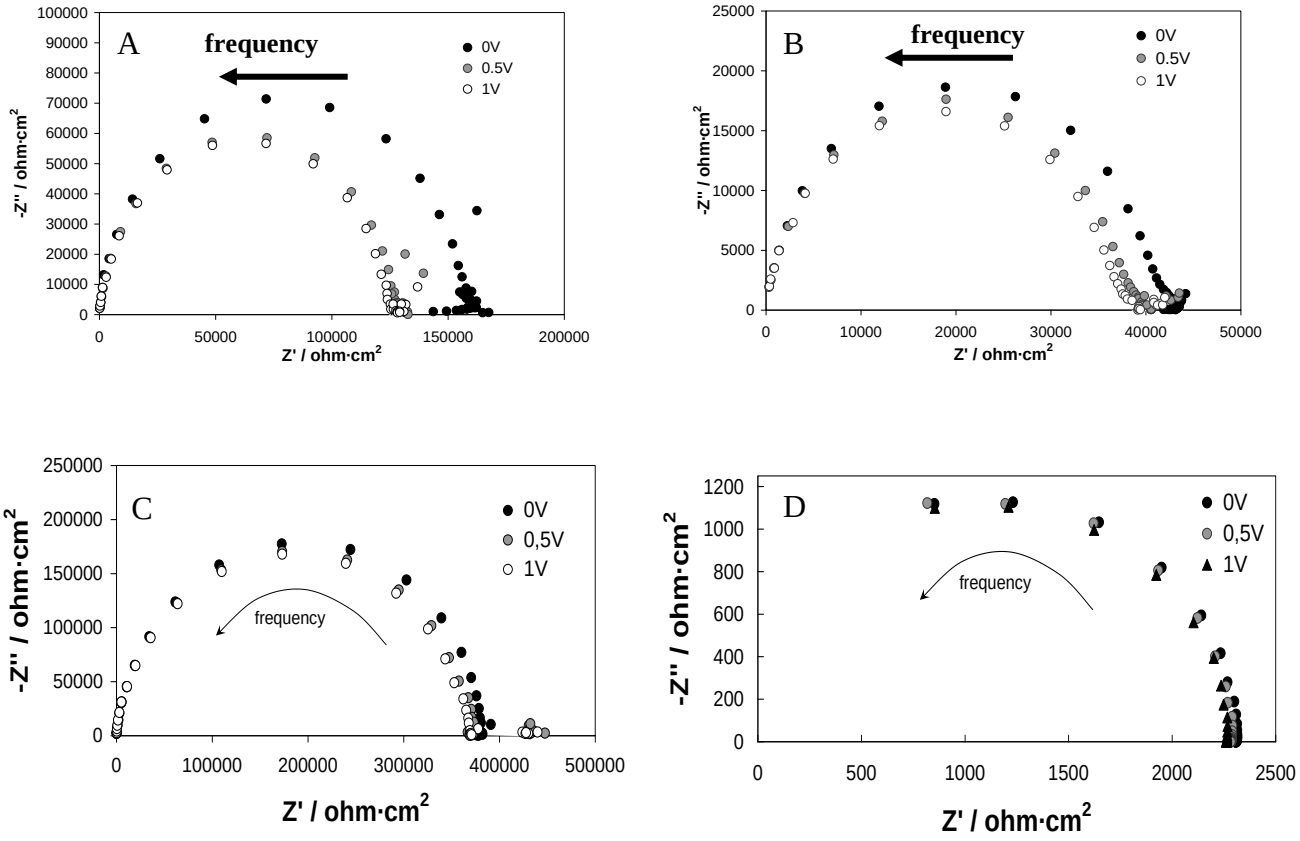

Figure 8.10.: Nyquist plot of the Sample no. (A) 18, (B) 36, (C) 17 and (D) 35.

The equivalent circuit that fits most adequately the impedance data of PANI/Fe_3O_4 composites corresponds to the parallel combination of capacitance and charge transfer resistance consistent with the conductivity of emeraldine salt. Overall resistance (R_t, intercept at low frequency) corresponded to the bulk resistance which arose from the resistance of the combination of *intra*-chain and *inter*-chain conductivity pathway. Series resistance (R_s, intercept at high frequency) was instead related to the lower band gap mechanism that was ascribed to the *intra*-chain charge transfer. Both were ascribed to the ability to transport charge carriers along the polymer chains. It is noteworthy of remark that in the spectra collected for the Sample no. 17, R_s was determined by adopting the same equivalent circuit of the other specimens. As it can be expected, with the decrease of the fixed voltage, the charge transfer resistance value decreased gradually and the PANI appeared to have a faster conductivity, generally related to the overcoming of band gap of *intra*-chain mechanism. By comparing the different behaviours of the samples under investigation (Table 8.7.), it is noteworthy that the samples prepared by MNPs ferrofluid-type (Sample no. 17 and 35)

showed a higher specific conductivity (about 4 times) than samples prepared with Fe_3O_4NPs powder-type (Sample no. 18 and 36). As previously said, the charge transfer resistance (R_{ct}, intercept at low frequency) was ascribed to the sum of the *inter*-chain and *intra*-chain conductivity and generally its value was determined by the voids inside the pellets.[474]

It should be pointed out that the effect of pressure, pressing time and interval between pressing and testing, which can modify the *inter*-chain and *intra*-chain conductivity of the polymers, were not evaluated. Unfortunately, to date, the different behaviour of the composites in terms of conductivity has not been explained.

8.2. The effect of nanoparticle size on the synthesis and properties of PANI/Fe_3O_4 nanocomposites

The dependence of the catalytic activity of Fe_3O_4NPs from their sizes in the oxidative polymerization of *N*-(4-aminophenyl)aniline was investigated. MNPs of three different sizes (MNPs_1= 27.0, MNPs_2= 10.0 and MNPs_3= 2.3 nm) were synthesized by two different techniques: high-temperature decomposition of iron precursor in non-coordinating solvents[573] and metal vapour synthesis.[574] These new PANI/Fe_3O_4 nanocomposites of second generation were characterized for their structural, morphological and magnetic attributes using specific probes like XRD, TEM, STEM, EELS, EDX and SQUID.

8.2.1. Catalytic polymerization

Tables 8.8. and 8.9. summarize the polymerization yields obtained by the oxidative polymerization of AD in the presence of magnetic nanoparticles of different sizes using hydrogen peroxide or molecular oxygen as the oxidizing agents respectively.

AD/MNPs (molar ratio)	Catalyst	Sample no.	% Yield
5	MNPs_3	37	98
10	MNPs_3	38	81
50	MNPs_3	39	39
5	MNPs_2	40	85
10	MNPs_2	41	68
50	MNPs_2	42	60
5	MNPs_1	43	58
10	MNPs_1	44	49
50	MNPs_1	45	46

Table 8.8.: Polymerization yields for the anaerobic oxidative polymerization of AD in the presence of MNPs. Reaction time= 24 h, reaction temperature= 25°C, H_2O_2/AD= 5, molar ratio.

AD/MNPs (molar ratio)	Catalyst	Sample no.	% Yield
5	MNPs_3	46	70
10	MNPs_3	47	63
50	MNPs_3	48	54
5	MNPs_2	49	87
10	MNPs_2	50	69
50	MNPs_2	51	53

Table 8.9.: Polymerization yields for the aerobic oxidative polymerization of AD in the presence of MNPs. Reaction time= 3 days, reaction temperature= 80°C, pO_2= 3 bar.

When H_2O_2 was employed as the oxidant, the catalytic activity of MNPs increased with decreasing their sizes, following the trend:

2.3 nm > 10 nm > 27.0 nm

However, this trend was not observed at higher values of AD/MNPs (molar ratio), where the catalytic activity of smaller MNP_3 was even lower than that of the larger MNPs_1 (Table 8.8.).
Also under aerobic conditions the catalytic activity of MNPs_3 resulted to be always lower than that of bigger ones (MNPs_2).
Such a behaviour of the smaller MNP_3 can be probably explained with an overoxidation of the nanoparticles to Fe_2O_3. The absence of the bivalent metallic center (Fe^{2+}) on the surface of NPs could interrupt the catalytic cycle, guaranteed by the couple Fe^{2+}/Fe^{3+}. However, at the moment, this hypothesis has not yet been confirmed.

Similarly, as reported in Section 8.1., the amount of MNPs embedded into some PANI/Fe_3O_4 composite samples was measured by AAS and the results are summarized in Table 8.10.

Sample no.	Catalyst	Oxidant	Loss of MNPs (%)
37	MNPs_3	H_2O_2	20
38			21
39			17
43	MNPs_1		3
44			3
45			6
46	MNPs_3	O_2	21
47			20
48			54

Table 8.10.: Loss of MNPs into the PANI/Fe_3O_4 composites measured by AAS.

Under both aerobic and anaerobic conditions smaller nanoparticles (MNPs_3) showed higher losses. Such a phenomenon confirmed that smaller NPs were more sensitive to the reaction conditions than the bigger ones.

Unlike that for all the other MNPs, in the case of MNPs_1 a large amount of oleic acid was employed to obtain a homogeneous organic dispersion of big nanoparticles. In order to investigate if large quantities of oleic acid effect the catalytic activity of MNPs, a sample of MNPs_1 containing 60% of oleic acid was abundantly washed with acetone to remove any trace of surfactant. Then, increasing amounts of oleic acid were added to MNPs and these latter were tested in the oxidative polymerization of AD. The results, reported in Graphic 8.2., demonstrated that the amount of oleic acid practically didn't affect the polymerization reaction.

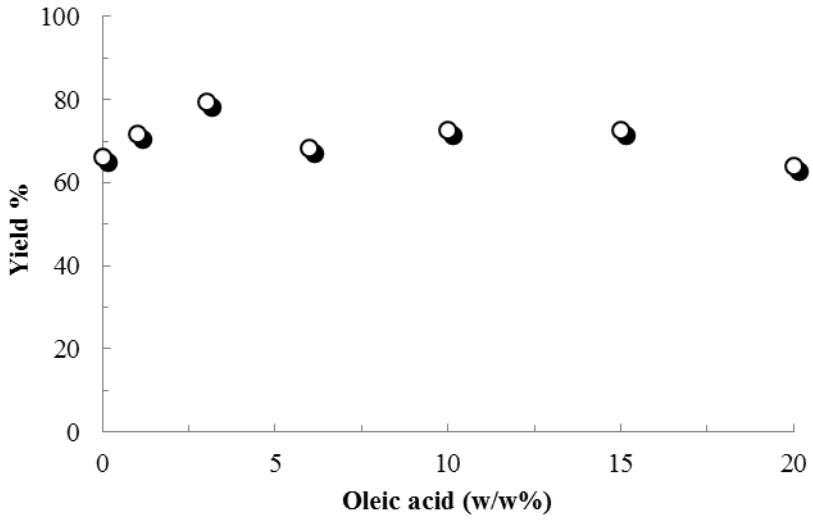

Graphic 8.2.: Yield % against oleic acid %. Reaction conditions: reaction time= 24 h, reaction temperature= 25°C, H_2O_2/AD= 5 (molar ratio), AD/MNPs= 50 (molar ratio).

All the materials were characterized by different techniques. FT-IR and UV-vis spectra resulted to be similar to those reported in Figures 8.1. and 8.2., confirming that into the composites polyaniline was in its conductive emeraldine form.

XRPD diffractograms of these second generation of PANI/Fe_3O_4 composites are reported in Figures 8.11. A-C.

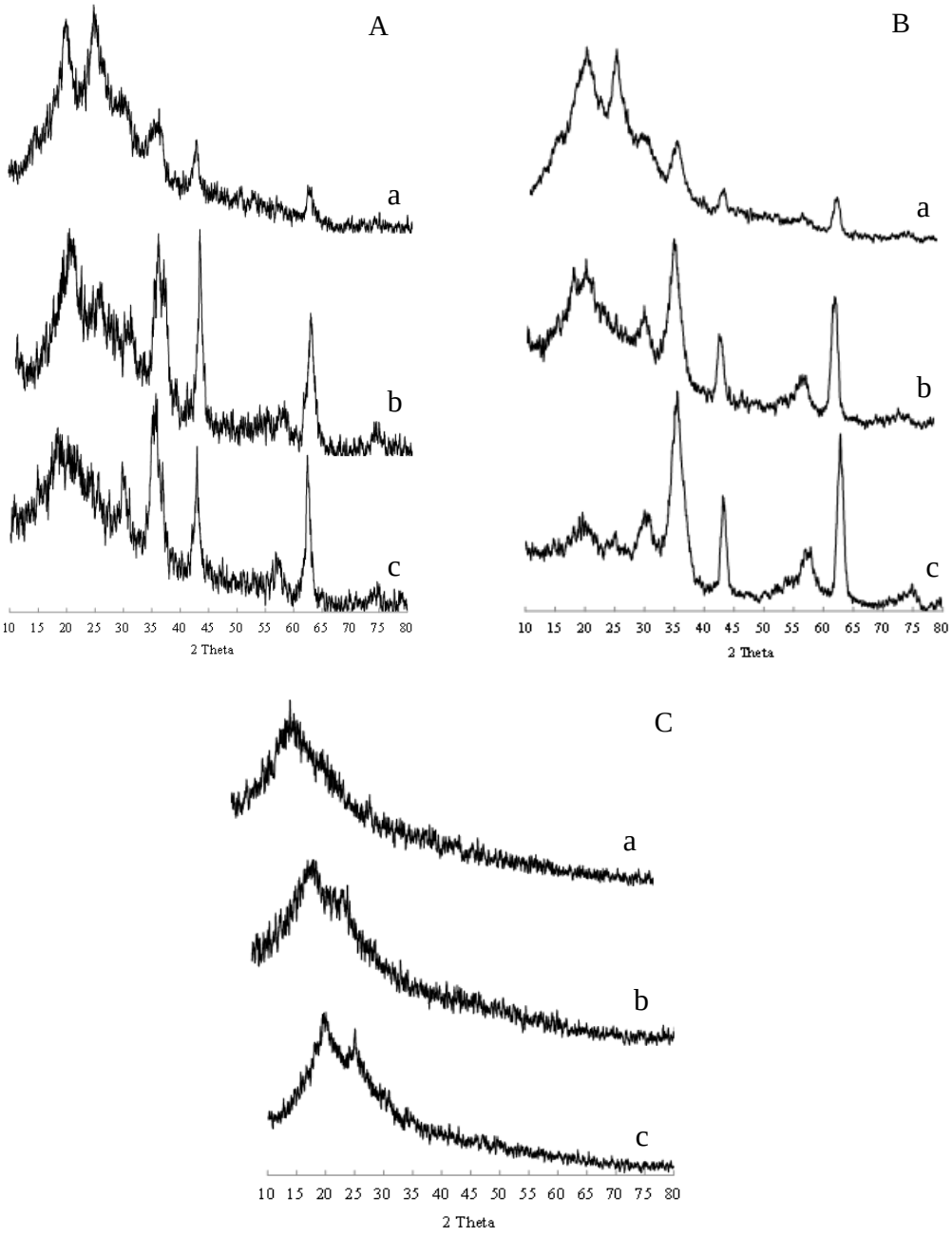

Figure 8.11.: XRPD patterns of A) composites containing MNPs_1 (a= sample no.45, b= sample no. 44, c= sample no. 43), B) composites containing MNPs_2 (a= sample no.42, b= sample no. 41, c= sample no. 40), C) composites containing MNPs_3 (a= sample no.39, b= sample no. 38, c= sample no. 37).

As it is possible to observe, the presence of the inorganic magnetic component resulted evident in the composite materials prepared with MNPs_1 and MNPs_2, whereas the absence of diffraction peaks of magnetite in composites synthesized in the presence of MNPs_3 might be attributed to the very small size of NPs.

8.2.2. Morphological characterization

The PANI/Fe_3O_4 composites were characterized for their structural and morphological attributes using specific probes like XRD, TEM, STEM, EELS and EDX and the results are reported below (Figure 8.12.).

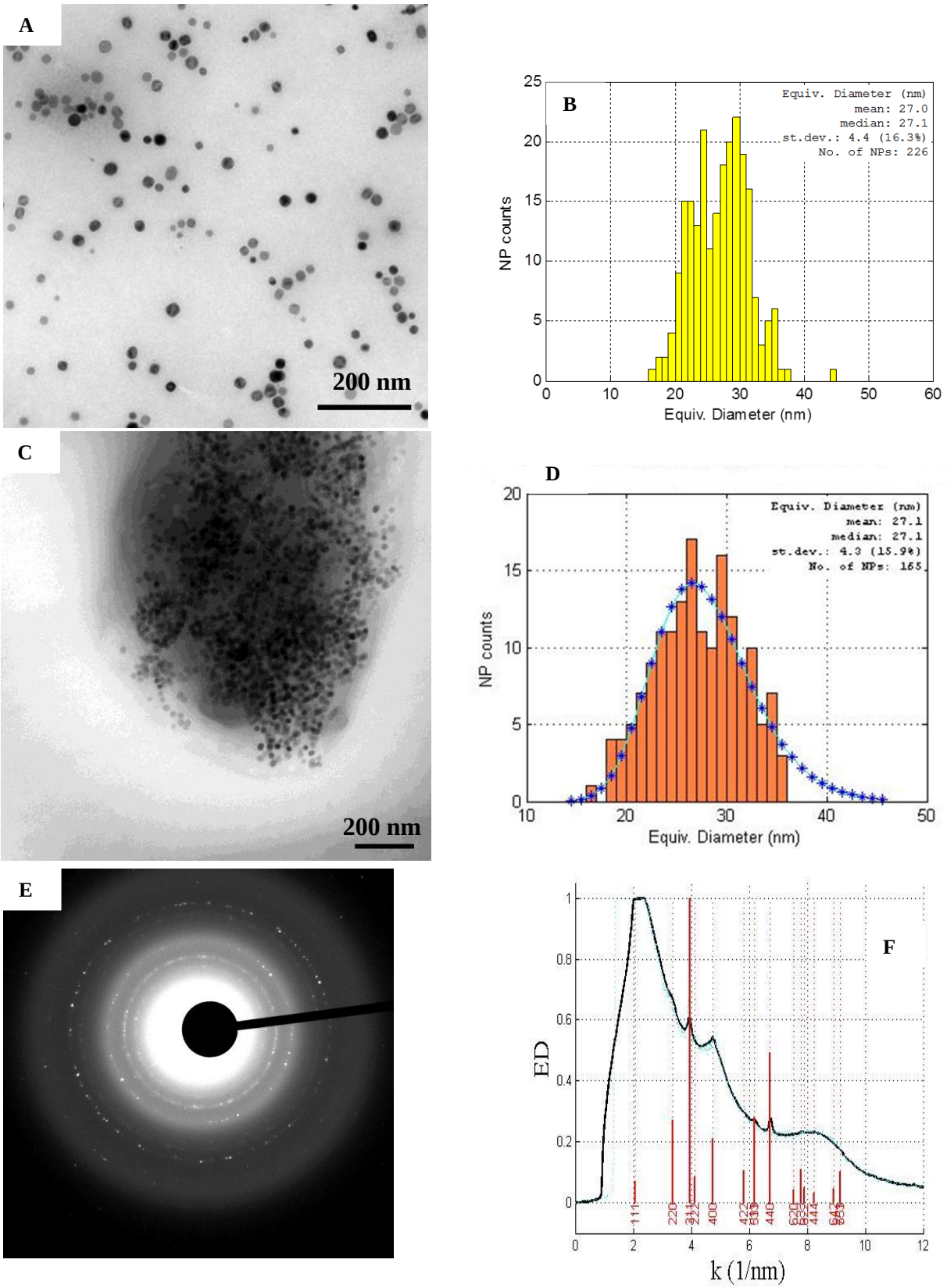

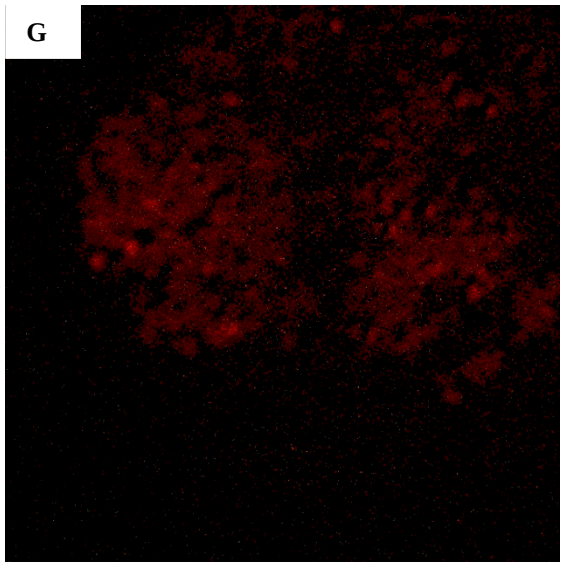
G

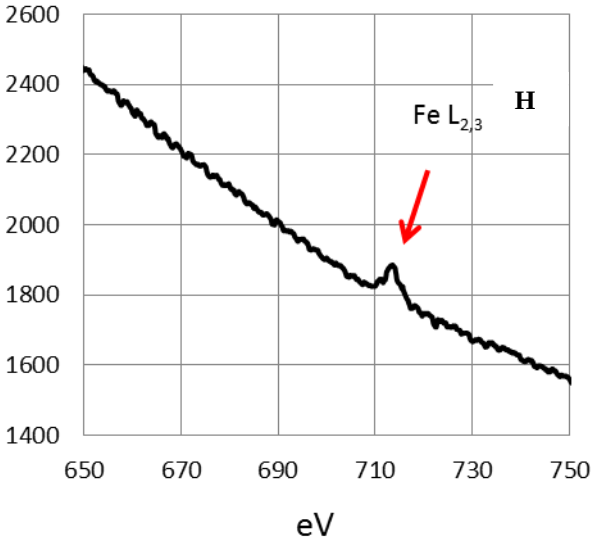
H
Fe L2,3
2600
2400
2200
2000
1800
1600
1400
650
670
690
710
730
750
eV

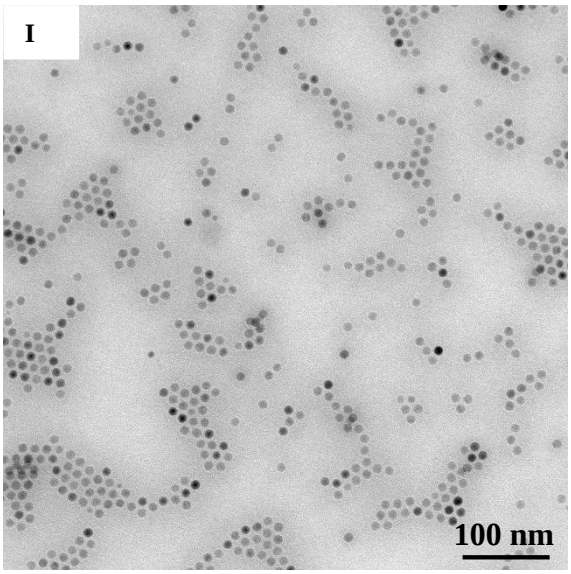
I
100 nm

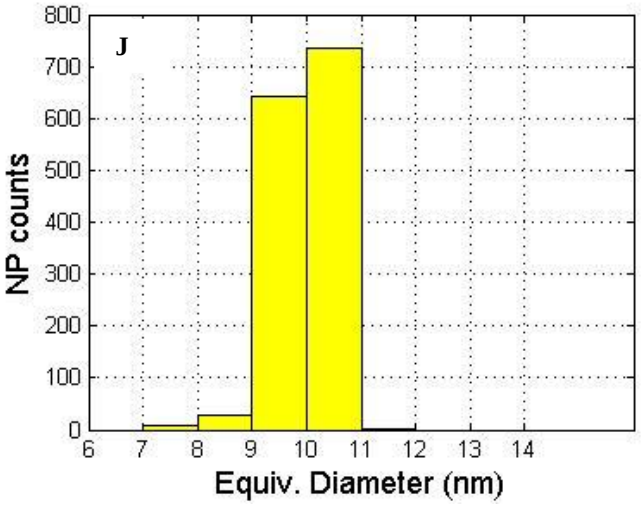
J
NP counts
800
700
600
500
400
300
200
100
0
6
7
8
9
10
11
12
13
14
Equiv. Diameter (nm)

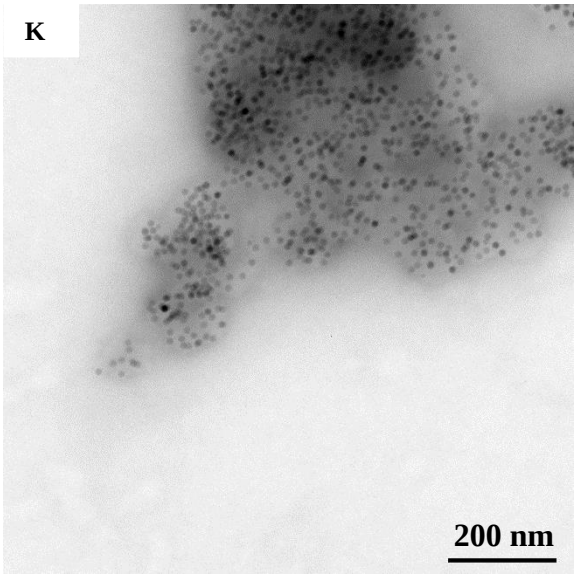
K
200 nm

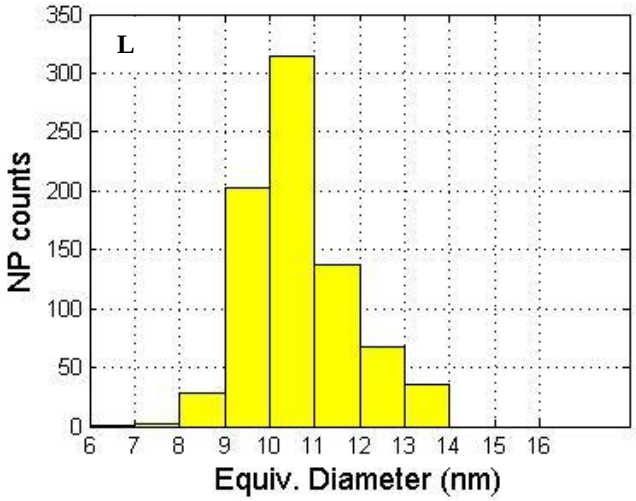
L
NP counts
350
300
250
200
150
100
50
0
6
7
8
9
10
11
12
13
14
15
16
Equiv. Diameter (nm)

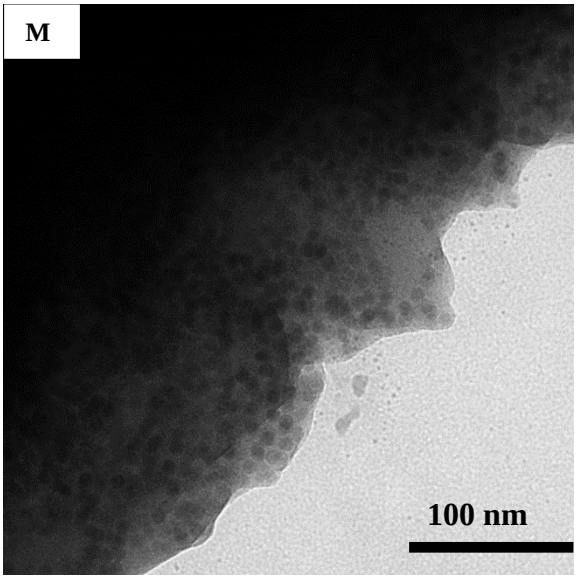
M
100 nm

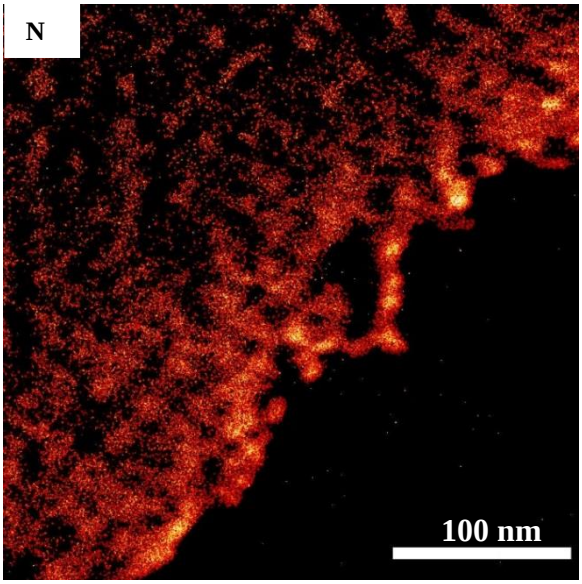
N
100 nm

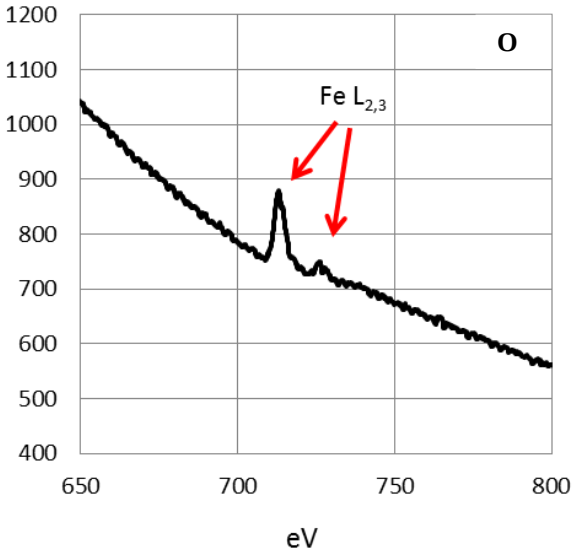
O
Fe L2,3
1200
1100
1000
900
800
700
600
500
400
650
700
750
800
eV

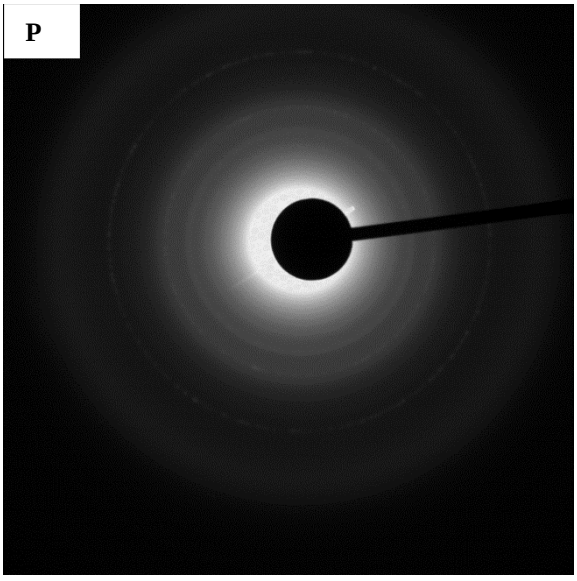
P

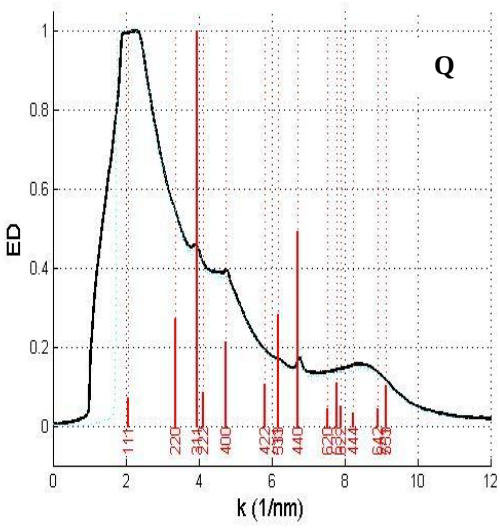
Q
ED
k (1/nm)
0
2
4
6
8
10
12
0.2
0.4
0.6
0.8
1
111
220
311
400
422
440
620
444

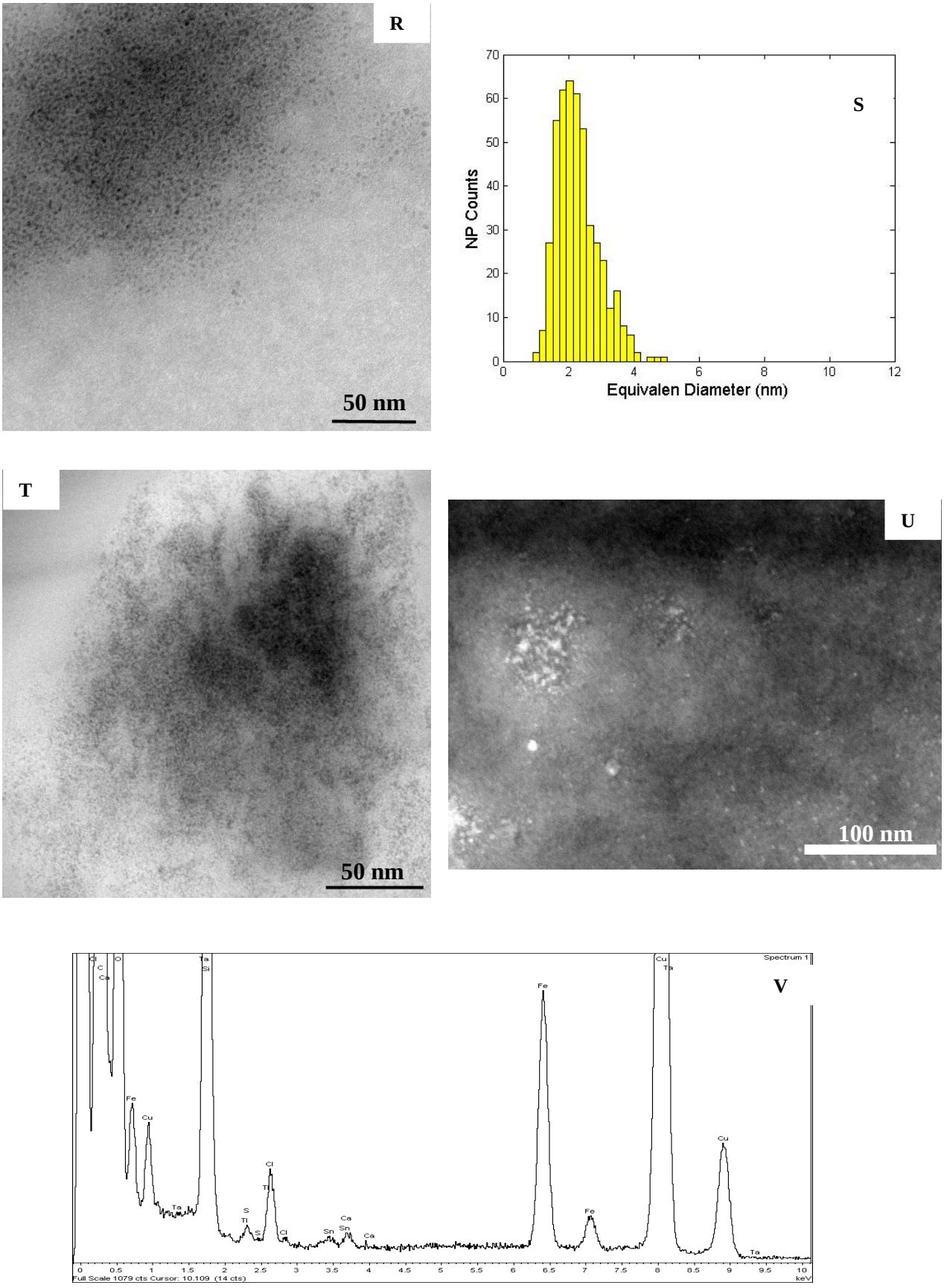

Figure 8.12.: A) TEM image of MNP_1, B) statistical distribution of MNP_1 diameters, C) TEM image of PANI/MNP_1 composite (Sample 43) with contrast improved by energy filtering, D) statistical analysis of size distribution of MNP_1 inside PANI/MNP_1 composite (Sample 43), E) electron diffraction pattern of PANI/MNP_1 composite and corresponding analysis (F), G) PANI/MNP_1 sample EFTEM (Energy Filtered

TEM) image: in red is reporder the image generated only from iron, H) EELS (Electron Energy loss Spectroscopy) spectrum of PANI/ MNP_1 sample the red arrow underlines the Fe $L_{2,3}$ signal, I) TEM image of MNP_2, J) statistical distribution of MNP_2 diameters, K) TEM image of PANI/MNP_2 composite (Sample 40) without any energy filtering, L) statistical analysis of size distribution of MNP_2 inside PANI/MNP_2 composite (Sample 40), M) PANI/MNP_2 sample(Sample 40) conventional TEM image, reference image for the EFTEM (Energy Filtered TEM) image (N): in red is reporder the image generated only from iron, O) EELS (Electron Energy loss Spectroscopy) spectrum of PANI/MNP_2 sample (Sample 40) the red arrows underline the Fe $L_{2,3}$ signal, P) electron diffraction pattern of PANI/MNP_2 sample (Sample 40) and corresponding analysis (Q), R) TEM image of MNP_3, S) statistical distribution of MNP_3 diameters, T) TEM image of PANI/MNP_3 composite (Sample 37) with contrast improved by energy filtering, U) PANI/MNP_3 (Sample 37) STEM image, V) PANI/MNP_3 (Sample 37) Energy Dispersive X-ray (EDX) spectrum.

To image the MNPs within the composite, and thus study their morphology and distribution, an energy filtered TEM was used to optimize the contrast between MNPs and polymer by using electrons with an energy loss of 30 eV, so that the polymer matrix appeared as a light gray halo instead of being very dark as occurs in conventional ZLF (zero-loss filtered) TEM.

In all cases the morphology of magnetic NPs resulted to be unchanged during the composite synthesis and a good dispersion within the PANI matrix was observed.

In order to verify that they didn't suffer from a change of crystal phase and/or chemical composition during the synthesis, several micro analytical techniques were used to examine the samples in depth.

Electron diffraction (ED) patterns confirmed that PANI/MNP_1 and PANI/MNP_2 (Figures 8.12. E and P) comprised magnetite MNPs with spinel structure. PANI/MNP_3 gave no detectable diffraction probably because of ring broadening brought about by their small size. So, in this case Scanning TEM (STEM) (Figure 8.12. U) and STEM/Energy Dispersive X-ray (EDX) spectroscopy (Figure 8.12. V) were performed: the MNP_3 nanoparticles were distinctly visible in STEM image and the EDX spectrum (not reported) showed the presence of Fe into the composite.

Electron Energy Loss Spectroscopy (EELS) and Energy Selected Imaging (ESI) experiments were also performed. In the EELS spectrum of the composites (Figures 8.12. H, G, N, O), the Fe-$L_{2,3}$ edge, with the typical "white lines", starting from 708 eV was clearly seen for all the three samples. ESI images selecting the Fe-$L_{2,3}$ edge energy were collected for PANI/MNP_1 and PANI/MNP_2, instrumental resolution being too low to image the individual NPs in PANI/MNP_3.

8.2.3. Magnetic measurements

Magnetic measurements were carried out by the use of a Quantum Design MPMS XL-5 SQUID magnetometer. The magnetic properties of PANI/MNPs nanocomposites were evaluated by measuring the hysteresis cycle in the field-cooling condition (HysFC, H_{cool} = 50 kOe) and the

temperature dependence of the magnetization in both Zero Field Cooling (ZFC) and Field Cooling (FC, H_{cool} = 10 Oe) modes. In both cases the measuring field was 10 Oe.

The saturation magnetization M_s, the remanence M_r and the coercive field H_c are reported in Table 8.11 and M-H curves are shown in Figure 8.13.

Parameter	Sample no. 37	Sample no. 40	Sample no. 43
M_s (emu/g)[a, b]	8.9	16.6	13.8
M_r (emu/g)[b]	0.03	4.0	2.1
M_r/M_s	0.003	0.24	0.15
H_c (Oe)	0.08	0.45	0.60
T_{irr} (K)	≈ 150	110	300
$T_{max,ZFC}$ (K)	5	90	310
$T_{der,ZFC}$ (K)	5	60	270

Table 8.11.: Magnetic properties of PANI/MNPs composites (Sample no. 37, 40 and 43). [a]M_s and M_r are referred to composite mass and at 50 kOe.

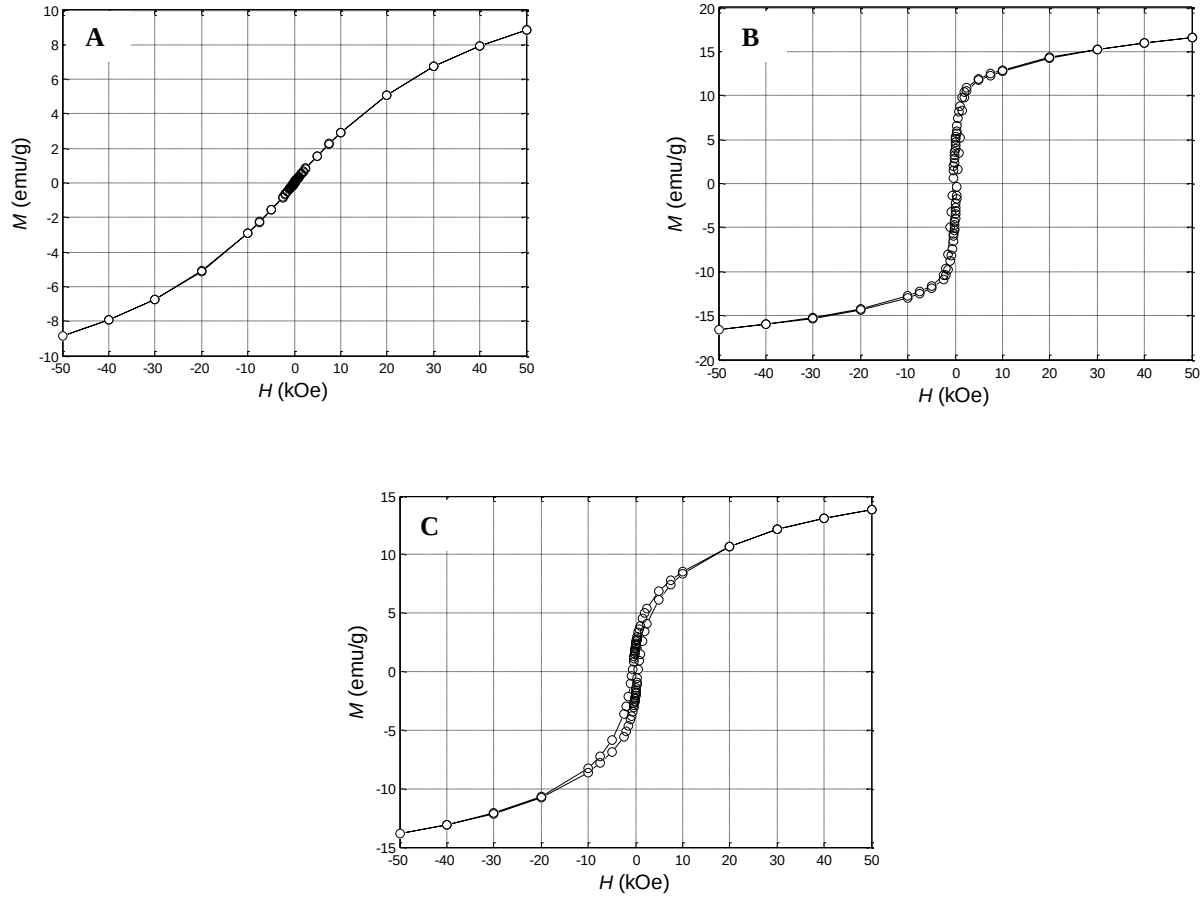

Figure 8.13.: Magnetization-demagnetization M-H curves of (a) Sample no.37, (b) Sample no. 40 and (c) sample 43.

As it is possible to observe, PANI/Fe_3O_4 composite (Sample no. 37) containing smaller magnetic nanoparticles didn't reach saturation even to 50 kOe, didn't exhibit remanence and coercitivity and didn't show hysteresis.

As expected, the other composites (Samples no. 40 and 43) saturated within 50 kOe, exhibited remanence and coercitivity and showed very small hysteresis that increased with the NPs sizes.

The unexpected trend observed for the M_r/M_s values, could be due to a different distribution of inorganic nanoparticles within the polymeric matrix. In fact, in general the value of this ratio increased with the NPs sizes.

To better understand the magnetic properties of PANI/Fe_3O_4 composites, ZFC (zero-field cooling) and FC (field cooling) magnetization were measured (Figure 8.14.). The characteristic temperatures derived from ZFC/FC data are reported in Table 8.11.

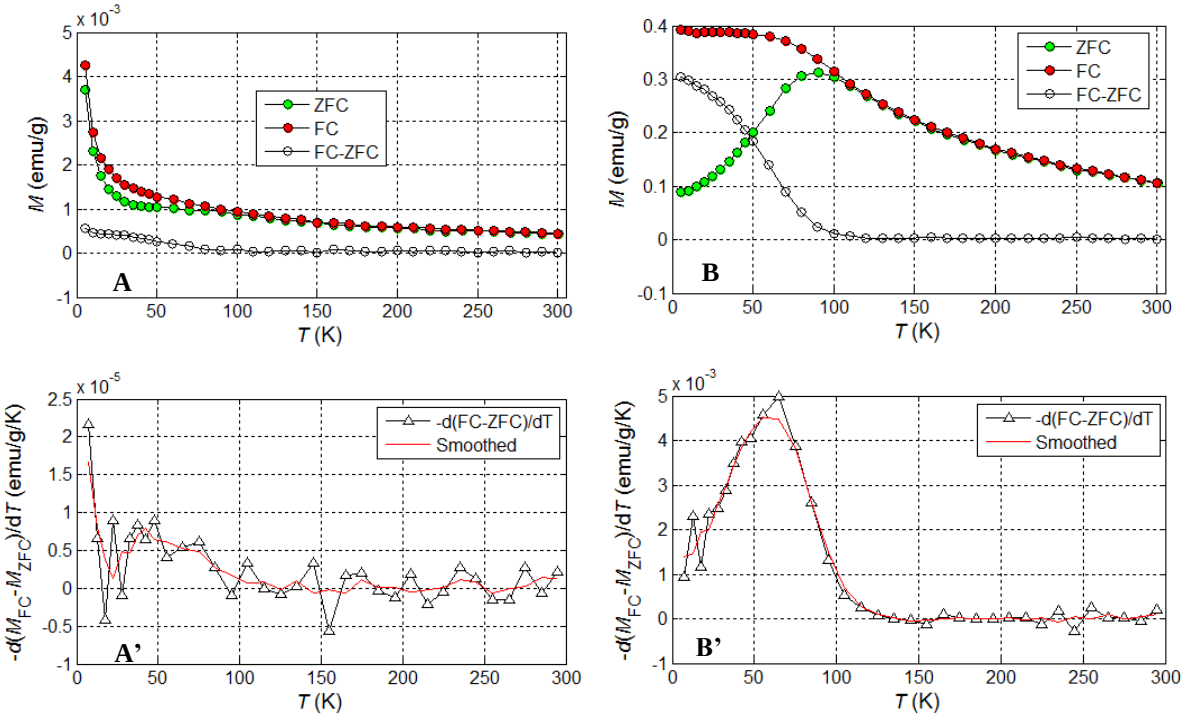

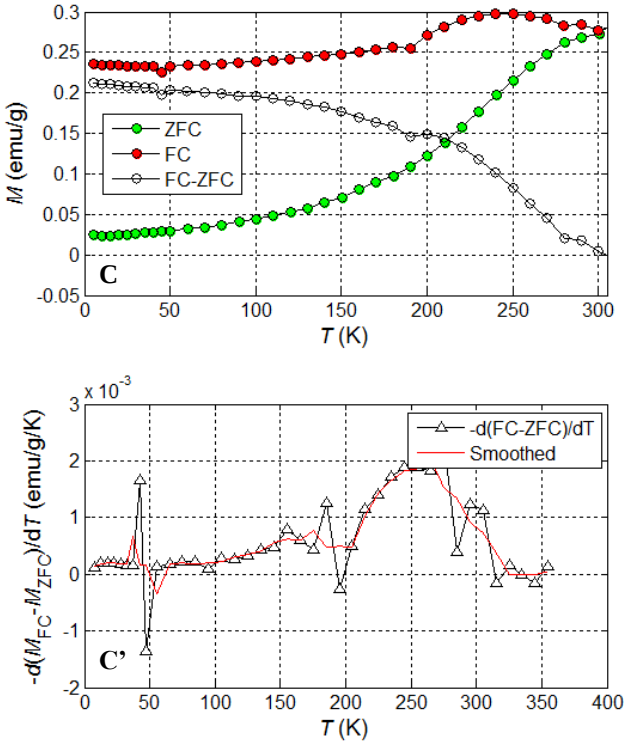

Figure 8.14.: ZFC and FC magnetization (100 Oe) of (a) Sample no.37, (b) Sample no. 40 and (c) sample 43 A_C: temperature dependence of M_{FC} (red dots), M_{ZFC} (green dots) and $M_{FC}-M_{ZFC}$ (white dots). A'-C': derivative $-d(M_{FC}-M_{ZFC})/dT$.

In particular, Sample no. 37 exhibited a reversible behaviour down to low temperature, whereas the ZFC/FC bifurcation about 100 K was probably due to aggregation phenomena of nanoparticles.

Sample no. 40 exhibited a typical behaviour of FeOx NPs with negligible aggregation. Derivative plot showed a barrier distribution between 5 and 100 K. There was no design of a spin-glass-like state at low temperature.

Coercivity at 5 K increased with the NPs size as expected due to SPM (superparamagnetic) effects.

Finally, Sample no. 43 exhibited an irreversible behaviour up to room temperature. A frozen, spin-glass-like state was observed at temperature as high as 200 K.

This means that these composite materials displayed a variety of magnetic behaviour which can be selected by choosing the NPs size; for example, the SPM regime can be shifted from above room temperature to T < 5 K. In any case, the small M_r/M_s ratio remains to be explained.

8.3. Synthesis and characterization of PANI/MFe_2O_4 composites: the role of the bivalent metal (M)

In order to extend the method described in Sections 8.1. and 8.2. to the preparation of polyaniline-based composites containing different ferrite components ($CoFe_2O_4$, $NiFe_2O_4$, $CuFe_2O_4$, etc.), the catalytic behaviour of other spinels was investigated in the oxidative polymerization of *N*-(4-

aminophenyl)aniline, replacing iron(II) with another metal (Mn, Co, Ni, Cu, Zn, Mg). This approach allowed to clarify what is the catalytically active metallic center in the spinel structure.
MFe_2O_4 materials (M= Co, Ni, Mn, Cu, Zn, Mg) were synthesized by chemical co-precipitation method and PANI/MFe_2O_4 composites were characterized by different techniques: FT-IR, UV-vis, XRPD, TEM and SQUID.

8.3.1. Catalytic polymerization using $CoFe_2O_4$ NPs as the catalysts

At first, Fe(II) was replaced with Co(II) and $CoFe_2O_4$NPs were produced as powder ($CoMNPs_p$) and ferrofluid (oleic acid-modified NPs dispersed in toluene, $CoMNPs_{ff}$).
Tables 8.12. and 8.13. report the results obtained in terms of yield in the oxidative polymerization of AD using H_2O_2 and molecular oxygen as the oxidants.

AD/$CoFe_2O_4$ (molar ratio)	$CoMNPs_{ff}$		$CoMNPs_p$	
	Sample no.	Yield (%)	Sample no.	Yield (%)
50	52	67	55	59
10	53	75	56	70
5	54	81	57	74

Table 8.12.: Polymerization yields for the aerobic oxidative polymerization of AD in the presence of CoMNPs. Reaction time= 3 days, reaction temperature= 80°C, pO_2= 3 bar.

AD/$CoFe_2O_4$ (molar ratio)	$CoMNPs_{ff}$		$CoMNPs_p$	
	Sample no.	Yield (%)	Sample no.	Yield (%)
50	58	80	61	53
10	59	89	62	70
5	60	98	63	83

Table 8.13: Polymerization yields for the anaerobic oxidative polymerization of AD in the presence of CoMNPs. Reaction time= 24 h, reaction temperature= 25°C, H_2O_2/AD= 5, molar ratio.

These results showed that both CoMNPs powder- and ferrofluid-type resulted to be good candidates as catalysts for the oxidative polymerization of AD.
However, contrary to what was observed for Fe_3O_4 NPs (Tables 8.1. and 8.2.), the catalytic activity of CoMNPs was higher under aerobic conditions than in the presence of hydrogen peroxide. In fact, as reported above (section 8.1.), hydrogen peroxide allowed to achieve polyaniline with 40% yield after 24 h also in the absence of any catalyst. This means that the starting point "zero" was different

for the two oxidants. Such an effect was more evident if yields were calculated according to Eq. 8.1. (Graphic 8.3.).

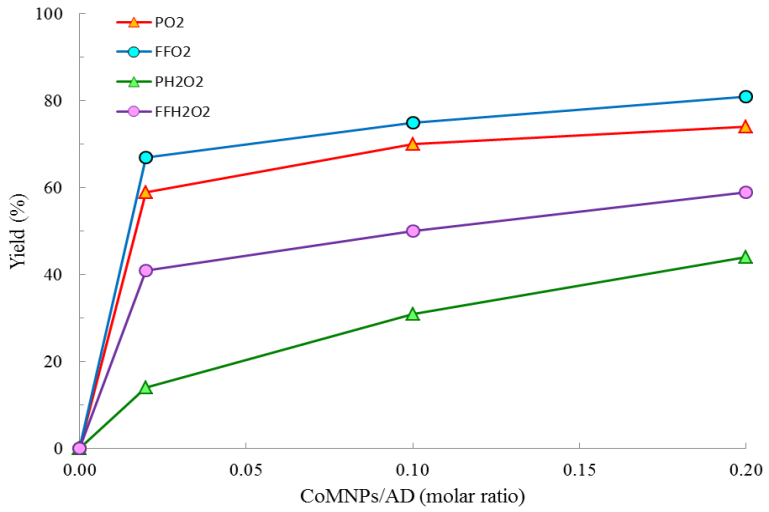

Graphic 8.3.: Dependence of the catalytic yields of the AD oxidative polymerization from the amount of CoMNPs.

As shown in Graphic 8.3., even though in the presence of molecular oxygen both CoMNPs powder- and ferrofluid-type exhibited similar catalytic activities, on the contrary using hydrogen peroxide they displayed different behaviours. In particular, $CoMNPs_{ff}$ showed higher catalytic performances if compared to the $CoMNPs_{p}$.

The different results obtained using different oxidants could be ascribed to the ability of CoMNPs to decompose H_2O_2. In fact, as reported by Lahiri *et al*., [575], spinel ferrites (in particular, manganese and cobalt ferrites) are active in the decomposition of H_2O_2. This means that the presence of CoMNPs into the reaction mixture might limit the presence of the oxidant thus producing polymer in low yield. However, when magnetic NPs were capped with oleic acid to give the corresponding ferrofluid-type NPs, their catalytic activity towards H_2O_2 decomposition was depressed and the polymer yield increased (Table 8.13. and Graphic 8.3.).

As reported in Section 8.1. for Fe_3O_4NPs, also in this case the content of inorganic component into the final composites was determined by atomic absorption spectroscopy (AAS) and the results, summarized in Table 8.14., confirmed that the inorganic component was totally incorporated into the final insoluble composites maintaining a constant Fe/Co molar ratio of 2.

Sample no.	$CoFe_2O_4$/composite % (w/w) calculated	$CoFe_2O_4$/composite % (w/w) measured
60	18.1	17.9
63	21.4	21.3
54	12.1	12.0
57	13.2	13.2

Table 8.14.: $CoFe_2O_4$ content in the PANI/$CoFe_2O_4$ composites

These results suggested that CoMNPs acted as a heterogeneous catalyst, because their performances are not attributable to corrosion phenomena in solution.

8.3.2. Morphological and spectroscopic characterization

Based on the experience of Fe_3O_4NPs, only $CoMNPs_{ff}$ were characterized by X-ray powder diffraction and TEM microscopy. The average crystallite domain size, calculated by the Debye-Scherrer equation (Eq. 2.2.), results to be 12 nm.

However, further investigations carried out by TEM microscopy allowed to demonstrate that CoMNPs were polydispersed with median diameter of <d> = 12 nm and standard deviation of 5 nm (Figure 8.15. b).

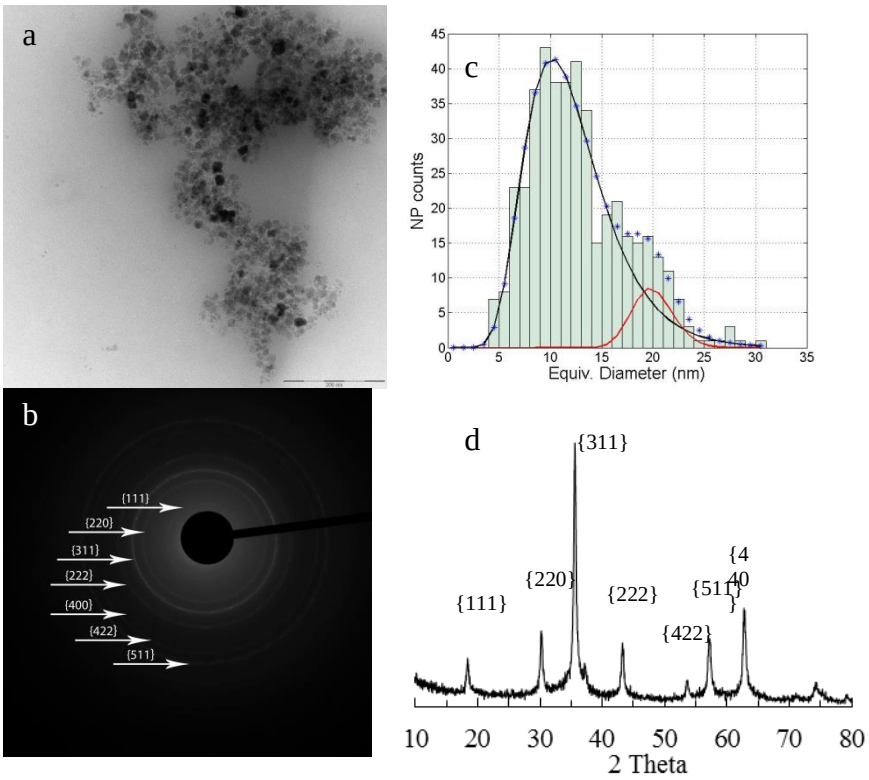

Figure 8.15.**:** TEM image of $CoMNPs_{ff}$ (a, bar=200 nm) with the corresponding ED pattern (b), particle size distribution (c), XRPD pattern of $CoMNPs_{ff}$ (d).

More in detail, the size histogram reported in Figure 8.15. b suggested that two different NP populations were present, the major one (95%) with <d> = 12 nm and the minor one (5%) with <d> = 20 nm. The spinel structure of MNPs, previously observed by the XRPD pattern (Figure 8.15. d), was confirmed by electron diffraction (ED) pattern (Figure 8.15. b), corresponding to the bright-field image (Figure 8.15. a).

The presence of CoMNPs into the composites, already established by AAS analyses (Table 8.14.) was confirmed by X-ray powder diffraction, as shown in Figure 8.16.

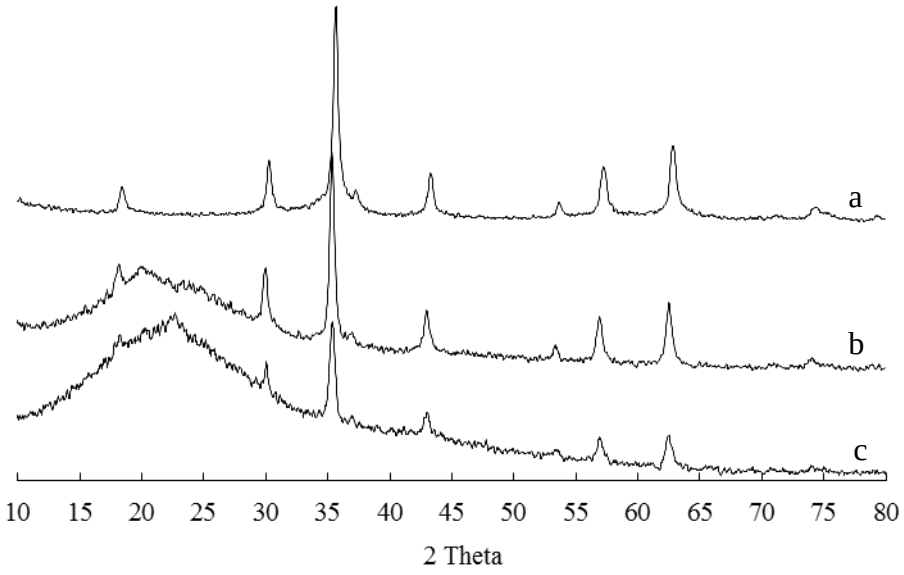

Figure 8.16.: XRPD patterns of $CoMNPs_{ff}$ (a) and its composites with PANI (b= sample no. 60, c= sample no. 59)

The broad peak at around 25°θ can be assigned to the amorphous polymeric matrix, whereas the other peaks can be assigned to pure cobalt ferrite phase with a cubic spinel structure, according to the literature.[576]

Moreover, the mean diameter of CoMNPs embedded into the polymeric matrix resulted to be unchanged (about 12 nm) if compared to that of pristine nanoparticles, as shown in Table 8.15.

Sample	Mean diameter (nm)
$MNPs_{ff}$	12.0
Sample no. 59	12.4
Sample no. 60	12.7

Table 8.15.: Mean diameter of the CoMNPs calculated by the Scherrer's equation

Similarly to what it was reported in section 8.1., the polymeric matrix in all the composites was characterized by FT-IR and UV-vis spectroscopies. Contrary to what it was observed when Fe_3O_4 NPs were used as the fillers and catalysts of the oxidative polymerization reaction of AD, in this case polyaniline was not obtained in half-oxidized emeraldine form, but rather in an intermediate oxidation state between leucoemeraldine and emeraldine (Figures 8.17. A and B).

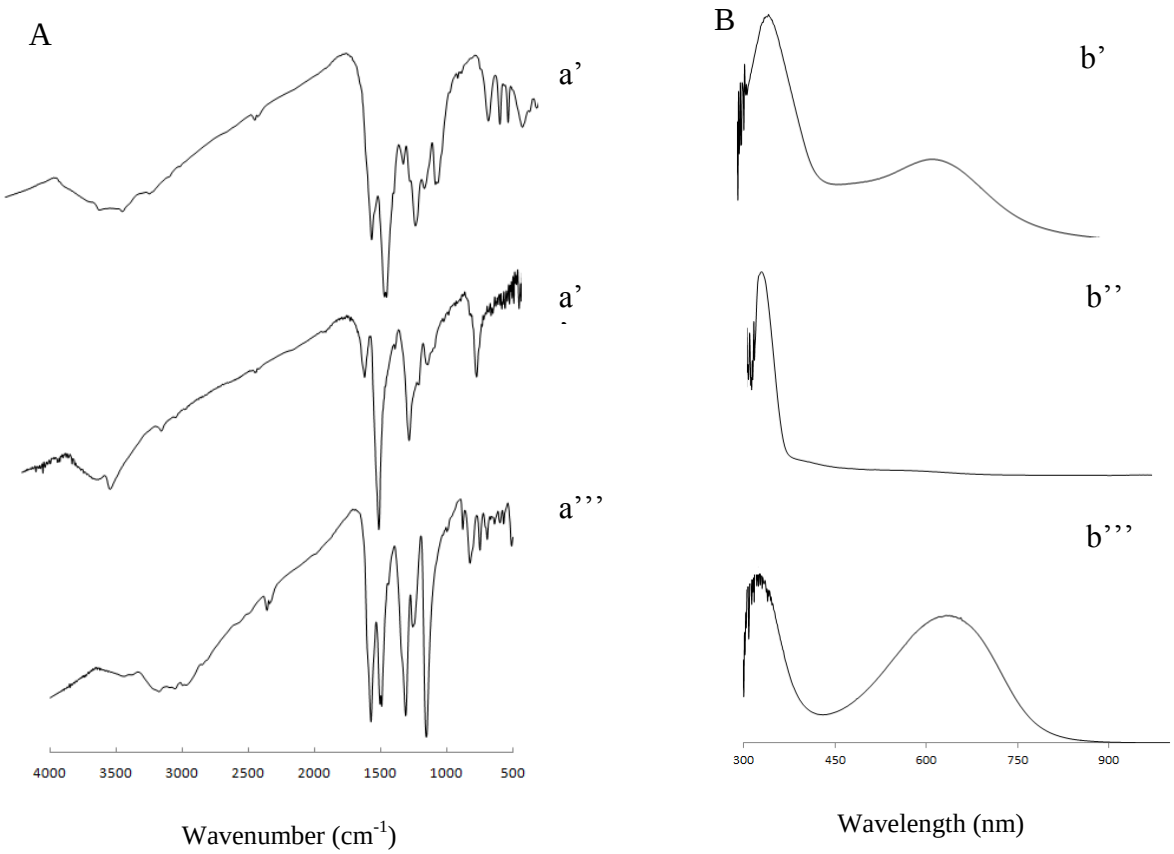

Figure 8.17.: A) FT-IR spectra and B) UV-vis spectra of (a', b') a typical PANI/CoMNPs composite, (a'', b'') leucoemeraldine and (a''', b''') emeraldine salt.

Spectra a' and b' clearly showed in PANI/CoMNPs composites polymeric structure resulted to be more similar to the reduced form of PANI, leucoemeraldine, than to the half-oxidized one, emeraldine.

In particular, in the FT-IR spectrum of composite (a') the ratio between the bands at around 1570 cm^{-1} (quinoid band) and 1498 cm^{-1} (benzenoid band) resulted to be minor than one and the intensity of the band at *ca.* 1144 cm^{-1} (electronic-like band) was strongly reduced. This was confirmed by the UV-vis spectroscopy. More in detail, in the UV-vis spectrum of PANI/CoMNPs composite (b') the first absorption band (*ca*. 330 nm), associated with a π-π^* transition of the conjugated ring system, was much higher than the second one (*ca*. 640 nm), assigned to a benzenoid to quinoid excitonic transition.

The FT-IR and UV-vis analyses, together with the reaction yields, showed that, even though CoMNPs exhibited catalytic activity in the oxidative polymerization of *N*-(4-amino phenyl)aniline, they stopped the reaction before that polymer reached the oxidation state of emeraldine.

In order to address the oxidative polymerization reaction towards conducting emeraldine form, a co-catalyst able to complete the oxidation process was added to the reaction mixture. Fe^{3+} (AD/Fe^{3+} = 1000 molar ratio) was chosen as the co-catalyst owing to its catalytic ability, as reported in the literature.[36] In this case the polymeric matrix of the composites was obtained in the conductive emeraldine form, as confirmed by FT-IR and UV-vis spectroscopies, that showed spectra similar to those reported in Figures 8.1. and 8.2., and by conductivity measurements (Table 8.16.)

Sample	σ (S · cm-1)
Emeraldine salt	$3.5 \cdot 10^{-3}$
Leucoemeraldine	$1.0 \cdot 10^{-8}$
Sample no. 59	$7.3 \cdot 10^{-5}$
Sampleno. 60	$4.9 \cdot 10^{-5}$
PANI/CoMNPs with co-catalyst	$5.5 \cdot 10^{-3}$

Table 8.16.: Conductivity values of emeraldine salt, leucoemeraldine, Sample no. 59, Sample no. 60 and PANI/CoMNPs composite prepared in the presence of Fe^{3+} as the co-catalyst.

As for PANI/Fe_3O_4 composites (Figure 8.7.), also for PANI/CoMNPs materials the positive effect of the presence of magnetic fillers into the polymeric matrix on its thermal stability was observed by TGA technique (Figure 8.18.).

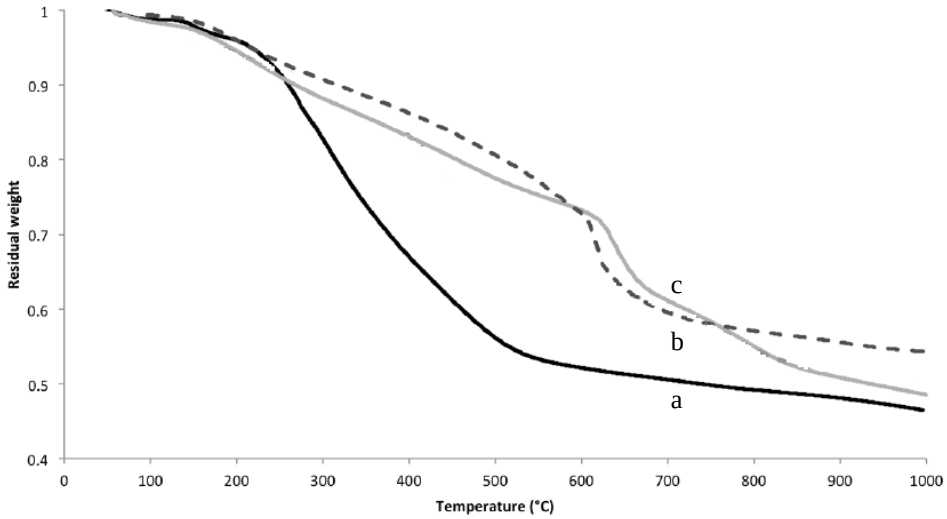

Figure 8.18.: TGA results for (a) pure PANI (Sample no. 20), (b) Sample no. 62 and (c) sample no. 63.

8.3.3. Magnetic measurements

In order to define a $CoFe_2O_4$ NP single-domain structure its diameter has to be < *ca.* 320 nm. Moreover, in order to reverse its magnetization by coherent rotation its diameter has to be < *ca.* 50 nm. XRD and TEM investigation (Fig. 8. 15) showed that individual CoMNPs reported above showed smaller diameters than these (329 n and 50 nm). It's well known from the literature,[577] that the blocking diameter for CoMNPs is 9 nm at 300 K and 2 nm at 5 K. For this reason CoMNPs and PANI/CoMNPs should exhibit a partial superparamagnetic behavior at high temperature. However, it should be stressed that these critical diameters – especially the blocking diameters – are valid for non-interacting NPs free from surface effects. The magnetization of $CoMNPs_{ff}$ and PANI/CoMNPs composites (Samples no.: 53, 54, 59 and 60) were measured either as a function of temperature in the range 300-5 K at low field (10 Oe) in ZFC and FC mode, and as magnetization isotherm (hysteresis loop) between ±50 kOe at 5 K after FC (+50 kOe) from 295 K.

Figure 8.19 shows the ZFC and FC magnetization curves and the main parameters are summarized in Table 8.17.

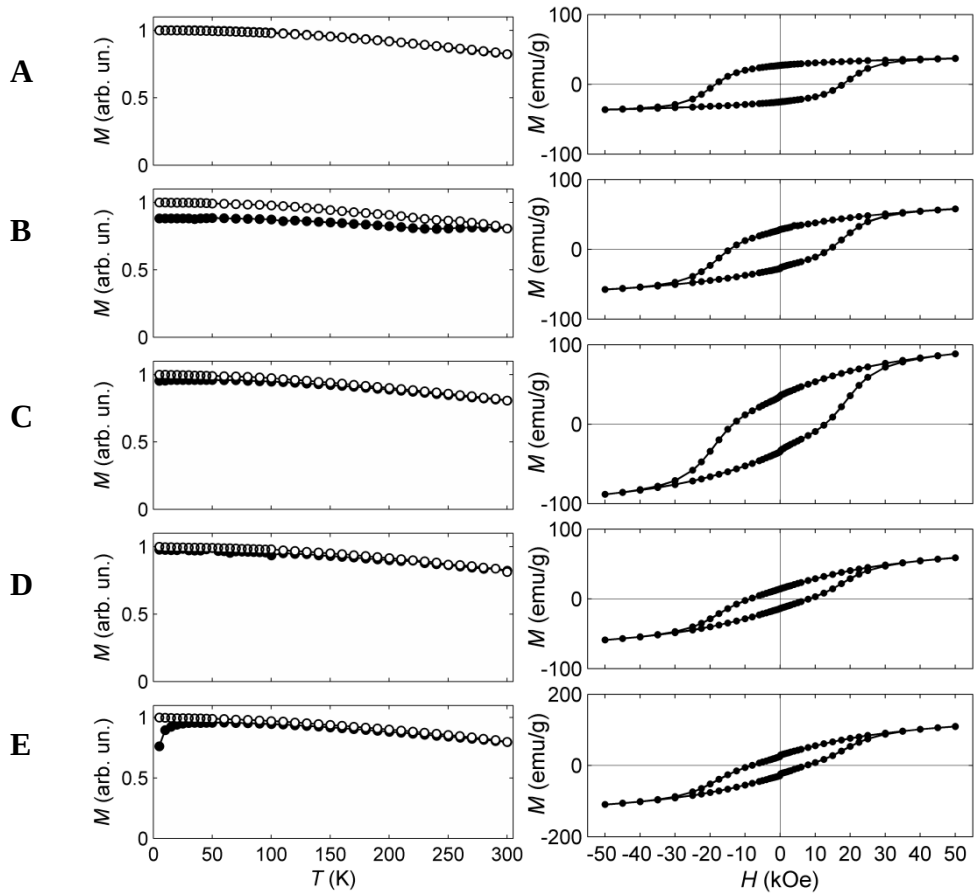

Figure 8.19.: Magnetization of $CoMNPs_{ff}$ and PANI/CoMNPs composites. Left: ZFC (solid circles) and FC (hollow circles) magnetization; right: magnetization isotherms (FC hysteresis loops). A), $CoMNPs_{ff}$, B) sample no. 54, C) sample no. 60, D) sample no. 53, E) sample no. 59.

Sample	T_0 (K)	a (K^{-b})	b
$CoMNPs_{ff}$	746±3	(3.4±0.3) 10^{-6}	1.91±0.01
54	783±12	(9±2) 10^{-6}	1.74±0.05
60	793±6	(12±2) 10^{-6}	1.69±0.02
53	727±7	(2.6±0.5) 10^{-6}	1.95±0.04
59	759±4	(9.1±0.9) 10^{-6}	1.75±0.02

[a] Generalized Bloch-type law: $M(T) = M(0)\,(1 - aT^b)$, $T_0 = a^{-1/b}$.

Table 8.17.: Optimal parameters from fitting the FC low-field magnetization of ferrofluid-type $CoFe_2O_4$ NPs and PANI-$CoFe_2O_4$ NP composites to the generalized Bloch-type law. [a]

The data showed that the samples did not reach saturation even at 50 kOe and had high coercivity. The values of saturation magnetization (Msat) at 50 kOe are in accordance with those reported in the literature for bulk CoFe2O4 [578].

The ZFC and FC curves of $CoMNPs_{ff}$ overlapped in the 5-300 K range and both M_{ZFC} and M_{FC} increased on cooling. These curves are very similar to those observed for bulk ferrites.[578] In the investigated temperature range, there was no evidence of superparamagnetic behavior with its

characteristic FC-ZFC bifurcation and magnetization blocking-unblocking processes, as often observed for CoMNPs where superparamagnetism dominates the magnetic behavior.
This behaviour could be explained by a dominant interparticle exhange interaction that overshadowed size and surface effects.

Comparing the results obtained by the use of Fe_3O_4 and $CoFe_2O_4$ NPs, it resulted to be clear that the change of the first metal into the spinel structure deeply affected the catalytic behaviour of these materials in the oxidative polymerization of aniline dimer.

8.3.4.Catalytic polymerization using MFe_2O_4 NPs as the catalysts (M= Mn, Co, Ni, Cu, Zn, Mg) and characterization

In order to clarify the effect of such a substitution, spinels containing other metals (Mn, Co, Ni, Cu, Zn, Mg) instead of iron(II) and Co(II) were prepared and tested under the same conditions.
All the MFe_2O_4 NPs were prepared by co-precipitation method. XRPD patterns (data not reported) showed that they were obtained in spinel structure with a mean diameter of about 10 nm (Table 8.18.), as resulted by the Debye-Scherrer equation (Eq. 2.2.).

Spinel	d (nm)	Fe/M (molar ratio)[a]
$MgFe_2O_4$	7.7	1.8
$NiFe_2O_4$	6.1	2.1
$ZnFe_2O_4$	7.3	1.8
$CuFe_2O_4$	11.0	1.9
$MnFe_2O_4$	11.8	2.1

Table 8.18.: Mean diameter of MFe_2O_4 NPs calculated by the Debye-Scherrer equation. [a] M= Mg, Ni, Zn, Cu and Mn. Data obtained by atomic absorption spectroscopy.

All these materials were tested in the reaction of oxidative polymerization of aniline dimer and the results are reported in Tables 8.19. and 8.20.

Sample no.	MFe_2O_4	AD/MFe_2O_4 (molar ratio)	Yield %
64	$NiFe_2O_4$	5	77
65		10	64
66		50	61
67	$CuFe_2O_4$	5	86
68		10	82
69		50	81
70	$ZnFe_2O_4$	5	61
71	$MgFe_2O_4$	5	63
72	$MnFe_2O_4$	5	48

Table 8.19.: Polymerization yields for the aerobic oxidative polymerization of AD in the presence of MFe_2O_4 NPs. Reaction time= 3 days, reaction temperature= 80°C, pO_2= 3 bar.

Sample no.	MFe_2O_4	AD/MFe_2O_4 (molar ratio)	Yield %
73	$NiFe_2O_4$	5	66
74		10	43
75		50	24
76	$CuFe_2O_4$	5	63
77		10	34
78		50	28
79	$ZnFe_2O_4$	5	31
80	$MnFe_2O_4$	5	21
81	$MgFe_2O_4$	5	18

Table 8.20.: Polymerization yields for the anaerobic oxidative polymerization of AD in the presence of MFe_2O_4 NPs. Reaction time= 24 h, reaction temperature= 25°C, H_2O_2/AD= 5, molar ratio.

As reported in Tables 8.19. and 8.20., under aerobic conditions all the ferrites showed interesting catalytic behaviours, exhibiting quite high polymerization yields (from 48 to 66%). On the contrary, when the reaction was carried out under anaerobic conditions, using H_2O_2 as the oxidant, good results in terms of yield were obtained only for $NiFe_2O_4$ and $CuFe_2O_4$ NPs.

Regarding MFe_2O_4, a different catalytic activity appeared when H_2O_2 was employed as the oxidant. As reported in the literature and discussed above,[575] spinels resulted to be good catalysts in the H_2O_2 decomposition reaction. This means that during AD oxidative polymerization part of the

oxidant could be subtracted to the polymerization reaction mixture, justifying the lower polymerization yield observed under these conditions.

Graphic 8.4. summarizes the results obtained in the oxidative polymerization of AD when spinels NPs (Fe_3O_4, $CoFe_2O_4$, $NiFe_2O_4$, $MnFe_2O_4$, $CuFe_2O_4$, $MgFe_2O_4$ and $ZnFe_2O_4$) were employed under the same reaction conditions in the presence of hydrogen peroxide as the oxidant.

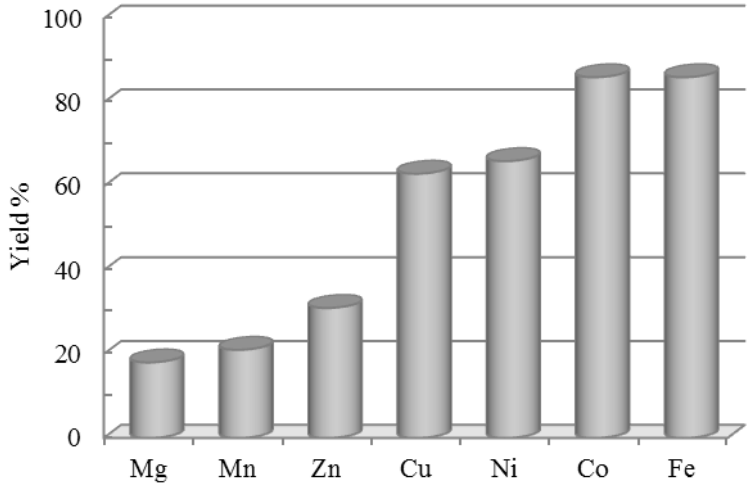

Graphic 8.4. Dependence of polymerization yields from the first metallic center of spinel structures. Reaction conditions: AD/MFe_2O_4= 5 (molar ratio), H_2O_2/AD= 5 (molar ratio), temperature= 25°C, reaction time= 24 h.

It looks clear that the catalytic effect of spinel ferrite NPs on PANI preparation was strictly related to the first metallic center, following the trend reported below:

$$Fe \geq Co > Ni \geq Cu >> Zn > Mn \geq Mg$$

The best results in terms of yield were obtained using Fe_3O_4, $CoFe_2O_4$, $NiFe_2O_4$ and $CuFe_2O_4$ NPs as the reaction catalysts and magnetic fillers, whereas in all the other cases PANI was obtained in very low yield.

In order to justify the trend observed, the results obtained in terms of yield were correlated to the their ability to decompose H_2O_2 and to the inversion degree of the ferrites.

Table 8.21. reveals that the catalytic activity of the ferrites in the decomposition of H_2O_2 follows the order: Mn > Co > Cu > Ni >Cd > Zn in MFe_2O_4.[575]

Spinels	Specific rate constants at 303 K ($g^{-1} \cdot min^{-1} \cdot 10^2 \pm 5\%$)
$ZnFe_2O_4$	2.46
$CdFe_2O_4$	11.51
$NiFe_2O_4$	14.96
$CuFe_2O_4$	25.56
$CoFe_2O_4$	221.00
$MnFe_2O_4$	1007.50
Fe_3O_4	0.00

Table 8.21.: Specific rate constants at 303K for the ferrite catalysts.

This order resulted to be deeply different from that observed for the catalytic activity of MFe_2O_4 in the PANI/MFe_2O_4 synthesis.

This means that, even though the different ability of the ferrites to decompose hydrogen peroxide can play a role in the oxidative polymerization reaction of AD, other factors have to be involved.

Table 8.22. reports the inversion degree (δ) of the ferrites, that is the fraction of tetrahedral sites occupied by Fe(III) ions and may vary between 0 for the perfectly normal case and 1 for the perfectly inverse case.

Spinel	δ
Fe_3O_4	1
$CoFe_2O_4$	0.8
$NiFe_2O_4$	1
$CuFe_2O_4$	0.85
$MnFe_2O_4$	0.2
$ZnFe_2O_4$	0
$MgFe_2O_4$	0.4-0.6

Table 8.22.: Inversion degree of the spinels.

Comparing data in Table 8.22. with the trend observed for the polymerization yield for PANI/MFe_2O_4 synthesis, it is possible to conclude that the catalytic activity of the spinels in the oxidative polymerization of AD is most likely correlated to the their inversion degree.

In fact, the ferrites NPs characterized by high inversion degree (Fe_3O_4, $CoFe_2O_4$, $NiFe_2O_4$ and $CuFe_2O_4$) exhibited high catalytic activity in the PANI/MFe_2O_4 preparation, whereas for direct spinels ($MnFe_2O_4$, $ZnFe_2O_4$, $MgFe_2O_4$) catalytic activity was very low.

The polymeric matrix contained into the composite materials was characterized by FT-IR spectroscopy and the results are shown in Figure 8.20.

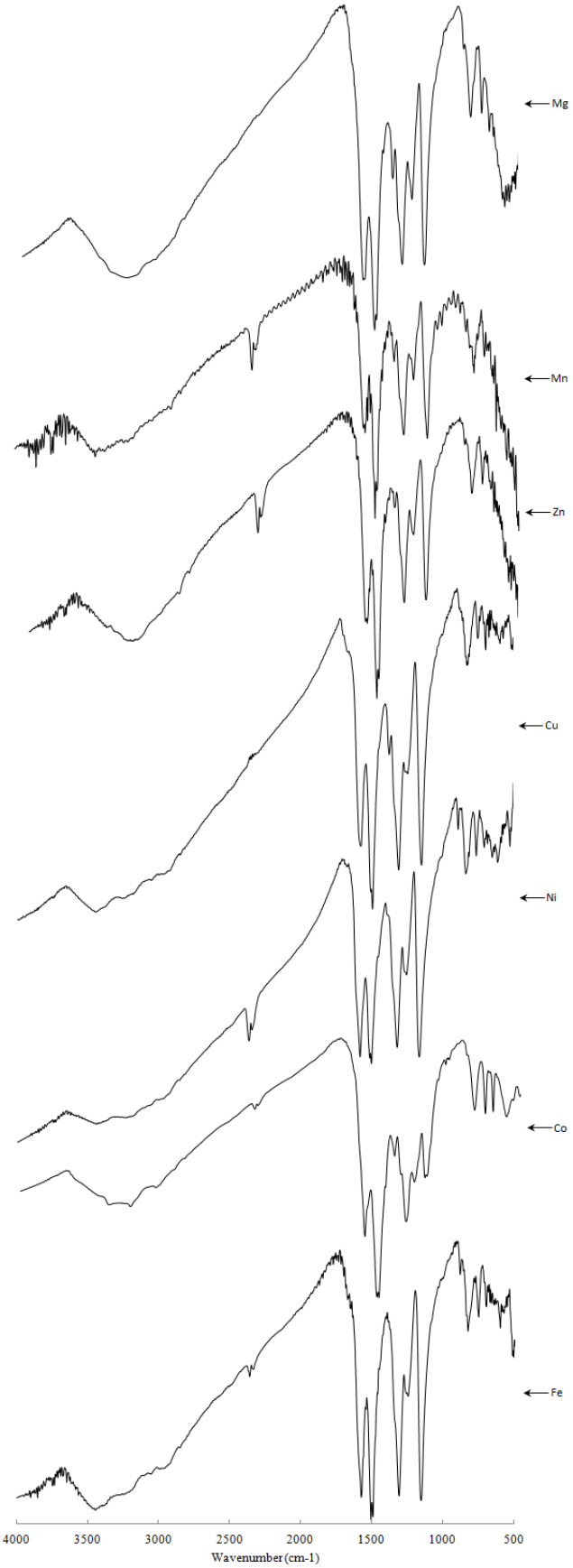

Figure 8.20.: FT-IR spectra of (Mg) Sample no. 81, (Mn) Sample no. 80, (Zn) Sample no. 79, (Cu) Sample no. 76, (Ni) Sample no. 73, (Co) Sample no. 63, (Fe) Sample no. 36.

FT-IR characterization showed that also the oxidation state of the polymeric matrix was affected by the type of bimetallic metal present into the spinel structure. Except for $CoFe_2O_4$ NPs, characterized by high H_2O_2 decomposition activity (see Table 8.21.), in all the other cases ferrites NPs characterized by high inversion degree produced PANI/MFe_2O_4 with a polymeric structure similar to emeraldine, whereas direct spinels produced PANI/MFe_2O_4 containing polyaniline in more reduced form (similar to leucoemeraldine), as confirmed by the conductivity values reported in Table 8.23.

Sample	σ (S/cm)
Leucoemeraldine	$1.00 \cdot 10^{-8}$
PANI/Fe_3O_4	$2.50 \cdot 10^{-3}$
PANI/$CoFe_2O_4$	$4.9 \cdot 10^{-5}$
PANI/$NiFe_2O_4$	$7.3 \cdot 10^{-4}$
PANI/$CuFe_2O_4$	$2.3 \cdot 10^{-5}$
Emeraldine	$3.50 \cdot 10^{-3}$

Table 8.23.: Conductivity values of leucoemeraldine, emeraldine and PANI/MFe_2O_4 composites.

As for PANI/Fe_3O_4 and PANI/$CoFe_2O_4$, also in this case the presence of magnetic nanoparticles into the composite materials was confirmed by X-ray powder diffraction and atomic absorption spectroscopy (loss of ferrites less than 10%).

It is possible to conclude that the catalytic effect of the spinels in the oxidative polymerization of *N*-(4-aminophenyl)aniline is related to two main factors: kind of oxidant and nature of the first metallic center.

In general, when the polymerization reaction was carried out under aerobic conditions all the ferrites exhibited good results (polymerization yields 48-82%). However, when H_2O_2 was used as the oxidant, replacing the first bivalent center (Fe^{2+}) with other metals the catalytic activity followed the trend: $Fe \geq Co > Ni \geq Cu >> Zn > Mn \geq Mg$.

The different behaviour of the ferrites under aerobic and anaerobic conditions could be related to their ability to decompose H_2O_2, subtracting it from the reaction mixture.

However, it was demonstrated for the first time that the catalytic activity of the spinels in the oxidative polymerization of AD in the presence of H_2O_2 resulted to be most likely correlated to the their inversion degree.

In fact, inverse spinels produced PANI/MFe_2O_4 composites in high yields, whereas more modest results were obtained in the presence of direct spinels.

Finally, inverse spinels led to composites containing PANI in conducting emeraldine form, whereas when direct spinels were used as the catalysts polymeric matrix resulted to be more reduced (similar to leucoemeraldine).

8.4. Electromagnetic characterization

Complex permittivity ($\varepsilon^* = \varepsilon' - i\,\varepsilon''$) and complex permeability ($\mu^* = \mu' - i\mu''$) were derived from the measured scattering parameters (S11 and S21). Measurements were carried out in waveguide WR42 between 18 and 26 GHz using an accurate deembedding procedure with calibrated standards. Two samples were prepared by mixing a host medium (PVA, polyvinyl acetate) with a polyaniline and PANI/Fe_3O_4 respectively, as described in Chapter 7, paragraph 7.9. Owing to the high amount of material necessary to carry out these measures, PANI/Fe_3O_4 composite was realized by mechanical mixing of PANI and Fe_3O_4 NPs (11 nm, prepared as describe in Chapter 6, paragraph 6.3.1.) maintaining a PANI/Fe_3O_4 ratio of 1:0.2 (w/w). The permittivity and permeability of both PANI and PANI/Fe_3O_4 materials were retrieved from the measured scattering parameters by Bruggeman's method.[579] It is well known that real (ε', μ') and imaginary (ε'', μ'') parts of complex permittivity and permeability characterize respectively the electric and magnetic polarizability and the energy loss due to electric and magnetic effects.[580, 581]

Figures 8.21 show the real and imaginary part of relative permittivity and permeability for each sample.

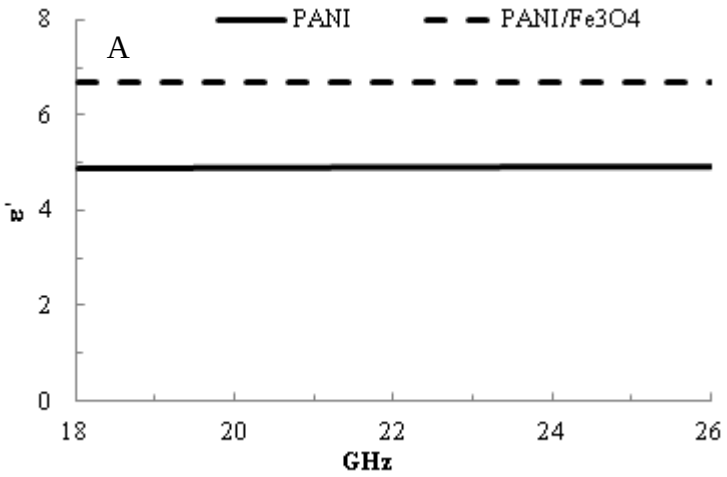

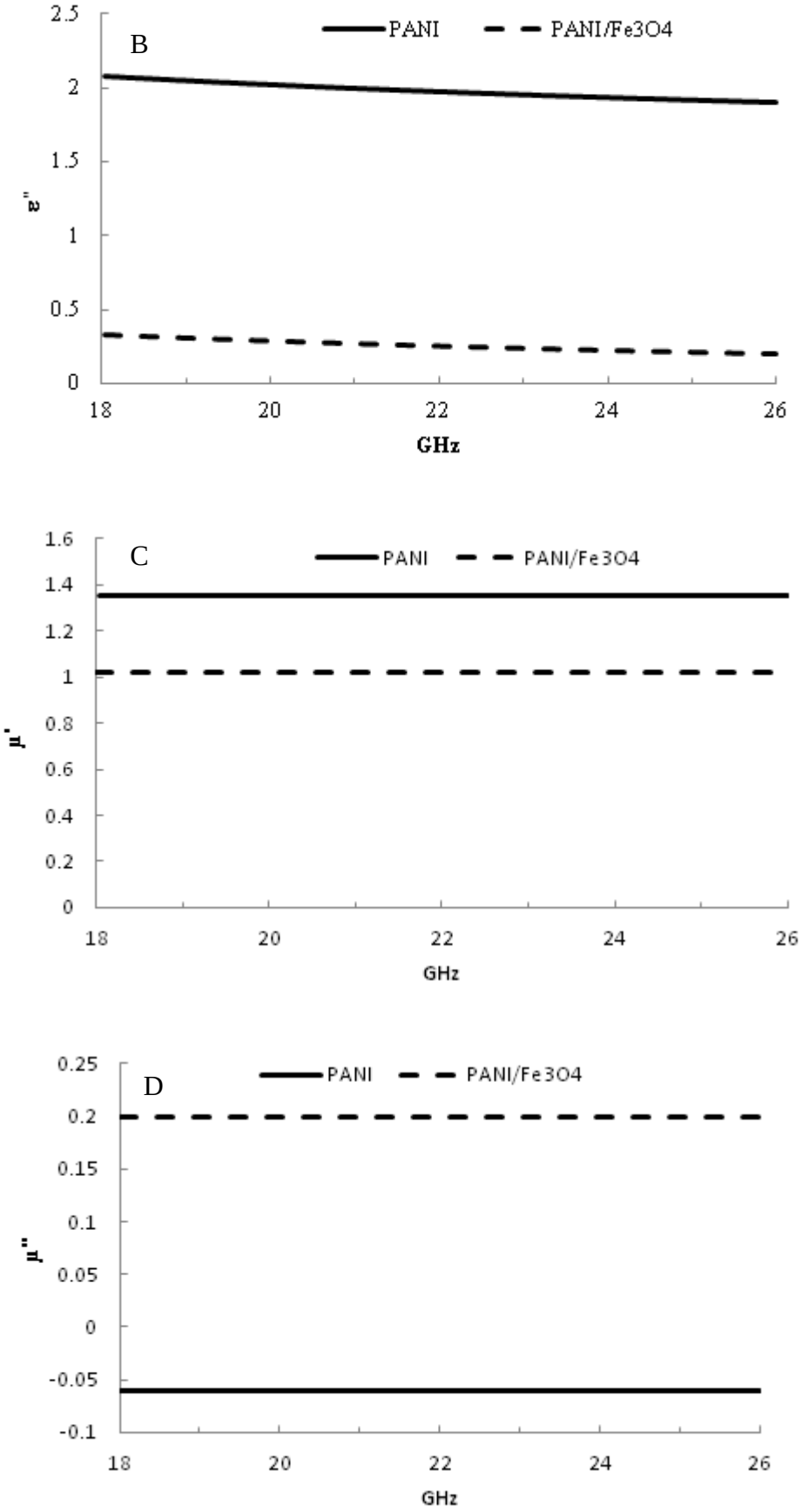

Figure 8.21.: Frequency dependence of real (A) and imaginary (B) part of complex permittivity and real (C) and imaginary (D) part of complex permeability for PANI and PANI/Fe_3O_4 composite

As it is possible to observe, when the magnetic filler was added into the conducting PANI matrix an increase of the real part of permittivity (ε') and the imaginary part (μ'') of permeability was observed, whereas the real part (μ') of permeability remained constant and the imaginary (ε'') part of permittivity dramatically decreased. Moreover, both real and imaginary parts didn't exhibit significantly variation with increasing frequency.

As reported in the literature,[582] in polyaniline system a strong polarization occurs due to the presence of polaron/bipolaron species, which leads to high values of ε' and ε''. The addition of magnetic Fe_3O_4 NPs resulted in an increase in the magnetic loss of the system but at the same time in a drop of the electric loss, probably due to the heterogeneity of the system that didn't guarantee a good network among conducting polymeric chains. In fact, the mechanical mixing of an insulating fraction into a conducting system caused an interruption of the ordered alignment of conducting chains and at the same time an increase of their distances. This phenomenon negatively affected the conductivity of the system and its dielectric loss.

Better results are expected for PANI/Fe_3O_4 composite prepared by the new one-pot synthesis reported in section 8.1. However, at the moment measurements are in progress. In any case, owing to the importance of the magnetic filler dispersion into the polymeric matrix, in Section 8.6. the work was addressed to the development of new synthetic approaches to prepare highly homogeneous PANI/Fe_3O_4 composite materials.

8.5. Microwave absorption properties

According to the transmission line theory,[582] when an electromagnetic wave is transmitted through a medium, its absorption property depends on many factors, such as a complex permittivity and permeability, sample thickness, specific surface area, and frequency. Theoretically, microwave reflection coefficient RC (dB) [584, 585] can be calculated from the relative permeability and permittivity for a given frequency and absorber thickness. In a single layered absorber, the electromagnetic wave absorbing property can be evaluated by the following Equation 8.2.:[586, 587]

$$RC\ (dB) = 20\log_{10}\left(\frac{iA\tan(kd)-1}{iA\tan(kd)+1}\right) \qquad \text{Eq. 8.2.}$$

$$\text{where } A = \sqrt{\frac{\mu}{\varepsilon}},\ k = \frac{2\pi f}{c}\sqrt{\mu\varepsilon},\ i = \sqrt{-1} \qquad \text{Eq. 8.3.}$$

In the above equations (Eq. 8.3.), μ and ε are, respectively, the complex permeability and permittivity of the absorbing material, k is the wavenumber, f is the frequency of the incident electromagnetic wave, c is the speed of light in vacuum and d is the thickness of the absorbing layer.

Figures 8.22. A-C present the variation of shielding effectiveness due to reflection (SE_R) and absorption (SE_A) in the frequency range of 18-26 GHz for PANI and PANI/Fe_3O_4 samples.

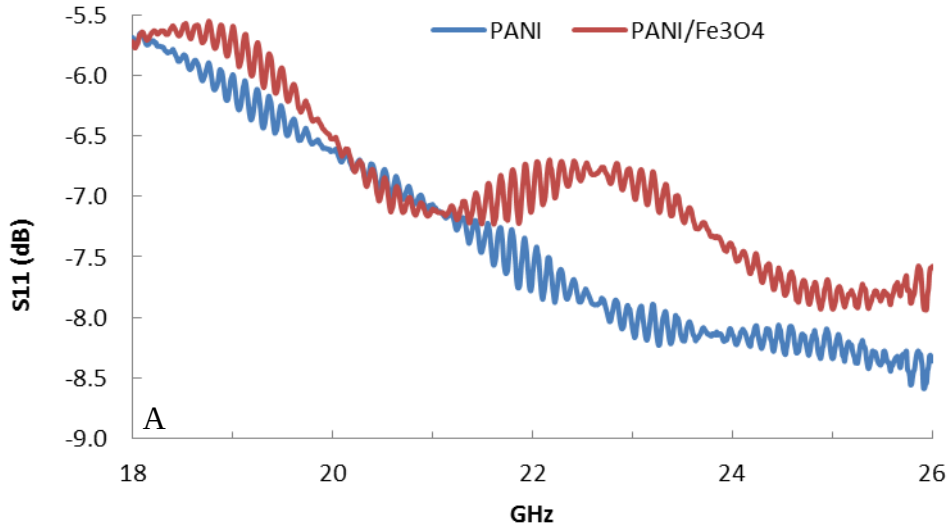

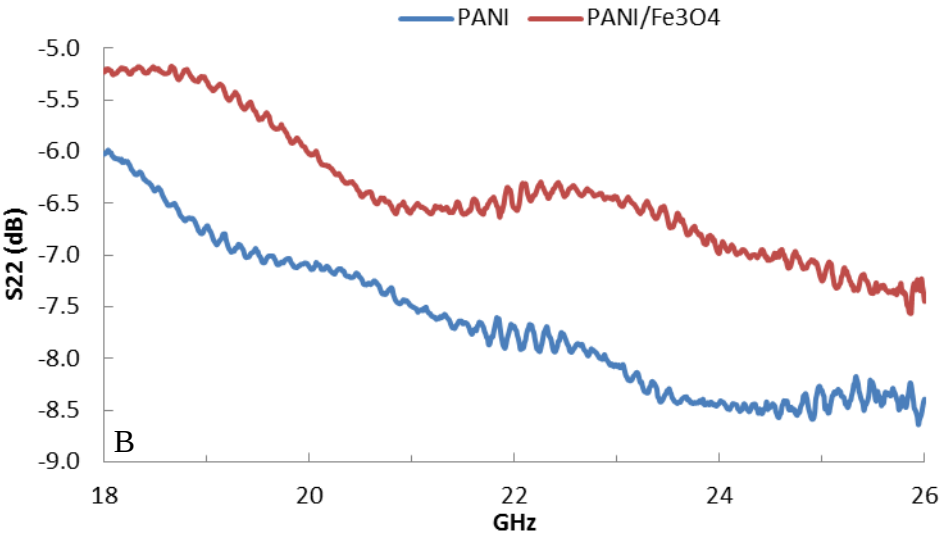

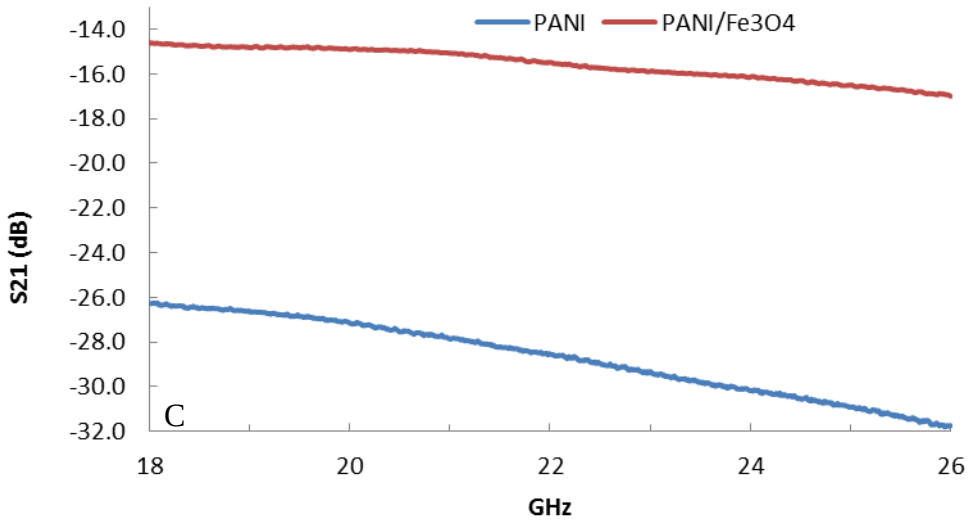

Figure 8.22.: Frequency dependence of reflection (A and B) and transmission (C) coefficients.

PANI sample showed a higher effect on microwave absorbing properties than PANI/Fe_3O_4 composite, revealing at 26 GHz values of reflection and transmission coefficient of -8dB and -32dB respectively, whereas under the same conditions PANI/Fe_3O_4 sample showed values of -7.5dB and -17dB. These results were interpreted in terms of non-homogeneous distribution of Fe_3O_4 NPs into the polymeric matrix that has a negative effect in the composite performance.

The calculated absorption spectra for all the samples have been compared with measured spectra and the shapes of both experimental and theoretically calculated spectra resulted to be similar (Figure 8.23.)

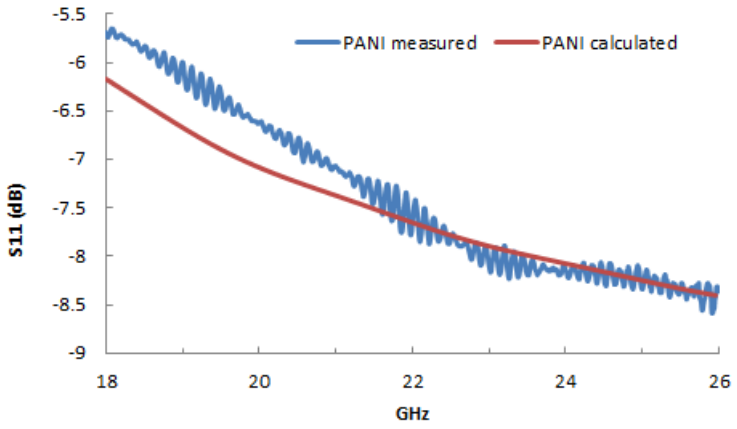

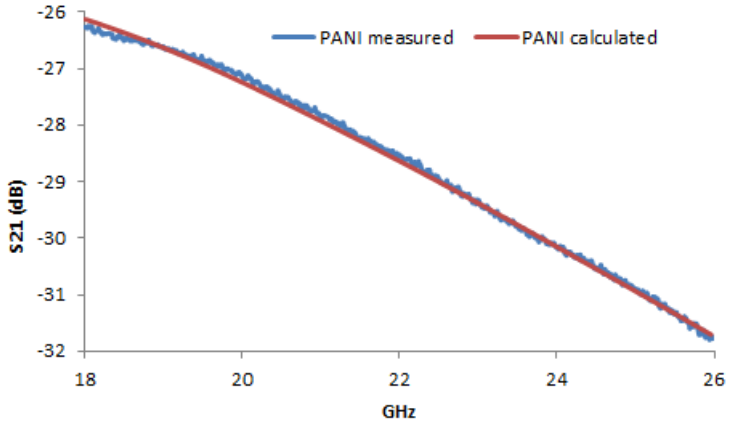
PANI measured
PANI calculated
S21 (dB)
-26
-27
-28
-29
-30
-31
-32
18
20
22
24
26
GHz

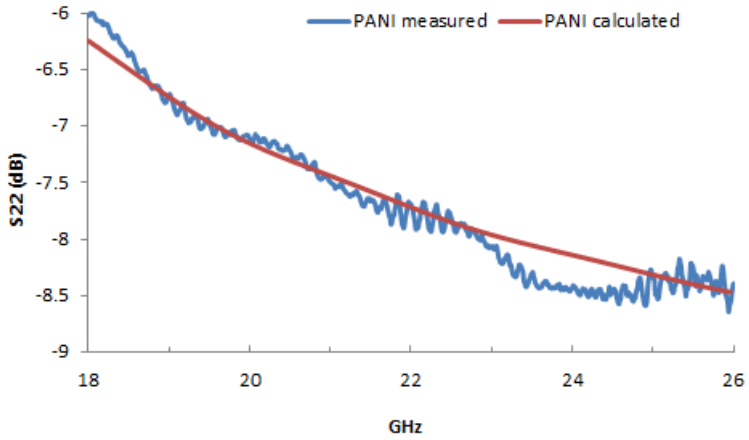
PANI measured
PANI calculated
S22 (dB)
-6
-6.5
-7
-7.5
-8
-8.5
-9
18
20
22
24
26
GHz

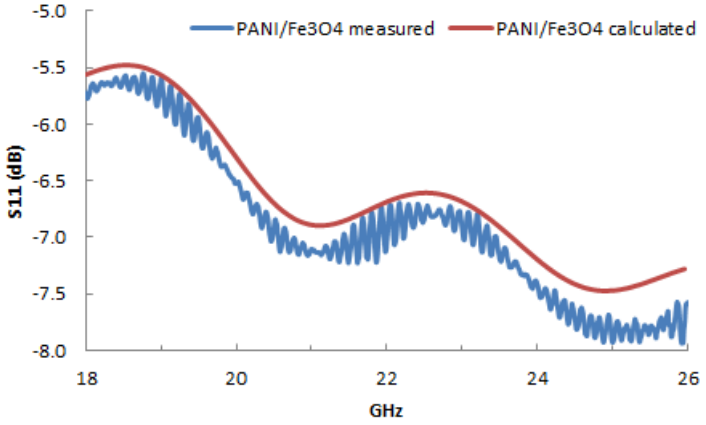
PANI/Fe3O4 measured
PANI/Fe3O4 calculated
S11 (dB)
-5.0
-5.5
-6.0
-6.5
-7.0
-7.5
-8.0
18
20
22
24
26
GHz

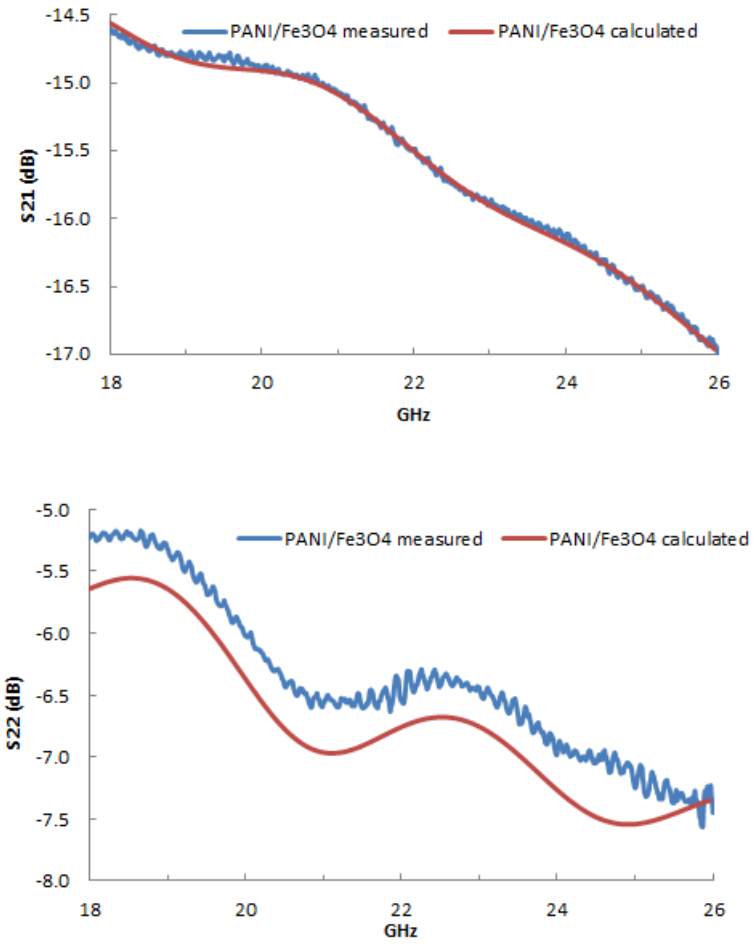

Figure 8.23.: Comparison between measured and calculated reflection and transmission coefficient**s.**

8.6. Towards well-dispersed PANI–Fe_3O_4 nanomaterials

Control over the dispersion of the magnetic NPs into the polymer matrix is critical for the magnetic properties of composite materials and their performances.

The inability to control the particle dispersion is mostly associated with clustering, which is influenced by particle–particle and particle–matrix interactions. Designing synthetic strategies in which the NPs are prevented from forming larger agglomerates is important to guarantee good properties and performances of the composite products.[588] In the scientific literature some authors have reported a new synthetic strategy to prepare polymer/magnetic NPs composites characterized by ordered structures, especially core shell.[589, 590] Preparing materials with highly ordered structure reduces the risk of NP aggregation that, however, may not completely be avoided. A possibility to overcome agglomeration phenomena is the use of ultrasonic irradiation that not only increases the NP dispersion but also favors the formation of organized structures.[34, 343, 344, 590-

592]. More recently, Lu *et al*. have increased Fe_3O_4 NPs dispersion into polyaniline matrix using an innovative method,[344] where aniline dimer was modified producing 4-Oxo-4-(4-(phenylamino)phenylamino)butanoic acid (ADCOOH). Carboxylic function was used to anchor magnetic nanoparticles producing ADCOOH-Fe_3O_4NPs specie. These materials were used as precursors in the subsequent oxidative polymerization reaction of aniline in the presence of a stoichiometric oxidant (ammonium persulfate).

In this section, this reaction was investigated in more detail. ADCOOH-Fe_3O_4NPs precursor was prepared by different approaches and used in the innovative oxidative polymerization of AD under mild conditions (H_2O_2 as the oxidant, room temperature). More accurate characterization of materials was carried out and interesting preliminary results will be presented.

8.6.1. ADCOOH characterization

4-Oxo-4-(4-(phenylamino)phenylamino)butanoic acid (ADCOOH) was prepared as described in the literature (Chapter 6 section 6.1.3.) [344] and an accurate spectroscopic characterization was furnished. Figure 8.24. reports the FT-IR spectrum of ADCOOH.

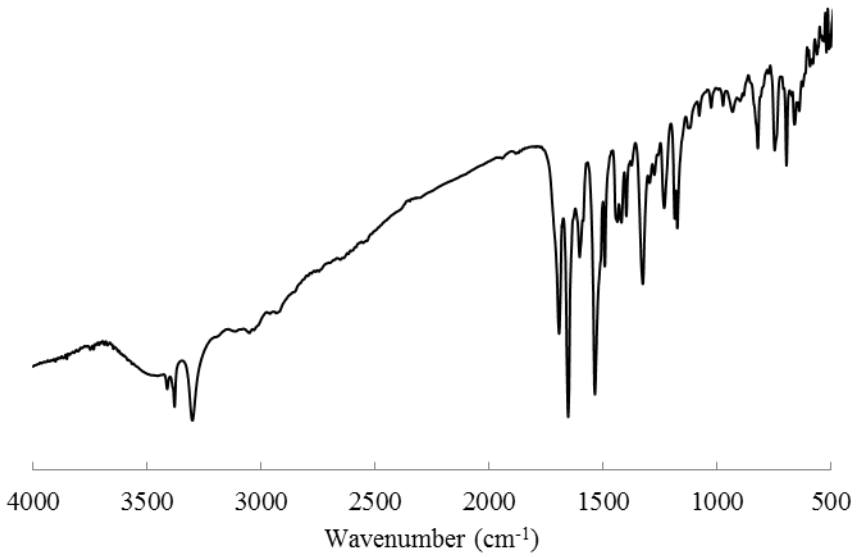

Figure 8.24.: FT-IR spectrum of ADCOOH.

The bands between 3000 and 3500 cm^{-1} can be assigned to N-H stretching for secondary amine and amide groups. Characteristic carbonyl stretching vibrations were observed at 1652 and 1692 cm^{-1} related to amidic and carboxylic groups respectively, whereas the bands at 1534 and 1600 cm^{-1} are characteristic of the benzenoid rings.

Comparing UV-vis spectra of AD and ACOOH (Figure 8.25. a and b) a shift of the band at *ca*. 290 nm to higher wavelengths was observed, indicating an increase in the conjugation degree.

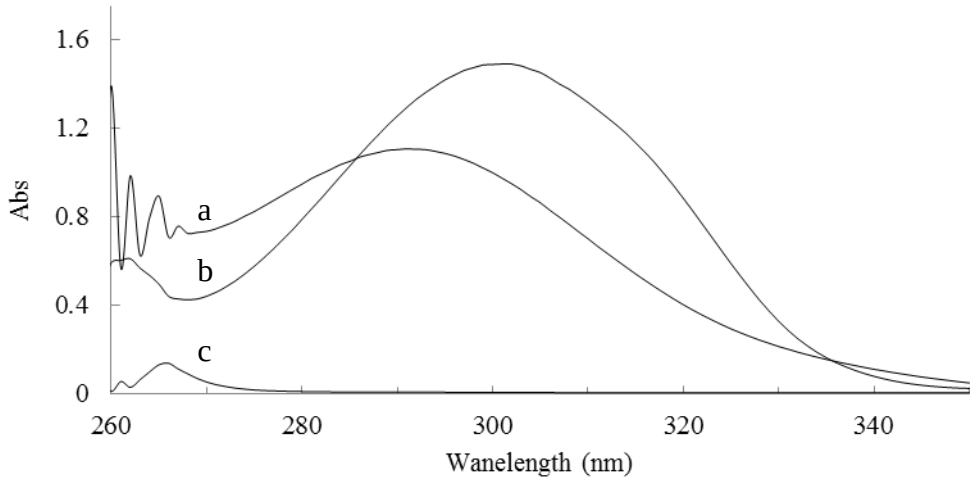

Figure 8.25.: UV-vis spectra of (a) AD, (b) ADCOOH and (c) succinic anhydride.

LSIMS (liquid secondary ionization mass spectroscopy) was used to determine the mass of the product (Figure 8.26.)

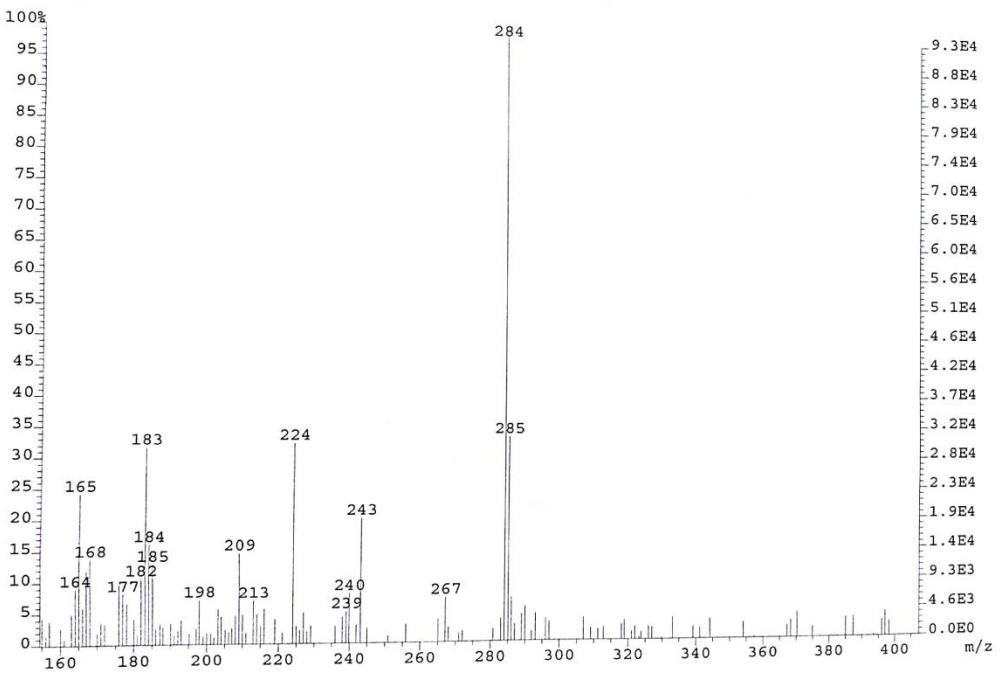

Figure 8.26.: Mass spectrum of ADCOOH.

The characteristic peak M+1 at 285 m/z corresponded to the mass of the expected product.
Finally, NMR spectrum (Figure 8.27.) confirmed the structure of the product obtained: 4-Oxo-4-(4-(phenylamino)phenylamino)butanoic acid.

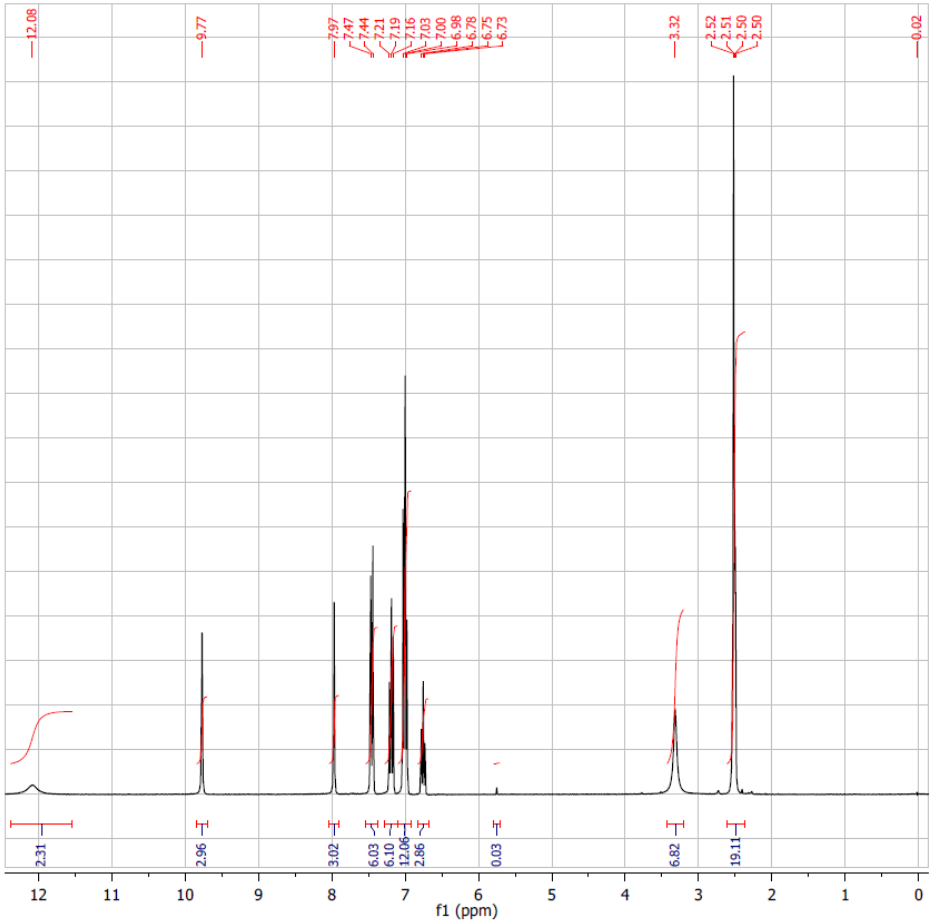

Figure 8.27.: NMR spectrum of 4-Oxo-4-(4-(phenylamino)phenylamino)butanoic acid in D_2O.

More in detail, the signals were assigned as reported in Table 8.24.

δ (ppm)	Protons
12.1	*H*OOC–CH_2–CH_2–
9.8	–CH_2–CO–N*H*–C_6H_4–
8.0	–C_6H_4–N*H*–C_6H_4–
6.7–7.5	benzenoid ring
3.3	H_2O
2.5	HOOC–CH_2–CH_2–CO

Table 8.24.: Chemical shift for 4-Oxo-4-(4-(phenylamino)phenylamino)butanoic acid

ADCOOH was used to anchor Fe_3O_4NPs and produce ADCOOH/Fe_3O_4NPs composites, then used as the precursors and catalysts in the subsequent oxidative polymerization of AD.

8.6.2. ADCOOH/Fe3O4 NPs preparation and characterization

ADCOOH/Fe_3O_4NPs composites were prepared through two different coupling approaches. The first one was a one-pot method reported in the literature [344] applying some modifications.

ADCOOH/Fe_3O_4NPs1 was prepared exactly as reported in ref. 344, adding ADCOOH to the reaction mixture during the Fe_3O_4 NPs synthesis, and used as a reference sample.

Then, the reaction was repeated changing the ADCOOH/Fe ratio (% w/w) into the reaction mixture. The results are summarized in Table 8.25.

Sample	ADCOOH/Fe (% w/w)	Mean diameter of NPs (nm)[a]
ADCOOH/Fe_3O_4NPs1	0.26	6.0
ADCOOH/Fe_3O_4NPs2	2.64	7.1
ADCOOH/Fe_3O_4NPs3	7.12	7.3

Table 8.25.: Different preparation for ADCOOH/Fe_3O_4NPs composites. Reaction conditions: [Fe]= 0.34 M. reaction temperature= 80°C, pH= 8, reaction time= 1h. [a] Data obtained by XRPD patterns through the Debye-Scherrer equation.

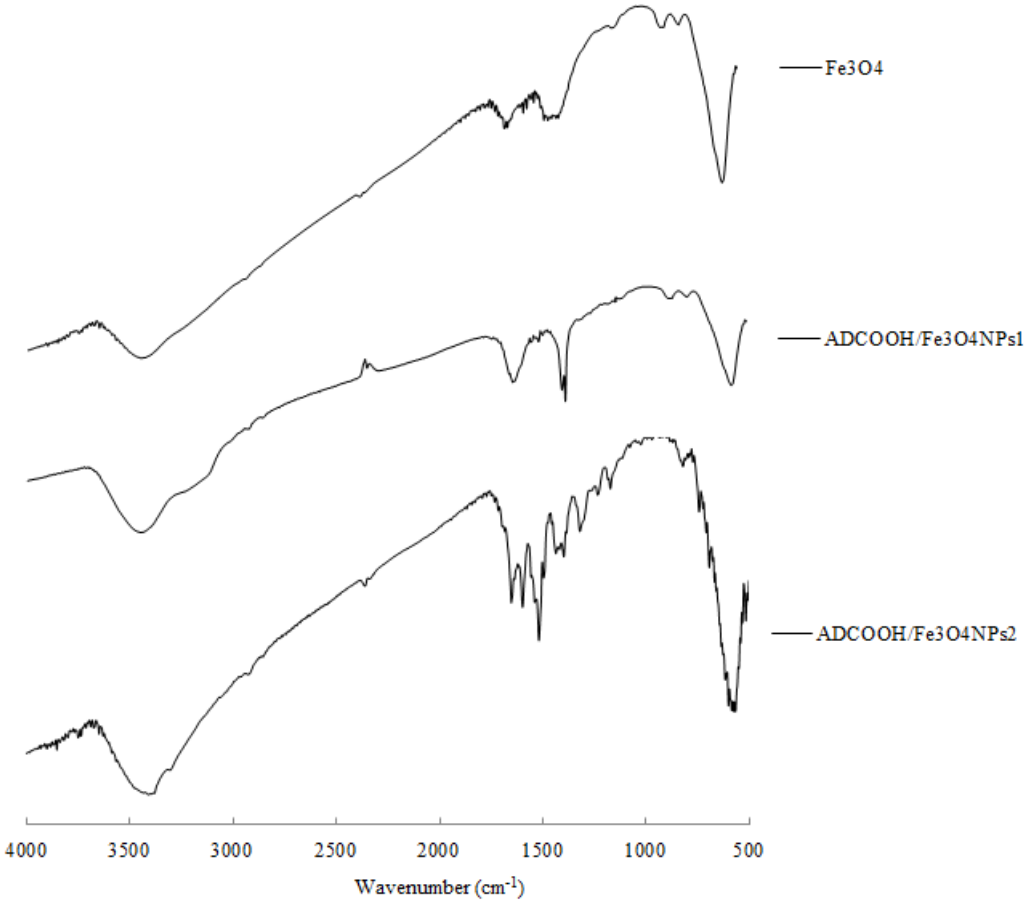

Figure 8.28. shows the FT-IR spectra of Fe_3O_4NPs, ADCOOH/Fe_3O_4NPs1 and ADCOOH/Fe_3O_4NPs2 composites.

As it is possible to observe, the characteristic bands of ADCOOH were more evident in ADCOOH/Fe_3O_4NPs2 than ADCOOH/Fe_3O_4NPs1 (Figure 8.28.). However, the band at 1692 cm^{-1}

for carboxyl group of ADCOOH was still very evident. As reported in the literature,[344] from a spectroscopic point of view a disappearance or attenuation of this band is strictly correlated to the presence of ADCOOH in its salt owing to its coordination with magnetic particles.

The amount of ADCOOH not involved in the coupling of Fe_3O_4NPs was removed from ADCOOH/Fe_3O_4NPs2 system by washing with ethanol. Such a cleaning produced a strong reduction of the band at 1692 cm^{-1} for carboxyl group, as shown in Figure 8.29.

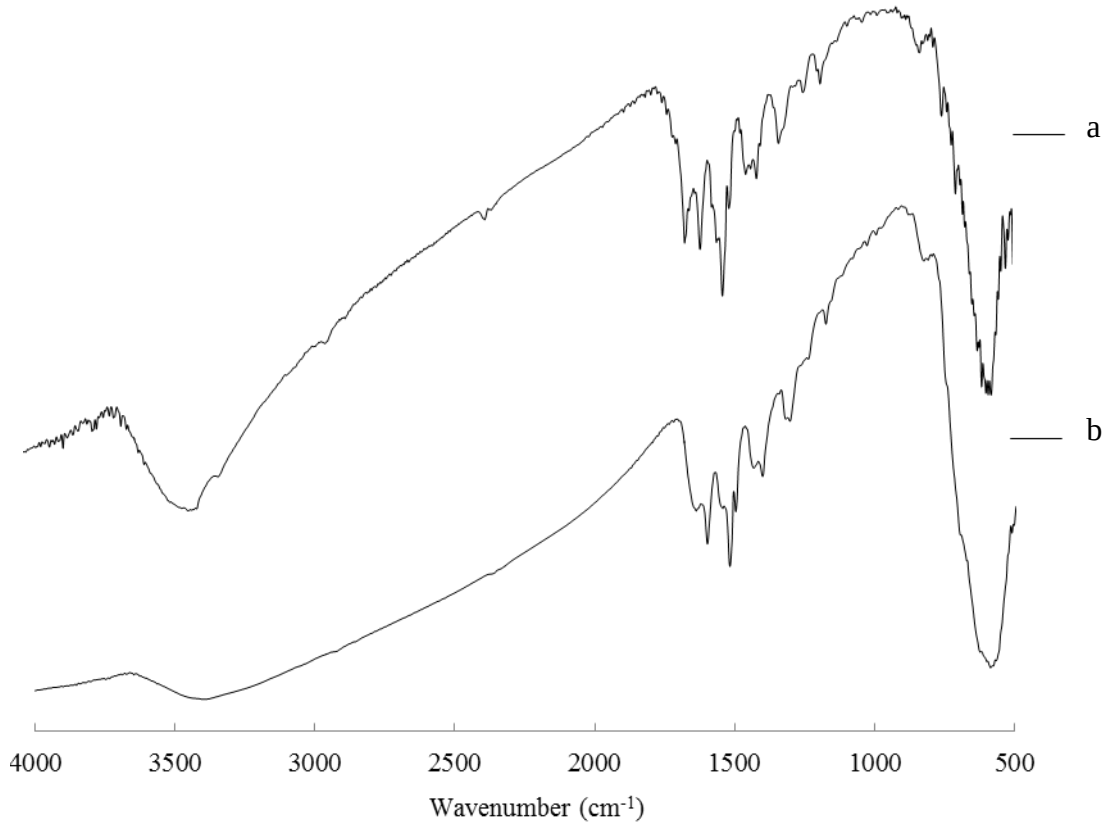

Figure 8.29.: FT-IR spectra of (a) ADCOOH/Fe_3O_4NPs2 before and (b) after purification.

Similar results were obtained for ADCOOH/Fe_3O_4NPs3.

The amount of Fe_3O_4 into the composites was determined by atomic absorption spectroscopy. The results showed that, in spite of the different ADCOOH/Fe ration used for their preparation, both ADCOOH/Fe_3O_4NPs2 and ADCOOH/Fe_3O_4NPs3 composites contained very similar amount of magnetic NPs: 70 and 78% respectively, demonstrating that the use of high ADCOOH/Fe ratios (w/w) led only to increase the amount of free ADCOOH subsequently removed by washing step.

All the ADCOOH/Fe_3O_4NPs composites were used as catalysts and precursors in the oxidative polymerization of AD, as described in Chapter 6 section 6.4.1., using an AD/Fe_3O_4NPs molar ratio of 5.

In all cases PANI/Fe_3O_4 composites were obtained with good yield (66-77%) and polymeric component resulted to be PANI in its conducting emeraldine form, suggesting that the coating on the inorganic nanoparticles didn't compromise their catalytic activity.
XRPD analyses confirmed the presence of inorganic materials into the polymeric matrix.

TEM characterizations are in progress to evaluate the effect of ADCOOH coating on the dispersion of the inorganic component into the composites.

8.6.3. ADCOOH/Fe_3O_4NPs composites prepared by a two-step method and their characterization

ADCOOH/Fe_3O_4NPs composites were prepared by a different approach: by a two-step method.
In this case Fe_3O_4NPs (mean diameter = 11 nm) were prepared in advance by a chemical co-precipitation method and then dispersed in toluene (amount Fe_3O_4 in toluene= 33mg/mL) using oleic acid as the surfactant (Chapter 6 section 6.3.1.1.). 1 mL of this dispersion was dried by the use of a rotary evaporator and Fe_3O_4 NPs_{ff} were washed several timed (*ca*. 10) with acetone to remove oleic acid and dried.
Different samples of these NPs (30 mg) were dispersed for 12 hours in 2 mL of different organic solution containing ADCOOH, as summarized in Table 8.26.

ADCOOH (mg)	Solvent (mL)	Concentration (mg/mL)
100	5	20
"	"	"
"	"	"
50	"	10

Table 8.26.: Concentration of different organic solutions containing ADCOOH

ADCOOH/Fe_3O_4NPs composites were recovered by centrifugation, dried at 60°C until constant weight, powdered with a mortar and characterized by FT-IR spectroscopy and XRPD diffraction, whereas liquid fractions were analyzed by UV-vis spectroscopy to measure the amount of free ADCOOH remained into the organic solution.
As it is possible to observe in Table 8.27., the percentage of ADCOOH absorbed on magnetic NPs decreased increasing the polarity of the solvent used, expressed as dielectric constant.

Solvent	Dielectric constant	%ADCOOH absorbed (w/w)
Dioxane	2.21	61
Tetrahydrofuran	7.58	50
Acetone	20.7	39
Methanol	32.7	21

Table 8.27.: Percentage of ADCOOH absorption on NPs in different solvents.

FT-IR spectra of ADCOOH-capped NPs in different solvents are similar to those reported in Figure 8.29. b, confirming the coordination between organic and inorganic component.

8.6.4. Synthesis of PANI/Fe_3O_4 composites using ADCOOH/Fe_3O_4NPs precursors prepared by a two-step method

All these materials were employed in the oxidative polymerization of AD as described in Chapter 6 Section 6.4.1., using an AD/Fe_3O_4NPs molar ratio of 5.

Also in this case PANI/Fe_3O_4 composites were obtained with good yield (57-71%) and polymeric component resulted to be PANI in its conducting emeraldine form. XRPD analyses confirm the inclusion of magnetic NPs into the polymeric matrix, whereas TEM characterization are in progress to evaluate the presence of agglomeration phenomena.

Figure 8.30. correlates the yields obtained in the presence of different ADCOOH/Fe_3O_4NPs materials with dielectric constants of solvents used to anchor magnetic NPs on ADCOOH and percentage of ADCOOH absorbed on magnetic NPs.

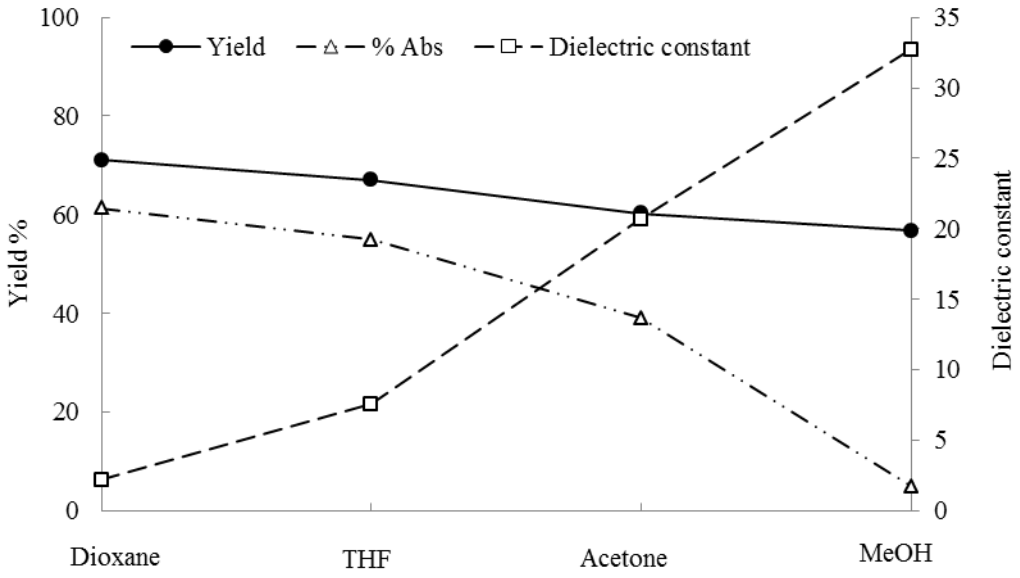

Figure 8.30.: Polymerization yields, dielectric constants of solvents and percentage of ADCOOH absorbed on magnetic NPs.

As it is possible to observe from Table 8.27. and Figure 8.30., the percentage of ADCOOH anchored on Fe_3O_4 NPs is closely related to the dielectric constant of solvents used. Solvents characterized by high dielectric constant caused low level of ADCOOH/Fe_3O_4 coupling, favoring the presence of free ADCOOH. Magnetic NPs characterized by low anchoring level had large surface area exposed to the reaction mixture, producing PANI/Fe_3O_4 composites in high yield. On the contrary, increasing the amount of ADCOOH anchored on magnetic NPs, their surface area exposed to the reaction mixture decreased slightly reducing their catalytic properties.

Chapter 9: Improvements in the preparation of polyaniline nanofibers by electrospinning technique and their biocompatibility. Towards pure electrospun polyaniline

Conducting polymers in nanostructured form, as nanofibers, nanotubes and nanowires, in particular polyaniline, have received a great deal of attention by the scientific community for their potential applications (electronic, magnetic, biomedical, optical fields).

Nanosized materials can be realized through many different methods and techniques.

In particular, PANI nanostructures can be synthesized through a "template synthesis" route. In this context different templates, such as zeolite channels, track-etched polycarbonate and nanosized alumina membrane, have been employed to direct growth of the PANI nanostructures.[21]

However, although this technique is attracting and elegant, the removal of the template at the end of the reaction is the biggest drawback. In fact, it is tedious and can compromise the morphology of the final products.

Recently, electrospinning has emerged as a promising technique for the production of wires and/or fibers of polymers with diameters ranging from 10 nm to 10 μm.[591-594] Unfortunately, the poor processability of the polyaniline in form of conducting emeraldine salt makes it difficult to be electrospun. In addition to poor processability, another limit for the PANI electrospinning is the low viscosity and surface tension of the polymer in organic solvents as chloroform.

As reported by Cao *et al*., the limitation of poor solubility can be overcome by the use of appropriate doping agents. In fact, polyanilines doped with sulfonic acids (camphorsulfonic acid, CSA, dodecylbenezensulfonic acids, DBSA, …) show higher processability in common solvents.[282]

As far as the low viscosity is concerned, another polymer can be added. However, it is in general an insulator material (polystyrene,[595] polyacrylonitrile,[596] polymethylmethacrylate (PMMA),[597] polyvinylpyrrolidone,[598] polyethylenoxide (PEO),[599]), that can compromise the electrical conductivity of the final product.

Mc Diarmid *et al.* spun big PANI fibers (*ca*. 1320 nm) doped with CSA blended with PEO, finding that for high content of PANI (72% weight with respect to PEO) single fibers exhibit high value of conductivity (33 S cm^{-1}) with respect to the conductivity of a pure polymer cast (10^{-1} S cm^{-1}).[167, 237]

In similar manner, many other authors produced PANI wires or fibers using different insulating co-polymers.

However, the possibility to produce pure PANI nanofibers (PANI NFs) is very tempting. This would allow to obtain materials characterized by very high electrical properties. Moreover, the complete removal of co-polymer would resolve possible problems of biocompatibility for medical and biomedical applications. It has been, in fact, recently demonstrated that pure PANI is biocompatible and not cytotoxic.[600]

For this purpose, two different synthetic methods (classical approach, $(NH_4)_2S_2O_8$ as the oxidant, PANI1),[544] and "green" approach (H_2O_2 as the oxidant,PANI2),[26] described in Chapter 6 sections 6.1.1. and 6.1.2., were followed for preparing PANI.

PEO and PMMA were chosen as the co-polymers and pure PANI NFs were produced by the use of two strategies.

Aim of the first part of the work was to optimize the minimum amount of co-polymer necessary for the electrospinning process in order to obtain PANI NFs as pure as possible. Moreover, the electrospinning parameters (type of collector, distance needle-collector, speed of solution) were varied in order to study these effects on the morphology of blended PANI NFs and on their electronic conductivity.

Instead, in the second part, the co-polymer was removed by a washing treatment after the electrospinning process.

9.1. PANI/PEO nanofibers: effect of different raw sources

9.1.1. Morphological characterization

Concerning PANI1/PEO blends, all the blended system solutions were homogeneous and showed no phase separation prior to the electrospinning process. In the absence of PEO, PANI1 didn't lead to fibers production during the electrospinning process. However, increasing PANI1 amount the consequent increase of viscosity of the blended solution guaranteed a more stable jet and, as a consequence, the fiber formation.[601]

Figure 9.1 shows the correlation between the nanofibers production and PEO/PANI1 ratio (w/w).

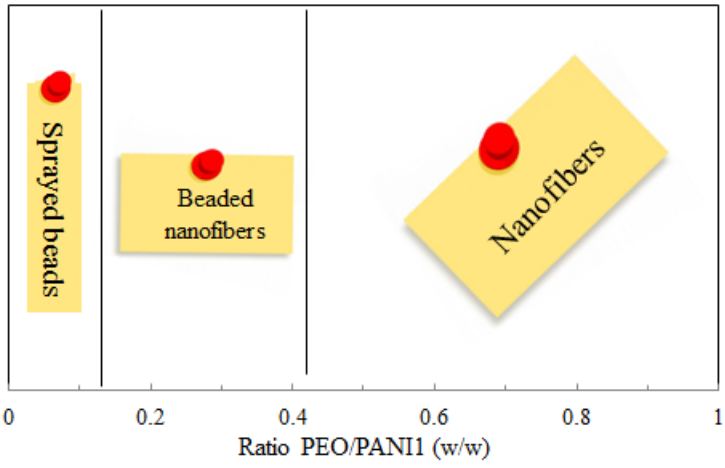

Figure 9.1.:Correlation between the nanofibers production and PEO/PANI1 ratio (w/w).

Figures 9.2. A-E report SEM images at low and high magnification of the nanofibers collected from solutions with different PEO/PANI1 and the diameters distribution using both a static (A-C) and a rotating collector (D-E).

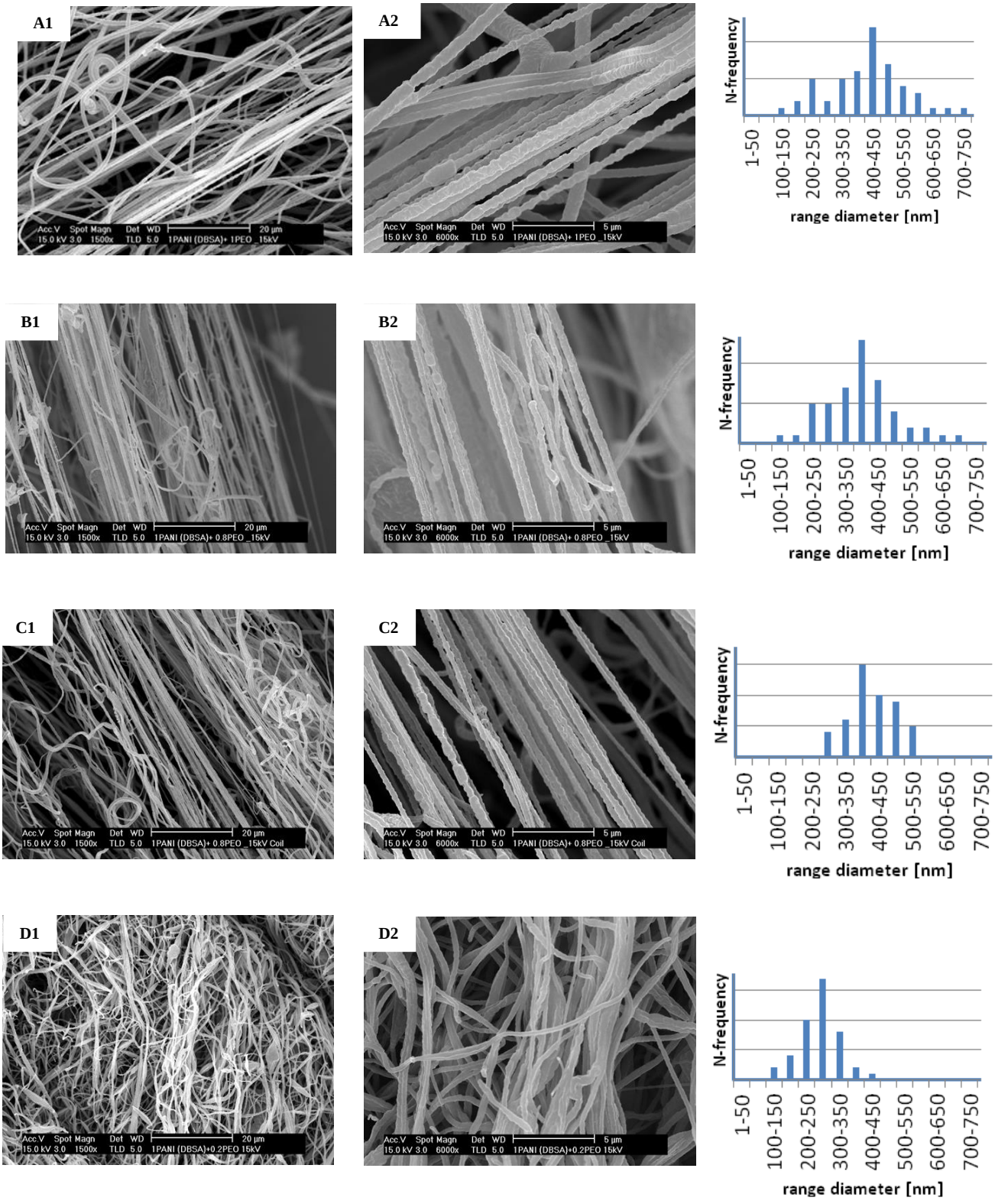

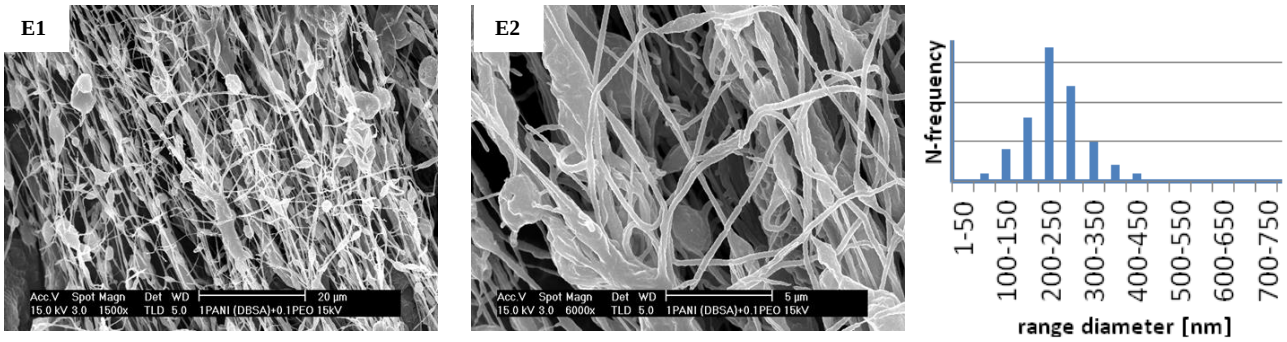

Figure 9.2.: SEM images at low and high magnification and diameters distribution for the composite nanofibers with a PANI1:PEO ratio of : A)1:1, B)1:0.8 collected on static collector and C)1:0.8 (w/w) D)1:0.2, E)1:0.1 (w/w) collected on rotating collector.

The morphological characterization shows that, increasing gradually the PANI1/PEO ratio from 1: 1 to 1: 0.1 the mean diameter of fibers is reduced by half (from 430 nm to 230 nm) and the surface morphology becomes rougher. Moreover, the size of the fibers is affected by the method used to collect them. In fact, the rotating collector promotes a narrow distribution of the diameters favoring a stretching effect (Figures 9.2. D and E) with respect to the static collector (Figures 9.2. A-C). However, when the PEO concentration is too low (PANI1/PEO 1:0.2) some defects (beads) appear on the polymer nanofibers (Figures 9.2. D and E). Their formation is probably due to capillary instability of jet caused by surface tension.

Figure 9.3. shows the results obtained using PANI2 in the electrospinning process changing the PEO/PANI2 ratio (w/w).

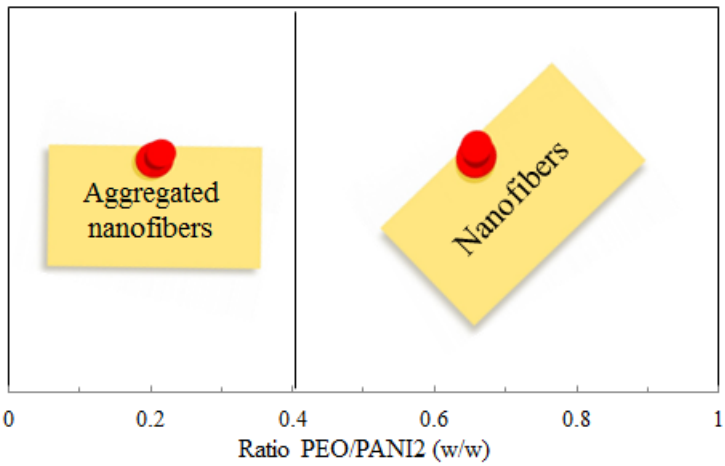

Figure 9.3.:Correlation between the nanofibers production and PEO/PANI1 ratio (w/w).

SEM characterizations are summarized in Figure 9.4.

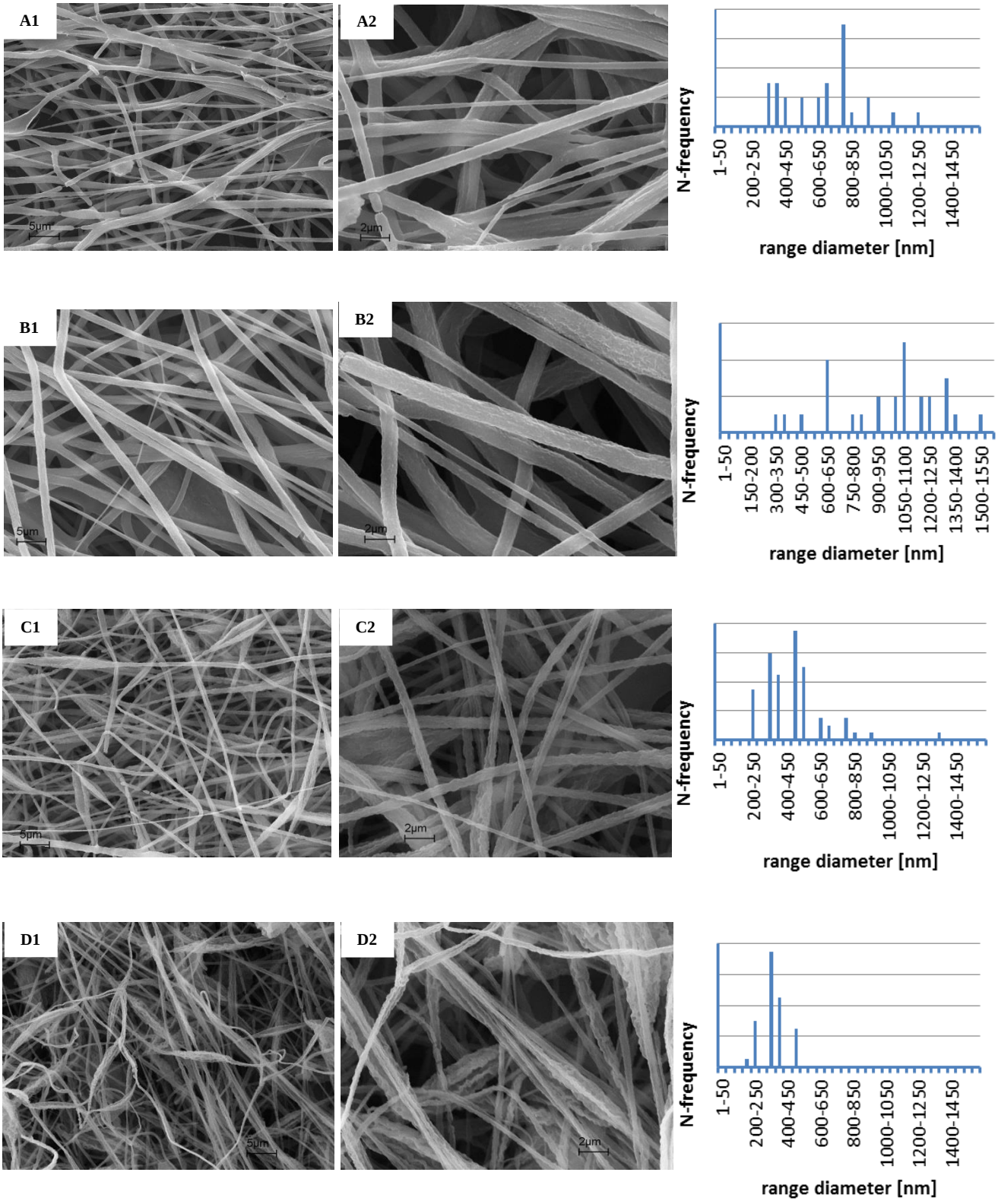
A1
5µm
A2
2µm
N-frequency
1-50
200-250
400-450
600-650
800-850
1000-1050
1200-1250
1400-1450
range diameter [nm]
B1
5µm
B2
2µm
N-frequency
1-50
150-200
300-350
450-500
600-650
750-800
900-950
1050-1100
1200-1250
1350-1400
1500-1550
range diameter [nm]
C1
5µm
C2
2µm
N-frequency
1-50
200-250
400-450
600-650
800-850
1000-1050
1200-1250
1400-1450
range diameter [nm]
D1
5µm
D2
2µm
N-frequency
1-50
200-250
400-450
600-650
800-850
1000-1050
1200-1250
1400-1450
range diameter [nm]

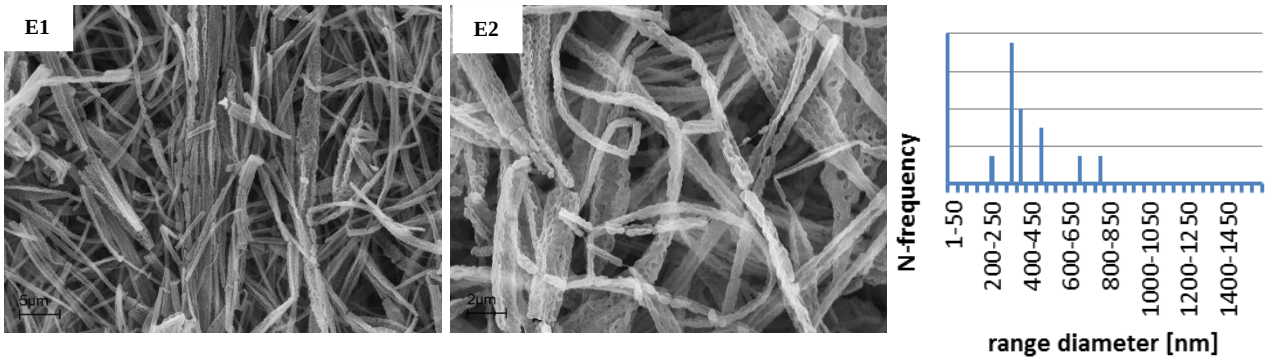

Figure 9.4.: SEM images at low and high magnification and diameters distribution for the composite nanofibers with a PEO:PANI2 ratio (w/w) of : A)1:1, B)1:0.8, C)1:0.6, D)1:0.4 and E)1:0.2 collected on static collector.

Also in the case of PANI2, increasing gradually the PANI2/PEO ratio from 1: 1 to 1: 0.2 the mean diameter of fibers is reduced by half from *ca*. 800 to *ca*. 300 nm. However, in this case it is more evident from the SEM images that coarse nanofibers are due to the agglomeration of smaller ones. This phenomenon is more important for high values of PANI2/PEO ratio. Moreover, a large distribution of diameters is observed, especially for the samples containing high amount of PEO (PEO/PANI2= 1: 1, 1: 0.8 and 1: 0.6). Unlike PANI1, for PANI2 the decrease of PEO amount into the blend doesn't compromise dramatically the nanofibers morphology. In fact, also for very low PEO amount nanofibers are obtained although with a higher roughness morphology.

9.1.2. Spectroscopic characterization

Figure 9.5.A shows FT-IR spectra of PANI1/PEO NFs (1:0.4, 1:1, w/w) and a sample of PANI1 not spun, while Figure 9.5.B reports the analogous FT-IR spectra of the materials prepared by PANI2.

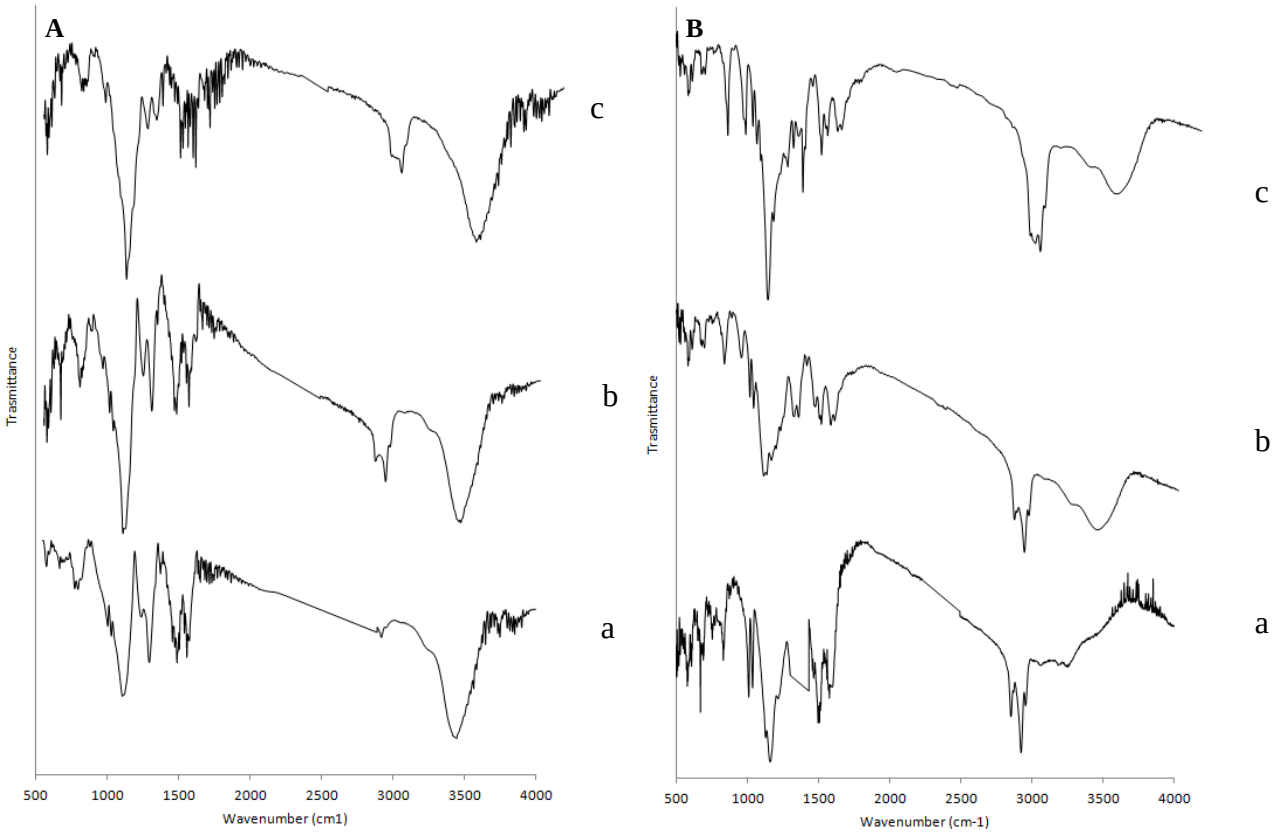

Figure 9.5.: FT-IR spectra of (A) PANI1 derivatives: a) PANI1 not spun, b) PANI1/PEO 1:0.4 spun nanofibers (static collector), c)PANI1/PEO 1:1 spun nanofibers (static collector), (B) PANI2 derivatives: a) PAND2 not spun, b) PAND2/PEO 1:0.4 spun nanofibers (static collector), c)PAND2/PEO 1:1 spun nanofibers (static collector).

All the spectra exhibit the characteristic absorptions for the conducting doped polyaniline . The bands at *ca.* 1350, 1050 and 1000 cm^{-1} can be assigned to the bending vibration mode of the S=O bonds. Whereas, the bands at *ca*. 1570, 1490 cm^{-1} are assigned respectively to the C=C stretching of the quinoid rings (N=Q=N) and to the C=C stretching vibration mode for the benzenoid rings (N-B-N). The typical characteristic spectral peak of PEO at around 2885 cm^{-1}[602] is not very prominent in the PANI1/PEO composites, probably due to its low concentration in the composites. No significant changes in intensities and frequencies were observed for the materials collected by rotating collector. For this reason only the FT-IR spectra of the fibers collected on the static collector have been reported.

Figure 9.6. shows UV-visible of PANI1 not spun and PANI1/PEO NFs collected on a static collector.

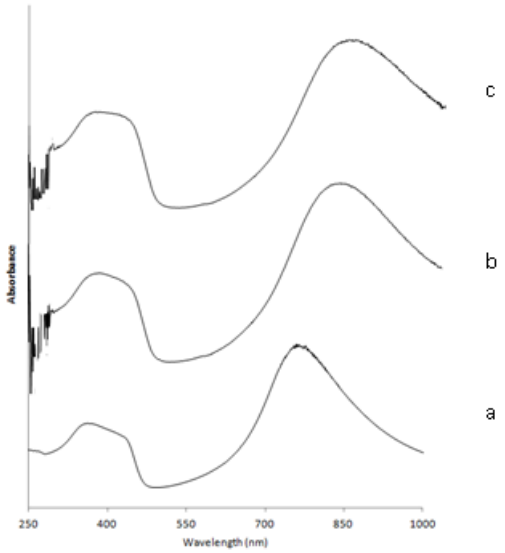

Figure 9.6.: Uv-Vis spectra a) PANI1 not spun, b) PANI1/PEO 1:0.4 NFs (static collector), c)PANI1/PEO 1:1 NFs.

Also in this case the spectra obtained for the composites collected on the rotating collector have led to similar results. The spectra show three absorption bands at *ca*. 330, 450 and 800 nm. The peak at 330 nm corresponds to the π-π* transition of the isolated benzenoid ring, that at 450 nm corresponds to the polaron to π* band transition. The presence of polaron band transitions indicates that the as-prepared PANI is in a conducting emeraldine salt form. The band at *ca.* 800 nm can be assigned to the excitation of the quinoid ring corresponding to the semi-conducting phase of PANI1 nanofibers. As it's possible to observe, the absorption spectra of PANI1/PEO spun nanofibers composites are similar to those of PANI1 not spun. In fact, no other absorption bands were observed in the visible region confirming that the high voltage used during the electrospinning process did not promote over-oxidation of the polyaniline chains.

The position of the bands at lower wavelength did not change significantly increasing the PEO amount in the spun nanofibers, instead the position of the high wavelength localized polaron band shifted to higher wavelengths. According to Zheng *et al*. [603] this shift in the position of the localized polaron band can be caused by de-aggregation of the polyaniline chains in solutions.

The materials spun from PANI2 solutions show some differences in their UV-vis spectra (Figure 9.7.).

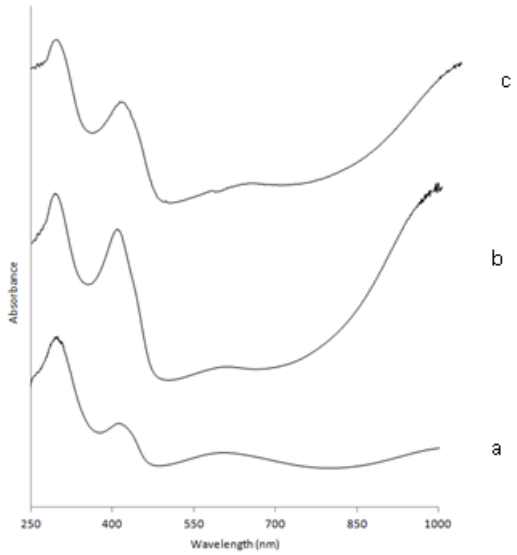

Figure 9.7.: Uv-Vis spectra a) PANI2 not spun, b) PANI2/PEO NFs (1:0.4), c) PANI2/PEO NFs (1:1).

In fact, the peaks at 330, 450 and 800 nm are shifted to *ca.* 270, 400 and 1000 nm, whereas a new peak at ca. 550 nm appears. The presence of two peaks (450 and 550 nm) in PANI2 based materials may arise from two types of polaron to π* band transitions, as these polyaniline nanostructures have two types of polaron bands, resulting from two types of polyaniline chain orientations. The significant intensity at 1000 nm can doubtlessly be attributed to the increase in the relative mass fraction of doped-PANI.[604]

9.1.3. Conductivity measurements

The complex impedance Z= Z'- jZ'', where Z' and Z'' are respectively the real and imaginary part of the impedance, describes the dielectric response of spun nanofiber composites. The frequency dependence of the real part of the sample impedance, which is governed by the resistance of the material for PANI1/PEO NFs and for a sample of PANI1 not spun is showed in Figure 9.8.

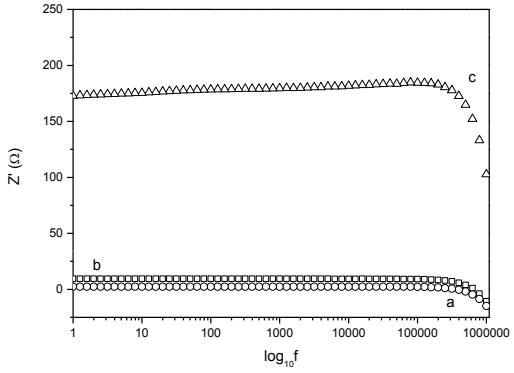

Figure 9.8.: Z' value by impedance spectroscopy of the samples a)PANI1 not spun, b) PANI1/PEO 1:0.4 spun nanofibers, c) PANI1/PEO 1:1 spun nanofibers, d) PANI1/PEO 1:0.4 blended system, e) PANI1/PEO 1:1 blended system.

It is observed that for doped PANI1 and for the spun sample with low content of PEO the real part of impedance for larger range of frequencies exhibits asymptotic value.

Figure 9.9. shows the imaginary part of impedance, it is noted that the peak present in pure PANI1 shifts at higher frequencies by increasing the PEO content probably because the nanofiber composites have less number of polarons and bipolarons thus providing multiple paths for the system to relax.[605]

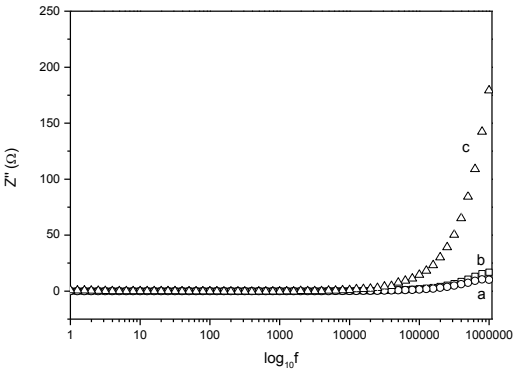

Figure 9.9.: Z'' value by impedance spectroscopy of the samples a)PANI1 not spun, b) PANI1/PEO 1:0.4 spun nanofibers, c) PANI1/PEO 1:1 spun nanofibers, d) PANI/PEO 1:0.4 blended system, e) PANI1/PEO 1:1 blended system.

Table 9.1. reports the impedance values at 100 Hz, 10 kHz and 100 kHz for the doped PANI1 and for nanocomposites spun fibers PANI1/PEO and also for cast blended systems for PANI1/PEO.

SAMPLE	f=10Hz			f=10kHz			f=100KHz		
	Z' [Ω]	Z'' [Ω]	σ [S/cm^{-1}]	Z' [Ω]	Z'' [Ω]	σ [S/cm^{-1}]	Z' [Ω]	Z'' [Ω]	σ [S/cm^{-1}]
PANI1	2.34	0.003	$2.14\cdot10^{-2}$	2.36	0.09	$2.12\cdot10^{-2}$	2.20	1.37	$2.27\cdot10^{-2}$
PANI1/PEO 1:0.4	9.38	0.006	$5.33\cdot10^{-3}$	9.36	0.14	$5.34\cdot10^{-3}$	9.11	1.98	$5.49\cdot10^{-3}$
PANI1/PEO 1:1	172	0.11	$2.91\cdot10^{-4}$	178	0.85	$2.81\cdot10^{-4}$	184	14.5	$2.72\cdot10^{-4}$
PANI1/PEO* 1:0.4	34.08	0.019	$1.47\cdot10^{-3}$	35.11	0.37	$1.42\cdot10^{-3}$	35.3	3.99	$1.42\cdot10^{-3}$
PANI1/PEO* 1:1	201	0.22	$2.49\cdot10^{-4}$	205	0.77	$2.44\cdot10^{-4}$	204.5	14.75	$2.44\cdot10^{-4}$
PANI2/PEO 1:1	220	0.31	$2.73\cdot10^{-4}$	212	0.71	$2.63\cdot10^{-4}$	205	14.82	$2.44\cdot10^{-4}$
PANI2/PEO* 1:1	218	0.30	$2.70\cdot10^{-4}$	220	0.86	$2.73\cdot10^{-4}$	208	16.32	$2.58\cdot10^{-4}$

Table 9.1.: Complex Impedance and conductivity at selected frequencies. * No spun, blended system.

Obviously increasing the content of PEO in the nanofibers, the Z' and Z'' values also increase and the correspondent conductivity values decrease. Comparing the same composite materials (PANI1/PEO) spun with the blended sample it is possible to notice that the spun system displays a better value of conductivity than the blended system indicating that the network of spun nanofibers improves the conduction mechanism. The conductivity values of the spun PANI2/PEO (1:1) are similar with respect to the analogue blended system. This result is probably due to the morphological characteristics of spun fibers.

To better analyze the data, a Cole-Cole plot for the various nano-composites samples of PANI1/PEO and for PANI1 is reported (Figure 9.10.).

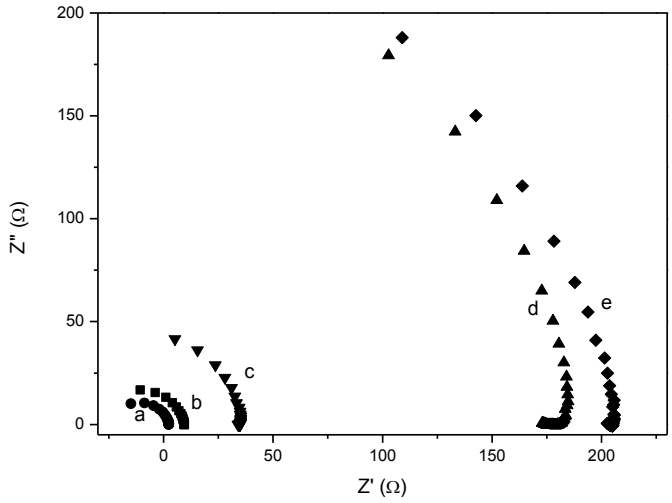

Figure 9.10.: Cole-Cole plot for the impedance of samples : a)PANI1 not spun, b) PANI1/PEO 1:0.4 spun nanofibers, c)PANI1/PEO 1:1 spun nanofibers, d) PANI1/PEO 1:0.4 blended system, e) PANI1/PEO 1:1 blended system.

The diagram, visibly asymmetric, confirms that at high frequency (greater than 100 KHz) the behavior of the materials is more and more similar to resistive-inductive (RL) response, while at frequencies near DC the resistive comportment is almost absolute, in dependence of the material typology. The presence of inductive effect is more marked with increasing the presence of PEO in the composite.

As reported in the scientific literature,[26] PANI2 is less conductive than PANI1. Such a different behaviour is not clear but could be related to a lower value of molecular weight of PANI2 than PANI1 or to their different degree of crystallinity (see Chapter 10, paragraph 10.1.2.).
For this reason, measurements of AC conductivity of samples resulted to be limited at low values of frequency. DC conductivity values are summarized in Table 9.2.

SAMPLE	σ [S/cm^{-1}]
PANI2*	$1.11 \cdot 10^{-6}$
PANI2/PEO 1:0.2	$7.15 \cdot 10^{-7}$
PANI2/PEO 1:0.4	$5.02 \cdot 10^{-7}$
PANI2/PEO 1:0.6	$4.68 \cdot 10^{-7}$
PANI2/PEO 1:0.8	$4.56 \cdot 10^{-7}$

Table 9.2.: conductivity values of PANI2/PEO NFs. * No spun.

However, also in this case, the values of conductivity of PANI2-based NFs increase as the PEO/PANI2 ratio (w/w) decreases.

9.1.4. Tests of cytocompatibility

In order to test direct and indirect PANI/PEO NFs cytocompatibility on a SH-SY5Y human cell line, PANI1/PEO and PANI2/PEO NFs (PANI:PEO ratio 1:0.4 w/w) were sterilized under different conditions: 15 minutes in EtOH 70%, 48 hours in PBS (phosphate buffer solution, pH 7.2-7.4) + 3% (v/v) of penicillin/streptomicyn and 10 minutes under UV irradiation (253.7 nm).
In all cases, PANI NFs suffered from degradation. Important fragmentation phenomena and indissolubility of the samples did not allow to carry out biological tests on PANI2 NFs.
Figure 9.11. shows the degradation of PANI1 NFs after the washing treatment.

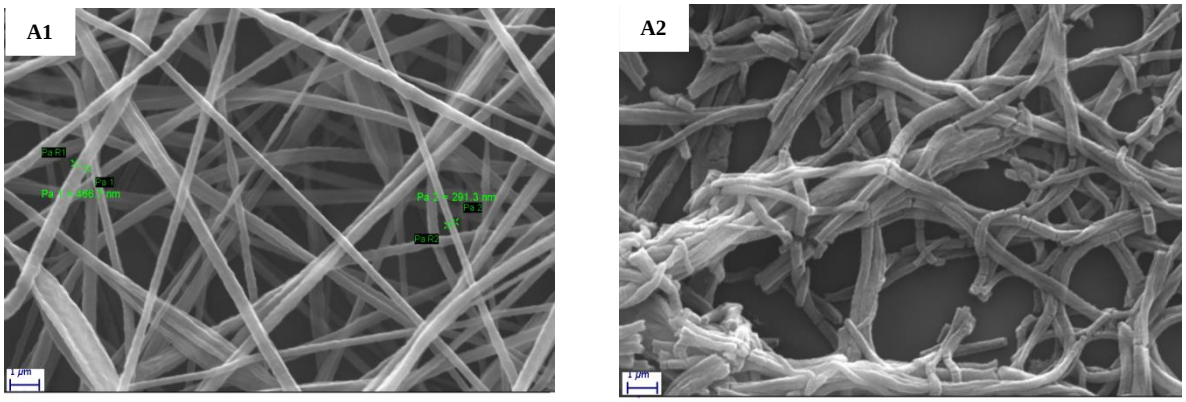

Figure 9.11.: SEM images of PANI1/PEO (1: 0.4 w/w) before (A1) and after (A2) EtOH treatment .

NFs degradation can be explained in terms of phase segregation phenomena. In fact, the sterilization process caused the removal of the small PEO amount present into NFs. Owing to the non-homogeneous distribution of PEO and PANI into the blend, this phenomenon dramatically compromised the morphology of NFs.

However, despite these drawbacks, PANI1 NFs exhibited good results in terms of cell viability, as shown in Figure 9.12.

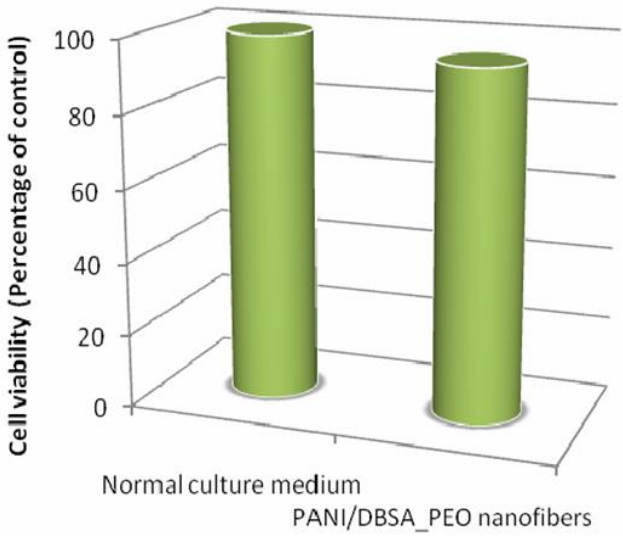

Figure 9.12.: Results of biocompatibility *in vitro* for PANI1/PEO NFs (1: 0.4 w/w): SH-SY5Y cells (human neuroblastoma cell line) viability after 48 h of incubation at 37°C, 5% CO_2.

Phase segregation phenomena observed in PANI/PEO NFs didn't allow a thorough biological characterization.

9.2. PANI/PMMA nanofibers: effect of washing

In order to overcome the drawback related to the degradation of PANI/PEO NFs after sterilization procedure, PEO was substituted with another polymer (PMMA) not soluble in water or ethanol but able to guarantee no segregation phenomena into the PANI/PMMA blend. This new approach allowed to spin PANI/PMMA NFs using high amount of insulating copolymer and remove it in a second step with a specific washing treatment.

9.2.1. Morphological characterization

PANI/PMMA solutions were prepared with the same procedure as used for PANI/PEO (see Chapter 6 paragraph 6.5.1) but using the PANI/PMMA ratio (w/w) reported in Figure 9.12.

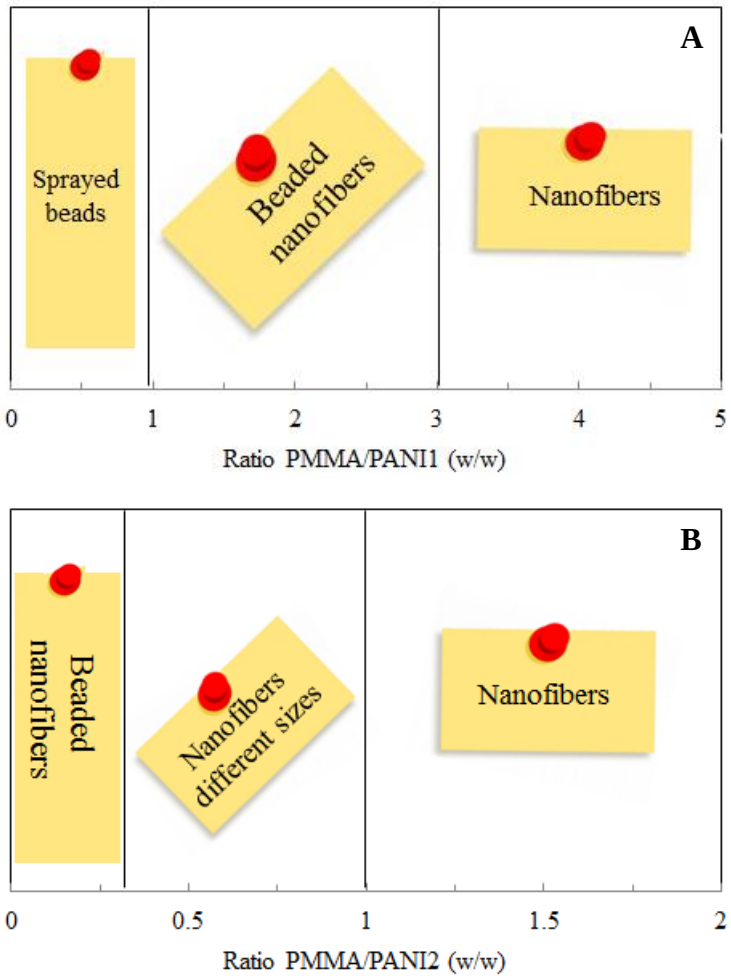

Figure 9.12.:Correlation between nanofibers production and (A) PMMA/PANI1 and (B) PMMA/PANI2 ratio (w/w).

In this case, a mixture of $CHCl_3$: DMF (dimethylformamide)= 5:1 was used as the solvent, in order to increase PANI solubility.

As shown in Figure 9.12 A, PANI1/PMMA NFs were obtained only when high amount of copolymer was used (PANI1: PMMA= 1:4). In fact, the low solubility of PANI1/DBSA in organic solvent leads to PANI1/PMMA organic mixtures characterized by low viscosity, that compromises jet stability.

On the contrary, the higher solubility of PANI2/DBSA allows to reduce the amount of copolymer used (PANI2: PMMA= 3:1).

Starting from the results obtained whit PEO as the copolymer, all PANI/PMMA NFs were washed for 2 minutes with 2-propanol after the electrospinning process and before the biological tests in order to remove PMMA from PANI NFs and investigate if some morphological modifications occur.

Figures 9.13. show the morphological characterization of PANI1/PMMA and PANI2/PMMA NFs obtained using different PANI/PMMA ratios before (Figures 9.13. A1, A2, C1, C2, E1, E2, G1 and G2) and after (Figures 9.13. A3, A4,C3, C4, E3, E4, G3 and G4) treatment with 2-propanol.

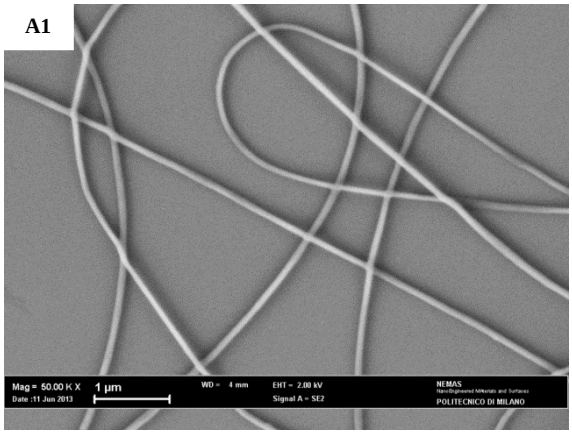

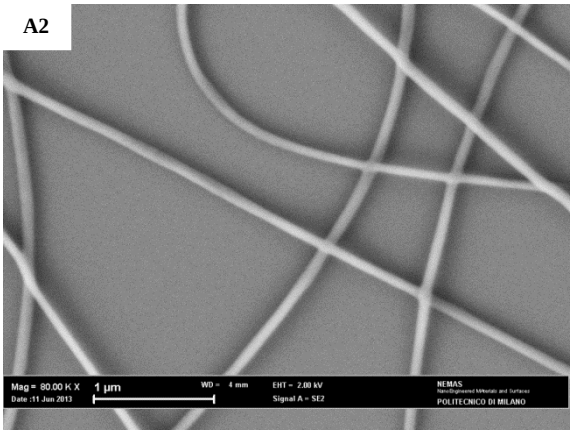

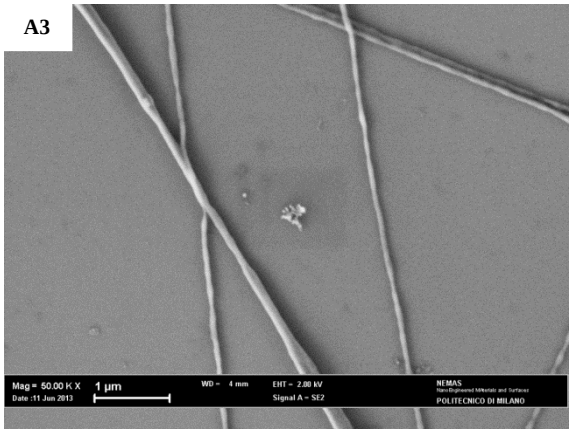

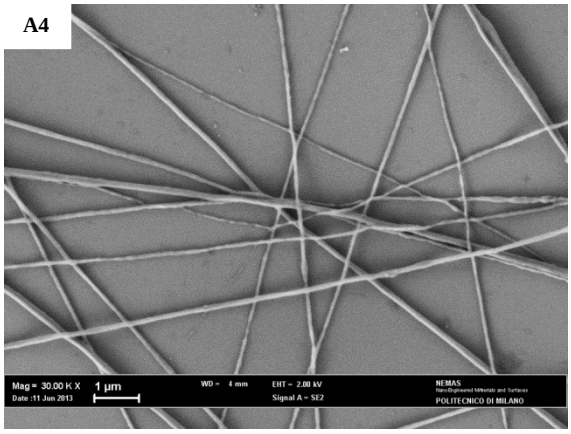

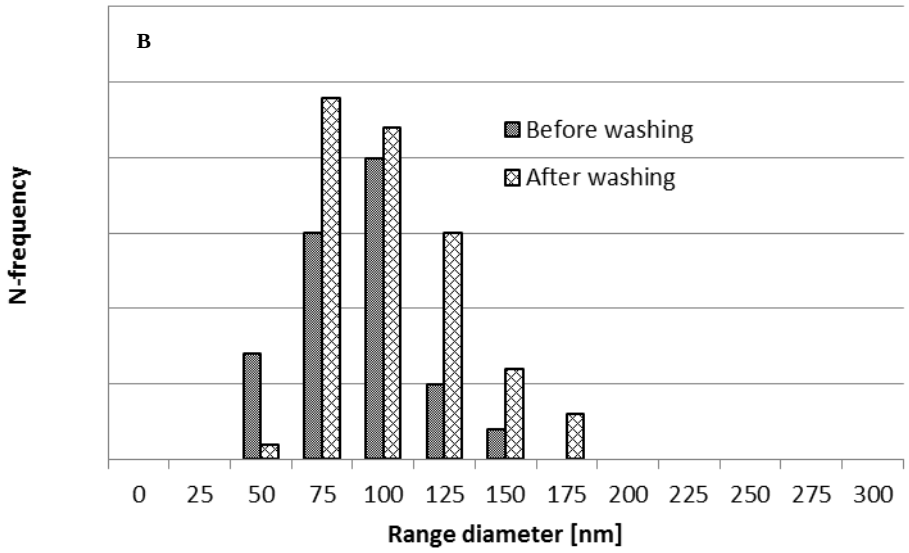
B
Before washing
After washing
N-frequency
0
25
50
75
100
125
150
175
200
225
250
275
300
Range diameter [nm]

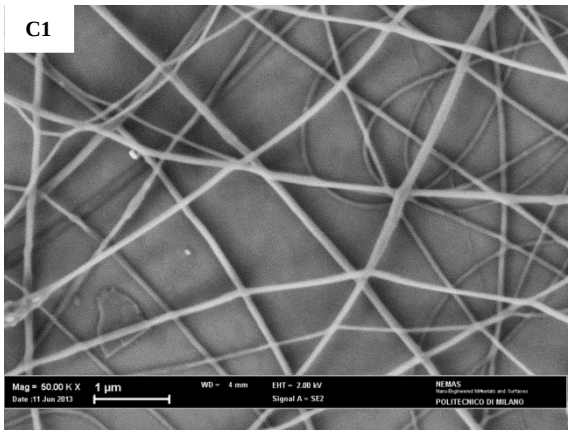
C1
Mag = 50.00 K X
1 µm
Date :11 Jun 2013
WD = 4 mm
EHT = 2.00 kV
Signal A = SE2
NEMAS
POLITECNICO DI MILANO

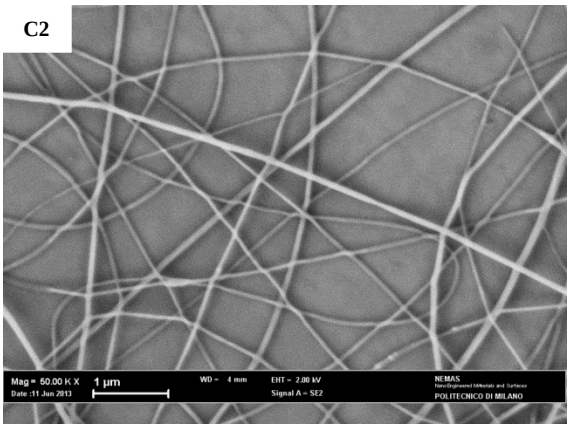
C2
Mag = 50.00 K X
1 µm
Date :11 Jun 2013
WD = 4 mm
EHT = 2.00 kV
Signal A = SE2
NEMAS
POLITECNICO DI MILANO

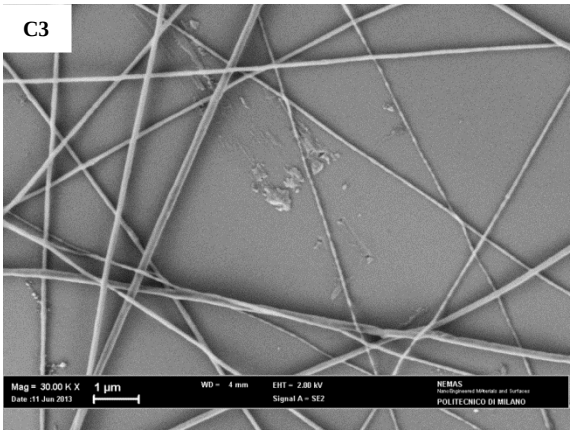
C3
Mag = 30.00 K X
1 µm
Date :11 Jun 2013
WD = 4 mm
EHT = 2.00 kV
Signal A = SE2
NEMAS
POLITECNICO DI MILANO

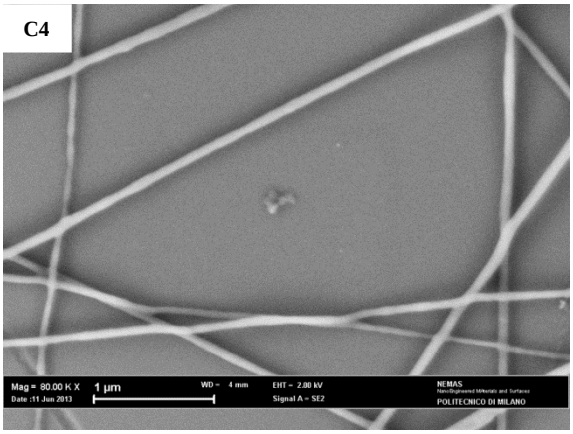
C4
Mag = 80.00 K X
1 µm
Date :11 Jun 2013
WD = 4 mm
EHT = 2.00 kV
Signal A = SE2
NEMAS
POLITECNICO DI MILANO

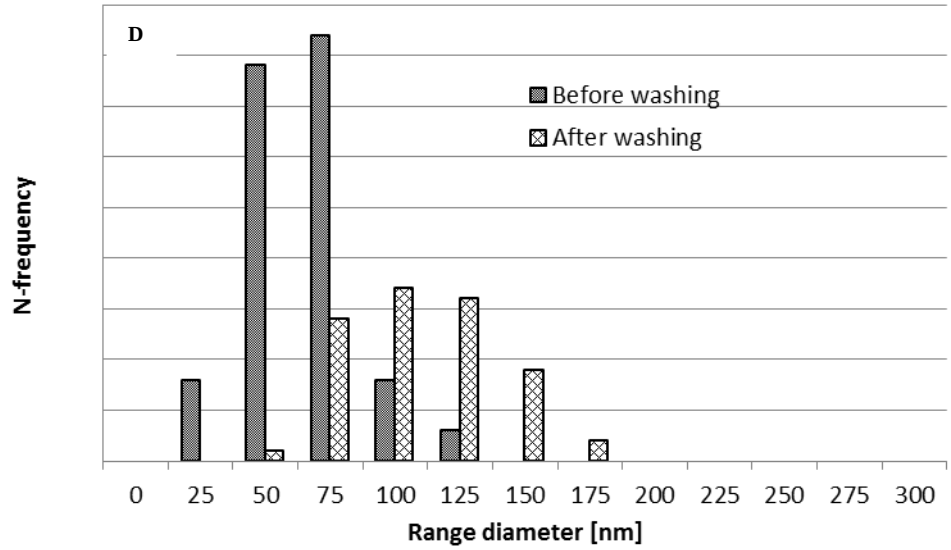
D
Before washing
After washing
N-frequency
0
25
50
75
100
125
150
175
200
225
250
275
300
Range diameter [nm]

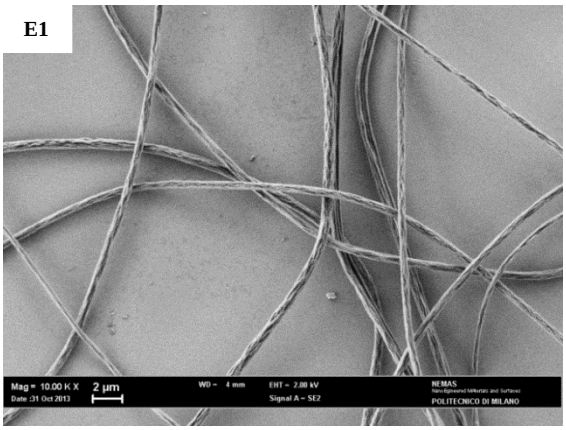
E1
Mag = 10.00 K X
2 µm
WD = 4 mm
EHT = 2.00 kV
Signal A = SE2
NEMAS
POLITECNICO DI MILANO

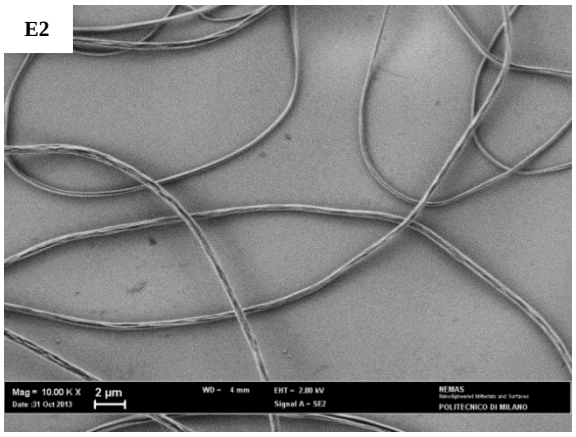
E2
Mag = 10.00 K X
2 µm
WD = 4 mm
EHT = 2.00 kV
Signal A = SE2
NEMAS
POLITECNICO DI MILANO

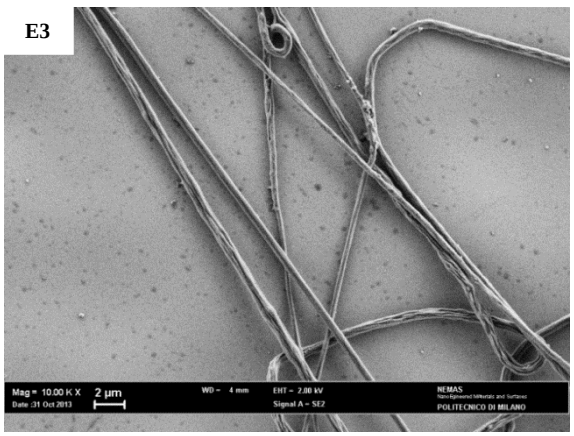
E3
Mag = 10.00 K X
2 µm
WD = 4 mm
EHT = 2.00 kV
Signal A = SE2
NEMAS
POLITECNICO DI MILANO

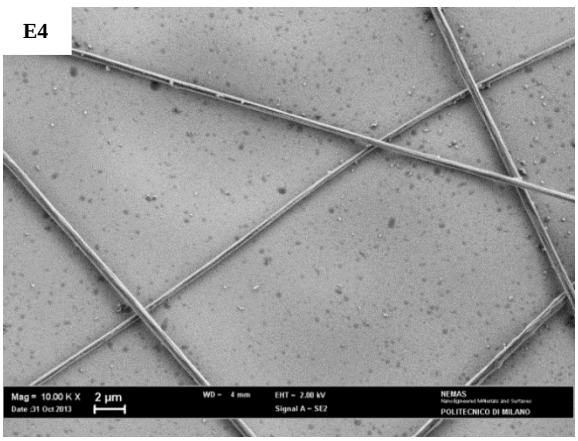
E4
Mag = 10.00 K X
2 µm
WD = 4 mm
EHT = 2.00 kV
Signal A = SE2
NEMAS
POLITECNICO DI MILANO

F

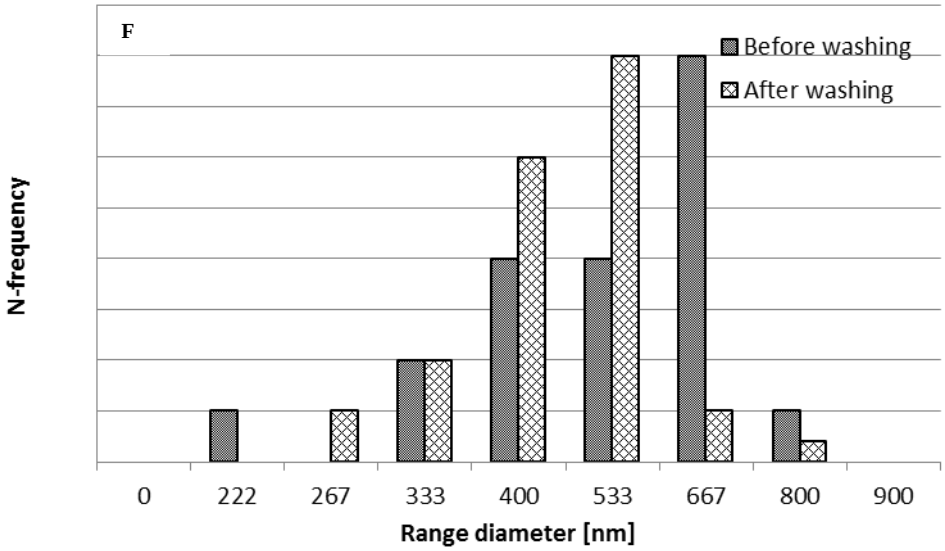
Before washing
After washing
N-frequency
0
222
267
333
400
533
667
800
900
Range diameter [nm]

G1

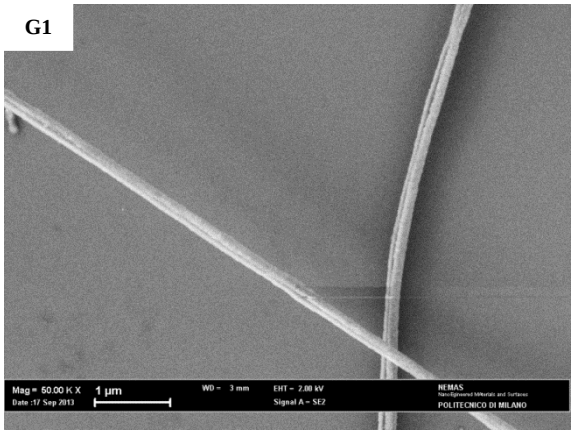
Mag = 50.00 K X
1 µm
WD = 3 mm
EHT = 2.00 kV
Signal A = SE2
NEMAS
POLITECNICO DI MILANO

G2

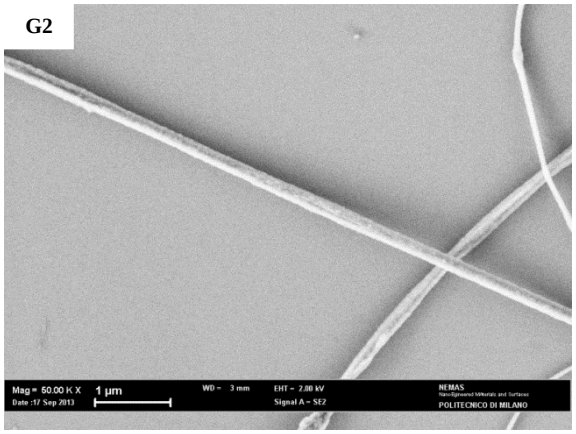
Mag = 50.00 K X
1 µm
WD = 3 mm
EHT = 2.00 kV
Signal A = SE2
NEMAS
POLITECNICO DI MILANO

G3

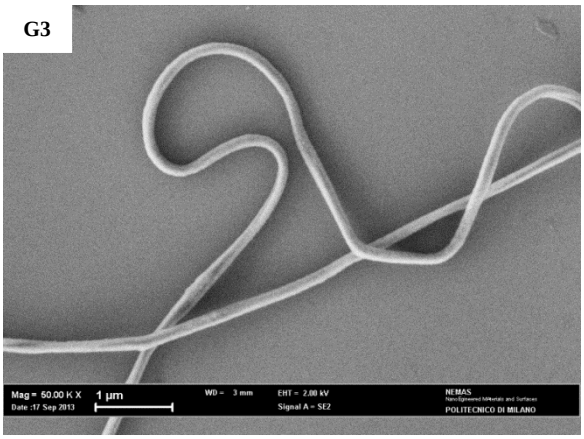
Mag = 50.00 K X
1 µm
WD = 3 mm
EHT = 2.00 kV
Signal A = SE2
NEMAS
POLITECNICO DI MILANO

G4

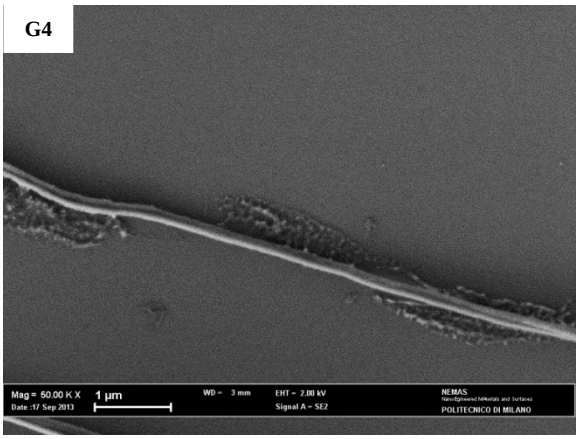
Mag = 50.00 K X
1 µm
WD = 3 mm
EHT = 2.00 kV
Signal A = SE2
NEMAS
POLITECNICO DI MILANO

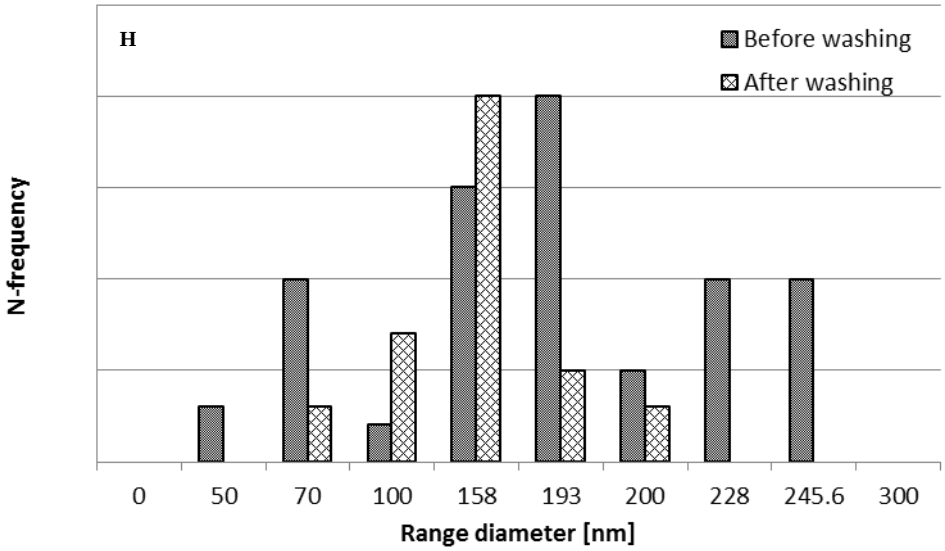

Figure 9.13.: SEM images and diameters distribution (B, D for PANI1 NFs, F and H for PANI2 NFs) of: PANI1 NFs with a PANI1:PMMA ratio w/w of (A)1:5 and (C)1:4 before (A1, A2, C1 and C2) and after (A3, A4, C3 and C4) washing with 2-propanol and the PANI2 NFs with a PANI2:PMMA ratio w/w of (E)1:2 and (G) 1:1 before (E1, E2, G1 and G2) and after (E3, E4, G3 and G4) washing with 2-propanol.

As it is possible to observe, as for PANI/PEO NFs, increasing the amount of conducting polymer into the PANI1/PMMA blend the mean diameter of NFs decreases significantly, passing from 103 to 78 nm.

Moreover, PANI1/PMMA NFs don't show phase segregation. In fact, the treatment with 2-propanol doesn't compromise neither their morphology nor sizes. An increase in the roughness of the surface of NFs confirms the PMMA removal.

Similar results were obtained using PANI2/PMMA blends. In fact, also in this case decreasing the amount of PMMA into the blend the mean diameter of NFs decreases passing form 600 to 200 nm and the treatment with 2-propanol doesn't dramatically change their size.

In terms of productivity of the process, the electrospinning technique allowed to produce hundreds milligrams of nanofibers per hour in the case of PANI2/PMMA blend, this rough value is smaller for PANI1/PMMA system (a few mg per hour). From an industrial point of view this limitation can be overcome applying on the instrument numerous syringes (or pipettes) that work simultaneously. Such a modification of the electrospinning apparatus resulted to be sufficient to improve the productivity for PANI2/PMMA system but not for PANI1/PMMA system.

For this reason only PANI2-based NFs will be characterized spectroscopically and by measurements of conductivity.

9.2.2. Spectroscopic characterization

Figure 9.14. shows UV-vis and FT-IR spectra of PANI2/PMMA NFs produced using a PANI2/PMMA ratio (w/w) of 1:2.

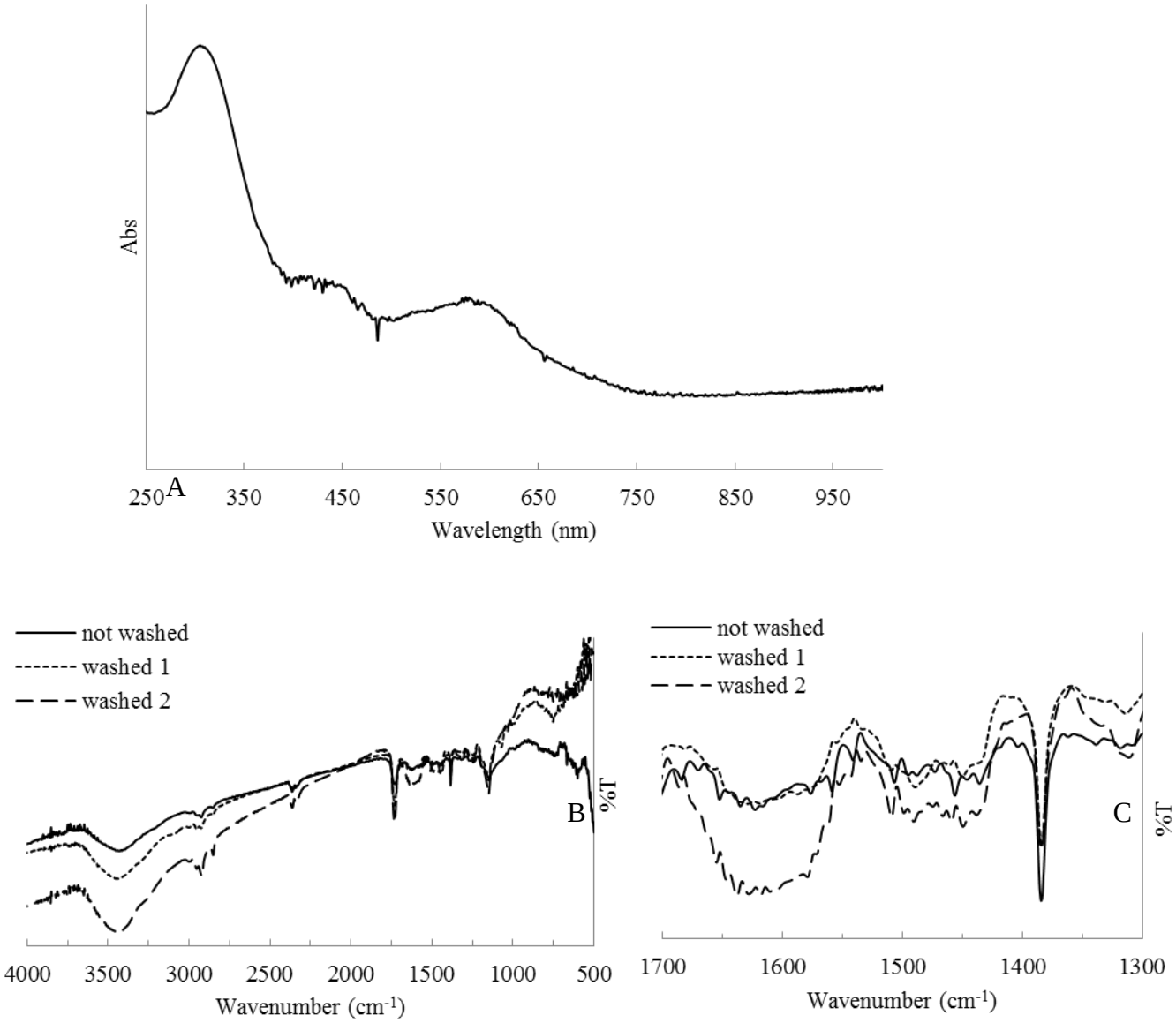

Figure 9.14.: (A) UV-vis and (B) FT-IR spectra and its magntification (C) of PANI2/PMMA NFs, PANI2/PMMA 1:2 (w/w).

UV-vis spectrum shows the characteristic band of PANI in its conducting emeraldine form, even though the band corresponding to the excitation of the quinoid ring that in protonated emeraldine is at around 800 nm, in this case is shifted to lower wavelength (600 nm). Such a shift is characteristic of unprotonated poyaniline.

FT-IR characterization was carried out before and after washing of the sample with 2-propanol in order to remove the excess of PMMA. As it is possible to observe (Figures 9.14. B and C), the

bands of PMMA, especially carbonylic band, are very intense and tend to cover that of PANI. However, after the washing step, the characteristic band of polyaniline at *ca.*1570 and 1490 cm^{-1} become more evident, confirming the effectiveness of the 2-propanol treatment.

9.2.3. Tests of cytocompatibility

Indirect cytocompatibility tests were carried out on SH-SY5Y cells (human neuroblastoma cell line).

For this scope, washed and unwashed PANI2/PMMA NFs were incubated for 1, 3 and 7 days in the culture medium to evaluate the possible release of toxic species.

At the time points selected, the supernatants were removed and used to culture SH-SY5Y cells.

In particular, three conditions were examined:

a) 31,250 cells/cm^2, 48 h of incubation with the supernatants;

c) 62,500 cells/cm^2, 72 h of incubation with the supernatants;

c) 93,750 cells/cm^2, 24 h of incubation with the supernatants.

As a control, SH-SY5Y cells were also cultured in fresh medium.

Then, cell viability was evaluated by MTS assay (Promega), according to the instructions provided by the manufacturer.

For all the conditions tested, the results (Figure 9.15.) have shown that after 1 and 3 days of exposure to the culture medium previously incubated with the NFs, SH-SY5Y cell viability was generally comparable with controls. After 7 days of exposure, SH-SY5Y cell viability was lower than controls for both washed and unwashed PANI2/PMMA NFs in the condition a) and only for unwashed PANI2/PMMA NFs in the condition b), while for both NFs it was comparable with controls under the other conditions.

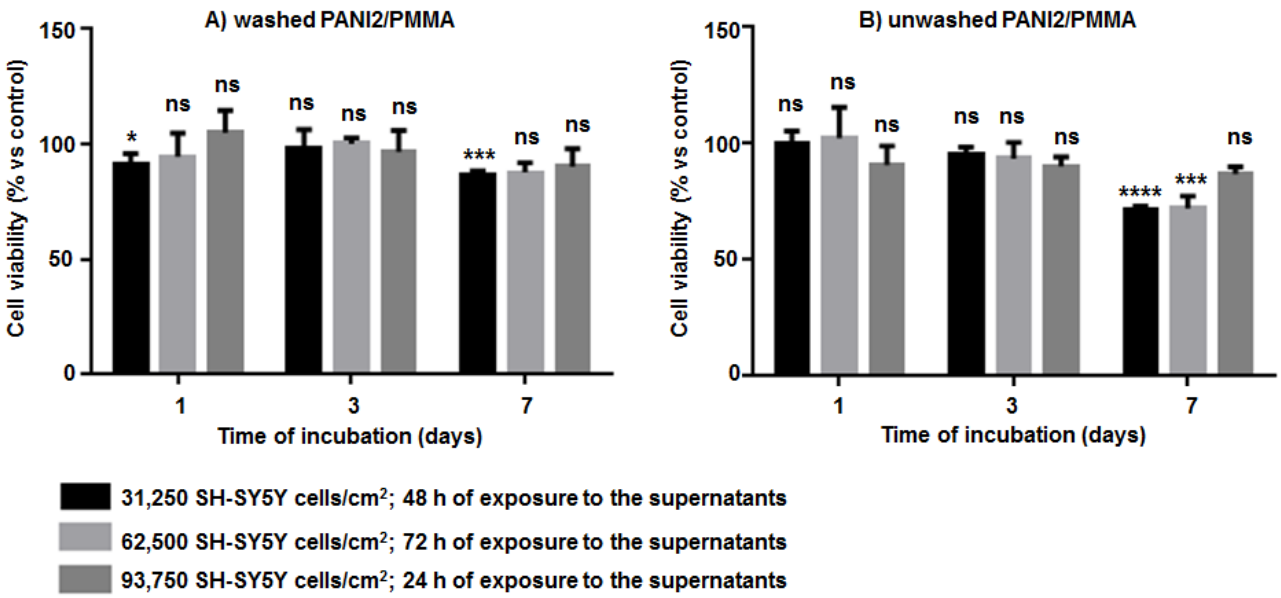

Figure 9.15.: Cytocompatibility tests. ns = p-value > 0.05, * = p-value < 0.05, ** = p-value < 0.001, **** = p-value < 0.0001

Even though preliminary, these results have suggested that washed PANI2/PMMA NFs might be a better substrate for culturing SH-SY5Y cells than unwashed PANI2/PMMA NFs.

To better investigate this aspect, direct cytocompatibility tests are in progress.

In particular, SH-SY5Y cells were cultured in contact with washed and unwashed PANI2/PMMA NFs for 24 h and 48 h and their morphology was observed by an optical and a scanning electron microscope (SEM).

The SEM analysis is still in progress, but the preliminary investigations by the optical microscope have shown that controls cultured in standard tissue culture plates have a more flattened and spread morphology than the SH-SY5Y cells cultured on the NFs.

Chapter 10: Electromechanical properties of polyaniline: towards low cost force and strain sensors

Pressure/force and strain sensors are based on electrical property changes of active materials when a mechanical stress is applied. Polyvinylidenefluoride (PVDF) is one of the most investigated active materials in this field. PVDF improves piezoelectric response when poled at high electric fields and generates an output voltage on the order of tens volts at $10N \cdot cm^{-2}$ pressure load.[606] However, the exponential growing of wireless sensors requires new active materials easily adaptable to versatile substrates. Among these materials, the ones with large piezoresisitive response are particularly interesting. These materials are developed for many different purposes, such as integrated systems for personal health care control, pressure sensors implemented into smart fabrics to monitor personal motion, heartbeat, etc. In this regard, conducting polymers and their composites are promising candidates for a new generation of sensors. Many authors reported conducting composites consisting on conducting fillers and elastic polymers for pressure/force sensor application. The fillers investigated include carbon black, [607, 608], carbon nanotube,[609] metals,[610] and conducting organic polymers.[611, 612]

Polyaniline and polypyrrole are particularly investigated for their ease of synthesis and low cost.

In this section the electromechanical behaviour of two different polyanilines will be presented.

PANI was prepared by two different synthetic methods: classical approach ($(NH_4)_2S_2O_8$ as the oxidant, PANI1),[544] and "green" approach (H_2O_2 as the oxidant, PANI2), [26] as described in Chapter 6 sections 6.1.1. and 6.1.2.

Both these materials were protonated with different acid dopants (H_2SO_4 and H_3PO_4) and their change in resistivity was tested under loading/unloading cycles at high (0-100 kN) and low (0-20 N) values of force at room temperature.

Moreover, the piezoresistive effect of PANI1 and PANI2 in form of film (doped with dodecylbenzenesulfonic acid, DBSA) at different temperatures was investigated.

10.1. Electromechanical characterization of PANI under high loading

PANI1 and PANI2 were doped with H_2SO_4 as described in Chapter 6 paragraph 6.2.2.

200 mg of each sample were pressed by the use of a hydraulic press at 11 ton in 13 mm diameter disks for 30 minutes, producing pellets of 1 mm thickness. The conductivity of each pellet was measured indirectly by the resistivity measurements using a multimeter during three cycles of loading and unloading under different force conditions (0-100 kN) carried out by the use of a MTS Alliance RT/100 testing machine. All the tests were carried out at room temperature.

Each pellet was sandwiched between two copper electrodes of area greater than the sample surface area for ensuring that field lines were parallel within the specimen, avoiding the field fringing which occurs at the electrode edges. The electrodes were connected to a multimeter, whereas a

cantilever allowed to measure the deformation of pellet. The experimental set-up is shown in Figure 10.1.

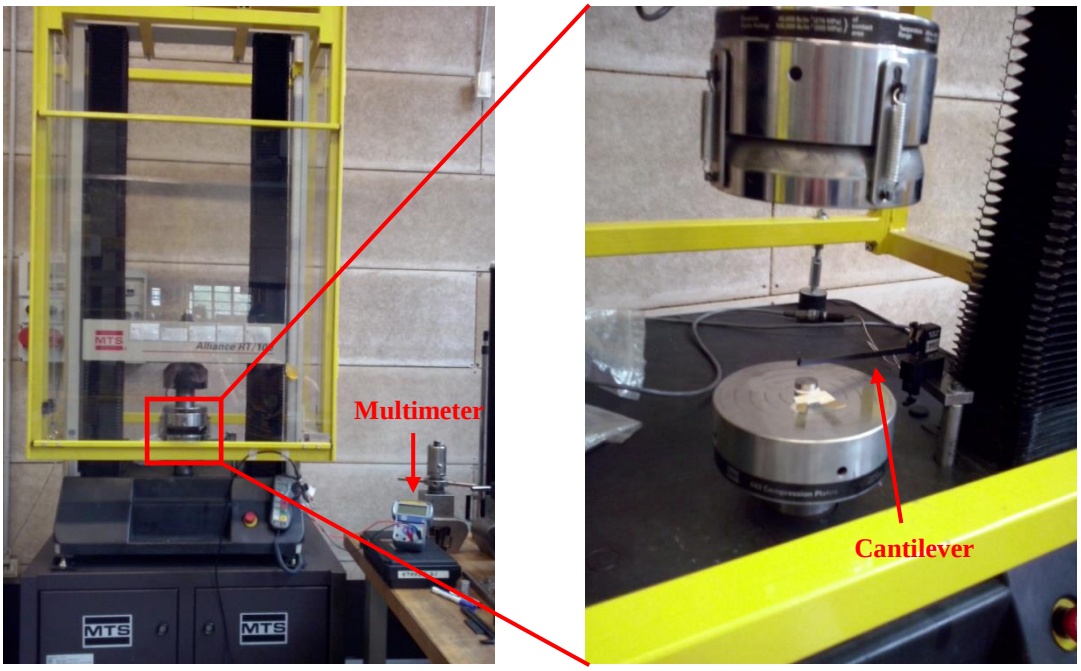

Figure 10.1.: Experimental set-up for the resistivity and strain measurements under loading/unloading cycles.

10.1.1. Electromechanical response

The mechanical hysteresis of PANI1 and PANI2 were characterized in stress–strain tests for three cycles (Figure 10.2.).

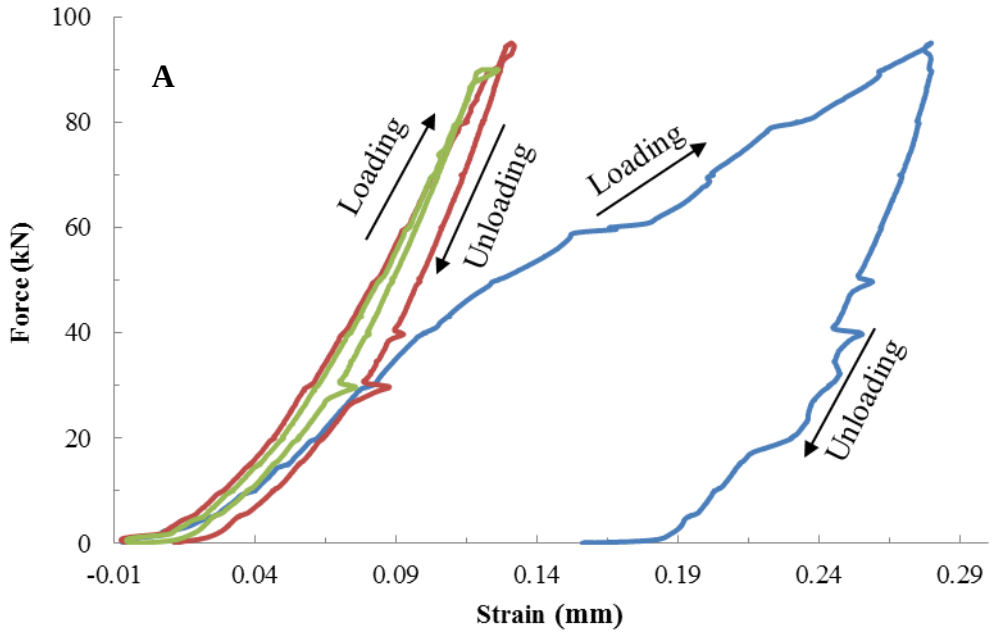

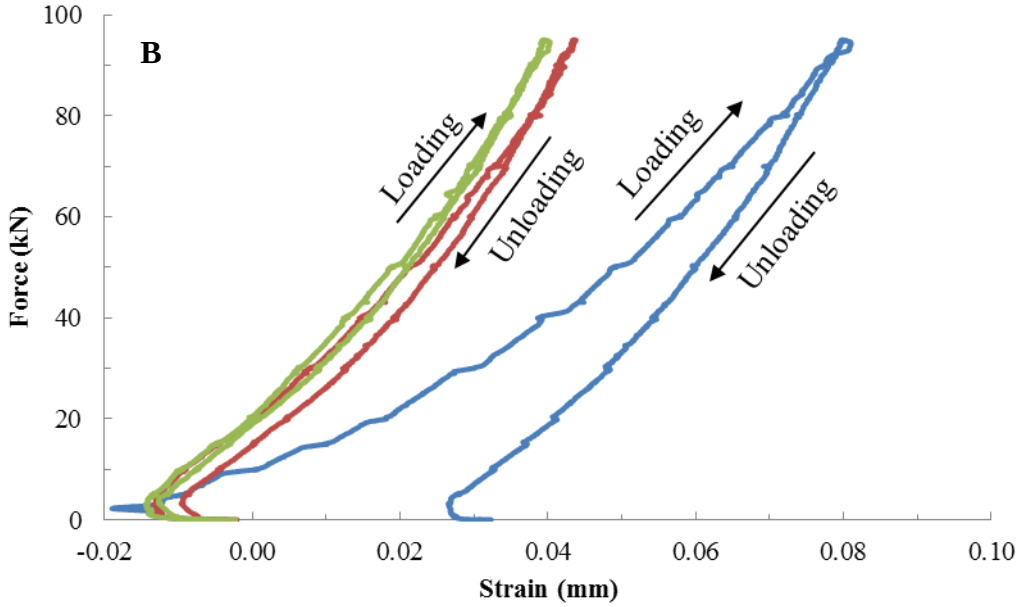

Figure 10.2.: Stress-strain curves under loading/unloading cycles for (A) PANI1/H_2SO_4 and (B) PANI2/H_2SO_4. Blue line= cycle no. 1, red line= cycle no. 2 and green line= cycle no. 3.

Negative values of strain at low forces can be attributed to the deformation of the circular thin copper foils not present during the zero setting of the testing machine.

It is possible to observe that the loading/unloading curves didn't coincide during the successive cycles and mechanical hysteresis were evident for both materials. As shown in Figure 10.2., the mechanical hysteresis decreased with increasing the number of cycles, suggesting a mechanical stabilization.

During the first cycle both materials displayed an irreversible deformation and the hysteresis was much larger than the others in both cases. This behavior could be attributed to the high stiffness of these materials that does not allow the reversal and recovery of the initial microstructure.

It is to notice the overall small nonlinear behaviour of PANI1 for deformations up to ~0.04 mm and a linear behaviour for deformations larger than ~0.04 mm. These two regimes can be mainly attributed to low deformation, mainly morphological reconfigurations of the polymer pellet, followed by a true stretching and reorientation of the polymer chains for larger deformations. On the contrary PANI2 showed a linear and almost hysteresis-free behaviour for all the range of deformation investigated, suggesting a higher stability of the morphology and compactness of this polymer.

10.1.2. Diffractometric characterization

The different behaviour of PANI1 and PANI2 can be attributed to their different degree of crystallinity, as shown in Figure 10.3.

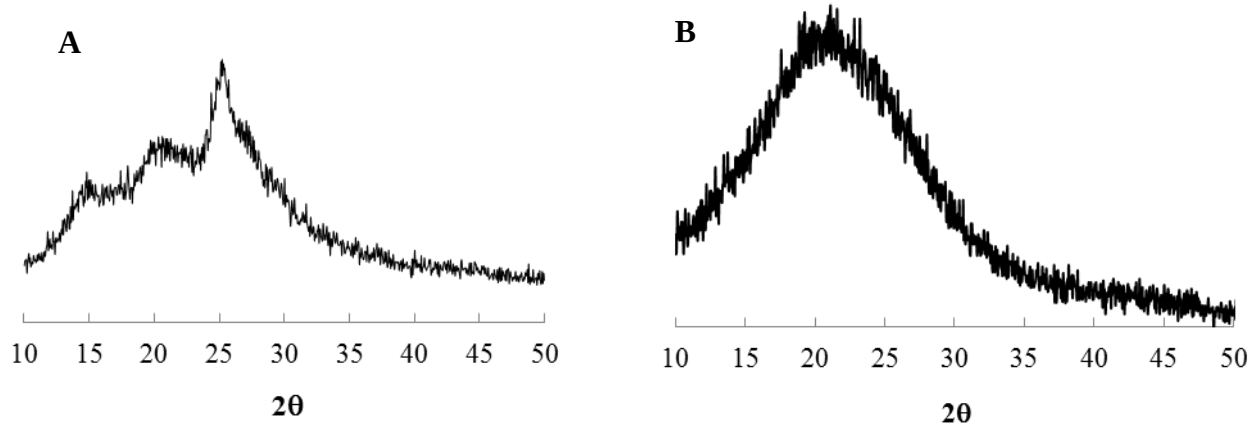

Figure 10.3.: XRPD patterns of (A) PANI1/H_2SO_4 and (B) PANI2/H_2SO_4.

The higher stiffness of PANI1 than PANI2 is confirmed by its higher degree of crystallinity that has a beneficial effect on its conductivity, as reported below (paragraph 10.1.3.).

10.1.3. Electrical conductivity

The resistance value of a resistor with length l and cross-sectional area A is given by the equation 10.1.:

$$R = \rho \frac{l}{A} \qquad \text{Eq. 10.1.}$$

where R is the electrical resistance (Ohm), ρ is the bulk resistivity (Ohm · cm), l is the length of the material (cm) and A is the cross-sectional area of the specimen (cm^2) that was maintained constant during the tests.

Consequently, there are two important ways by which the resistance value can change with applied strain: the dimensions, including the length and cross section, and resistivity. The change in dimensions is generally small, whereas for certain materials the change in resistivity may deeply change as a function of strain.

The maximum values of conductivity for PANI1 and PANI2, measured for all the loading/unloading cycles, are reported in Table 10.1.

Sample	σ_{cycle1}(S/cm)	σ_{cycle2}(S/cm)	σ_{cycle3}(S/cm)
PANI1	$1.01 \cdot 10^{-2}$	$1.27 \cdot 10^{-2}$	$1.29 \cdot 10^{-2}$
PANI2	$4.84 \cdot 10^{-5}$	$4.76 \cdot 10^{-5}$	$4.78 \cdot 10^{-5}$

Table 10.1.: Maximum value of conductivity for each cycle for PANI1 and PANI2.

As it is possible to observe, PANI2 showed maximum values of conductivity constant but much lower than those of PANI1. The difference in conductivity can be explained in terms of different degree of crystallinity (Figure 10.3) but also with a different molecular weight (not investigated in this thesis). As reported in Chapter 2 paragraph 2.4., the electrical properties of polyaniline are strongly influenced by the structure of chains. It has been observed that with the increase in crystallinity the conductivity increased, because the structure becomes more organized.[133] In this case the higher crystallinity of PANI1 guaranteed high values of conductivity (Table 10.1.) but at the same time lower mechanical characteristics, as shown by stress-strain curves (Figure 10.2. A). On the contrary, the low degree of crystallinity of PANI2 causes lower value of conductivity but higher mechanical properties.

10.1.4. Piezoresistive effect

By strict definition, piezoresistors refer to resistors whose resistivity changes with applied strain (more details are reported in §10.3.)

The fractional change in the electrical resistivity (DR/R0) plotted against the applied force and the change of deformation (Dl/l0) for both PANI1 and PANI2 is reported in Figure 10.4.

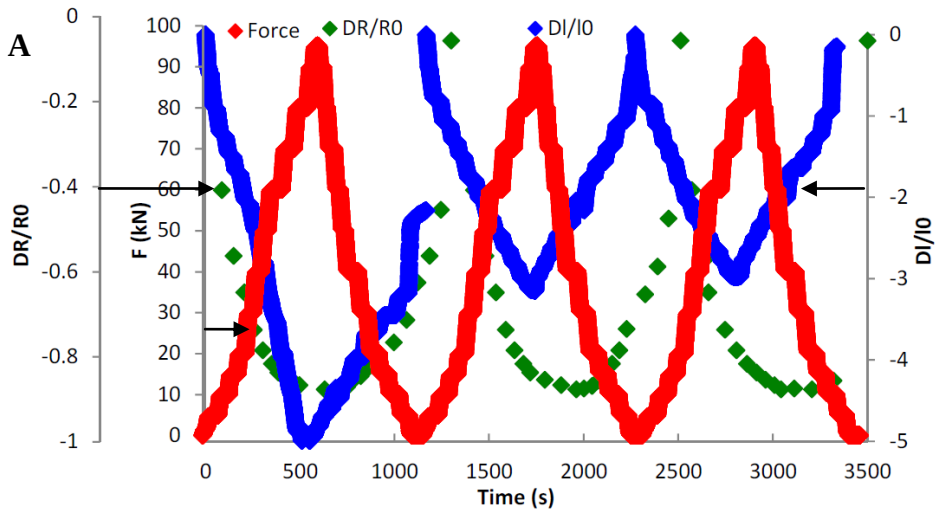

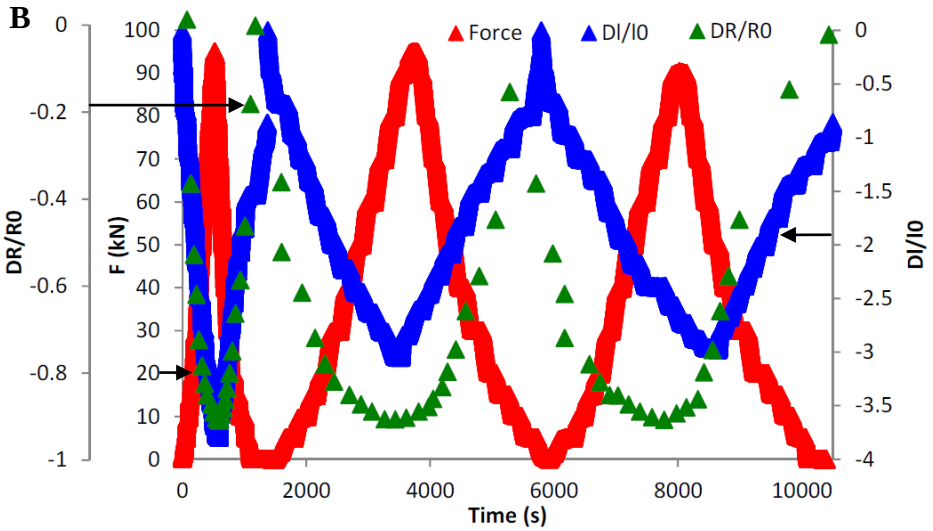

Figure 10. 4.: Change in resistance against applied force and change of deformation for PANI1 (A) and PANI2 (B). Blue (change of deformation), red (force), green (change of resistance)

As it is possible to observe from Figure 10.4., a fractional change in the electrical resistance for both PANI1 and PANI2 was observed under uniaxial compression. This change went up to 87% and 90% for PANI1 and PANI2 respectively when the compressive stress was in the range of 0-100 kN. The change in electrical resistance reversibly decreased upon loading and increased upon unloading in each cycle. Moreover, it is important to notice the complete reproducibility for the three loading and unloading processes for both materials, PANI1 and PANI2. The relationship between change in resistance and deformation was expressed in terms of gauge factor (Equation 10.2.):

$$GF = \frac{\Delta R/R0}{\Delta L/L} \qquad \text{Eq. 10.2.}$$

where R0 is the steady-state electrical resistance of the material without deformation (l0) and ΔR is the resistance change caused by the change in length (Δl).[607] It quantifies the magnitude of the piezoresistivity effect.

According to the linear regression, i.e., Y = kX, the relationship between the fractional change in electrical resistivity (DR/R0) and the deformation (Dl/l0) for both PANI1 and PANI2 is shown in Figure 10.5.

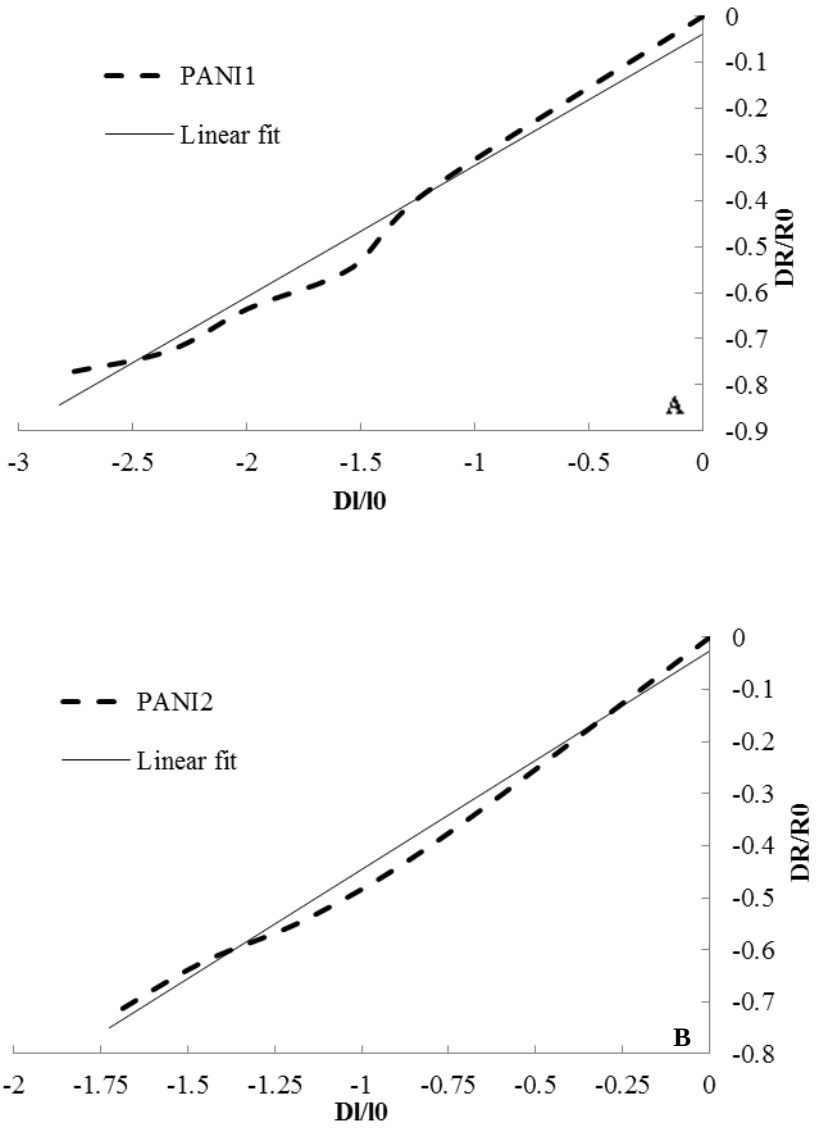

Figure 10.5.: Fractional change in electrical resistance as a function of the deformation for PANI1 (A) and PANI2 (B).

The slope of the linear fit, according to Eq. 10.2. (obtained with a R-square higher than 0.90), corresponds to the GF of the samples.

For PANI1 and PANI2 GF resulted to be 0.29 and 0.42 respectively. These values of GF are typical of commercial stress/strain sensors (GF of 0.1-2), that only show geometric effect.

However, it is known that the piezoresistive behaviour of polyaniline is strictly related to its mechanism of conduction, as described in Chapter 2, paragraph 2.4.

More in detail, the conductivity of PANI is the sum of two contributions: the ability of the charge carriers to move along the polymer backbone (*intra*-chain mechanism) and the ability of the charge carriers to hop between the polymer chains (*inter*-chain mechanism).[148] This second contribution becomes particularly important when the material is subjected to stress/strain processes.

During the compression (stress) processes the distance among polymeric chains is gradually reduced, promoting the movement of charge carriers among the polymeric chains. This phenomenon leads to a gradual decrease of resistance values and, therefore, to an increase of conductivity of the material.

On the contrary, if the material is subjected to strain processes the consequent increased *inter*-chains distance reduces the ability of charge carriers to hop among them, causing an increase of resistance values (low conductivity).

In this context, the low values of GF obtained for both PANI1 and PANI2 in this section was attributed to the use of the materials in form of pellet. For this reason PANI1 and PANI2 were produced in form of film using DBSA (dodecylbenzenesulfonic acid) or CSA (camphorsulfonic acid) as the dopant and their piezoresistive behaviour was carried out by 4-point bending tests (Paragraph 10.3). However, similar behaviour of both PANI1 and PANI2 under these conditions encourage a more detailed investigation of PANI2 for its application in the field of stress/strain sensors. In fact, the higher solubility of PANI2 in common organic solvents and its lower conductivity make it ideal for application as piezoresistor in form of thin film.

10.2. Electromechanical characterization of PANI under low loading

In the last years the application of polyaniline as new material for polymeric resistors has been investigated only at high values of force. In this regarding, starting from the previous results obtained under these conditions, the variation of resistivity of pellets of PANI1/ H_2SO_4 and PANI2/ H_2SO_4 was investigated also at low value of applied force (0-20 N).

It was sandwiched between two copper electrodes of area greater than the sample surface area for ensuring that field lines were parallel within the specimen, avoiding the field fringing which occurs at the electrode edges. The electrodes were connected to the multimeter and placed on digital balance. Each material was tested at room temperature. The values of force were gradually increased and decreased by the use of a screw, as shown in Figure 10.6.

Figure 10.6.: Experimental set-up for the measurements of the resistivity variation during loading/unloading cycles (0-20 N).

The conductivity of each pellet was measured indirectly by the resistivity measurements using a multimeter during the four cycles of loading and unloading under different force conditions (0-20 N).

Figure 10.7. shows that also at low value of force PANI1 and PANI2 doped with H_2SO_4 exhibited a linear relationship between the resistance and the applied force during the loading and unloading processes. However, in this case the experimental set-up used didn't allow to measure the change of deformation.

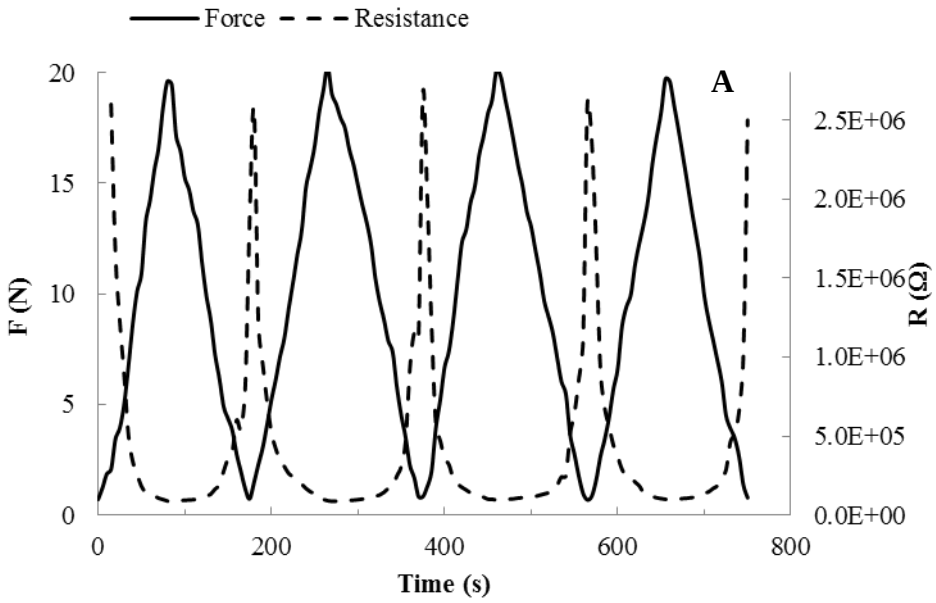

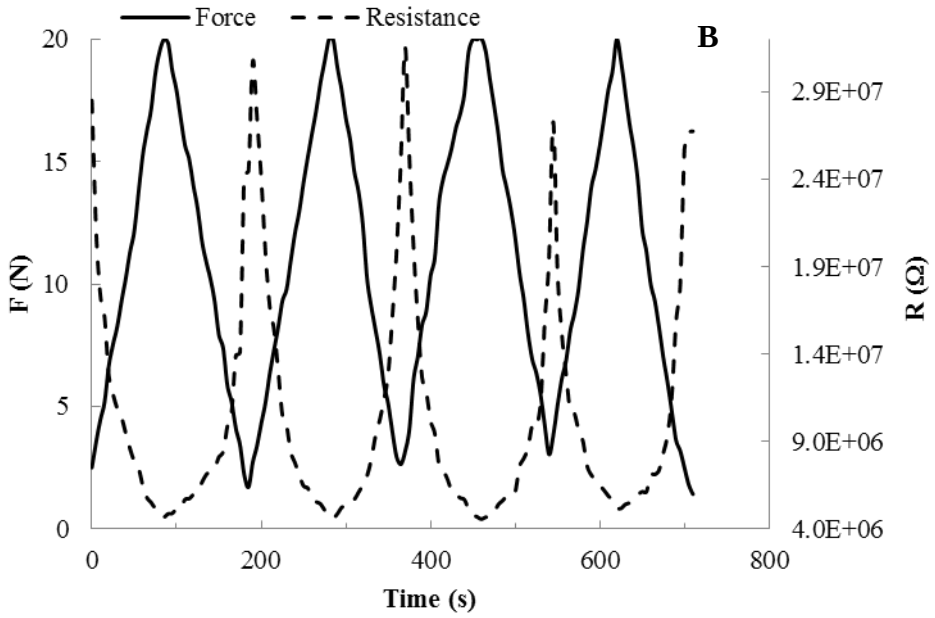

Figure 10.7.: Resistance against applied force for PANI1 (A) and PANI2 (B).

Also at low values of applied force both PANI and PANI2 show similar behaviour, exhibiting a good linear relationship between resistance and force. However, because of the high values of resistance of PANI2, this material becomes conductive at higher values of force (about 2.5 N).

The maximum values of conductivity for both PANI1 and PANI2 during different cycles are reported in Table 10.2.

Sample	σ_{cycle1}(S/cm)	σ_{cycle2}(S/cm)	σ_{cycle3}(S/cm)	σ_{cycle4}(S/cm)
PANI1	$9.83 \cdot 10^{-7}$	$9.66 \cdot 10^{-7}$	$8.80 \cdot 10^{-7}$	$8.66 \cdot 10^{-7}$
PANI2	$1.77 \cdot 10^{-8}$	$1.79 \cdot 10^{-8}$	$1.81 \cdot 10^{-8}$	$1.60 \cdot 10^{-8}$

Table 10.2.: Maximum value of conductivity for each cycle for PANI1 and PANI2.

The values of conductivity of PANI1 are higher than those of PANI2. However, in this case the difference is not as evident as in the measurements at high applied force (Table 10.1.).

This suggests that working at low values of force the differences in crystallinity of both materials become less important, not compromising their values of conductivity that in this case resulted to be more similar. Unfortunately, the impossibility to measure the deformation of pellets during loading/unloading cycles didn't allow to calculate the values of GF under these conditions.

10.3. Piezoresistive effect in polyaniline. The effect of different raw materials and doping agents

Electrical strain gauges are based on the measurement of an inherent electrical property (most often resistance) as function of an induced strain.

Piezoresistivity describes change in the electrical resistivity as function of a mechanical strain.

Piezoresistive films are used to produce macroscopic strain gauges or small devices useful as force transducers, such as accelerometers, pressure and/or deformation sensors.

The magnitude of the piezoresistivity effect is often quantified by the gauge factor (GF) (Eq. 10.3.).

Many commercially available thin film piezoresistive strain gauges are metal foils deposited on flexible polymer substrates. Generally, they are used to measure deformation in bridges, buildings, machine parts, etc. However, their performances are not good for other applications, such as measuring strain in biological tissues and large movements in robotic devices, among others, due to their limited flexibility.[617]

An additional problem with metal film strain gauges is their delamination and the low inherent resistivity and resistivity variation with strain.

Many approaches have been developed to obtain strain gauge resistance which is large enough to be distinguished from lead wire resistance.

For example, metal films can be designed to have a large length/width ratio (about 500) to increase the resistance. The metal pattern is folded back upon itself so as to take up as little space as possible, but the size of the overall strain gauge is dictated by the required length/width ratio. Commercial metal film strain gauges have a typical resistance of 50-100 Ohms. In this case, the contribution of lead wire resistance to the total strain gauge resistance cannot be ignored and introduces errors of several percent.[618]

To eliminate the effect of lead wire resistance, a multiple-terminal resistance measurement can be employed. However, more than two leads must be connected to the device and this makes this method more complicated for practical applications.

Another important material useful for micromachined sensors is silicon.[619, 620] However, the use of silicon limits the choice of substrate. Moreover, owing to its low flexibility it cannot be used for large-scale applications.

More recently polymer-based strain gauges have been suggested as a more useful flexible substitute.[620]

In general, these materials are insulating polymers whose conductivity is increased by the incorporation of conductive materials, generally metallic particles or carbon nanotubes. At high enough loading the contact among conducting grains guarantees current flow.

The piezoresistitive effect results from the change of grains distances during compression or expansion.[465, 618]

Some problems are associated to the use of those materials, too. For example, the particulate nature of the films prevents small geometry patterning. Another drawback is the delamination of the polymer from the particle surface. This phenomenon is ascribed to poor wetting and poor adhesion of the filler to the polymer matrix. Moreover, it is difficult to obtain a uniform dispersion of polymer and metal particles.[618]

The discovery of homogeneously flexible conductive polymers that exhibit piezoresistive properties without embedding carbon or metal conductive fillers opened the way to a new era of strain gauges.

Strain gauges formed from piezoresistive, homogeneous conductive polymer films show several advantages. They maintain the same advantage of the polymer composites with respect to processing and eliminate the necessity to apply multiple-terminal resistance measurements, essential in the case of metal strain gauges, having high resistance.

Moreover, thanks to their homogeneity, they can be produced in highly uniform films.

Intrinsically conductive polymers, such as PANI, can be used for this scope. Concerning polyaniline, there are not enough data and investigations on its piezoresistive properties. Moreover, these results are conflicting. Lillemose *et al*.[621] reported a negative GF of ~ 5 in 4-point-bending experiments, that means an increase in conductivity for large deformations owing to the alignment of the polymeric chains.[622] However, the 4-point-bending experiment does not provide the large deformation needed for the alignment of polymeric chains. More recently, Pereira *et al*.[623] describe the piezoresistive effect of a commercial polyaniline, prepared in form of thin film, and report GF values from 10 to 22 for different samples.

In this work PANI1 and PANI2 were doped with organic acid, dodecylbenzenesulfonic acid (DBSA) and camphorsulfonic acid (CSA), (see Chapter 6 section 6.2.3.) in order to be solubilized in chloroform. Films of PANI1 and PANI2 doped with DBSA and CSA were produced by drop-casting process using a plate of PET (polyethylene terephthalate) as support. In all the samples a pair of gold rectangular electrodes with 6×2 mm and 1 mm apart were deposited by sputtering. On the top of each electrode, a copper wire with 0.125 mm diameter was glued with silver ink, as shown in Figure 10.8, and their piezoresistive effect was investigated.

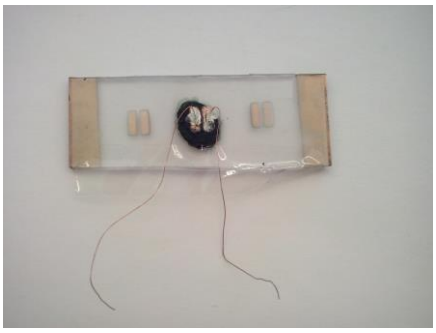

Figure 10.8.: Sample of PANI for measurement of piezoresistivity.

The relationship between electrical response and mechanical solicitations was evaluated and the values of the gauge factor were calculated.

In order to quantify the piezoresistive effect, 4-point bending tests were performed. In these tests, the electrical resistance changes with strain were measured. Figure 10.9. shows a diagram of the 4-point bending jig.

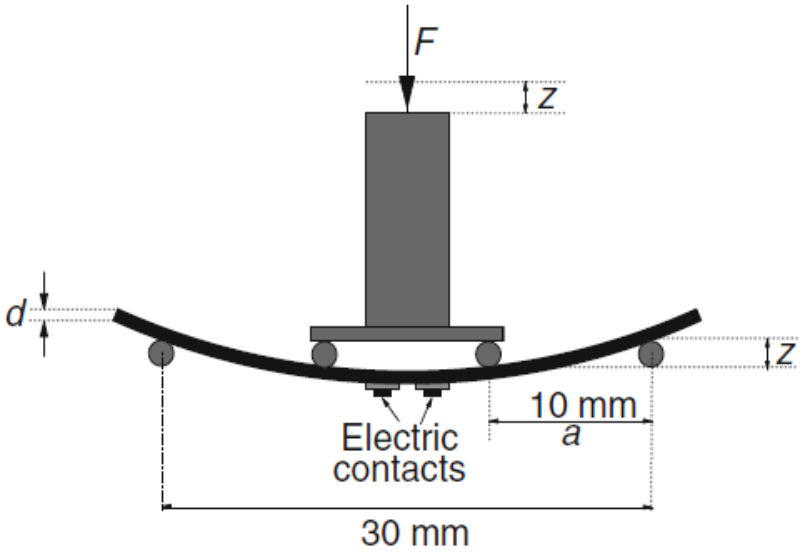

Figure 10.9.: Diagram of the 4-point bending jig used in the present study.

In 4-point-bending experiments, the strain along the longitudinal direction (εl), calculated from the theory of pure bending of a plate, to form a cylindrical surface between the inner loading points, is given by Equation 10.3., according with ref. 65:

$$\varepsilon l = \frac{3dz}{5a^2} \qquad \text{Eq. 10.3.}$$

where d is the distance from the neutral plane to the plane of the sample, which in this case is approximately equal to the thickness of the substrate (1 mm), z is the vertical displacement of the and a is the distance between the first and the second points of the 4-point bending load cell (10 mm).

The 4-point-bending tests were performed in a Shimadzu-AG-IS 500 N testing instrument at speeds from 0.1 to 10 mm/min and a maximum vertical (z axis) displacement from 0.1 to 2.5 mm (Figure 10.10.)

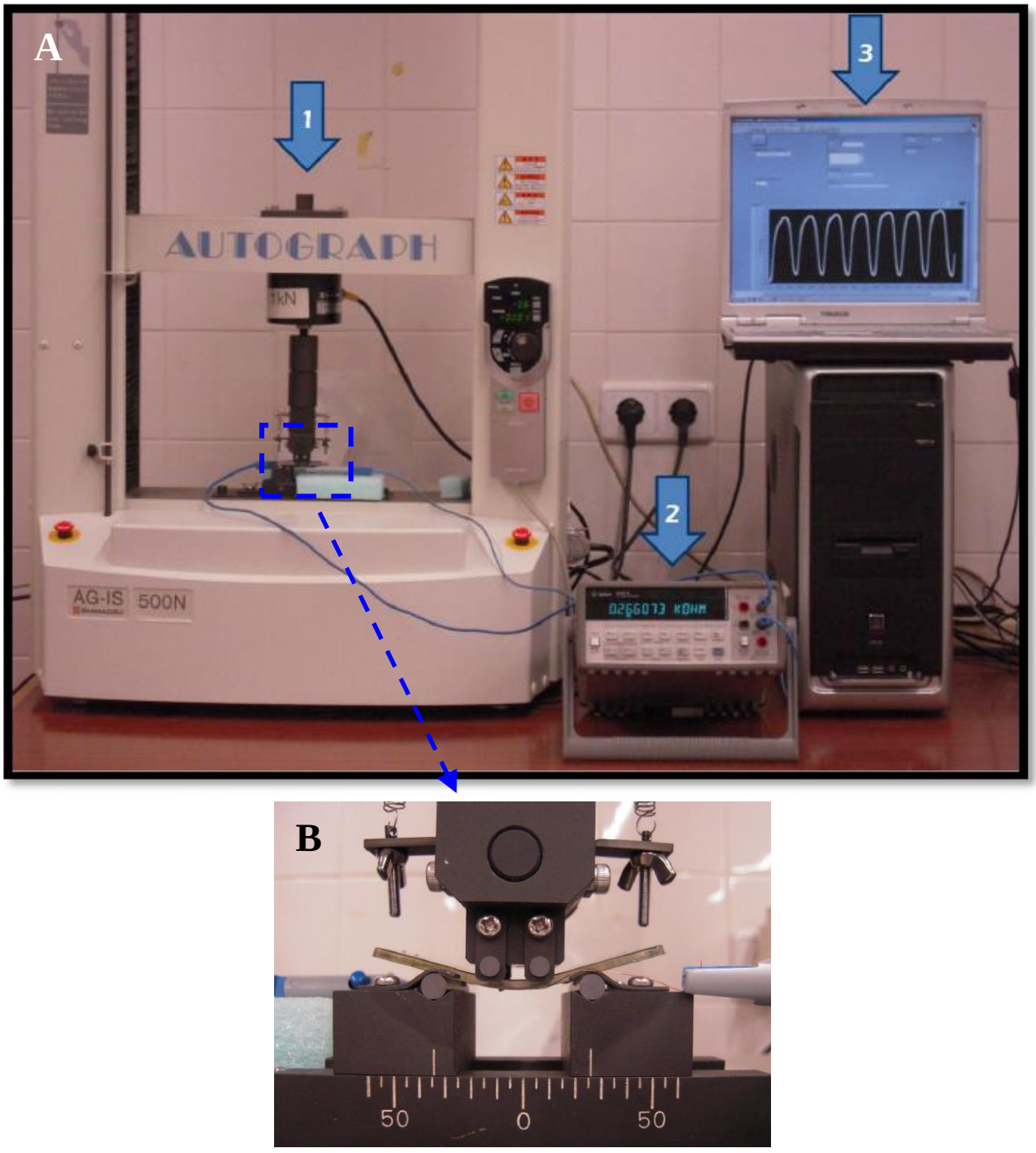

Figure 10.10.: A) 1: Universal *Shimadzu - AG-IS 500 N* testing machine, 2: digital multimeter, 3: computer; B) Photograph of a sample in a test deformation during 4-point-bending.

Each test was composed by four cycles of deformation. Stability tests were also performed in selected samples up to 40 cycles.

10.3.1. Electrical conductivity

The d.c. electrical conductivity of the materials was calculated from the slope of I–V curves measured with an automated Keithley 487 picoammeter/voltage source and the resistivity of the samples (ρ) was calculated by the equation 10.1.The corresponding values of electrical conductivity are summarized in Table 10.3. Figure 10.11. shows the I–V plots for PANI1 and PANI2 doped with DBSA and CSA. Samples doped with DBSA were also subjected to a thermal treatment (1 hour at 70°C) in order to remove any trace of solvent ($CHCl_3$) among the polymeric chains and remove residual stresses in order to guarantee the mechanical stabilization.

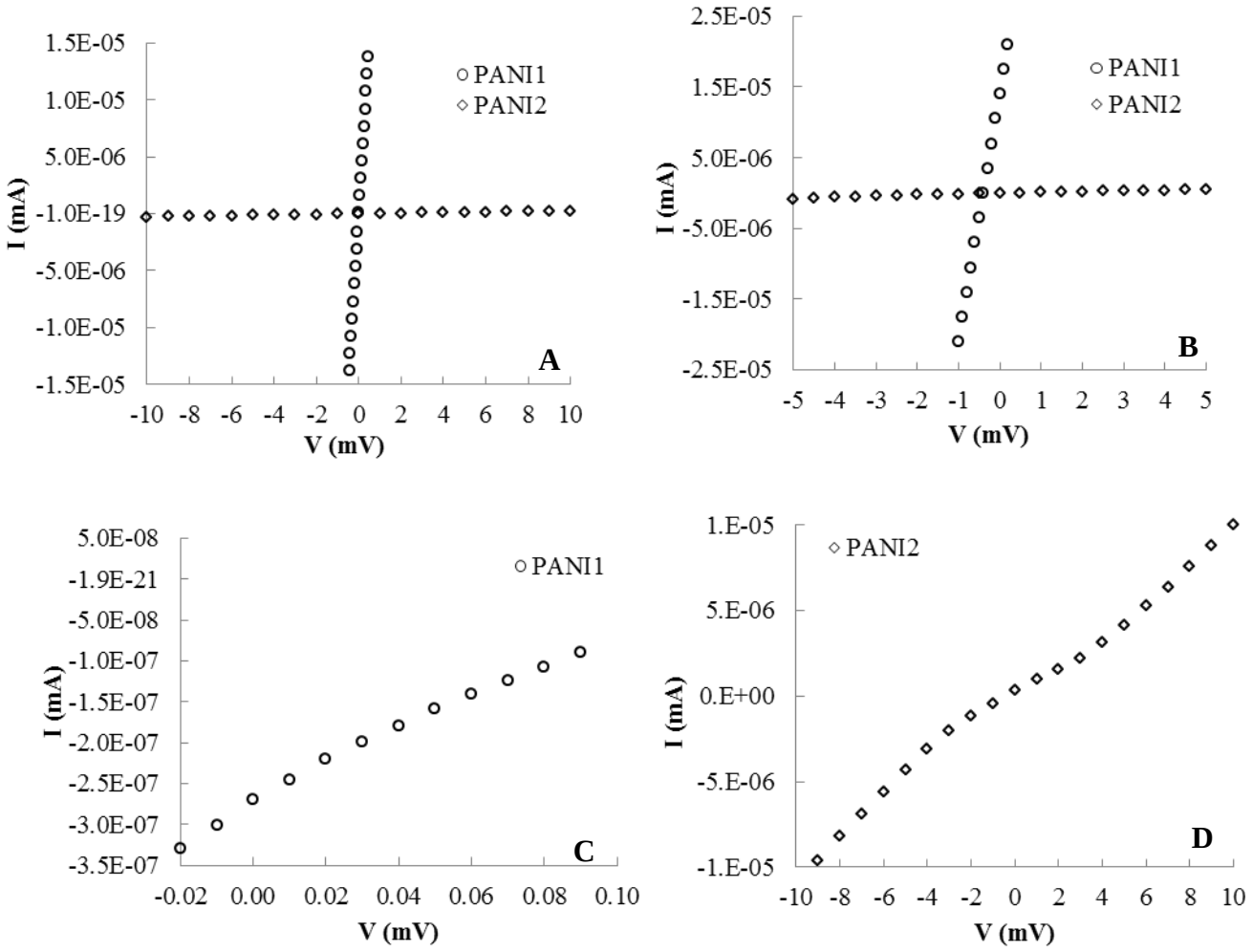

Figure 10.11.: I–V plots for PANI1/DBSA and PANI2/DBSA at room temperature (A). PANI1/DBSA and PANI2/DBSA after thermal treatment (1 h at 70°C) (B), PANI1/CSA (C) and PANI2/CSA (D) at room temperature.

Sample	σ (S/cm)*	σ (S/cm)**
PANI1/DBSA	$5.12 \cdot 10^{-6}$	$5.82 \cdot 10^{-6}$
PANI2/DBSA	$4.17 \cdot 10^{-9}$	$1.80 \cdot 10^{-8}$
PANI1/CSA	$2.19 \cdot 10^{-7}$	-
PANI2/CSA	$1.67 \cdot 10^{-7}$	-

Table 10.3.: Values of conductivity of samples at room temperature (*) and after thermal treatment (1 h at 70°C) (**).

When DBSA is used as the doping agent, PANI1 exhibits higher values of electrical conductivity than PANI2, probably due to the longer polymeric chains and higher molecular weight. Moreover, the electrical conductivity of PANI1/DBSA does not change after thermal treatment, whereas for PANI2/DBSA it increases 10 times, suggesting a better packing of polymeric chains.

On the contrary, concerning CSA, PANI1 and PANI2 show similar values of conductivity.

The differences observed when DBSA and CSA are employed as dopants can be attributed to the different characteristics of these organic acids. In fact, due to its smaller counterion size CSA guarantees stronger *inter*-chain interactions, that implies higher values of electrical conductivity, more evident in PANI2 than in PANI1.

10.3.2. Morphological characterization

The morphological characterization of all the samples was carried out by SEM microscopy and the results are shown in Figure 10.12.

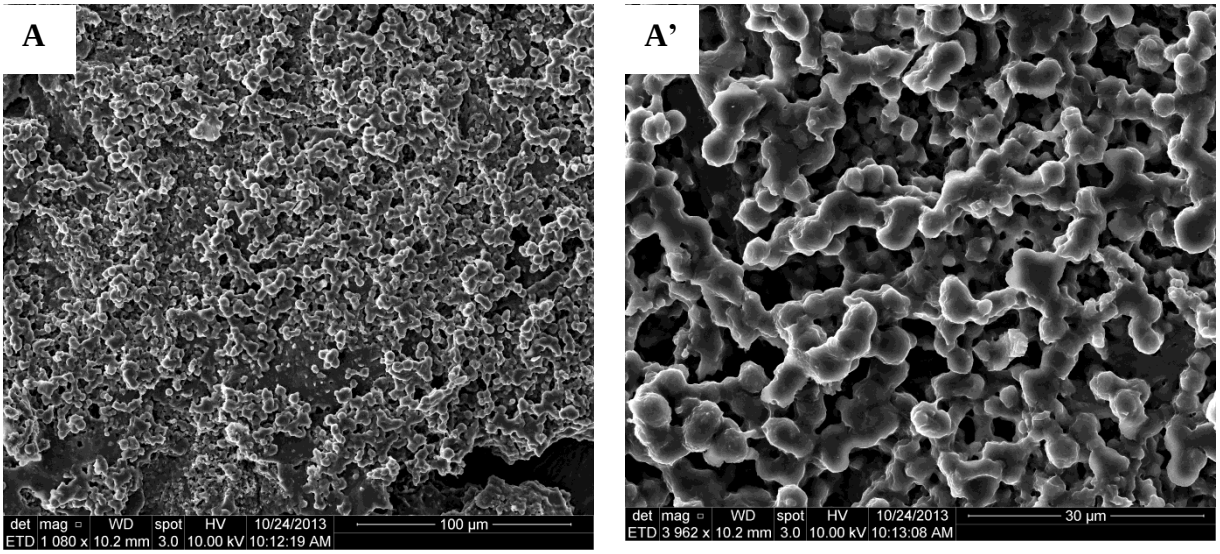

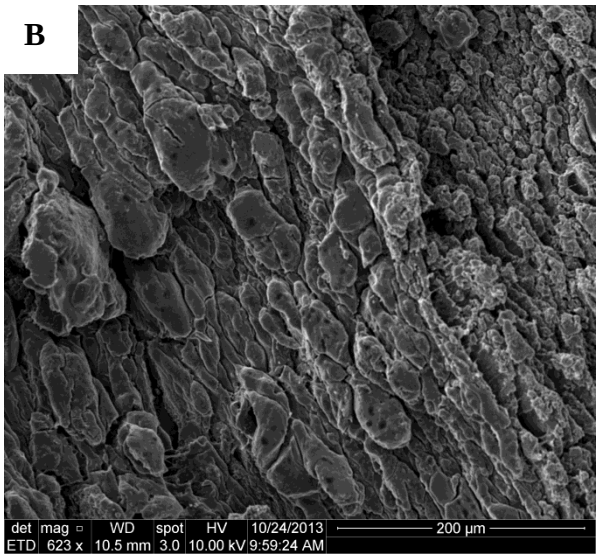
B
det mag WD spot HV 10/24/2013
ETD 623 x 10.5 mm 3.0 10.00 kV 9:59:24 AM
200 µm

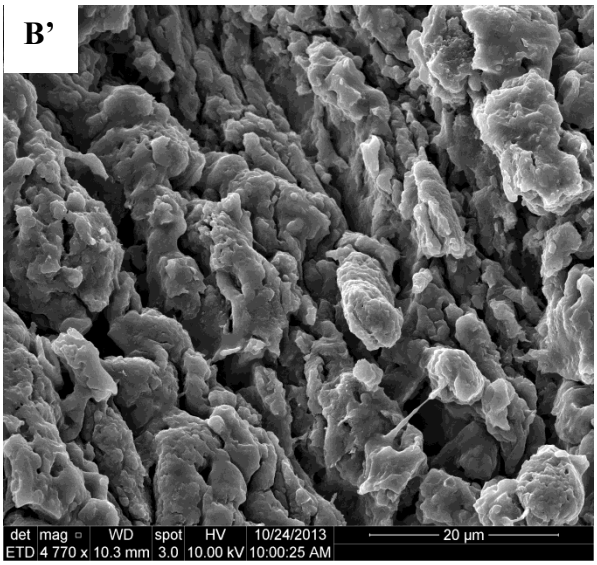
B'
det mag WD spot HV 10/24/2013
ETD 4 770 x 10.3 mm 3.0 10.00 kV 10:00:25 AM
20 µm

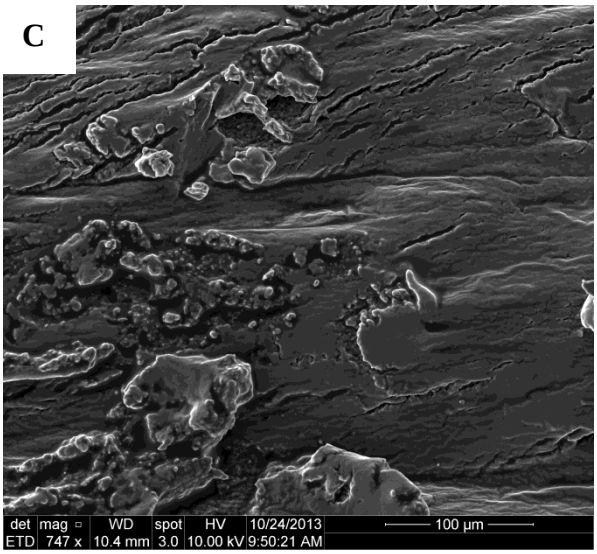
C
det mag WD spot HV 10/24/2013
ETD 747 x 10.4 mm 3.0 10.00 kV 9:50:21 AM
100 µm

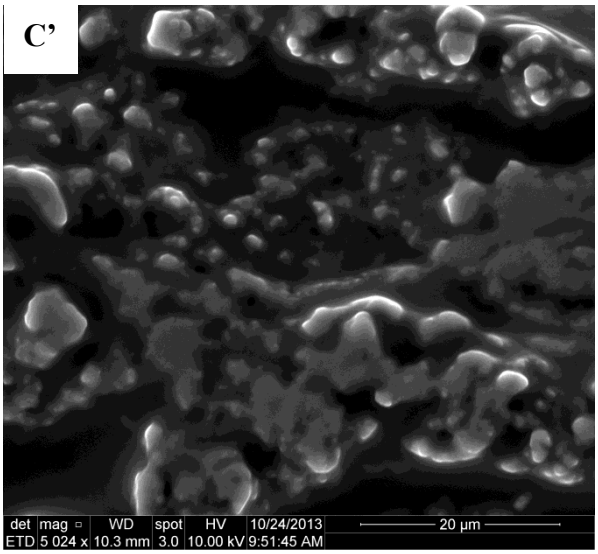
C'
det mag WD spot HV 10/24/2013
ETD 5 024 x 10.3 mm 3.0 10.00 kV 9:51:45 AM
20 µm

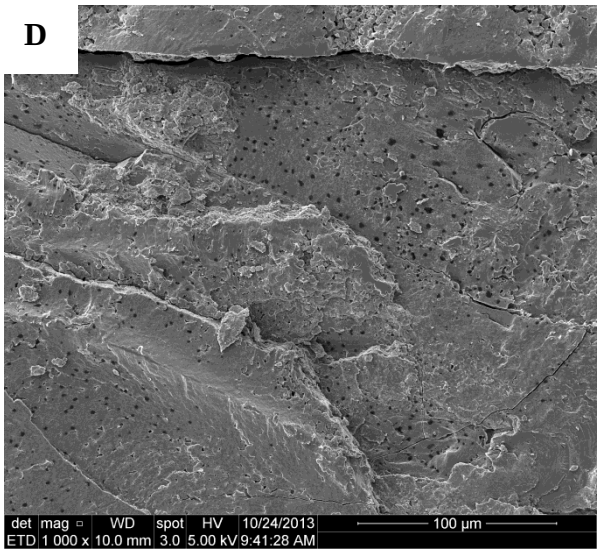
D
det mag WD spot HV 10/24/2013
ETD 1 000 x 10.0 mm 3.0 5.00 kV 9:41:28 AM
100 µm

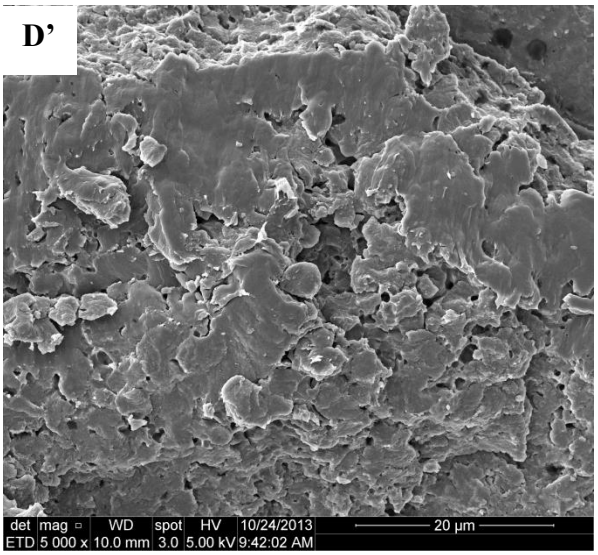
D'
det mag WD spot HV 10/24/2013
ETD 5 000 x 10.0 mm 3.0 5.00 kV 9:42:02 AM
20 µm

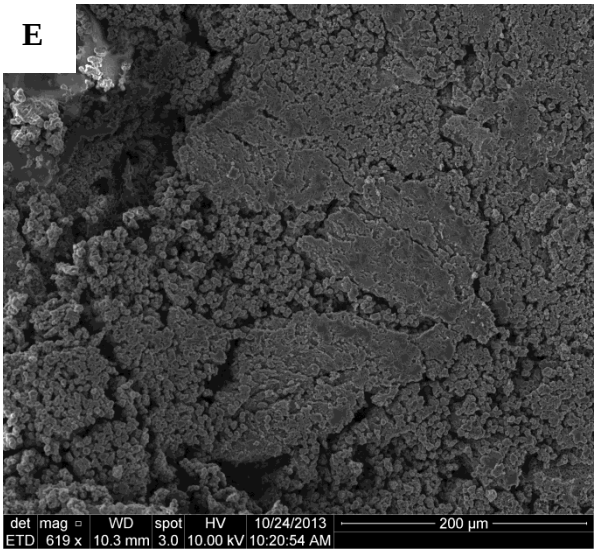
E
det mag WD spot HV 10/24/2013
ETD 619 x 10.3 mm 3.0 10.00 kV 10:20:54 AM
200 µm

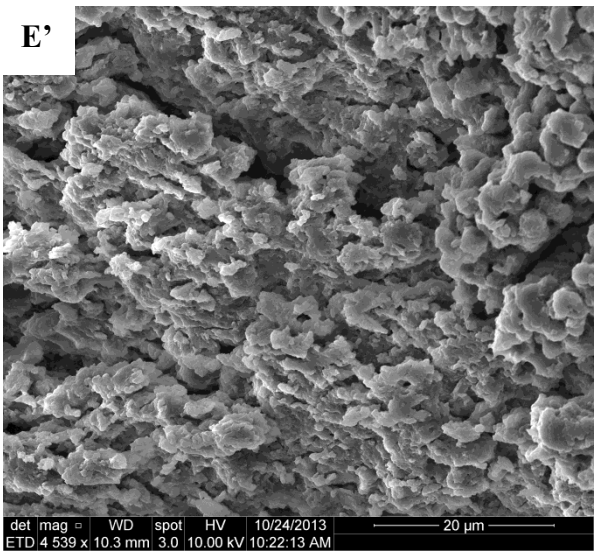
E'
det mag WD spot HV 10/24/2013
ETD 4 539 x 10.3 mm 3.0 10.00 kV 10:22:13 AM
20 µm

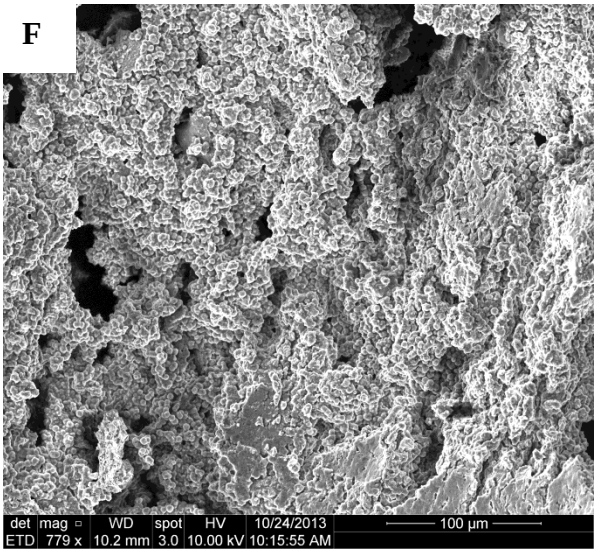
F
det mag WD spot HV 10/24/2013
ETD 779 x 10.2 mm 3.0 10.00 kV 10:15:55 AM
100 µm

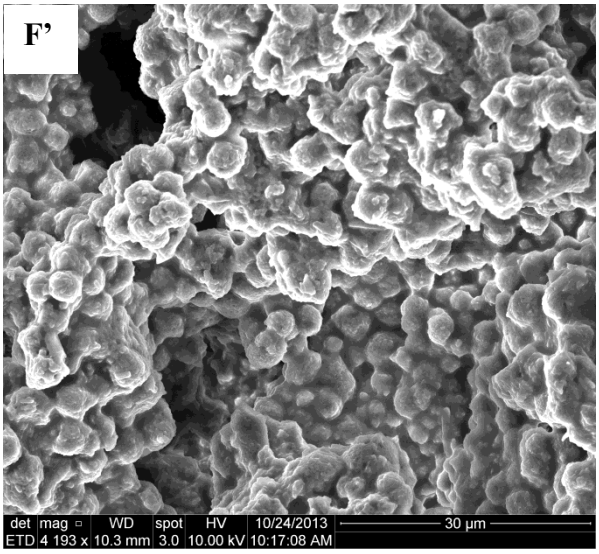
F'
det mag WD spot HV 10/24/2013
ETD 4 193 x 10.3 mm 3.0 10.00 kV 10:17:08 AM
30 µm

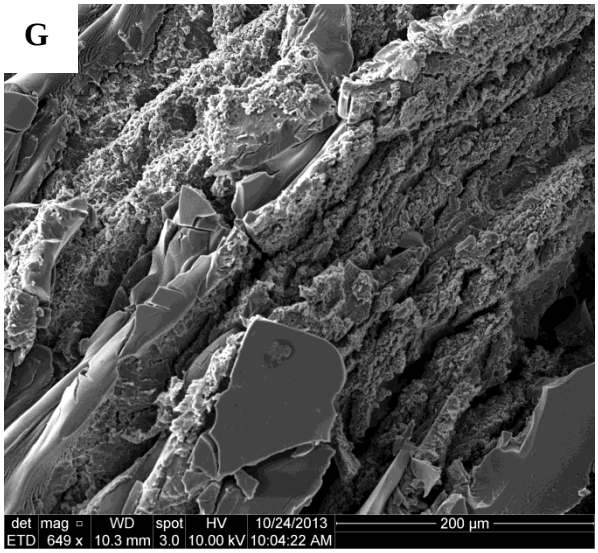
G
det mag WD spot HV 10/24/2013
ETD 649 x 10.3 mm 3.0 10.00 kV 10:04:22 AM
200 µm

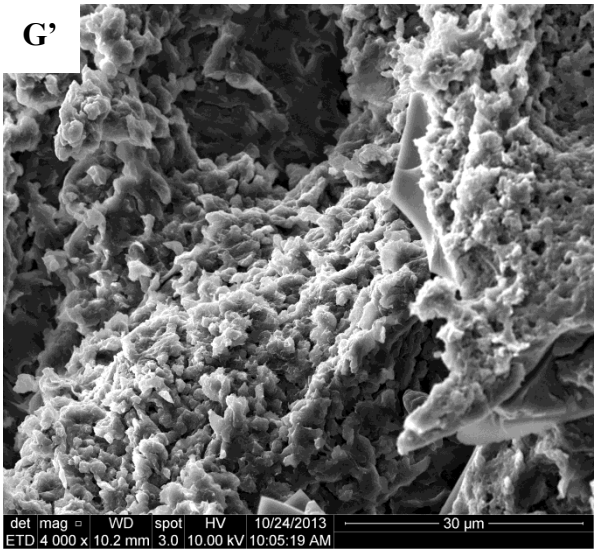
G'
det mag WD spot HV 10/24/2013
ETD 4 000 x 10.2 mm 3.0 10.00 kV 10:05:19 AM
30 µm

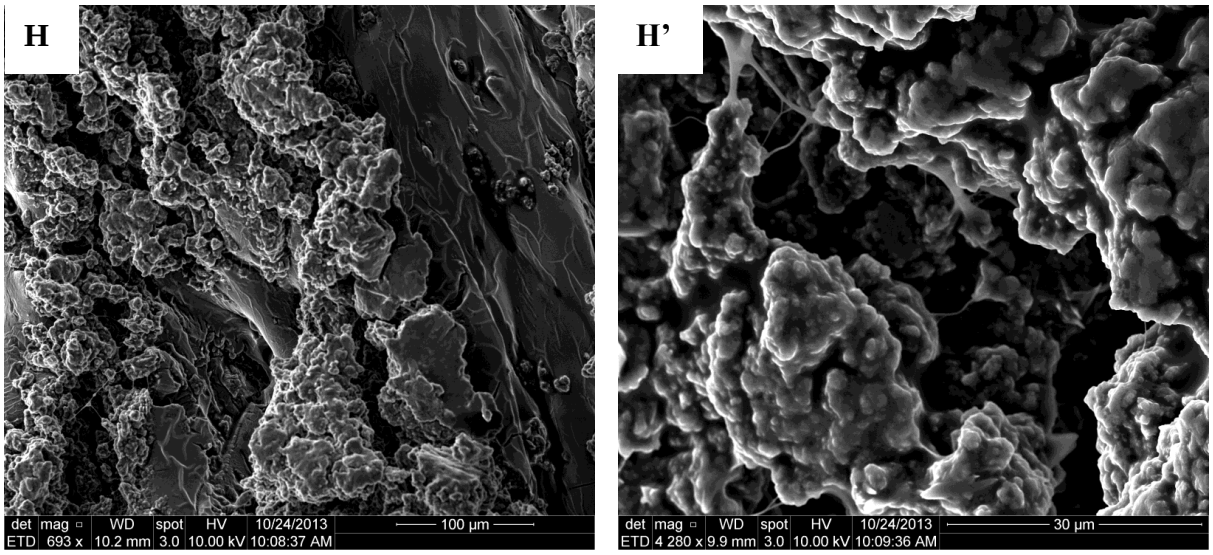

Figure 10.12.: SEM images at low and high magnification for PANI1/DBSA at room temperature (A and A'), PANI1/DBSA after thermal treatment (B and B'), PANI2/DBSA at room temperature (C and C'), PANI2/DBSA after thermal treatment (D and D'), PANI1/CSA at room temperature (E and E'), PANI1/CSA after thermal treatment (F and F'), PANI2/CSA at room temperature (G and G'), PANI2/CSA after thermal treatment (H and H').

As shown in Figure 10.12. and confirmed by the piezoresistive response (see § 10.3.4.), at room temperature the materials prepared by PANI1 show more regular globular-like structures than PANI2 and after a thermal treatment, when any trace of solvent and residual stresses are removed, their morphology becomes more compact. Concerning PANI2, at room temperature the morphology of the polymer deeply changes with the dopant used. In fact, PANI2/DBSA shows higher uniformity than PANI2/CSA, even though lower than PANI1. Moreover, after thermal treatment the removal of solvent leads to a porous and more compact morphology (Figure 10.12.D) that positively affects the piezoresistive behaviour of the material (see later).

Finally, the very high irregular morphology of PANI2/CSA before and after the thermal treatment justifies the poor piezorestive response of this material in all the conditions.

10.3.3. Electromechanical response

The mechanical properties of polyaniline (initial modulus, maximum strain and hysteresis) are key issues for its application as piezoresistive sensors, since the mechanical properties play a critical role in sensor response and reliability. The mechanical hysteresis is important to analyse reproducibility of stress–strain tests in sensor applications. Good linearity of electrical resistance depends on the mechanical properties of the material.

Figure 10.13. shows stress-strain curves for PANI1 and PANI2 doped with DBSA and CSA.

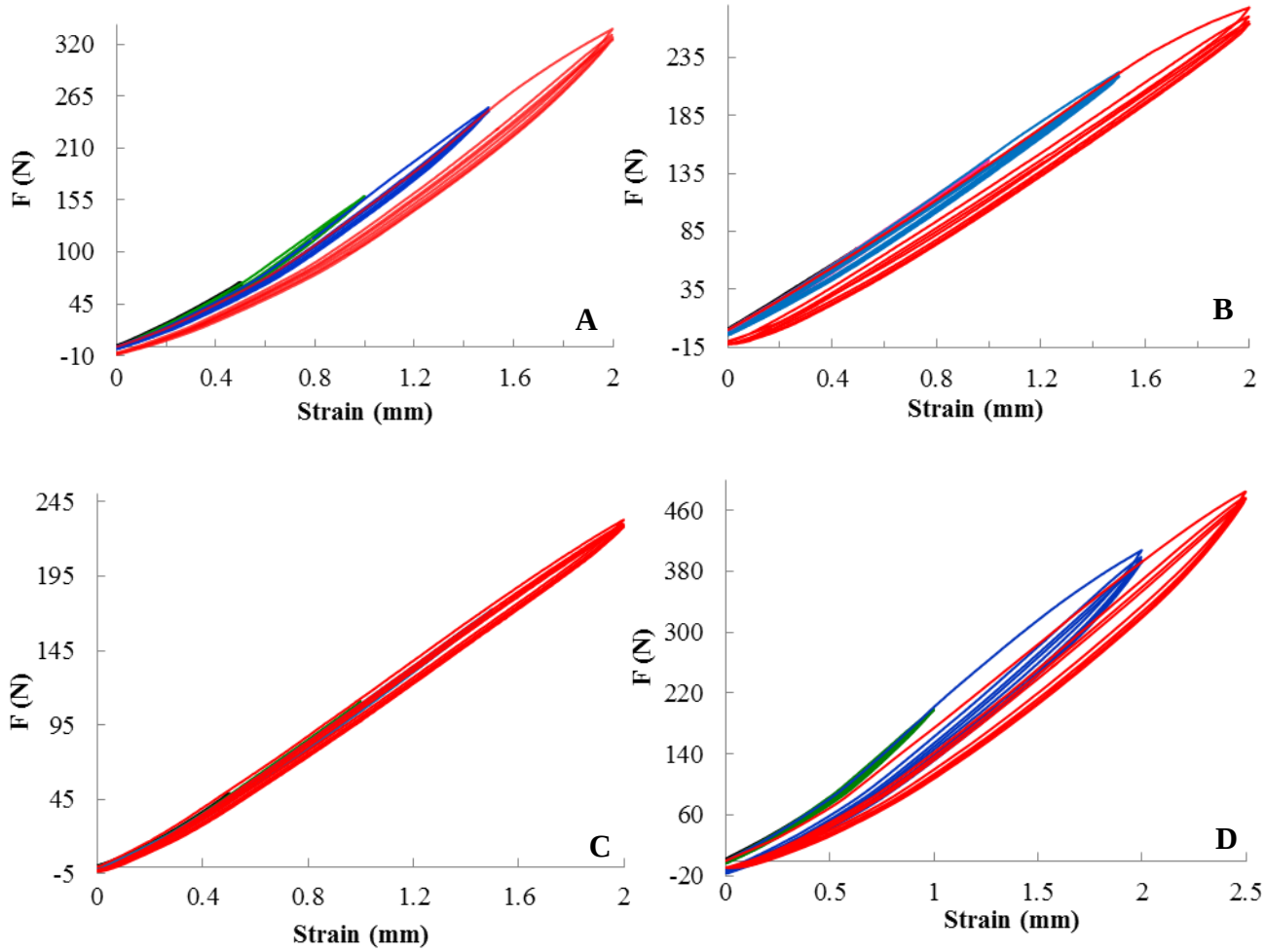

Figure 10.13.: Stress-strain curves of PANI1/DBSA (A),PANI2/DBSA (B), PANI1/CSA (C) and PANI2/CSA (D).

As it is possible to observe, loading and unloading curves do not coincide during successive cycles, given evidence of a mechanical hysteresis in the material. In all cases, the mechanical hysteresis decreases with increasing number of cycles, in particular for the first cycle, and increases for increasing strain. Among all the samples investigated, only PANI1/CSA shows lower hysteresis, explained with a more compact and flexible structure (Figures 10.12. E and E'), whereas PANI2 always exhibits higher hysteresis than PANI1, according with a more irregular structure (Figure 10.12. C and C', H and H').

It is to notice the overall small nonlinear behaviour of the samples with a linear and almost hysteresis free behaviour for deformations up to ~0.4 mm and another linear behaviour for deformations larger than ~0.6 mm. These two regimes can be mainly attributed to low deformation, mainly morphological reconfigurations of the porous polymer film, followed by a true stretching and reorientation of the polymer chains for larger deformations. The stress-strain curves of the samples after thermal treatment do not show any modifications

10.3.4. Piezoresistive effect

Figure 10.14. shows typical examples of the electromechanical experiments performed with the different samples, where it can be observed the electrical resistance variation to repeated loading–unloading cycles following the procedure described in Figure 10.9.

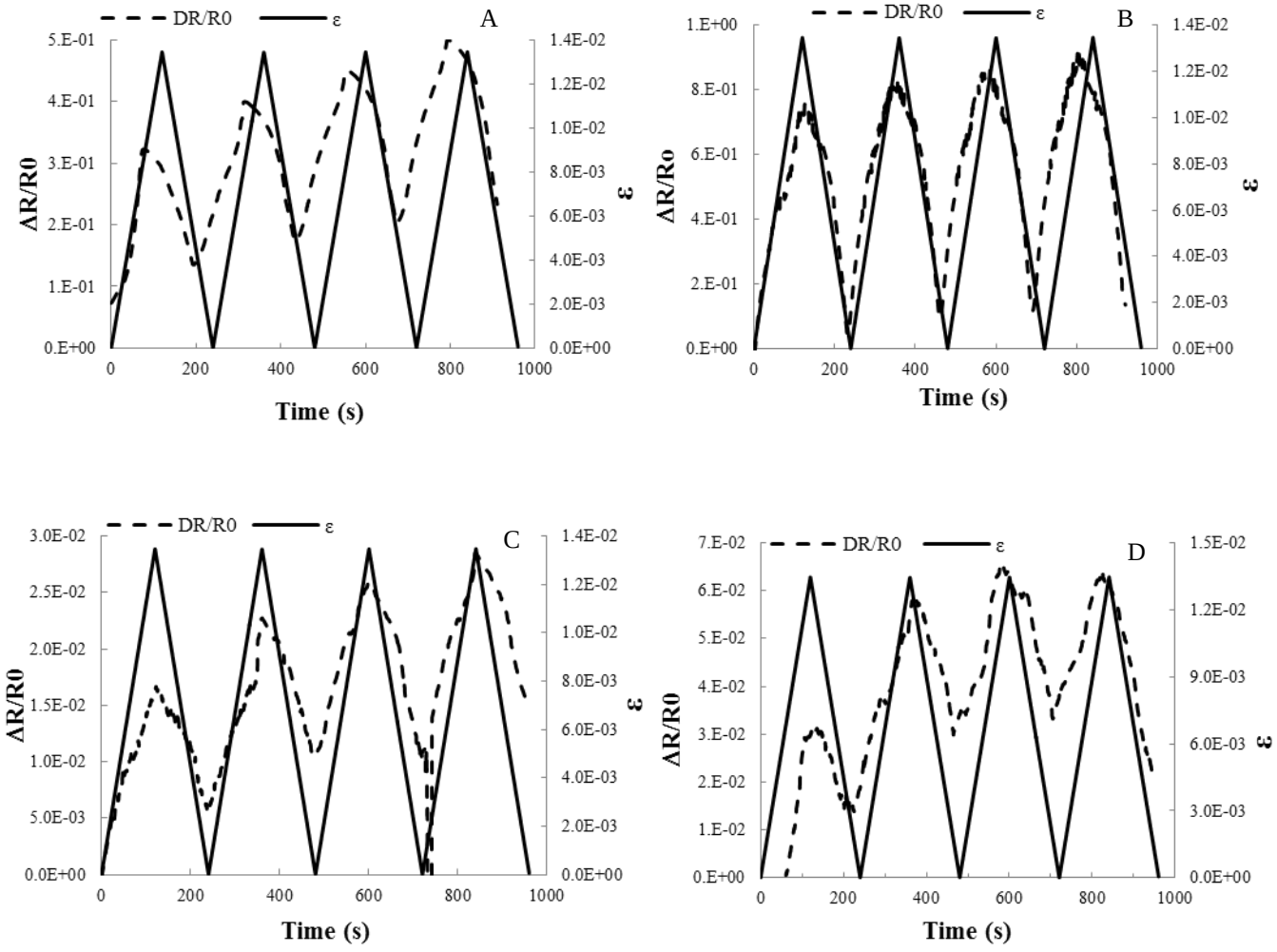

Figure 10.14.: Cyclic piezoresistive response as a function of time for (A) PANI1/DBSA, (B) PANI2/DBSA, (C) PANI1/CSA and (D) PANI2/CSA. Experimental conditions: bending of 2 mm, deformation velocity of 1mm/min at room temperature.

It is observed that the electrical resistance changes fairly linearly with the applied strain and the linearity is maintained for the different cycles and for the different samples.

The curves were thus fitted by linear regression as shown in Fig. 10.15. The slope of the linear fit with Eq. 10.2. (obtained with a R-square higher than 0.90) corresponds to the GF of the samples, which is reported in Table 10.4.

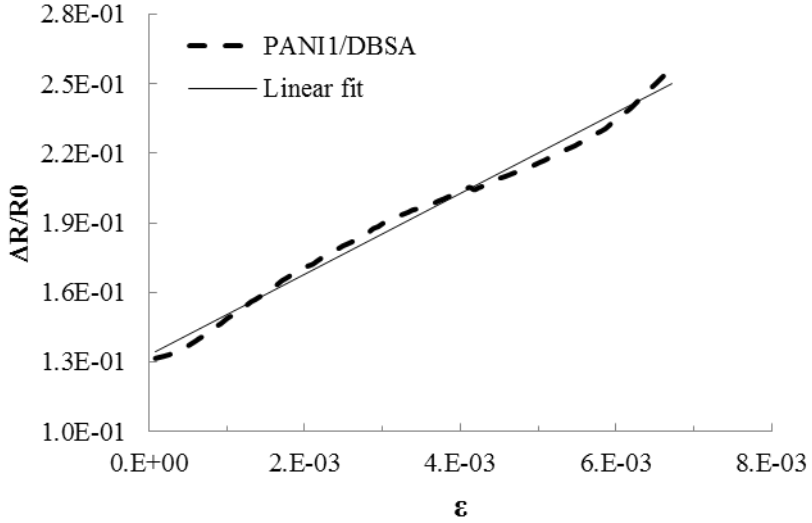

Figure 10.15.: Relative change in electrical resistance as a function of the strain in a 4-point bending test for PANI1/DBSA.

Sample	GF (up)	Standard error	GF (down)	Standard error
PANI1/DBSA	21.97	2.17	16.84	1.45
PANI2/DBSA	44.16	6.12	61.98	0.08
PANI1/CSA	1.10	0.10	1.02	0.18
PANI2/CSA	2.36	0.37	2.44	0.64

Table 10.4.: GF values resulting of the linear fit of $\Delta R/R_0$ as function of stress.

It is to notice in Table 10.4. that, in general, the value of GF is strictly related to the nature of the dopant used. In fact, PANI1/DBSA and PANI2/DBSA exhibit GFs extraordinarily high (commercial piezoesistors have GF ranging from 1 to 2),[618, 624, 625] whereas PANI1/CSA and PANI2/CSA show low GFs. Moreover, the latter displays interesting piezoresistive behaviour only up 1.5 mm of deformation.

As reported in Equation 10.1. the resistance R variation results from the contribution of the dimensional change (l/S), that is a geometrical effect, and from variations in the resistivity (ρ), that is characteristic of each material and therefore an intrinsic contribution. GF of 1-2 are typical of those materials for which the change of resistance is related to geometrical effects (e. g. metals).[614] This suggests that for both PANI1 and PANI2 doped with CSA only the geometrical variations contribute to the GF.

In order to explain the different GF values of PANI1 and PANI2 when different dopants are used, it is worth to notice that the small counterion size of CSA reduces the *inter*-chain distances ensuring

high values of conductivity (Table 10.3.). However, at the same time it can cause poor mobility of chains increasing the rigidity of the polymer and making polyaniline a metal-like material.

On the contrary, big organic dopants, such as DBSA, make polyaniline less conductive but allows a higher mobility of chains during the loading/unloading process, leading to molecular modifications of the polymer that affect its resistivity.

In all cases, samples display an increasing trend in electrical resistance with increasing the number of cycles (Figure 10.14). This irregular behaviour is attributed to structural modifications in the polymers during the subsequent loading/unloading processes. For this reason all the samples were tested for a higher number of cycles (up to 40) in order to guarantee a complete mechanical stabilization. The results are reported in Figure 10.16.

.

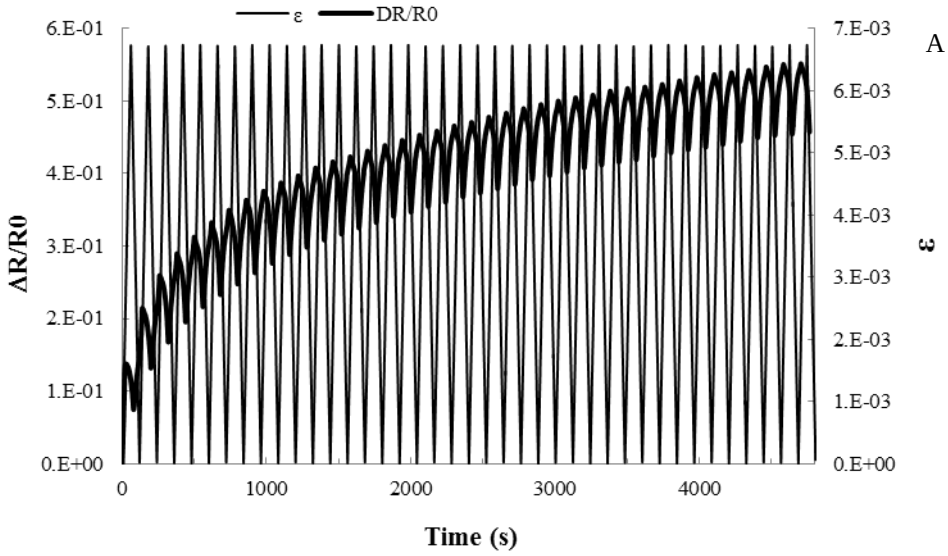

A

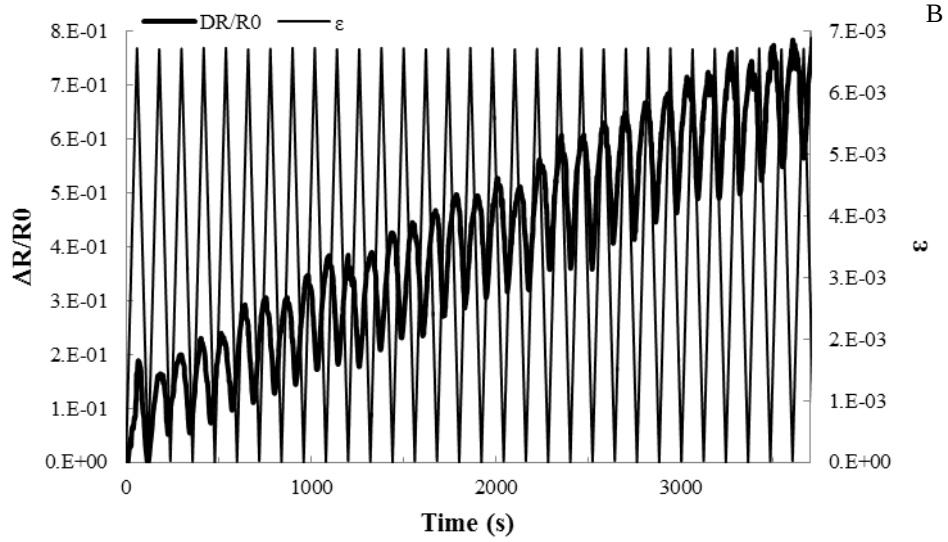

B

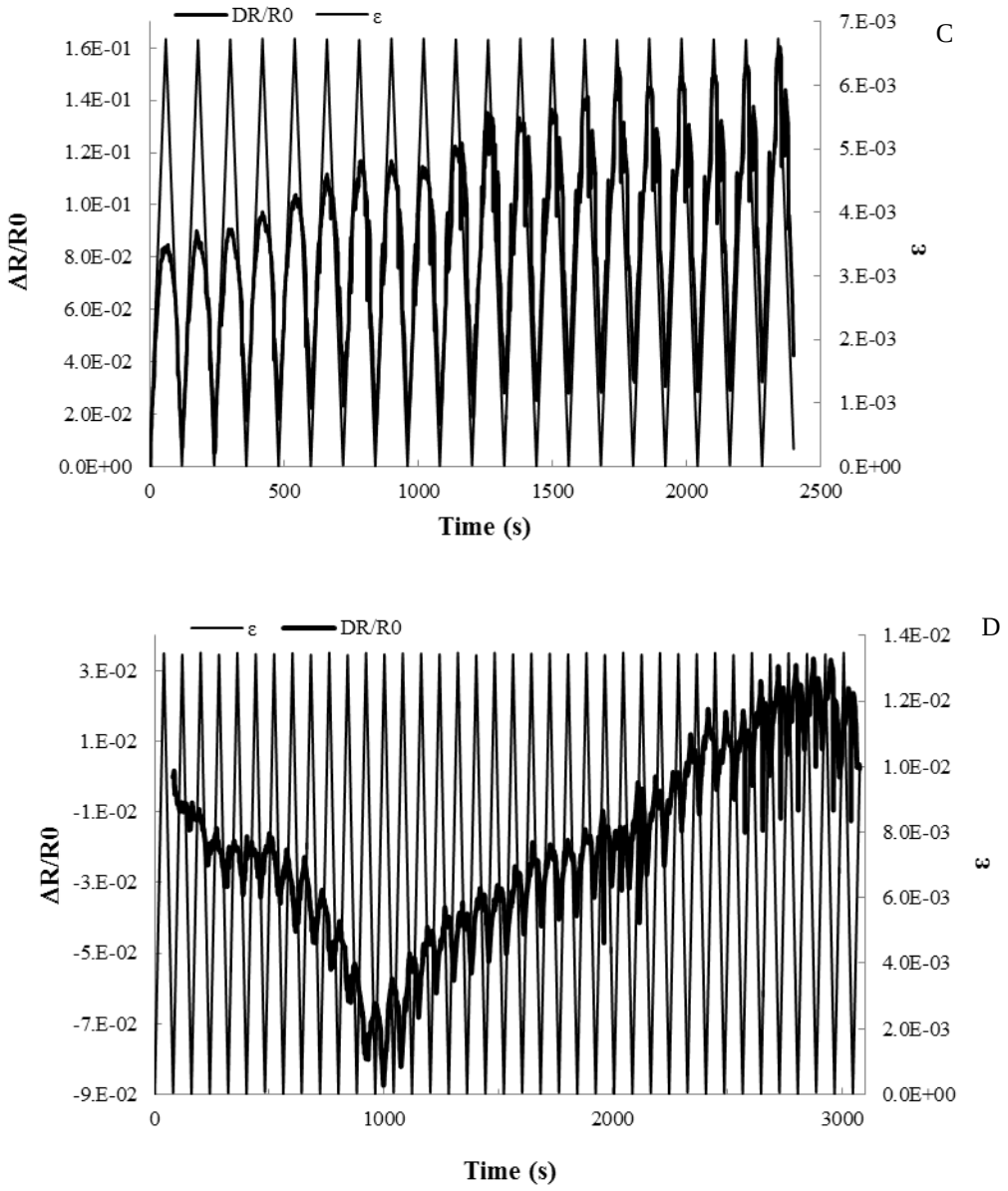

Figure 10.15.: Cyclic piezoresistive response as a function of time for (A) PANI1/DBSA, (B) PANI2/DBSA, (C) PANI1/CSA and (D) PANI2/CSA. Experimental conditions: bending of 1 mm, deformation velocity of 1mm/min at room temperature, number of cycles= 40 for A, B and D and 20 for C.

Figure 10.16. shows that PANI1/DBSA and PANI1/CSA reach stabilization after 40 and 7 cycles respectively, whereas PANI2/DBSA still shows a growing trend after 40 cycles and PANI2/CSA is completely unstable. It is interesting to notice that even if the overall resistance increases in the first cases, the resistance variation, i.e. the GF, remains practically stable over the different cycles (see Figure 10.17.)

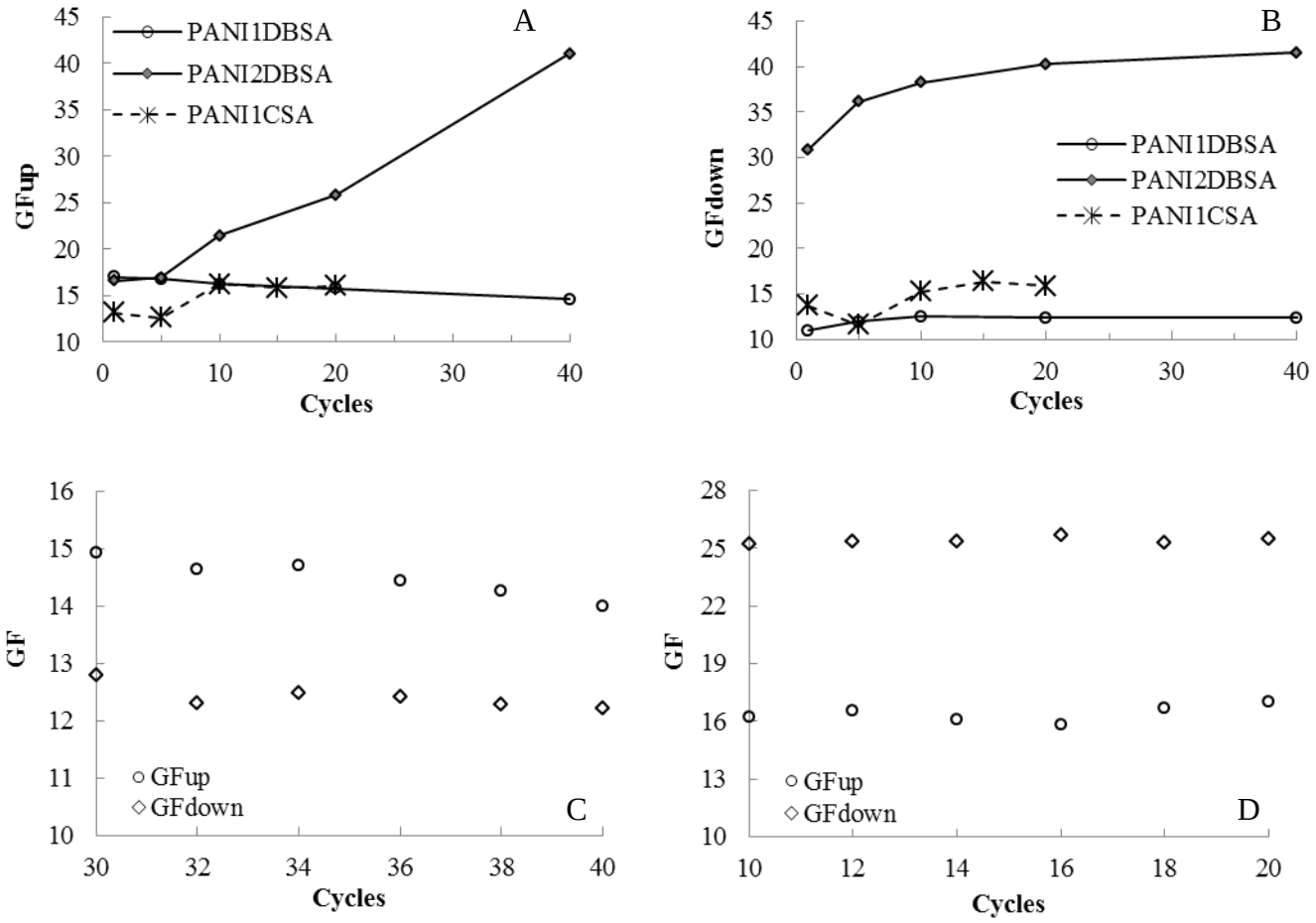

Figure 10.17.: (A and B) GF variation with the number of cycles for PANI1/DBSA, PANI2/DBSA and PANI1/CSA, GF stabilization for (C) PANI1/DBSA and (D) PANI1/CSA in the last 10 cycles.

This is important because the material can be used from the beginning without treatment as a sensor, as the R variation with the number of cycles is not that large and can be compensated/calibrated.

The instability of both PANI2 samples can be explained in terms of irregular morphology and poor compactness, as show in Figure 10.12.

Table 10.5. reports the GF for samples that reached mechanical stabilization increasing the number of loading/unloading cycles.

Sample	GF (up)	Standard error	GF (down)	Standard error
PANI1/DBSA	14.55	0.11	12.40	0.27
PANI2/DBSA	40.71	0.33	40.71	0.13
PANI1/CSA	16.00	0.56	16.68	0.95

Table 10.5.: GF values resulting from the linear fit of $\Delta R/R_0$ as function of stress after mechanical stabilization.

As it is possible to observe the mechanical stabilization affects also the values of GF. In fact, PANI1/DBSA and PANI2/DBSA maintain high GF values but lower standard errors, confirming the stabilization of the polymers during the loading/unloading cycles, whereas PANI1/CSA under these conditions exhibits GF very similar to that of PANI1/DBSA, suggesting a complete modification of the original molecular structure.

In order to obtain materials stable for all the loading/unloading cycles and at the same time remove any trace of solvent ($CHCl_3$) that can compromise their *inter*-chains network, all the samples were subjected to a thermal treatment (1 hour at 70°C) and tested again. PANI2/DBSA and PANI1/CSA maintain the same behaviours shown at room temperature, even though the former becomes stable more quickly (after 25 cycles). The higher stability of PANI2/DBSA can be explained by the morphology change (Figures 10.12 D and D'). As it is possible observe, the removal of solvent leads to a quite porous and more regular morphology that positively affects the piezoresistive behaviour. On the contrary, also after the thermal treatment PANI2/CSA exhibits an unstable trend, justified by the high irregular morphology of the sample before and after the thermal aging process. Only PANI1/DBSA shows a complete stabilization and for this reason it was tested at different velocity of deformation, as shown in Figure 10.18. and GF variation is summarized in Figure 10.19.

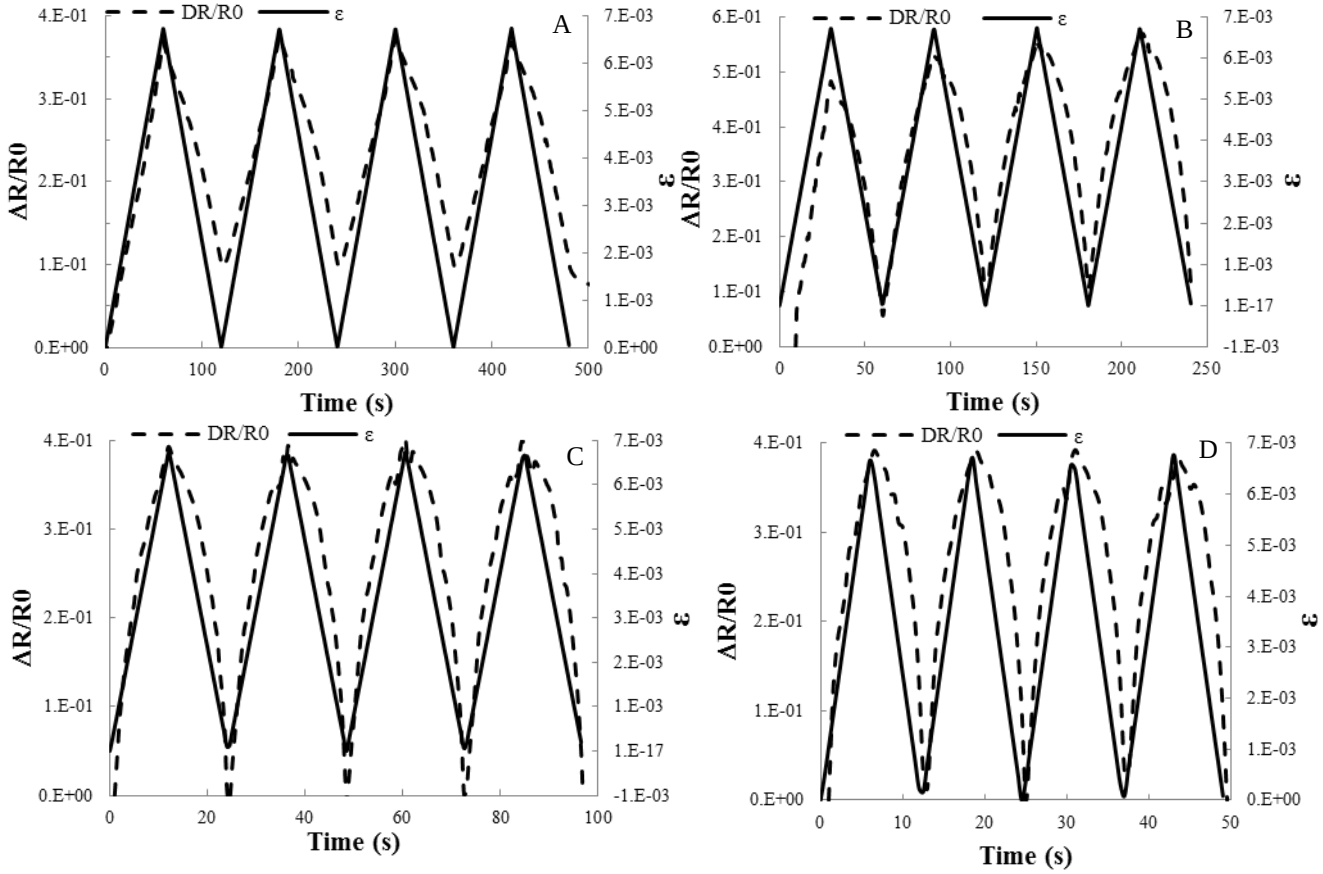

Figure 10.18.: Cyclic piezoresistive response as a function of time for PANI1/DBSA after thermal treatment (1 h at 70°C). Experimental conditions: bending of 1 mm, deformation velocity of (A) 1mm/min, (B) 2 mm/min, (C) 5 mm/min and (D) 10 mm/min.

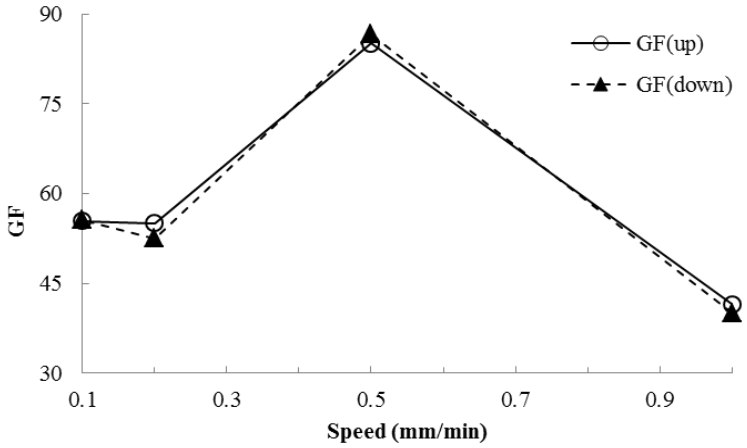

Figure 10.19.: GF as a function of the of the 4-point bending speed for PANI1/DBSA after thermal treatment (1 h at 70°C).

An increase of the deformation speed reveals that it affects the value of GF. In fact, GF increase for higher velocity reaching the maximum value of 85. This electro-mechanical behaviour is related to the structure of the polymer matrix and therefore to the mechanical time response.
Figure 10.20. shows the behaviour of the GF with increasing deformation.

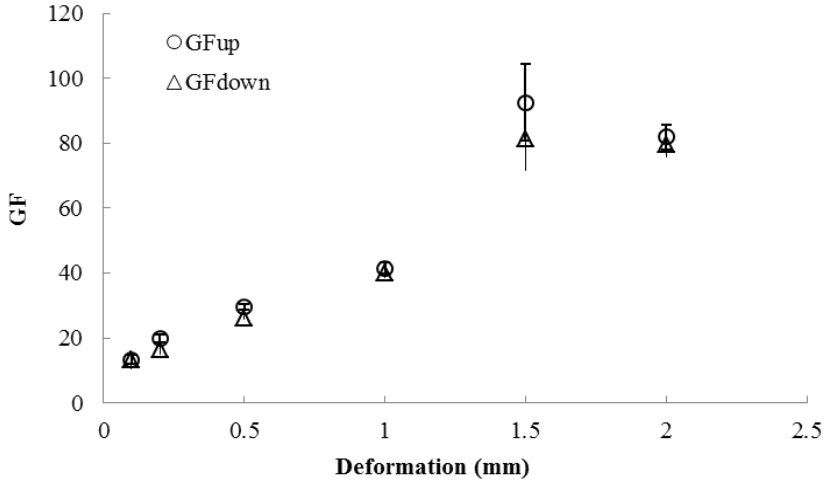

Figure 10.20.: GF as a function of the of the 4-point bending deformation for PANI1/DBSA after thermal treatment (1 h at 70°C).

The GF increases with increasing deformation up to a maximum at ~1.5 mm/min in which the GF seems to stabilize. The linear growth on the GF with increasing deformation indicates a strong effect of the deformation on the conduction mechanism of the polymer, far beyond the geometrical effect or even the morphological effects on the sample. The strong resistivity variations strongly increase for larger deformations indicating a direct effect on electron mobility due to polymer chain stretching. This effect seems to be stabilized for deformations larger than 1.5 mm.

PART IV: Conclusions

The chemical industry of the next few years will be shaped by a number of emerging global mega trends strictly related to the growth and aging of the world population (nine billion people in 2050), that will result in demand of innovative materials able to solve new needs in many fields: health, communication, energy, environmental sustainability, etc. In all these big new challenges conducting organic polymers (COPs) will have an important role thanks to their surprising properties. Among them polyaniline (PANI) is one of the more investigated COPs owing to its peculiar properties which make it valid substitute of conventional materials in different fields (electronics, fenestration, textile industry, sensors and many others). However, to date many aspects related to its synthesis and application are still open. In this context, this three-year PhD thesis allowed to examine in depth many aspects related to PANI-based materials syntheses and their application in some of those fields reported above.

Recently, an extensive effort has been spent to develop shielding materials able to reduce the electromagnetic interference (EMI) originated by the increasing use of electronic devices and telecommunication equipment. In this field conducting/magnetic materials are particularly tempting for their ability to reduce the electromagnetic interferences (EMI) originated by the increasing use of electronic devices and telecommunication equipment. For this purpose in the first part of the work new green protocols to prepare PANI/magnetic nanoparticles composites were presented and preliminary results in terms of their microwave absorbing properties were shown.

For the first time the double role of Fe_3O_4 nanoparticles (NPs) as catalysts and magnetic fillers in the aerobic polymerization of *N*-(4-aminophenyl)aniline (AD) to produce PANI/Fe_3O_4 nanocomposites was described. TEM and SEM microscopies demonstrated that using Fe_3O_4 NPs in ferrofluid form as catalysts and magnetic fillers all the products were obtained in a specific morphology of nanorods with diameter ranging from 30 to 110 nm. On the contrary, when Fe_3O_4 NPs in powder form were used the products displayed more irregular structures. For such a morphological effect a mechanism of reaction similar to a interfacial polymerization was proposed. The PANI/Fe_3O_4 composites exhibited superparamagnetic behaviour at room temperature but at low temperature they resulted to be in a blocked state where remanence and coercivity were observed. In terms of conductivity PANI/Fe_3O_4 composites showed values of the same order of magnitude as that of pristine PANI.

Preliminary results in terms of microwave absorption properties carried out on PANI prepared by a new green approach and a PANI/Fe_3O_4 composite prepared by mechanical mixing demonstrated the surprising properties in this field. The addition of magnetic Fe_3O_4 NPs resulted in an increase in the magnetic loss of the system but at the same time in a drop of the electrical loss, probably due to the heterogeneity of the system that didn’t guarantee a good network among conducting polymeric

chains. The best results are expected for PANI/Fe_3O_4 composite prepared by the new catalytic approach reported in this thesis.

The dependence of the catalytic activity of Fe_3O_4NPs from their sizes in the oxidative polymerization of *N*-(4-aminophenyl)aniline was also investigated and it was demonstrated that the catalytic effect of magnetic nanoparticles increased as their size decreased. Fe_3O_4NPs didn't undergo chemical or crystallographic change during the polymerization reaction and resulted to be almost uniformly dispersed in the polymer matrix guaranteeing a good homogeneity of the magnetic properties within the sample. Moreover, PANI/Fe_3O_4 nanocomposites showed tunable magnetic properties as a function of the magnetic NPs size.

In order to clarify what was the catalytically active metallic center in the spinel structure of magnetite, Fe(II) was substituted with another metal (Mn, Co, Ni, Cu, Zn, Mg) and the effect of such a substitution on the catalytic performance was investigated.

It was observed that the catalytic effect of the spinels in the oxidative polymerization of *N*-(4-aminophenyl)aniline was related to two main factors: kind of oxidant and nature of the first metallic center. In general, when the polymerization reaction was carried out under aerobic conditions all the ferrites exhibited good results in terms of polymerization yield. However, when H_2O_2 was used as the oxidant, replacing the first bivalent center (Fe^{2+}) with other metals the catalytic activity followed the trend: $Fe \geq Co > Ni \geq Cu >> Zn > Mn \geq Mg$.

The different behaviour of the ferrites under aerobic and anaerobic conditions could be related to their ability to decompose H_2O_2, subtracting it from the reaction mixture.

However, it was demonstrated for the first time that the catalytic activity of the spinels in the oxidative polymerization of AD in the presence of H_2O_2 resulted to be most likely correlated to the their inversion degree. In fact, inverse spinels produced PANI/MFe_2O_4 composites in high yields and led to composites containing PANI in conducting emeraldine form, whereas more modest results were obtained in the presence of direct spinels producing more reduced polymeric matrix (similar to leucoemeraldine).

In the second part of this thesis interesting results in the preparation of highly pure polyaniline nanofibers (NFs) by the electrospinning technique were presented. These nanostructured materials showed high values of conductivity and good cytocompatibility. Highly pure PANI NFs were produced by two strategies: reducing as much as possible the co-polymer amount (polyethylene oxide, PEO) within the PANI/insulating blend used to spun NFs or removing the co-polymer (polymethylmetacrylate, PMMA) after the electrospinning process by a washing step. Moreover, in the first case two different kinds of collector were used (static and rotating) and the effect on the morphology of blended PANI/PEO NFs was investigated.

It was observed a decrease of the fiber size and an increase of the conductivity values by reducing PEO amount. Moreover, the use of a rotating collector had a stretching effect on the nanofibers, promoting a narrow distribution of diameters. However, the sterilization treatment carried out on PANI NFs before to test their cytocompatibility resulted to affect negatively their morphology. This phenomenon was explained in terms of phase segregation. In fact, owing to the non-homogeneous distribution of PEO and PANI into the blend, the sterilization process caused the removal of a small co-polymer amount present into the NFs thus dramatically compromising their morphology. Substituting PEO with another co-polymer (PMMA), not soluble in water or ethanol but able to guarantee no segregation phenomena, it was possible to spun PANI/PMMA NFs using a high amount of the insulating copolymer and remove it in a second step with a specific washing treatment: 2 minutes in 2-propanol. After the washing step PANI NFs didn't change size and morphology. Their cytocompatibility was tested on SH-SY5Y cells (human neuroblastoma cell line). Preliminary results suggested that washed PANI/PMMA NFs result to be a better substrate for culturing SH-SY5Y cells than unwashed PANI/PMMA NFs. To better investigate this aspect, direct cytocompatibility tests are in progress

The mechanical monitoring in large and small scale (buildings/touch-technology) needs of highly sensitive stress/strains sensors and in the third part the amazing piezoelectric properties of PANI film will be for the first time presented.

In the first part of this section the electromechanical characterization of PANI pellets doped with H_2SO_4 was carried out under high and low force loading. The variation of resistance with the deformation was expressed in terms of gauge factor, GF, and resulted to be similar to that of commercial stress/strain sensors (0.1-2), whose change in resistance is strictly related to geometrical factors.

However, at molecular level the conductivity of PANI is the sum of two contributions: the ability of the charge carriers to move along the polymer backbone (intra-chain mechanism) and the ability of the charge carriers to hop between the polymer chains (inter-chain mechanism). This second contribution is particularly important when the material is subjected to stress/strain processes. In order to emphasize this second contribution and increase the intrinsic piezoresistive effect PANI was produced in film form and tested in strain/stress tests. The extraordinary high GF values obtained under specific conditions (more than 10 times higher than those of commercial strain gauges) open the way to innovative applications of polyaniline in the world of low cost stress/strain sensors.

References

[1] L. Rupprecht, *Conductive polymers and plastics in industrial applications*, William Andrew (1999);

[2] M. Bryning, M. Islam, J. Kikkawa, A. Yodh, *Advanced Materials*, 17 (2005) 1186-1191;

[3] R. Ramasubramaniam, J. Chen, H. Liu, *Applied Physics Letters*, 83 (2003) 2928-2930;

[4] C. K. Chiang, C. R. Fincher, Jr. Y. W. Park, A. J. Heeger, H. Shirakawa, E. J. Louis, S. C. Gau, A. G. MacDiarmid, *Physical Review Letters*, 39 (1977) 1098-1107;

[5] T. A. Skotheim, R. L. Elsenbaumer, J. R. Reynolds, *Handbook of Conducting Polymers*;

[6] D. Verma, D. Dutta, *Journal of Physics: Condensed Matter*, 19 (2007) 186212-186217;

[7] H. Karami, M. F. Mousavi, M. Shamsipur, *Journal of Power Sources*, 117 (2003) 255-259;

[8] M. M. Gvozdenović, B. Z. Jugović, T. L. Trišović, J. S. Stevanović, B. N. Grgur, *Materials Chemistry and Physics*, 125 (3) (2011) 601-605;

[9] D. N. Huyen, N. T. Tung, N. D. Thien, L. H. Thanh, *Sensor*, 11 (2011) 1924-1931;

[10] G. Natta, G. Mazzanti, P. Corraddini, *Atti della Accademia Nazionale dei Lincei. Rendiconti Classe di Scienze Fisiche, Matematiche e Naturali*, 25 (1958) 3;

[11] H. Shirakawa, E. J. Luis, A. G. MacDiarmid, C. K. Chiang, A. J. Heeger, *Journal of the Chemical Society, Chemical Communications*, (1977) 578-580;

[12] G. Zerbi, *La Chimica e l'Industria*, 73 (1991) 355;

[13] P. Chandrasekhar, *Conducting Polymers, Fundamentals and Applications*, Kluwer Academic Publishers (1999);

[14] J. L. Bredas, G. B. Street, *Accounts of Chemical Research*, 18 (1985) 309-315;

[15] P. W. Anderson, *Physical Review Letters*, 34 (1975) 953-955;

[16] W. P. Su, J. R. Schrieffer, A. J. Heeger, *Physical Review Letters*, 42 (1979) 1698-1701;

[17] D. S. Boudreaux, R. R. Chance, J. L. Brédas, R. Silbey, *Physical Review B: Condensed Matter*, 28 (1983) 6927-6936;

[18] H. Thomann, L. R. Dalton, Y. Tomkiewicz, N. S. Shiren, T. C. Clarke, *Physical Review Letters*, 50 (1983) 533-536;

[19] S. Roth, *Introduction To The Physics Of Conducting Polymers. Mater. Sci. Forum*, 21 (1987) 1–12;

[20] M. S. Dresslhaus, G. Dresselhaus, A. Jorio, A. G. Souza Filho, R. Saito, *Carbon*, 40 (2002) 2043-2061;

[21] K. Mallick, M. J. Witcomb, A. Dinsmore, M. S. Scurrell, *Langmuir*, 21 (2005) 7964-7967;

[22] Y. Wang, Z. Liu, B. Han, Z. Sun, Y. Huang, G. Yang, *Langmuir*, 21 (2005) 833-836;

[23] Z. Sun, Y. Geng, J. Li, X. Wang, X. Jing, F. Wang, *Journal of Applied Polymer Science*, 72 (1999) 1077-1084;

[24] T. K. Sarma, D. Chowdhury, A. Paul, A. Chattopadhyay, *Chemical Communications*, (2002) 1048-1049;

[25] N. Toshima, S. Hara, *Progress in Polymer Science*, 20 (1995) 155-183;

[26] Z. Chen, C. Della Pina, E. Falletta, M. Rossi, *Journal of Catalysis*, 267 (2009) 93-96;

[27] C. Della Pina, E. Falletta, M. Lo Faro, M. Pasta, M. Rossi, *Gold Bulletin*, 42 (2009) 27-33;

[28] Z. Chen, C. Della Pina, E. Falletta, M. Lo Faro, M. Pasta, M. Rossi, N. Santo, *Journal of Catalysis*, 259 (2008) 1-4;

[29] H.V.R. Dias, R. M. G. Rajapakse, D. M. M. Krishantha, M. Fianchini, X. Wang, R. L. Elsenbaumer, *Journal of Material Chemistry*, 17 (2007) 1762-1768;

[30] H. V. R. Dias, X. Wang, R. M. G. Rajapakse, R. L. Elsenbaumer, *Chemical Communication*s, (2006) 976-978;

[31] H. Liu, X. B. Hu, J. Y. Wang, R. I. Boughton, *Macromolecules*, 35 (2002) 9414-9419;

[32] J. Huang, S. Virji, B. H. Weiller, R. B. Kaner, *Journal of American Chemical Society*, 125 (2003) 314-315;

[33] J. Huang, R. B. Kaner, *Journal of American Chemical Society*, 126 (2004) 851-855;

[34] X. Lu, H. Mao, D. Chao, W. Zhang, Y. Wei, *Macromolecular Chemistry and Physics*, 207 (2006) 2142–2152;

[35] K. Doblhofer, K. Rajeshwar, T. A. Skotheim, R. L. Elsenbaumer, J. R. Reynolds (Eds.), *Handbook of Conducting Polymers*, 2nd ed., Marcel Dekker, (1998) 531;

[36] C. Della Pina, E. Falletta, M. Rossi, *Catalysis Today* 160 (2011) 11–27;

[37] B. L. Funt, A. F. Diaz, *Organic Electrochemistry: an Introduction and a Guide*, Marcel Dekker, (1991) 1337;

[38] E. M. Genies, G. Bidan, A. F. Diaz, *Journal of Electroanalytical Chemistry*, 149 (1983) 101;

[39] R. J. Waltman, J. Bargon, *Canadian Journal of Chemistry*, 64 (1986) 76-95;

[40] R. J. Waltman, J. Bargon, *Tetrahedron*, 40 (1984) 3963-3970;

[41] S. Asavapiriyanont, G. K. Chandler, G. A. Gunawardena, D. Pletcher, *Journal of Electroanalytical Chemistry*, 177 (1984) 229-244;

[42] J. Wang, D. Zhang, *Advances in Polymer Technology*, 32 (S1) (2013) E323–E368;

[43] www.marketsandmarkets.com;

[44] O. Unverdorben, *Annual Physical Chemistry*, 8 (1826) 397;

[45] F. F. Runge, *Annual Physical Chemistry*, 31 (1834) 513;

[46] J. Frtzche, *Journal fur Praktische Chemie*, 20 (1840) 454;

[47] A. G. MacDiarmid, A. J. Epstein, *Faraday Discussions*, 88 (1989) 317-332;

[48] H. Letheby, *Journal of Chemical Society*, 15 (1862) 161-163;

[49] A. Green, A. Woodhead, *Journal of Chemical Society Transactions*, 101 (1912) 1117-1123;

[50] A. Green, A. Woodhead, *Journal of Chemical Society Transactions*, 97 (1910) 2388-2403;

[51] E. Noelting, *Scientific and Industrial History of Aniline Black*, WM. J. Matheson& Co, (1889);

[52] R. Willstätter, C. W. Moore, *Berichte der Deutschen Chemischen Gesellschaft*, 40 (1907) 2665;

[53] J. Chiang, A. MacDiarmid, *Synthetic Metals*, 13 (1986) 193-205;

[54] G. G. Wallace, G. M. Spinks, P. R. Teasdale, *Conductive Electroactive Polymers*, CRC Press, London (2002);

[55] G. G. Wallace, G. M. Spinks, L. A. P. Kane-Maguire, P. R. Teasdale, *Conductive Electroactive Polymers: Intelligent Polymer Systems*, CRC Press, London(2009);

[56] J. E. de Albuquerque, L. H. C. Mattoso, R. M. Faria, J. G. Masters, A. G MacDiarmid, *Synthetic Metals*, 146 (2004) 1-10;

[57] Y. Xia, J. M. Wiesinger, A. G. MacDiarmid, A. J. Epstein, *Chemistry of Materials*, 7 (1995) 443-445;

[58] W. S. Huang, A. G. MacDiarmid, *Polymer*, 34 (1993) 1833-1845;

[59] A. Boyle, J. P. Penneau, E. Genies, C. Riekiel, *Journal of Polymer Science, Part B: Polymer Physics*, 30 (1992) 265-274;

[60] J. Chiang, A. MacDiarmid, *Synthetic Metals*, 13 (1986) 193-205;

[61] K. Mallick, M. J. Witcomb, A. Dinsmore, M. S. Scurrell, *Langmuir*, 21 (2005) 7964-7967;

[62] Y. Wang, Z. Liu, B. Han, Z. Sun, Y. Huang, G. Yang, *Langmuir*, 21 (2005) 833-836;

[63] Z. Sun, Y. Geng, J. Li, X. Wang, X. Jing, F. Wang, *Journal of Applied Polymer Science*, 72 (1999) 1077-1084;

[64] T. K. Sarma, D. Chowdhury, A. Paul, A. Chattopadhyay, *Chemical Communications*, (2002) 1048-1049;

[65] P. N Adams, P. J.Laughlin, A. P. Monkman, A. M. Kenwright, *Polymer*, 37 (1996) 3411-3417;

[66] J.E. Österholm, Y.Cao, F.L. Klavetter, P.Smith, Synth. Met. 55 (1993) 1034.

[67] S. Trakhtenberg, Y. Hangun-Balkir, J. C. Warner, F. F. Bruno, J. Kumar, R. Nagarajan, L. A. Samuelson, *Journal of the American Chemical Society*, 127 (2005) 9100-9104;.

[68] W. Liu, A. Anagnostopoulos, F. F. Bruno, K. Senekal, J. Kumar, S. Tripathy, L. Samuelson, *Synthetic Metals*, 101 (1999) 738-741;

[69] N. Bicak, B. Karagoz, *Journal of Polymer Science Part A: Polymer Chemistry*, 44 (2006) 6025-6031;

[70] N. Toshima, S. Hara, *Progress in Polymer Science*, 20 (1995) 155-183;

[71] S. E. Bourdo, B. C. Berry, T. Viswanathan, *Journal of Applied Polymer Science*, 98 (2005) 29-33;

[72] W. Liu, A. L. Cholli, R. Nagarajan, J. Kumar, S. Tripathy, F. F. Bruno, L. Samuelson, *Journal of the American Chemical Society*, 121 (1999) 11345-11355;

[73] W. Liu, J. Kumar, S. Tripathym, J. Senecal, L. Samuelson, *Journal of the American Chemical Society*, 121 (1999) 71-78;

[74] D. K. Moon, K. Osokada, T. Maruyama, T. Yamamoto, *Macromolecular Chemistry and Physics*, 193 (1992) 17231728;

[75] M. Sivakumar, A. Gedanken, *Synthetic Metals*, 148 (2005) 301-306;

[76] Y. Wei, G. W. Jang, Ch. Ch. Chan, K. F. Hsuen, R. Hariharan, S. A. Patel, C. K. Whitecar, *Journal of Physical Chemistry*, 94 (1990) 7716-7721;

[77] Y. Wei, X. Tang, Y. Sun, W. W. Focke, *Journal of Polymer Science Part A: Polymer Chemistry*, 27 (1989) 2385-2396;

[78] Y. Wei, R. Hariharan, S. A. Patel, *Macromolecules*, 23 (1990) 758-764;

[79] Y. Wei, K. F. Hsueh, G. W. Jang, *Polymer*, 35 (1994) 3572-3575;

[80] C. Della Pina, M. Rossi, A. M. Ferretti, A. Ponti, M. Lo Faro, E. Falletta, *Synthetic Metals*, 162 (2012) 2250-2258;

[81] D. M. Mohilner, R. N. Adams, W. J. Argersinger Jr., *Journal of the American Chemical Society*, 84 (1962) 3618-3622;

[82] J. Bacon, R. N. Adams, *Journal of the American Chemical Society*, 90 (1968) 6596-6599;

[83] G. Ćirić-Marjanović, unpublished results.

[84] N. Gospodinova, L. Terlemezyan, *Progress in Polymer Science*, 23 (1998) 1443-1484;

[85] G. Ćirić-Marjanović, M. Trchová, J. Stejskal, *Collection of Czechoslovak Chemical Communications*, 71 (2006) 1407-1426;

[86] G. Ćirić-Marjanović, E.N. Konyushenko, M. Trchová, J. Stejskal, *Synthetic Metals*, 158 (2008) 200-211;

[87] N. Gospodinova, L. Terlemezyan, P. Mokreva, K. Kossev, *Polymer*, 34 (1993) 2434-2437;

[88] Y. Ding, A. B. Padias, H. K. Hall Jr., *Journal of Polymer Science Part A: Polymer Chemistry*, 37 (1999) 2569-2579;

[89] R. Madathil, S. Ponrathnam, H. J. Byrne, *Polymer*, 45 (2004) 5465-5471;

[90] E. M. Genies, C. Tsintavis, *Journal of Electroanalytical Chemistry*, 195 (1985) 109-128;

[91] E. M. Genies, M. Łapkowski, *Journal of Electroanalytical Chemistry*, 236 (1987) 199-208;

[92] G. Vidotto, A. Crosato-Arnaldi, G. Talamini, *Macromolecular Chemistry and Physics*, 122 (1969) 91–104;

[93] M. Carenza, G. Palma, *European Polymer Journal*, 21 (1985) 41–47;

[94] A. Guyot, Salamone JC, Editor-in-Chief. *Polymeric materials encyclopedia*, Boca Raton: CRC Press, 9 (1996) 7228–7237;

[95] H. D. H. Stover, Salamone JC, Editor-in-Chief. *Polymeric materials encyclopedia*, Boca Raton: CRC Press, 9 (1996) 7237–7238;

[96] E. A.Gruike, Kroschwitz JI. Executive editor., *Encyclopedia of polymer science and engineering*, NewYork: John Wiley & Sons, 16 2nd Ed. (1989) 443–473;

[97] H. Bieringer, K. Flatau, D. Reese, *Angewandte Makromolekulare Chemie*, 123 (1984) 307–334;

[98] H. G. Yuan, G. Kalfas, W. H. Ray, *Journal of Macromolecular Science - Reviews in Macromolecular Chemistry & Physics*, 31 (1991) 215–299;

[99] K. E. J. Barrett, *Dispersion polymerization in organic media*, London: John Wiley & Sons, (1975);

[100] S. Palaniappan, M. Sairam, *Journal of Applied Polymer Science*, 108 (2008) 825–32;

[101] J. Stejskal, *Journal of Polymer Materials*, 18 (2001) 225–258;

[102] J. Stejskal, *Dendrimers, assemblies, nanocomposites*, Arshady R, Guyot A, Editors, London, Citus Books (2002) 195–281;

[103] V. R. Gowariker, N. V. Viswanathan, J. Sreedhar, *Polymer Science*, New Delhi, India, New Age International (P) Limited (1996) 73;

[104] F. Yan, G. Xue, *Journal of Material Chemistry*, 9 (1999) 3035–3039;

[105] E. Ruckenstein, Y. Sun, *Synthetic Metals*, 74 (1995) 107–113;

[106] H. Huang, H. Zhang, J. Li, S. Cheng, F. Hu, B. Tan, *Journal of Applied Polymer Science*, 68 (1998) 2029–2039;

[107] H. Huang, H. Zhang, Z. Ai, J. Li, S. Cheng, F. Hu, Z. Ai, B. Tan, S. Cheng, J. Li, *Journal of Applied Polymer Science*, 73 (1999) 315–322;

[108] E. Marie, R. Rothe, M. Antonietti, K. Landfester, *Macromolecules*, 36 (2003) 3967–3973;

[109] J. Li, K. Fang, H. Qiu, S. Li, W. Mao, Q. Wu, *Synthetic Metals*, 145 (2004) 191–194;

[110] S. Ding, H. Mao, W. J. Zhang, *Applied Polymer Science*, 109 (2008) 2842–2847;

[111] P. Dallas, D. Stamopoulos, N. Boukos, V. Tzitzios, D. Niarchos, D. Petridis, *Polymer*, 48 (2007) 3162–3169;

[112] J. Chen, D. Chao, X. Lu, W. Zhang, *Materials Letters*, 61 (2007) 1419–1423;

[113] Q. Guo, C. Yi, L. Zhu, Q. Yang, Y. Xie, *Polymer*, 46 (2005) 3185–3189;

[114] J. Y. Kim, E. Y. Kim, Y. S. Won, H. S. Lee, K. S. Suh, *Synthetic Metals*, 139 (2003) 485–489;

[115] J. Y. Kim, S. J. Kwon, S. W. Han, Y. K. Min, *Japanese Journal of Applied Physcs*, 43 (2004) 5660–5664;

[116] J. Y. Kim, J. H. Lee, S. J. Kwon, *Synthetic Metals*, 157 (2007) 336–342;

[117] K. S. Suslick, *Science*, 1990, 3, 1439-1445;

[118] X. L. Jing, Y. Y. Wang, D. Wu, L. She, Y. Guo, *Journal of Polymer Science Part A: Polymer Chemistry*, 44 (2006) 1014–1019;

[119] X. Jing, Y. Wang, D. Wu, J. P. Qiang, *Ultrasonic Sonochemistry*, 14 (2007) 75–80;

[120] S. Kobayashi, H. Uyama, S. Kimura, *Chemical Review*, 101 (2001) 3793–3818;

[121] E. Arias-Marin, J. Romero, A. S. Ledezma-Perez, S. Kniajansky, *Polymer Bulletin*, 37 (1996) 581–587;

[122] L. Mejias, M. H. Reihmann, S. Sepulveda-Boza, H. Ritter, *Macromolecular Bioscience*, 2 (2002) 24–32;

[123] N. Kobayashi, K. Teshima, R. Hirohashi, *Journal of Material Chemistry*, 8 (1998) 497–506;

[124] R. A. Barros, W. M. Azevedo, F. M. Aguiar, *Materials Characterization*, 50 (2003) 131–134;

[125] P. K. Khanna, N. Singh, S. Charan, A. K. Viswanath, *Materials Chemisty and Physics*, 92 (2005) 214–219;

[126] C. Nastase, F. Nastase, A. Dumitru, M. Ionescu, I. Stamatin, *Composites Part A: Appl ied Science and Manufacturing*, 36 (2005) 481–485;

[127] F. Nastase, I. Stamatin, C. Nastase, D. Mihaiescu, A. Moldovan, *Progress in Solid State Chemistry*, 34 (2006) 191–199;

[128] A. G. MacDiarmid, J. C. Chiang, A. F. Richter, N. L. D. Somasiri, *Conducting Polymers*, Alcacer, L., Ed.; Reidel: Dordrecht, The Netherlands (1986);

[129] E. R. Holland, S. J. Pomfret, P. N. Adams, L. Abell, A. P. Monkmann, *Synthetic Metals*, 84 (1997) 777–778;

[130] P. Kiattibutr, L. Tarachiwin, L. Ruangchuay, A. Sirivat, J..Schwank, *Reactive and Functional Polymers*, 53 (2002) 29–37;

[131] M. D. Catedral, A. K. G. Tapia, R. V. Sarmago, J. P. Tamayo, E. J. del Rosario, *Science Diliman*, 16/2 (2004) 41-46;

[132] M. Doriomedoff, F. Hautiere-Cristofini, R. De Surville, M. Jozefowicz, L.T. Yu, R .Buvet, *Journal de Chimie Physique et de Physico-Chimie Biologique*, 68 (1971) 1063;

[133] Q. Zhou, J. Wang, Y. Ma, C. Cong, F. Wang, *Colloid & Polymer Science*, 285 (2007) 405–411;

[134] Y. Wei, G. W. Jang, K. F. Hsueh, E. M. Scherr, A. G. MacDiarmid, A. J. Epstein, *Polymer*, 33 (1992) 314–322;

[135] H. Farrokhzad, T. Van Gerven, B. Van der Bruggen, *European Polymer Journal*, in press;

[136] A.G. MacDiarmid, A. J. Epstein, *Materials Research Society Symposium Proceedings*, 247 (1992) 565-576;

[137] A. Ohtani, M. Abe, M. Ezoe, T. Doi, T. Miyata, A. Miyake, *Synthetic Metals*, 55-57 (1993) 3696-3701;

[138] P. N. Adams, P. J. Laughlin, A. P. Monkman, A. M. Kenwright, *Polymer*, 37 (1996) 3411-3417;

[139] P. N. Adams, P. J. Laughlin, A. P. Monkman, *Synthetic Metals*, 76 (1996) 157-160;

[140] P. G. de Gennes, *Comptes rendus de l'Académie des Sciences Paris*, 2/302 (1986) 1;

[141] D. S. Pearson, P. A. Pincus, G. W. Heffner, S. M. Dahman, *Macromolecules*, 26 (1993) 1570-1575;

[142] S. Bhadra, N. K. Singha, D. Khastgir, *Synthetic Metals*, 156 (2006) 1148–1154;

[143] S. Bhadra, S. Chattopadhyay, N. K. Singha, D. Khastgir, *Journal of Polymer Science Part B: Polymer Physics*, 45 (2007) 246–259;

[144] S. Bhadra, N. K. Singha, D. Khastgir, *Polymer International*, 56 (2007) 919–927;

[145] S. Bhadra, N. K. Singha, D. Khastgir, *Journal of Applied Polymer Science*, 104 (2007) 1900–1904;

[146] S. Bhadra, D. Khastgir, *Polymer Degradation and Stability*, 92 (2007) 1824–1832;

[147] A. Wolter, P. Rannou, J. P. Travers, B. Gilles, D..Djurado, *Physical Review B*, 58 (1998) 7637–7647.;

[148] W. W. Focke, G. E. Wnek, Y. Wei, *Journal of Physical Chemistry*, 91/22 (1987) 5813-5818;

[149] M. Nechtstein, C. Santier, *Journal de Physique*, 47 (1986) 935-937;

[150] S. Quillard, G. Louarn, S. Lefrant, A. G. MacDiarmid, *Physical Review B*, 50 (1994) 12496-12508;

[151] E. Kang, K. Neoh, T. Tan, S. Khor, K. Tan, *Macromolecules*, 23 (1990) 2918-2926;

[152] A. G. MacDiarmid, A. Epstein, *Faraday Discussions of the Chemical Society*, 88 (1989) 317-332;

[153] A. G. MacDiarmid, A. J. Epstein, *Science and Applications of Conducting Polymers*, W.R. Salaneck, D.T. Clark, and E.J. Samuelson, Eds. Adam Hilger, Bristol, UK, (1991) 117-127;

[154] J. Laska, *Journal of Molecular Structure*, 701 (2004) 13-18;

[155] Y. Xis, J. M. Wiesinger, A. G. MacDiarmid, *Polymer*, 7 (1995) 443-445;

[156] R. H. Baughman, J. F. Wolf, H. Eckhardt, W. Shacklette, *Synthetic Metals*, 25 (1988) 121-137;

[157] W. Fosong, T. Jinsong, W. Lixiang, Z. Hongfang, M. Zhishen, *Molecular Crystals and Liquid Crystals*, 160 (1988) 175-184;

[158] Y. B. Moon, Y. Cao, P. Smith, A. J. Heeger, *Polymer Communications*, 30 (1989) 196-199;

[159] J. P. Pouget, M. E. Jdzefowiczt, A. J. Epstein, X. Tang, A. G. MacDiarmid, *Macromolecules*, 24 (1991) 779-789;

[160] M. E. Jbzefowicz, R. Laversanne, H. H. S. Javadi, A. J. Epstein, J. P. Pouget, X. Tang, A. G. MacDiarmid, *Physical Review B*, 39 (1989) 12958-12961;

[161] S. Pruneanu, E. Veress, I. Marian, L. Oniciu, *Journal of Material Science*, 34 (1999) 2733–2739;

[162] P . Snauwaert, R. Lazzaroni, J . Riga, J . Verbist, D. Gonbeau, *Electronic Properties of Conjugated polymers III*, Springer Series in Solid State Sciences, edited by H. Kuzmany, M. Mehring and S. Roth, Springer, Berlin, 91 (1989) 301–304;

[163] R. L. Hand, R. F . Nelson, *Journal of the American Chemical Society*, 96 (1974) 850-860;

[164] V. B. Shim, M. S. Won, S . M. Park, *Journal of the Electrochemical Society*, 137 (1990) 538-544;

[165] D. C. Trivedi, S . K. Dhawan, *Synthetic Metals*, 58 (1993) 309-324;

[166] R. Greef, R. Peat, L. M. Peter, D. Pletcher, J. Robinson, *Instrumental Methods in Electrochemistry*, Ellis Horwood, Chichester, (1980) 25;

[167] A.G. MacDiarmid, W.E. Jones Jr., I. D. Norris, J. Gao, A. T. Johnson Jr.,N. J. Pinto, J. Hone, B. Han, F. K. Ko, H. Okuzaki, M. Llaguno, *Synthetic Metals*, 119 (2001) 27–30;

[168] N. J. Pinto, A. T. Johnson Jr., A. G. MacDiarmid, C. H. Mueller, N. Theofylaktos, D. C. Robinson, F. A. Miranda, *Applied Physics Letters*, 83 (2003) 4244–4246;

[169] Y. X. Zhou, M. Freitag, J. Hone, C. Staii, N. J. Pinto, A. T. Johnson Jr., A. G. MacDiarmid, *Applied Physics Letters*, 83 (2003) 3800–3802;

[170] P. K. Kahol, N. J. Pinto, *Synthetic Metals*, 140 (2004) 269–272;

[171] H. X. He, C. Z. Li, N. J. Tao, *Applied Physics Letters*, 78 (2001) 811–813;

[172] C. He, Y. W. Tan, Y. F. Li, *Journal of Applied Polymer Science*, 87 (2003) 1537–1540;

[173] X. Y. Zhang, R. Chan-Yu-King, A. Jose, S. K. Manohar, *Synthetic Metals*, 145 (2004) 23–29;

[174] S. Virji, J. X. Huang, R. B. Kaner, B. H. Weiller, *Nano Letters*, 4 (2004) 491–496;

[175] S. K. Pillalamarri, F. D. Blum, A. T. Tokuhiro, J. G. Story, M. F. Bertino, *Chemistry of Materials*, 17 (2005) 227–229;

[176] J. X. Huang, R. B. Kaner, *Angewandte Chemie International Edition*, 43 (2004) 5817–5821;

[177] C. R. Martin, L. S. Van Dyke, Z. Cai, W. Liang, *Journal of the American Chemical Society*, 112 (1990) 8976–8977;

[178] R. M. Penner, C. R. Martin, *Journal of the Electrochemical Society*, 133 (1986) 2206–2207;

[179] C. R. Martin, *Science*, 266 (1994) 1961–1966;

[180] C. R. Martin, *Accounts of Chemical Research*, 28 (1995) 61–68;

[181] C. R. Martin, *Chemistry of Materials*, 8 (1996) 1739–1746;

[182] C. G. Wu, T. Bein, *Science*, 264 (1994) 1757–1759;

[183] C. W. Wang, Z. Wang, M. K. Li, H. L. Li, *Chemical Physics Letters*, 341 (2001) 431–434;

[184] Z. Wang, M. A. Chen, H. L. Li, *Materials Science and Engineering A*, 328 (2002) 33–38;

[185] S. M. Yang, K. H. Chen, Y. F. Yang, *Synthetic Metals*, 152 (2005) 65–68;

[186] M. Delvaux, J. Duchet, P. Y. Stavaux, R. Legras, S. Demoustier-Champagne, *Synthetic Metals*, 113 (2000) 275–280;

[187] C. Y. Peng, A. K. Kalkan, S. J. Fonash, B. Gu, A. Sen, *Nano Letters*, 5 (2005) 439–444;

[188] H. Cao, C. Tie, Z. Xu, J. Hong, H. Sang, *Applied Physics Letters*, 78 (2001) 1592–1594;

[189] H. J. Qiu, M. X. Wan, B. Matthews, L. M. Dai, *Macromolecules*, 34 (2001) 675–677;

[190] J. Liu, M. X. Wan, *Journal of Materials Chemistry*, 11 (2001) 404–407;

[191] Y. Z. Long, Z. J. Chen, P. Zheng, N. L. Wang, Z. M. Zhang, M. X. Wan, *Journal of Applied Physics*, 93 (2003) 2962–2965;

[192] Z. X. Wei, M. X. Wan, *Journal of Applied Polymer Science*, 87 (2003) 1297–1301;

[193] Z. M. Zhang, Z. X. Wei, M. X. Wan, *Macromolecules*, 35 (2002) 5937–5942;

[194] Y. S. Yang, J. Liu, M. X. Wan, *Nanotechnology*, 13 (2002) 771–773;

[195] A. D. W. Carswell, E. A. O'Rear, B. P. Grady, *Journal of the American Chemical Society*, 125 (2003) 14793–14800;

[196] X. Y. Zhang, S. K. Manohar, *Chemical Communications*, (2004) 2360–2361;

[197] P. Nickels,W. U. Dittmer, S. Beyer, J. P.Kotthaus, F. C. Simmel, *Nanotechnology*, 15 (2004) 1524–1529;

[198] Y. F. Ma, J. M. Zhang, G. J. Zhang, H. X. He, *Journal of the American Chemical Society*, 126 (2004) 7097–7101;

[199] J. M. Liu, S. C. Yang, *Journal of the Chemical Society, Chemical Communications*, (1991) 1529–1531;

[200] S. J. Choi, S. M. Park, *Advanced Materials*, 12 (2000) 1547–1549;

[201] T. Hatano, M. Takeuchi, A. Ikeda, S. Shinkai, *Chemistry Letters*, 32 (2003) 314–315;

[202] L. M. Huang, Z. B. Wang, H. T. Wang, X. L. Cheng, A. Mitra, Y. X. Yan, *Journal of Material Chemistry*, 12 (2002) 388–391;

[203] J. Kan, R. Lv, S. Zhang, *Synthetic Metals*, 145 (2004) 37–42;

[204] J. Q. Kan, S. L. Zhang, G. L. Jing, *Journal of Applied Polymer Science*, 99 (2006) 1848–1853;

[205] M. X. Wan, J. C. Li, *Journal of Polymer Science Part A: Polymer Chemistry*, 38 (2000) 2359–2364;

[206] Y. Z. Long, Z. J. Chen, N. L. Wang, Z. M. Zhang, M. X. Wan, *Physica B: Condensed Matter*, 325 (2003) 208–213;

[207] L. J. Zhang, M. X. Wan, *Nanotechnology*, 13 (2002) 750–755;

[208] Y. Z. Long, L. J. Zhang, Y. J. Ma, Z. J. Chen, N. L. Wang, Z. Zhang, M. X. Wan, *Macromolecular Rapid Communications*, 24 (2003) 938–942;

[209] Y. Z. Long, J. L. Luo, J. Xu, Z. J. Chen, L. J. Zhang, J. C. Li, M. X. Wan, *Journal of Physics: Condensed Matter*, 16 (2004) 1123–1130;

[210] Y. Z. Long, Z. J. Chen, N. L. Wang, Y. J. Ma, Z. Zhang, L. J. Zhang, M. X. Wan, *Applied Physics Letters*, 83 (2003) 1863–1865;

[211] K. Huang, M. X. Wan, *Chemistry of Materials*, 14 (2002) 3486–3492;

[212] Y. S. Yang, M. X. Wan, *Journal of Materials Chemistry*, 12 (2002) 897–901;

[213] H. J. Qiu, J. Zhai, S. H. Li, L. Jiang, M. X. Wan, *Advanced Functional Materials*, 13 (2003) 925–928;

[214] N. J. Pinto, P. L. Carrión, A. M. Ayala, M. Ortiz-Marciales, *Synthetic Metals*, 148 (2005) 271–274;

[215] J. H. Hwang, S. C. Yang, *Synthetic Metals*, 29 (1989) 271–276;

[216] Z. M. Zhang, Z. X. Wei, L. J. Zhang, W. X. Wan, *Acta Materialia*, 53 (2005) 1373–1379;

[217] J. Huang, M. X. Wan, *Journal of Polymer Science Part A: Polymer Chemistry*, 37 (1999) 151–157;

[218] U. Beginn, *Advanced Materials*, 10 (1998) 1391–1394;

[219] M. Bockstaller, W. Köhler, G. Wegner, D. Vlassopoulos, G. Fytas, *Macromolecules*, 33 (2000) 3951–3953;

[220] L. K. Werake, J. G. Story, M. F. Bertino, S. K. Pillalamarri, F. D. Blum, *Nanotechnology*, 16 (2005) 2833–2837;

[221] N. R. Chiou, A. J. Epstein, *Advanced Materials*, 73 (2005) 1679–1683;

[222] N. R. Chiou, A. J. Epstein, *Synthetic Metals*, 153 (2005) 69–72;

[223] R. V. Parthasarathy, C. R. Martin, *Chemistry of Materials*, 6 (1994) 1627–1632;

[224] J. P. Spatz, B. Lorenz, K. Weishaupt, H. D. Hochheimer, *Physical Review B*, 50 (1994) 14888–14892;

[225] X. Y. Zhang, W. J. Goux, S. K. Manohar, *Journal of the America Chemical Society*, 126 (2004) 4502–4503;

[226] W. G. Li, H. L. Wang, *Journal of the American Chemical Society*, 126 (2004) 2278–2279;

[227] M. H. Yun, N. V. Myung, R. P. Vasquez, C. S. Lee, E. Menke, R. M. Penner, *Nano Letters*, 4 (2004) 419-422;

[228] M. Li, Y. Guo, Y. Wei, A. G. MacDiarmid, P. Y. Lelkes, *Biomaterials*, 27 (2006) 2705-2715;

[229] G. E. Wnek, M. E. Carr, D. G. Simpson, G. I. Bowlin, *Nano Letters*, 3 (2003) 213-216;

[230] H. Schreuder-Gibson, P. Gibson, K. Senecal, M. Sennett, J. Walker, W. Yeomans, D. Ziegler, P. P. Tsai, *Journal of Advanced Materials*, 34 (2002) 44-55;

[231] P. Gibson, H. S. Gibson, D. Rivin, *Colloids and Surfaces A*, 2001, 187, 469-481;

[232] C. Kim, K. S. Yang, *Applied Physics Letters*, 83 (2003) 1216-1218;

[233] S. W. Choi, S. M. Jo, W. S. Lee, Y. R. Kim, *Advanced Materials*, 15 (2003) 2027-2032;

[234] H. Liu, J. Kameoka, D. A. Czaplewski, H. G. Craighead, *Nano Letters*, 4 (2004) 671-675;

[235] D. Aussawasathien, J. H. Dong, L. Dai, *Synthetic Metals*, 154 (2005) 37-40;

[236] K. M. Manesh, A. I. Gopalan, K. P. Lee, P. Santhosh, K. D. Song, D. D. Lee, *IEEE Transactions on Nanotechnology*, 6 (2007) 513-518;

[237] I. D. Norris, M. M. Shaker, F. K. Ko, A. G. MacDiarmid, *Synthetic Metals*, 114 (2000) 109-114;

[238] K. H. Hong, T. J. Kang, *Journal of Applied Polymer Science*, 99 (2006) 1277-1286;

[239] M. Wei, B. W. Kang, C. M. Sung, J. Mead, *Macromolecular Materials and Engineering*, 2006, 291, 1307-1314;

[240] P. H. S. Picciani, E. S. Medeiros, Z. Pan, W. J. Orts, L. H. C. Mattoso, B. G. Soares, *Journal of Applied Polymer Science*, 112 (2009) 744–753;

[241] B. Gupta, N. Revagade, J. Hilborn, *Progress in Polymer Science*, 32 (2007) 455-482;

[242] R. Langer, J. P. Vacanti, *Tissue Engineering Science*, 260 (1993) 920-926;

[243] X. Zong, K. Kim, D. Fang, S. Ran, B. S. Hsiao, B. Chu, *Polymer*, 43 (2002) 4403-4412;

[244] H. Hou, Z. Jun, A. Reuning, A. Schaper, J. H. Wendorff, A. Greiner, *Macromolecules*, 35 (2002) 2429-2431;

[245] Z. Jun, H. Hou, A. Schaper, J. H. Wendorff, A. Greiner, *e-Polymers*, 9 (2003)1-9;

[246] S. P. Armes, *Current Opinion in Colloid & Interface Science*, 1/2 (1996) 214–220;

[247] S. P. Armes, M. J. Aldissi, *Journal of the Chemical Society, Chemical Communications*, 2 (1989) 88–89;

[248] S. P. Armes, M. J. Aldissi, M. Hawley, J. G. Beery, S. Gottesfeld, *Langmuir*, 7/7 (1991) 1447–1452;

[249] N. Gospodinova, P. Mokreva, L. Terlemezyan, *Journal of the Chemical Society, Chemical Communications*, 13 (1992) 923–924;

[250] H. Eisazadeh, G. Spinks, G. G. Wallace, *Polymer International*, 37/2 ((1995) 87–91;

[251] J. Stejskal, P. Kratochvil, M. Helmstedt, *Langmuir*, 12/14 (1996) 3389–3392;

[252] B. Vincent, J. Waterson, *Journal of the Chemical Society, Chemical Communications*, 1990;9:683–4.

[253] J. Stejskal, M. Špirkova, A. Riede, M. Helmstedt, P. Mokreva, J. Prokeš, *Polymer*, 40/10 (1999) 2487–2492;

[254] D. Chattopadhyay, M. Chakraborty, B. M. Mandal, *Polymer International*, 50/5 (2001) 538–544;

[255] P. B. Banerjee, M. L. Digar, S. N. Bhattacharyya, B. M. Mandal, *European Polymer Journal*, 30/4 (1994) 499–501;

[256] P. Beadle, S. P. Armes, S. Gottesfeld, C. Mombourquette, R. Houlton, W. D. Andrews, S. F. Agnew, *Macromolecules*, 25/9 (1992) 2526–2530;

[257] M.Morita, *Journal of Polymer Science: Polymer Physics*, 32/2 (1994) 231–242;

[258] R. Gangopadhyay, A. De, G. Ghosh, *Synthetic Metals*, 123/1 (2001) 21–31;

[259] K. Ogura, T. Saino, M. Nakayama, H. Shiigi, *Journal of Materials Chemistry*, 7/7 (1997) 2363–2366;

[260] A. Malinauskas, *Polymer*, 4/9 (2001) 3957–3972;

[261] R. Anbarasan, J. Jayaseharan, M Sudha, J. L. Devi, P. V. Nirmala, A. J. Gopalan, *Applied Polymer Science*, 2001;81(2):468–78;

[262] R. Anbarasan, T. Vasudevan, A. Gopalan, *Journal of Materials Science*, 35/3 (2000) 617–25;

[263] K. W. Oh, K. H. Hong, S. H. Kim, *Journal of Applied Polymer Science*, 74/8 (1999) 2094–2101;

[264] G. A. Tishchenko, J. Dybal, J. Stejskal, V. Kudela, M. Bleha, E. Y. Rosova, G. K. Elyashevich, *Journal of Membrane Science*, 196 (2002) 279–287;

[265] G. K. Elyashevich, L. Terlemezyan, I. S. Kuryndin, V. K. Lavrentyeva, P. Mokreva, E. Y. Rosova, Y. N. Sazanov ,*Thermochima Acta*, 374/1 (2001) 23–30;

[266] B. Das, S. Kar, S. Chakraborty, D. Chakraborty, S. Gangopadhyay, *Journal of Applied Polymer Science*, 69/5 (1998) 841–844;

[267] M. Chakraborty, D. C. Mukherjee, B. M. Mandal, *Synthetic Metals*, 98/3 (1999) 193–200;

[268] J. Anand, S. Palaniappan, D .N. Sathyanarayana, *Progress in Polymer Science*, 23/6 (1998) 993–1018;

[269] T. Fukunada, K. Fuse, K. Kobayashi, *Japan Patent*, 62-139896 (1987);

[270] O. Niwa, T. Tamamura, *Journal of Chemical Society, Chemical Communications*, 13 (1984) 817–818;

[271] M. A. De Paoli, R. J. Waltman, A. F. Diaz, J. Bargon, *Journal of Chemical Society, Chemical Communications*, 15 (1984) 1015–1016;

[272] M. G. Han, S. S. Im, *Polymer*, 42/17 (2001) 7449–7454;

[273] T. Jeevananda, Siddaramaiah, *European Polymer Journal*, 39/3 (2003) 569–578;

[274] T. Vikki, L. O. Pietilä, H. Österholm, L. Ahjopalo, A. Takala, A. Toivo, K. Levon, P. Passiniemi, O. Ikkala, *Macromolecules*, 29/8 (1996) 2945–2953;

[275] Y. Wei, W. W. Focke, G. E. Wnek, A. Ray, A. G..MacDiarmid, *Journal of Physical Chemistry*, 93 (1989) 495–499;

[276] M. Leclerc, J. Guay, L. H. Dao, *Macromolecules*, 22/2 (1989) 649–653;

[277] D. Macinnes, B. L. Funt, *Synthetic Metals*, 25/3 (1988) 235–242;

[278] J. Yue, A. J. Epstein, A. G. MacDiarmid, *Molecular Crystals and Liquid Crystals*, 189 (1990) 255–261;

[279] J. Yue, Z. H. Wang, K. R. Cromack, A. J. Epstein, A. G. MacDiarmid, *Journal of the American Chemical Society*, 113/7 (1991) 2665–2671;

[280] X. L. Wei, Y. Z. Wang, S. M. Long, C. Bobeczko, A. J..Epstein, *Journal of the American Chemical Society*, 118/11 (1996) 2545–2555;

[281] X. G. Li, M. R. Huang, L. H. Zhu, Y. L. Yang, *Journal of Applied Polymer Science*, 82/4 (2001) 790–798.;

[282] Y. Cao, P. Smith, A. J. Heeger, *Synthetic Metals*, 48/1 (1992) 91–97;

[283] A. J. Heeger, *Synthetic Metals*, 57/1 (1993) 3471–3482;

[284] A. Pron, J. E. Österholm, P. Smith, A. J. Heeger, J. Laska, M. Zagorska, *Synthetic Metals*, 57/1 (1993) 3520–3525;

[285] Y. Cao, P. Smith, A. J. Heeger, *Synthetic Metals*, 57/1 (1993) 3514–3519;

[286] M. Angelopoulos, C. E. Asturias, S. P. Ermer, E. Ray, E. M. Scherr, A. G. MacDiarmid, M. A. Akhtar, Z. Kiss, A. J. Epstein, *Molecular Crystals and Liquid Crystals*, 160 (1988) 151–163;

[287] D. Gonçalves, A. Waddon, F. E. Karasz, L. Akcelrud, *Synthetic Metals*, 74/3 (1995) 197–199;

[288] J. Anand, S. Palaniappan, Siddaramaiah, P. Srinivasan, D. N. Sathyanarayana, *European Polymer Journal*, 35/3 (1999) 499–507;

[289] U. A. Sevil, O. Guven, Ö. Birer, S. Süzer, *Synthetic Metals*, 110/3 (2000) 175–179;

[290] S. A. Chen, G. W. Hwang, *Polymer*, 38/13 (1997) 3333–3346;

[291] I. Yamaguchi, T. Yasuda, T. Yamamoto, *Journal of Polymer Science, Polymer Chemistry*, 39/18 (2001) 3137–3143;

[292] P. N. Adams, P. Devasagayam, S. J. Pomfret, L. Abell, A. P. Monkman, *Journal of Physics: Condensed Matter*, 10/37 (1998) 8293–8303;

[293] S. J. Pomfret, P. N. Adams, N. P. Comfort, A. P. Monkman, *Synthetic Metals*, 101/1-3 (1999) 724–725;

[294] T. E. Olinga, J. Fraysse, J. P. Travers, A. Dufresne, A. Pron, *Macromolecules*, 33/6 (2000) 2107–2113;

[295] J. Fraysse, J. Planés, A. Dufresne, A. Guermache, *Macromolecules*, 34/23 (2001) 8143–8148;

[296] H. S. Moon, J. K. Park, *Journal of Polymer Science, Polymer Chemistry*, 36/9 (1998) 1431–1439;

[297] S. Yang, E. Ruckenstein, *Synthetic Metals*, 59/1 (1993) 1–12;

[298] E. Ruckenstein, S. Yang, *Synthetic Metals*, 53/3 (1993) 283–292;

[299] E. Ruckenstein, Y. Sun, *Synthetic Metals*, 74/2 (1995) 107–113;

[300] Y. Sun, E. Ruckenstein, *Synthetic Metals*, 74/2 (1995) 145–150;

[301] T. Jeevananda, Siddaramaiah, V. Annadurai, R. Somashekar, *Journal of Applied Polymer Science*, 82/2 (2001) 383–388;

[302] V. Jousseaume, M. Morsli, A. Bonnet, *Journal of Applied Physics*, 84 (2002) 1848–1855;

[303] Q. Zhang, X. Wang, Y. Geng, D. Chen, X. Jing, *Journal of Polymer Science, Polymer Physics*, 40/22 (2002) 2531–2538;

[304] A. Andreatta, P. Smith, *Synthetic Metals*, 55/2-3 (1993) 1017–1022;

[305] L. W. Shacklette, G. G. Miller, R. L. Elsenbaumer, C. C. Han, B. M. Webling, B. Wessling, *US Patent* 5,281,363 (1994);

[306] S. Koul, R. Chandra, S. K. Dhawan, *Sensors and Actuator B*, 75/3 (2001) 151–159;

[307] Y. Wang, X. Wang, J. Li, H. Zhang, Z. Mo, X. Jing, F..Wang, *Journal of Polymer Science, Polymer Physics*, 40 (2002) 605–612;

[308] T. Ondarcuhu, C. Joachim, *Europhysics Letters*, 42/2 (1998) 215–220;

[309] L. Feng, S. Li, H. Li, J. Zhai, Y. Song, L. Jiang, *Angewandte Chemie International Edition*, 41/7 (2002) 1221–1223;

[310] P. X. Ma, R. Zhang, *Journal of Biomedical Materials Research*, 46 (1999) 60–72;

[311] G. J. Liu, J. F. Ding, L. J. Qiao, A. Guo, B. P. Dymov, J. T. Gleeson, *Chemistry: A European Journal*, 5 (1999)2740–2749;

[312] G. M. Whitesides, B. Grzybowski, *Science*, 295 (2002) 2418–2421;

[313] J. M. Deitzel, J. Kleinmeyer, J. K. Hirvonen, N. C. Beck Tan, *Polymer*, 42 (2001) 8163–8170;

[314] H. Fong, D. H. Reneker, *Electrospinning and formation of nanofibers*, Salem DR editor, *Structure formation in polymeric fibers*, Munich: Hanser, (2001) 225–246;

[315] X. Fang, D. H. Reneker, *Journal of Macromolecular Science: Physics*, B36 (1997) 169–173;

[316] G. I. Taylor, *Electrically driven jets*, Proc R Soc London, Ser A, 313 (1969) 453–475;

[317] J. Doshi, D. H. Reneker, *Journal of Electrostatics*, 35/2-3 (1995) 151–160;

[318] K. H. Hong, T. J. Kang, *Journal of Applied Polymer Science*, 99 (2006) 1277-1286;

[319] A. Lagashetty, A. Venkataraman, *Resonance*, (2005) 49-60;

[320] M. D. Ventra, S. Evoy, J. R. Heflin, *Introduction to Nanoscale Science and Technology*, Kluwer Academic Publishers, (2004);

[321] S. Aoshima , F. R. Costa , L. J. Fetters , G. Heinrich , S. Kanaoka, A. Radulescu , D. Richter , M. Saphiannikova, U. Wagenknecht, *Advances in Polymer Science*, Springer-Verlag Berlin Heidelberg, 210 (2008);

[322] J. Jiang, L. Li, M. Zhu, *Reactive & Functional Polymers*, 68 (2008) 57–62;

[323] M. Wan, J. Fan, *Polymer Science Part A: Polymer Chemistry*, 36 (1998) 2749-2755;

[324] Y. I. Kim, D. Kim, C. Lee, *Physica B*, 337 (2003) 42–51;

[325] Y. Qu, H. Yang, N. Yang, Y. Fan, H. Zhu, G. Zou, *Materials Letters*, 60 (2006) 3548–3552;

[326] M. P. Gonzalez-Sandoval, A. M. Beesley, M. M. Yoshida, L. F. Cobas, J. A. M. Aquino, *Journal of Alloys and Compounds*, 369 (2004) 190–194;

[327] R. M. Cornell, U. Schwertmann, *The Iron Oxides: Structure, Properties, Reactions, Occurences and Uses*, Wiley-VCH Verlag GmbH & Co. KGaA, Weinheim, ISBN: 3-527-30274-3, (2003);

[328] Z. Jing, Y. Wang, S. Wu, *Sensors and Actuators B: Chemical*, 113/1 (2006) 177-181;

[329] Y. Gao, Y. Bao, M. Beerman, A. Yasuhara, D. Shindo, M. K. Krishman, *Applied Physics Letters*, 84 (2004) 3361-3363;

[330] A. K. Gupta , M. Gupta, *Biomaterials*, 26/18 (2005) 3995-4021;

[331] D. K. Bora, P. Deb, *Nanoscale Research Letters*, 4 (2009)138–143;

[332] Q. Liu, Z. Cui, Z. Ma, S. Bian, W. Song, L. Wan, *Nanotechnology*, 18 (2007) 385605-385610;

[333] M. A. Willard, L. K. Kurihara, E. E. Carpenter, S. Calvin, V. G. Harris, *International Materials Reviews*, 49 (2004) 125-170;

[334] C. Jovalekic, M. Zdujic, A. Radakovic, M. Mitric, *Materials Letters*, 24 (1995) 365-368;

[335] S. Lee, J. Jeong, S. Shin, J. Kim, J. Kim, *Journal of Magnetism and Magnetic Materials*, 282 (2004) 147-150;

[336] J. Rockenberger, E. C. Scher, A. P. Alivisatos, *Journal of the American Chemical Society*, 121 (1999) 11595-11596;

[337] H. Lu, W. Schmidt, N. Matoussevitch, H. Bönnemann, B. Spliethoff, B. Tesche, E. Bill, W. Kiefer, F. Schüth, *Angewandte Chemie International Edition*, 43/3 (2004) 4304-4306;

[338] A. K. Gupta, M. Gupta, *Biomaterials*, 26/18 (2005) 3995-4021;

[339] S. Mornet, S. Vasseur, F. Grasset, P. Verveka, G. Goglio, A. Demourgues, J. Portier, E. Pollert, E. Duguet, *Progress in Solid State Chemistry*, 34 (2006) 237-247;

[340] T. Hyeon, *Chemical Communications*, (2003) 927-934;

[341] J. J. Watkins, T. J. McCarthy, Chemistry of Materials, 7/11 (1995) 1991-1994;

[342] Z. Zhang, M. Wan, Y. Wei, *Nanotechnology*, 16 (2005) 2827-2832;

[343] Y. Long, Z. Chen, J. L. Duvail, Z. Zhang, M. Wan, *Physica B*, 370 (2005) 121-130;

[344] X. Lu, Y. Yu, L. Chen, H. Mao, H. Gao, J. Wang, W. Zhang, Y. Wei, *Nanotechnology*, 16 (2005) 1660-1665;

[345] M. Kryszewski, J. K. Jeszka, *Synthetic Metals*, 94 (1998) 99–104;

[346] M. X. Wan, W. Zhou, J. C. Li, *Synthetic Metals*, 78 (1996) 27–31;

[347] Q. Xiao, X. Tan, L. Ji, J. Xue, *Synthetic Metals*, 157 (2007) 784-791;

[348] W. Xue, K. Fang, H. Qiu, J. Li, W. Mao, *Synthetic Metals*, 156 (2006) 506–509

[349] J. C. Aphesteguy, P. G. Bercoff, S. E. Jacobo, *Physica B*, 398 (2007) 200–203;

[350] G. Liu, M. S. Freund, *Macromolecules*, 30 (1997) 5660–5665;

[351] S. Xiong, Q. Wang, Y. Chen, *Journal of Applied Polymer Science*, 111 (2009) 963–969;

[352] T. H. Hsieh, K. S. Ho, C. H. Huang, Y. Z. Wang , Z. L. Chen, *Synthetic Metals*, 156 (2006) 1355–1361;

[353] Z. M. Zhang, M. X. Wan, *Synthetic Metals*, 132 (2003) 205–212;

[354] Z. M. Zhang, M. X. Wan, Y. Wei, *Nanotechnology*, 16 (2005) 2827–2832;

[355] C. Cui, Y. Huang, J. Lee, *US Patent* 5,451,526;

[356] M. Hirata, R. Yosomiya, S. Takenishi, *US Patent* 5,252,292;

[357] F. Yamagishi, C. Van Ast, L. Miller, *US Patent* 5,331,287;

[358] R. Yodice, R. Gapinski, *US Patent* 4,791,374;

[359] A. Epstein, J. Yue, *US Patent* 5,208,301;

[360] M. Wrighton, H. White Jr, G. Kittlesen, *US Patent* 5,034,192;

[361] J. Lai, X. Huang, S. Chen, T. Nehl, *Industry Applications IEEE Transactions*, 40 (2004) 178-185;

[362] V. Sadchikov, Z. Prudnikova, *Steel in Translation*, (1997) 66-69;

[363] W. Biter, P. Jamnicky, W. Coburn, *International sample electronics conference*, (1994) 234;

[364] C. Grimes, Proceedings IEEE Aerospace Applications Conference, (1994) 211-221;

[365] S. A. Schelkunoff, *Electromagnetic Waves*, D. Van Nostrand, Princeton, NJ, (1943);

[366] R. B. Schulz, V. C. Plantz, D. R. Brush, *IEEE Transactions on Electromagnetic Compatibility*, 30/3 (1988) 187-201;

[367] S. Yang, K. Lozano, A. Lomeli, H. D. Foltz, R. Jones, *Composites: Part A*, 36 (2005) 691-697;

[368] D. M. Bigg, E. J. Bradbury, *Conducting Polymers*, Ed. R. B. Seymour,. Plenum press: New York, (1981) 23;

[369] A. C. Niranjanappa, R. Biliya, D. C. Trivedi, Seminar on *State of the Art in EMI—EMC and Future Trends*; India, (1996);

[370] E. J. Carlson, *Materials Performance*, 29 (1990) 76-80;

[371] *EMI Shielding—NDC Quality Magnesium Castings*, www.northerndiecast.com;

[372] J. C. Huang, *Advances Polymer Technology*, 14 (1995) 137-150;

[373] J. R. Ellis, *Handbook of Conducting Polymers*, Ed. T.A. Skotheim, Marcel Dekker, New York, 1 (1986) 501;

[374] N. V. Mandich, *Plating and Surface Finishing*, 81 (1994) 60-63;

[375] M. Stefecka, M. Kando, H. Matsuo, Y. Nakashima, M. Koyanagi, T. Kamiya, M. Cernak, *Journal Materials Science*, 39 (2004) 2215-2217;

[376] B. F. J. Calleja, R. K. Bayer, T. A. Ezquerra, *Journal of Materials Science*, 33/23 (1998) 1411;

[377] Y. Ramadin, S. A. Jawad, S. M. Musameh, M. Ahmad, A. M. Zihlif, A. Paesano, E. Martuscelli, G. Ragosta, *Polymer International*, 34 (1994) 145-150;

[378] N. C. Das, D. Khastgir, T. K. Chaki, A. Chakraborty, *Composites Part A:Applied Science and Manufacturing*, 31 (2000) 1069-1081;

[379] R. M. Simon, *Conducting Polymers*, Ed. R. B. Seymour, Plenum press, New York, (1981) 49;

[380] X. Luo, D. D. L. Chung, *Carbon*, 34 (1996) 1293-1294;

[381] D. C. Trivedi, S. K. Dhawan, Journal of Materials Chemistry, 2 (1992) 1091-1096;

[382] D. C. Trivedi, S. K. Dhawan, *Polymer Science Contemporary Themes*, Ed. S. Sivaram, Tata McGraw-Hill, New Delhi, 2 (1991) 746;

[383] S. K. Dhawan, D. C. Trivedi, *Electromagnetic Compatibility Journal*, 4 (1991) 1-4;

[384] D. C. Trivedi, S. K. Dhawan, *Polymers for Advanced Technologies*, 4 (1993) 335-340;

[385] D. C. Trivedi, S. K. Dhawan, *Frontiers of Polymer Research*, Eds. J. K. Nigam, P. N. Prasad, Plenum, New York, (1992) 419;

[386] P. Kathirgamanathan, *Journal of Materials Chemistry*, 3 (1993) 259-262;

[387] C. Y. Lee, H. G. Song, K. S. Jang, E. J. Oh, A. J. Epstein, J. Loo, *Synthetic Metals*, 102 (1999) 1346-1349;

[388] T. Makela, S. Pienimaa, T. Taka, S. Jussila, H. Isotalo, *Synthetic Metals*, 85 (1997) 1335-1336;

[389] T. Makela, J. Sten, A. Hujanen, H. Isotala, *Synthetic Metals*, 101 (1999) 707;

[390] R. P. Pant, S. K. Dhawan, N. D. Kataria, D. K. Suri, *Journal of Magnetism and Magnetic Materials*, 252 (2002) 16-19;

[391] D. C. Trivedi, S. K. Dhawan, *Bulletin of Materials Science*, 16 (1993) 371-380;

[392] K. Hong, C. Y. Lee, C. K. Jeong, J. H. Sim, K. Kim, J. Joo, M. S. Kim, J. Y. Lee, S. H. Jeong, S. W. Byun, *Current Applied Physics*, 1 (2001) 439-442;

[393] J. A. Pomposa, J. Rodriguez, H. Grande, *Synthetic Metals*, 104 (1999) 107-111;

[394] N. C. Foulds, C. R.Lowe, *Journal of the Chemical Society, Faraday Transations*, 82 (1986) 1259–1264;

[395] M. Umana, J. Waller, *Analytical Chemistry*, 58 (1986) 2979–2983;

[396] J. Y. Wong, R. Langer, D. E. Ingber, *Proceedings of the National Academy of Sciences USA*, 91 (1994) 3201–3204;

[397] G. Shi, M. Rouabhia, Z. Wang, L. H. Dao, Z..Zhang, *Biomaterials*, 25 (2004) 2477–2488;

[398] L. C. Clark, C. Lyons, *Annals of the New York Academy of Sciences*, 102 (1962) 29–45;

[399] M. Gerard, A. Chaubey, B. D. Malhotra, *Biosensors and Bioelectronics*, 17 (2002) 345–359;

[400] P. C. Pandey, A. P. Mishra, *Analyst*, 113 (1988) 329–331;

[401] A. Gambhir, M. Gerard, A. Mulchandani, B. D. Malhotra, *Applied Biochemistry and Biotechnology*, 96 (2001) 249–257;

[402] B. D Malhotra, A. Chaubey, S. P. Singh, *Analytica Chimica Acta*, 578 (2006) 59–74;

[403] T. Ahuja, I. A. Mir, D. Kumar, Rajesh, *Biomaterials*, 28 (2007) 791–805;

[404] C. Mousty, B. Galland, S. Cosnier, *Electroanalysis*, 13 (2001) 186–190;

[405] S. Fabiano, C. Tran-Minh, B. Piro, L. A. Dang, M. C. Pham, O. Vittori, *Materials Science and Engineering C*, 21 (2002) 61–67;

[406] T. F. Otero, J. M. Sansihena, *Bioelectrochemistry and Bioenergetics*, 42 (1997) 117–122;

[407] T. F. Otero, M. T. Cortes, *Sensors and Actuators B*, 96 (2003) 152–156;

[408] E. Smela, *Advanced Materials*, 15 (2003) 481–494;

[409] M. R. Gandhi, P. Murray, G. M. Spinks, G. G. Wallace, *Synthetic Metals*, 73 (1995) 247–256;

[410] B. Garner, A. Georgevich, A. J. Hodgson, L. Liu, G. G. Wallace, *Journal of Biomedical Materials Research*, 44 (1999) 121–129;

[411] B. Garner, A. J. Hodgson, G. G. Wallace, P. A. Underwood, *Journal of Materials Science: Materials in Medicine*, 10 (1999) 19–27;

[412] A. J. Hodgson, M. J. John, T. Campbell, A. Georgevich, S. Woodhouse, T. Aoki, *Proceedings in SPIE International Society of Optical Engineering*, 2716 (1996) 164–176;

[413] C. E. Schmidt, V. R. Shastri, J. P. Vacanti, R. Langer, *Proceedings of the National Academy of Sciences USA*, 94 (1997) 8948–8953;

[414] X. Wang, X. Gu, C. Yuan, S. Chen, P. Zhang, T. Zhang, J. Yao, F. Chen, G. Chen, *Journal of Biomedical Materials Research*, 68A (2004) 411–422;

[415] H. K. Song, B. Toste, K. Ahmann, D. Hoffman-Kim, G. T. R. Palmore, *Biomaterials*, 27 (2006) 473–484;

[416] W. R. Stauffer, X. T. Cui, *Biomaterials*, 27 (2006) 2405–2413;

[417] N. Gomez, J. Y. Lee, J. D. Nickels, C. E. Schmidt, *Advanced Functional Materials*, 17 (2007) 1645–1653;

[418] D. D. Ateh, P. Vadgama, H. A. Navsaria, *Tissue Engineering*, 12 (2006) 645–655;

[419] H. Castano, E. A. O'Rear, P. S. McFetridge, V. I. Sikavitsas, *Macromolecular Bioscience*, 4 (2004) 785–794;

[420] A. Boyle, E. Geniès, M. Fouletier, *Journal of Electroanalytical Chemistry*, 279 (1990) 179–86;

[421] M. Pyo, G. Maeder, R. T. Kennedy, J. R. Reynolds, *Journal of Electroanalytical Chemistry*, 368 (1994) 329–332;

[422] M. Pyo, J. R. Reynolds, *Journal of Materials Chemistry*, 8 (1996) 128–133;

[423] E. Hakansson, A. Kaynak, T. Lin, S. Nahavandi, T. Jones, E. Hu, *Synthetic Metals*, 144 (2004) 21–28;

[424] A. N. Zelikin, D. M. Lynn, J. Farhadi, I. Martin, V. Shastri, R. Langer, *Angewandte Chemie International Edition*, 41 (2002) 141–145;

[425] G. Shi, M. Rouabhia, Z. Wang, L. H. Dao, Z. Zhang, *Biomaterials*, 25 (2004) 2477–2488;

[426] P. R. Bidez, S. Li, A. G. MacDiarmid, E. C. Venancio, Y. Wei, P. I. Lelkes, *Journal of Biomaterials Science: Polymer Edition*, 17 (2006) 199–212;

[427] Z. F. Li, E. Ruckenstein, *Journal of Colloid and Interface Science*, 264 (2003) 370–377;

[428] D. Cheng, H. Xia, H. S. Chan, *Journal of Nanoscience and Nanotechnology*, 5 (2005) 466–473;

[429] E. Guterman, S. Cheng, K. Palouian, P. Bidez, P. Lelkes, Y. Wei, *Polymer Preprints, American Chemical Society, Division of Polymer Chemistry*, 43 (2002) 766–767;

[430] R. Wadhwa, C. F. Lagenaur, X. T. Cui, *Journal of Controlled Release*, 110 (2006) 531–541;

[431] M. R. Abidian, D. H. Kim, D. C. Martin, *Advanced Materials*, 18 (2006) 405–409;

[432] Y. Li, K. G. Neoh, E. T. Kang, *Journal of Biomedical Materials Research Part A*, 73A (2005) 171–181;

[433] L. Kulinsky, H. Xu, H. K. A. Tsai, M. Madou, *Proceedings in SPIE International Society of Optical Engineering*, (2006) 6173;

[434] D. Svirskin, J. Travas-Sejdic, A. Rodgers, S . Garg, *Journal of Controlled Release*, 146 (2010) 6-15;

[435] P. M. George, D. A. LaVan, J. A. Burdick, C. Y. Chen, E. Liang, R. Langer, *Advanced Materials*, 18 (2006) 577–581;

[436] F. Selampinar, L. Toppare, U. Akbulut, T. Yalcin, S. Suzer, *Synthetic Metals*, 68 (1995) 109–116;

[437] J. E. G. De Souza, B. B. Neto, F. L. Dos Santos, C. P. DeMelo, M. S. Santos, T. B. Ludermir, *Synthetic Metals*, 102 (1999) 1296–1298;

[438] M. Hirata, L. Sun, *Sensors and Actuators A*, 40 (1994) 159–163;

[439] K. H. Hong, K. W. Oh, T. J. Kang, *Journal of Applied Polymer Science*, 92 (2004) 37–42;

[440] S. K. Dhawan, D. Kumar, M. K. Ram, S. Chandra, D. C. Trivedi, *Sensors and Actuators B*, 40 (1997) 99–103;

[441] S. Takeda, *Thin Solid Films*, 343–344 (1999) 313–316;

[442] S. Sharma, C. Nirkhe, S. Pethkar, A. A. Athawale, *Sensors and Actuators B*, 85 (2002) 131–136;

[443] A. A. Athawale, M. V. Kulkarni, *Sensors and Actuators B*, 67 (2000) 173–177;

[444] G. E. Collins, L. J. Buckley, *Synthetic Metals*, 78 (1996) 93–101;

[445] C. P. De Melo, C. G. Dos Santos, A. M. S. Silva, F. Dos Santos, J. E. G. De Souza, *Molecular Crystals and Liquid Crystals Science and Technology: Section A*, 374 (2002) 543–548;

[446] J. X. Huang, S. Virji, B. H. Weiller, R. B. Kaner, *Chemistry: A European Journal*, 10 (2004) 1314–1319;

[447] G. F. Li, C. Martinez, J. Janata, J. A. Smith, M. Josowicz, S. Semancik, *Electrochemical and Solid-State Letters*, 7 (2004) H44–H47;

[448] M. R. Ganjali, P. Norouzi, M. Rezapour, *Encyclopedia of Sensors, Potentiometric Ion Sensors*, American Scientific Publisher (ASP), Los Angeles, 8 (2006) 197-288;

[449] F. Faridbod, M. R. Ganjali, R. Dinarvand, P. Norouzi, S. Riahi, *Sensors*, 8 (2008) 1645-1703;

[450] M. Tudorache, C. Bala, *Analytical and Bioanalytical Chemistry*, 388 (2007) 565-578;

[451] J. Bobacka, A. Ivaska, A. Lewenstam, *Electroanalysis*, 5–6 (2003) 366-374;

[452] T. Lindfors, A. Ivaska, *Journal of Electroanalytical Chemistry*, 531 (2002) 43-52;

[453] M. Kaempgen, S. Roth, *Journal of Electroanalytical Chemistry*, 586 (2006) 72-76;

[454] K. Crowley, E. O. Malley, A. Morrin, M. R. Smyth, A. J. Killard, *Analyst*, 133 (2008) 391-399;

[455] A. Michalska, M. Wojciechowski, W. Jedral, E. Bulska, K. Maksymiuk, *Journal of Solid-State Electrochemistry*, 13 (2009) 99-106;

[456] G. A. Evtugyn, I. I. Stoikov, S. V. Belyakova, E. E. Stoikova, R. V. Shamagsumova, A. Yu. Zhukov, I. S. Antipin, H. C. Budnikov, *Talanta*, 2008, 76, 441-447;

[457] T. Lindfors, A. Ivaska, *Analytica Chimica Acta*, 2000, 404, 111-119;

[458] S. de Marcos, N. Alcubierre, J. Galbán, J. R. Castillo, *Analytica Chimica Acta*, 502 (2004) 7-13;

[459] L. Zhang, C. Zhang, J. Lian, *Biosensors in Bioelectronics*, 24 (2008) 690-695;

[460] N. M. Kocherginsky, Z. Wang, *Journal of Electroanalytical Chemistry*, 611 (2007) 162-168;

[461] S. Ivanov, V. Tsakova, V. M. Mirsky, *Electrochemistry Communications*, 2006, 8, 643-646;

[462] M. Ates, A. S. Sarac, *Progress in Organic Coatings*, 66 (2009) 337-358;

[463] V. V. Abalyaeva, O. N. Efimov, *Russian Journal of Electrochemistry*, 2005, 41, 1180-1184;

[464] J. M. Gutiérrez, L. Moreno-Barón, M. I. Pividori, S. Alegret, M. del Valle, *Microchimica Acta*, 169 (2010) 261-268;

[465] S. Radhakrishnan, B. Kar Swarnendu, Sensors and Actuators A: Physical, 120 (2005) 474-481;

[466] J. Vilčáková, M. Paligová , M. Omastová, P. Sáha, O. Quadrat, *Synthetic Metals*, 146 (2004) 121-126;

[467] M. Pelíšková, J. Vilčáková, M. Omastová, P. Sáha, C. Li, O. Quadrat, *Smart Materials and Structures*, 14 (2005) 949-952;

[468] A. Allaoui, S. V. Hoa, P. Evesque, J. B. Bai, *Scripta Materialia*, 61 (2009) 628-631;

[469] N. D. Alexopoulos, C. Bartholome, P. Poulin, Z. Marioli-Riga, *Composites Science and Technology*, 70/12 (2010) 1733-1741;

[470] N. D. Alexopoulos, C. Bartholome, P. Poulin, Z. Marioli-Riga, *Composites Science and Technology*, 70/2 (2010) 260-271;

[471] K. Mosbach, B. Danielsson, *Analytical Chemistry*, 53 (1981) 83A-94A;

[472] B. H. Weiller, S. Virji, R. B. Kaner, J. Huang, *US8012326 B2*;

[473] S. J. Cui, D. P. Xu, W. H. Su, F. S. Wang, S. L. Wang, *Chinese Journal of High Pressure Physics*, 1 (1987) 71-75;

[474] D. Zhang, *Polymer Testing*, 26 (2007) 9-13;

[475]] Z. X. Bao, C. X. Liu, N. J. Pinto, *Synthetic Metals*, 87 (1997) 147–150;

[476] S. J. Varma, S. Jayalekshmi, *Journal of Applied Polymer Science*, 117 (2010) 138-142;

[477] Z. X. Bao, C. X. Liu, N. J. Pinto, *Synthetic Metals*, 87 (1997) 147-150;

[478] J. Prokes, M. Varga, I. Křivka, A. Rudajevová, J. Stejskal, *Journal of Materials Chemistry*, 21 (2011) 5038-5045;

[479] J. Mikat, I. Orgzall, H. D. Hochheimer, *Physical Review B*, 65 (2002) 174202;

[480] J. Mikat, I. Orgzall, B. Lorenz, S. Sapp, C. R. Martin, J. L. Burris, H. D. Hochheimer, *Physica B: Condensed Matter*, 265/1–4 (1999) 154–159;

[481] I. Orgzall, B. Lorenz, S. T. Ting, P.-H Hor, V. Menon, C. R. Martin, H. D. Hochheimer, *Physical Review B*, 54 (1996) 16654–16658;

[482] J. Engel, N. Chen, C. Tucker, C. Liu, S. H. Kim, D. Jones, *Proceedings of the IEEE Sensors*, Exco, Daegu, Korea, Oct 2006, 563–566;

[483] B. J. Kane, M. R. Cutkosky, G. T. A. Kovacs, *Journal of Microelectromechanical Systems*, 9/4 (2000) 425–434;

[484] T. Mei, W. J. Li, Y. Ge, Y. Chen, L. Ni, M. H. Chan, *Sensors and Actuators*, 80 (2000) 155–162;

[485] T. Lomas, A. Tuantranont, V. M. Bright, *NSTI Nanotechnology Conference*, (2004);

[486] K. Kim, K. R. Lee, D. S. Lee, N. Cho, W. H. Kim, K. Park, H. Park, Y. Kim, Y. Park, J. Kim, *Journal of Physics, Conference Series*, 34 (2006) 399–403;

[487] A. Wisitsoraat, V. Patthanasetakul, T. Lomas, A. Tuantranont, *Sensors and Actuators A*, 139 (2007) 17–22;

[488] J. H. Shan, T. Mei, L. Sun, D. Y. Kong, Z. Y. Zhang, L. Ni, M. Meng, J. R. Chu, *Proceedings of the IEEE/RSJ International conference on intelligent robots and systems*, (2005) 1818–1823;

[489] K. Nakamura, T. Toriyama, S. Sugiyama, *IEE Journal of Transactions on Electrical and Electronic Engineering*, 5 (2010) 157–163;

[490] T. Salo, T. Vancura, O. Brand, H. Baltes (2003), *IEEE MEMS, Micro Electro Mechanical Systems*, Kyoto, Japan, (2003) 590–593;

[491] M. Leineweber, G. Pelz, M. Schmidt, H. Kappert, G. Zimmer, *Sensors and Actuators*, 84 (2000) 236–245;

[492] U. Paschen, M. Leineweber, J. Arnelung, M. Schmidt, G. Zammer, *Sensors and Actuators*, 68 (1998) 294–298;

[493] B. L. Gray, R. S. Fearing, *IEEE International conference robotics and automation*, (1996);

[494] H. K. Lee, S. I. Chang, E. Yoon, *Proceedings of the 19th International conference on micro electro mechanical systems MEMS2006*, Istambul, Turkey, (2006) 606–609;

[495] G. Hellard, R. A. Russell, *Proceedings of the Australasian conference on robotics and automation 2006*, Auckland, New Zealand, (2006);

[496] R. S. Dahiya, M. Valle, G. Metta, L. Lorenzelli, *14th IEEE International conference on electronics, circuits and systems (ICECS)*, (2007) 1075–1078;

[497] T. Lomas, A. Tuantranont, V. M. Bright, *NSTI Nanotechnology conference*, (2004);

[498] http://pressureprofile.com/products-robotouch

[499] http://www.shadowrobot.com

[500] K. Weiss, H. Wörn, *IEEE International conference on manipulation and grasping IMG*, Genua, Italy (2004);

[501] G. Cannata, M. Maggliali, *Proceedings of the 2006 IEEE International conference on multisensor fusion and integration for intelligent systems*, (2006) 160–166;

[502] M. Shimojo, A. Namiki, M. Ishikawa, R. Makino, K. Mabuchi, *IEEE Sensors Journal*, 4/5 (2004) 589–596;

[503] http://www.tekscan.com

[504] http://www. peratech.com

[505] T. Someya, T. Sekitani, S. Iba, Y. Kato, H. Kawaguchi, T. Sakurai, *Proceedings of the National Academy of Sciences USA*, 101/27 (2004) 9966–9970;

[506] E. Ochoteco, J. A. Pomposo, T. Sikora, F. Vidal, F. Martinez, G. Obieta, H. Grande, *Microsystem Technologies*, 14/8 (2008) 1089–1097;

[507] D. Xie, Y. Jiang, W. Pan, D. Li, Z. Wu, Y. Li, *Sensors and Actuators B: Chemical*, 81 (2002) 158-164;

[508] X. B. Yan, Z. J. Han, Y. Yang, B. K. Tay, *Sensor and Actuators B: Chemical*, 123 (2007) 107-113;

[509] W. Prissanaroon, L. Ruangchuay, A. Sirivat, J. Schwank, *Synthetic Metals*, 114 (2000) 65-72;

[510] F. Mohammad, *Journal of Physics D: Applied Physics*, 31 (1998) 951-959;

[511] Y. Sakurai, H. S. Jung, T. Shimanouchi, T. Inoguchi, S. Morita, R. Kuboi, K. Natsukawa, *Sensors and Actuators B: Chemical*, 83 (2002) 270-275;

[512] T. Hanawa, S. Kuwabata, H. Hashimoto, H. Yoneyama, *Synthetic Metals*, 30 (1989) 173-181;

[513] L. Torsi, M. C. Tanese, N. Cioffi, M. Gallazzi, L. Sabbatini, P. G. Zambonin, *Sensors and Actuators B: Chemical*, 98 (2004) 204-207;

[514] J. Reemts, J. Parisi, D. Schlettwein, *Thin Solid Films*, 466, (2004) 320-325;

[515] B. Li, S. Santhanam, L. Schultz, M. Jeffries-EL, M. C. Iovu, G. Sauve, J. Cooper, R. Zhang, J. C. Revelli, A. G. Kusne, *Sensors and Actuators B*, 123 (2007) 651-660;

[516] B. Vercelli, S. Zecchin, N. Comisso, G. Zotti, A. Berlin, E. Dalcanale, L. B. Groenendaal, *Chemistry of Materials*, 14 (2002) 4768-4774;

[517] L. Ruangchuay, A. Sirivat, J. Schwank, *Synthetic Metals*, 140 (2004) 15-21;

[518] C. K. Tan, D. J. Blackwood, *Sensors and Actuators B: Chemical*, 71 (2000) 184-191;

[519] E. Segal, R. Tchoudakov, M. Narkis, A. Siegmann, W. Yen, *Sensors and Actuators B: Chemical*, 104 (2005) 140-150;

[520] A. J. Cunningham, *Introduction to bioanalytical sensors*, New York, Wiley, (1998) 112;

[521] S. Achmatowicz, M. Jakubowska, E. Zwierkowska, R. Koncki, L. Tymecki, *Proceedings XXIV International Microelectronics and Packaging Society (IMAPS)*, Poland Conference, Rytro (2000);

[522] A. Cadogan, Z. Gao, A. Lewenstam, A. Iraska, D. Diamond, *Analytical Chemistry*, 64 (1992) 2496–2501;

[523] M. Careri, A. Casnati, A. Guarinoni, R. Mangia, G. Mori, A. Pochini, R. Ungaro, *Analytical Chemistry*, 65 (1993) 3156–3160;

[524] K. Suzuki, K. Watanabe, Y. Matsumoto, M. Kobayashi, S. Sato, D. Siswanta, H. Hisamoto, *Analytical Chemistry*, 67 (1995) 324–334;

[525] Y. Tsujimura, M. Yokoyama, K. Kimura, *Analytical Chemistry*, 67 (1995) 2401–2404;

[526] T. Lindfors, A. Ivaska, *Analytica Chimica Acta*, 437 (2001) 171–183;

[527] F. A. Nada, A. Galal, H. B. Mark Jr., T. Yu, P. L. Bishop, *Talanta*, 47 (1998) 987–999;

[528] Q. J. Wang, X. J. Zhang, C. G. Zhang, X. Y. Zhu, *Chemical journal of Chinese Universities*, 18 (1997) 226-228;

[529] C. A. Lindino, L. O. S. Bulhoes, *Analytica Chimica Acta*, 334 (1996) 317-322;

[530] D. T. MacQuade, A. E. Pullen, T. M. Swagen, *Chemical Reviews*, 100 (2000) 2537-2574;

[531] A. A. Karyakin, M. Vuki, L. V. Lukachova, E. E. Karyakina, A. V. Orlov, G. P. Karpachova, J. Wang, *Analytical Chemistry*, 71 (1999) 2534-2540;

[532] S. De Marcos, O. S. Wolbeis, *Analytica Chemica Acta*, 334 (1996) 149-153;

[533] Z. Ge, C. W. Brown, L. Sun, S. C. Yang, *Analytica Chimica Acta*, 65 (1993) 2335-2338;

[534] E. Pringsheim, E. Terpetschning, O. S. Wolbeis, *Analytica Chimica Acta*, 357 (1997) 247-252;

[535] U. W. Grummt, A. Pron, M. Zagorska, S. Lefrant, *Analytica Chimica Acta*, 357 (1997) 253-259;

[536] Z. Jin, Y. Su, Y. Duan, *Sensors and Actuators B: Chemical*, 71 (2000) 118-122;

[537] E. C. Venancio, L. H. C. Mattoso, P. S. D. Herrmann, A. G. Mac Diarmid, *Sensors and Actuator B: Chemical*, 130 (2008) 723–729;

[538] T. T. Wu, Y. Y. Chen, T. H. Chou, *Journal of Physics D: Applied Physics*, 41 (2008) 085101;

[539] F. W. Zeng, X. X. Liu, D. Diamond, K. T. Lau, *Sensors and Actuator B: Chemical*, 143 (2010) 530–534;

[540] G. Lee, H. Joo, J. Lee, *Journal of Molecular Catalysis B: Enzymatic*, 54/3-4 (2008) 116–121;

[541] M. Kyotani, H. Goto, K. Suda, T. Nagai, Y. Matsui, K. Akagi, *Journal of Nanoscience and Nanotechnology*, 8/4 (2008) 1999–2004;

[542] A. Janosevic, G. C. Marjanovic, B. Marjanovic, M. Trchová, J. Stejskal, *Materials Letters*, 64/21 (2010) 2337–2340;

[543] J. Wang, D. Zhang, *Advances in Polymer Technology*, 32/S1 (2013) E323–E368;

[544] J. C. Chang, A. G. MacDiarmid, *Synthetic Metals*, 13 (1986) 193-205;

[545] J. G. Deng, C. L. He, Y. X. Peng, J. H. Wang, X. P. Long, P. Li, *Synthetic Metals*, 139 (2003) 295–301;

[546] J. H. Xu, L. Cui, N. Tong, H. Gu, *Journal of the American Chemical Society*, 128 (2006) 15582–15583;

[547] G. Vitulli, C. Evangelisti, A. M. Caporusso, P. Pertici, N. Panziera, S. Bertozzi, P. Salvadori, *Metal Nanoclusters in Catalysis and Materials Science: The Issue of Size Control*, Edited by B. Corain, G. Schmid, N. Toshima, (2008) 437-452;

[548] T. Hyeon, S. S. Lee, J. Park, Y. Chung, H. B. Na, *Journal of the American Chemical Society*, 123 (2001) 12798-12801;

[549] J. Park, K. An, Y. Hwang, J. G. Park, H. J. Noh, J. Y. Kim, J. H. Park, N. M. Hwang, T. Hyeon, *Nature Materials*, 3 Dec (2004) 891-895;

[550] N. Guskos, E. A. Anagnostakis, V. Likodimos, T. Bodziony, J. Typek, M. Maryniak, U. Narkiewicz, I. Kucharewicz, S. Waplak, *Journal of Applied Physics*, 97 (2005) 024304;

[551] K. Suri, S. Annapoorni, R.P. Tandon, N.C. Mehra, *Synthetic Metals*, 126 (2002) 137–142;

[552] X. Yang, L. Xu, N. S. Choon, C. S. O. Hardy, *Nanotechnology*, 14 (2003) 624–629;

[553] D. G. Shchukin, I. L. Radtchenko, G. B. Sukhorukov, *Materials Letters*, 57 (2002) 1743–1747;

[554] M. Wang, W. Li, *Journal of Polymer Science*, 35 (1997) 2129–2136;

[555] H. Xia, D. Cheng, C. Xiao, H. S. O. Chan, *Journal of Materials Chemistry*, 15 (2005) 4161–4166;

[556] A. C. V. Araújo, R. J. de Oliveira, J. S. Alves, A. R. Rodrigues, F. L. A. Machado, F. A. O. Cabral, W. M. de Azevedo, *Synthetic Metals*, 160 (2010) 685–690;

[557] C. Yang, J. Du, Q. Peng, R. Qiao, W. Chen, C. Xu, Z. Shuai, M. Gao, *Journal of Physical Chemistry B*, 113 (2009) 5052–5058;

[558] L. Gao, J. Zhuang, L. Nie, J. Zhang, N. Gu, T. Wang, J. Feng, D. Yang, S. Perrett, X. Yan, *Nature Nanotechnology*, 2 (2007) 577–583;

[559] J. Zhang, J. Chen, Z. Wang, *Materials Letters*, 61 (2007) 1629-1632;

[560] J. Sun, S. Zhou, P. Hou, Y. Yang, J. Weng, X. Li, M. Li, *Journal of Biomedical Materials Research Part A*, 80A (2007) 333-341;

[561] G. Qiu, Q. Wang, M. Nie, *Journal of Applied Polymer Science*, 102 (2006) 2107-2111;

[562] H. Gu, Y. Huang, X. Zhang, Q. Wang, J. Zhu, L. Shao, N. Haldolaarachchige, D. P. Young, S. Wei, Z. Guo, *Polymer*, 53 (2012) 801-809;

[563] S. Xing, H. Zheng, G. Zhao, *Synthetic Metals*, 158 (2008) 59–63;

[564] L. Del Bianco, D. Fiorani, A. M. Testa, E. Bonetti, L. Savini, S. Signoretti, *Physical Review B*, 66 (174418) (2002) 1–11;

[565] X. Batlle, A. Labarta, *Journal of Physics D: Applied Physics*, 35 (2002) R15–R42;

[566] S. Bedanta, W. Kleemann, *Journal of Physics D: Applied Physics*, 42/013001 (2009) 1–28;

[567] L. Del Bianco, A. Hernando, D. Fiorani, *Surface Effects in Magnetic Nanoparticles*, Springer, New York, (2005) 217–238;

[568] Z. Liu, J. Wang, D. H. Xie, G. Chen, *Small*, 4 (2008) 462–466;

[569] D. Farrell, Y. Cheng, R. W. McCallum, M. Sachan, S. A. Majetich, *Journal of Physical Chemistry B*, 109 (2005) 13409–13419;

[570] G. C. Papaefthymiou, E. Devlin, A. Simopoulos, D. K. Yi, S. N. Riduan, S. S. Lee, J. Y. Ying, *Physical Review B*, 80 (2009) 024406;

[571] V. Calero-Diaz del Castillo, C. Rinaldi, *IEEE Transactions on Magnetics*, 46 (2010) 852–859;

[572] E. De Biasi, C. A. Ramos, R. D. Zysler, H. Romero, *Physical Review B*, 65 (2002) 144416;

[573] J. Park, K. An, Y Hwang, J. G. Park, H. J. Noh, J. Y. Kim, J. H. Park, N. M. Hwang, T. Hyeon, *Nature Materials*, 3 (2004) 891-895;

[574] G. Vitulli, C. Evangelisti, A. M. Caporusso, P. Pertici, N. Panziera, S. Bertozzi, P. Salvadori, *Metal Nanoclusters in Catalysis and Materials Science: The Issue of Size Control*, Edited by B. Corain, G. Schmid, N. Toshima, (2008) 437-452;

[575] P. Lahiri, S. Sengupta, *Canadian Journal of Chemistry*, 69 (1991) 33-36;

[576] H. Wang, J. Huang, L. Ding, C. Wang, Y. Han, *Journal of Wuhan University of Technology-Materials Science Edition*, 26 (2011) 257-261;

[577] J. M. D. Coey, *Magnetism and Magnetic Materials*, CUP, Cambridge (2009);

[578] J. Smit, H. Wijn, *Ferrites*, Philips, (1959);

[579] K. Karkkainen, A. Shivole, K. Nikoskinen, "Analysis of a Three-Dimensional Dielectric Mixture with Finite Difference Method", IEEE Trans. Geoscience and Remote Sensing, Vol. 39, No. 5, May 2001, pp. 1013-1018.

[580] K. Singh, A. Ohlan, A.K. Bakhshi, S.K. Dhawan, Materials Chemistry and Physics 119 (2010) 201–207;

[581] C. Hou, T. Li, T. Zhao, W. Zhang, Y. Cheng, Materials & Design 33 (2012) 413–418

[582] Y. Yao, H. Jiang, J. Wu, D. Gu, L. Shen, Procedia Engineering 27 (2012) 664–670

[583] E. Michielssen, J.-M. Sajer, S. Ranjithan, R. Mittra, IEEE Transactions on Microwave Theory and Techniques 41 (1993) 024–1031.

[584] D. Micheli, C. Apollo, R. Pastore, M. Marchetti, Composites Science and Technology 70 (2010) 400–409.

[585] D. Micheli, C. Apollo, R. Pastore, R. Bueno Morles, S. Laurenzi, M. Marchetti, Acta Astronautica 69 (2011) 747–757

[586] C. A.Balanis, *Advanced Engineering Electromagnetics*, New York, John Wiley and Sons; (1989);

[587] S.W. Phang, R. Daik, M.H. Abdullah, *Thin Solid Films*, 477 (2005) 125–130.

[588] J. Gass, P. Poddar, J. Almand, S. Srinath, H. Srikanth, *Advanced Functional Materials*, 16 (2006) 71–75;

[589] J. Deng, X. Ding, W. Zhang, Y. Peng, J. Wang, X. Long, P. Li, A. S. C. Chan, *Polymer*, 43 (2002) 2179-2184;

[590] X. Lu, H. Mao, D. Chao, W. Zhang, Y. Wei, *Journal of Solid State Chemistry*, 179 (2006) 2609-2615;

[591] H. Xia, Q. Wang, *Chemistry of Materials*, 14 (2002) 2158-2165;

[592] J. H. Yu, G. C. Rutledge, *Electrospinning*, in Encyclopedia of Polymer Science and Technology, Online Edition, John Wiley & Sons, New Jersey, (2007);

[593] D. Li, Y. Xia, *Advanced Materials*, 16/14 (2004) 1151-1170;

[594] Y. Zhu, J. Zhang, Y. Zheng, Z. Huang, L. Feng, L. Jiang, *Advanced Functional Materials*,16 (2006) 568-574;

[595] W. Pan, Q. Zhang, Y. Chen, *Optoelectronics And Advanced Materials – Rapid Communications*, 4/12 (2010) 2118-2122;

[596] J. B. Veluru, K. K. Satheesh, D.C. Trivedi, M. V. Ramakrishna, T. N.Srinivasan, *Journal of Engineered Fibers and Fabrics*, 2/2 (2007) 25-31;

[597] A. Bishop, P. Gouma, *Reviews on Advanced Materials Science*, 10 (2005) 209-214;

[598] P. Frontera, C. Busacca, P. Antonucci, M. Lo Faro, E. Falletta, C. Della Pina, M. Rossi, *American Institute of Physics Conference Proceedings*, 1459 (2012) 253-255;

[599] P. Humpolicek, V. Kasparkova, P. Saha, J. Stejskal, *Synthetic Metals*, 162 (2012) 722– 727;

[600] W. K. Son, J. H. Youk, T. S. Lee, W. H. Park, *Polymer*, 45 (2004) 2959-2966;

[601] http://www.sigmaaldrich.com/spectra/ftir/FTIR002642.PDF;

[602] W. Zheng, Y. Min, A. G. MacDiarmid, M. Angelopoulos, Y. H. Liao, A. J. Epstein, *Synthetic Metals*, 84 (1997) 109-110;

[603] B. K. Kuila, M. Stamm, *Journal of Material Chemistry*, 20 (2010) 6086-6094;

[604] N. J. Pinto, A. A. Acosta, G. P. Sinha, F. M. Aliev, Synthetic Metals, 113 (2000) 77-81;

[605] A. V. Shirinov,W. K. Schomburg, *Sensors and Actuator A: Physical*; 142 (2008) 48-55;

[606] A. E. Job, F. A. Oliveira, N. Alves, J. A. Giacometti, L. H. C. Mattoso, *Synthetic Metals*, 135–136 (2003) 99-100;

[607] M. Knite, V. Teteris, A. Kiploka, J. Kaupuzs, *Sensors and Actuators A: Physical*, 110 (2004) 142-149;

[608] G. T. Pham, Y. B. Park, Z. Liang, C. Zhang, B. Wang, *Composites Part B: Engineering*, 39 (2008) 209-216;

[609] G. Carotenuto, B. Martorana, G. LaPeruta, A. Longo, P. Perlo, L. Nicolais, *Sensors and Actuators A: Physical*, 132 (2006) 541-546;

[610] M. N. Kalasad, M. A. Gadyal, R. K. Hiremath, I. Mohamed Ikram, B. G. Mulimani, I. M. Khazi, S. K. Anantha Krishnan, M. K. Rabinal, *Composites Science and Technology*, 68 (2008) 1787-1793;

[611] F. Cataldo, P. Maltese, *Polymers for Advanced Technology*, 12 (2001) 293-299;

[612] M. V Andrés, K. W. H Foulds, M. J Tudor, *Sensor and Actuators*, 15 (1988) 417-426;

[613] P. Lorenzini, J. M Dusseau, J. L Robert, V. Mosser, S. Contreras, *Sensors and Actuators A: Physical*, 33 (1992) 53-56;

[614] E. Defaÿ, C. Millon, C. Malhaire, D. Barbier, *Sensors and Actuators A: Physical*, 99 (2002) 64-67;

[615] A. Ettouhami, N. Zahid, M. Elbelkacemi, *Comptes Rendus Mecanique*, 332 (2004) 141-146;

[616] S. Beeby, G. Ensell, M. Kraft, N. White, *MEMS mechanical sensors*, Boston, Artech House, (2004);

[617] S. Yang, N. Lu, Sensors, 13 (2013) 8577-8594;

[618] R. E. Giedd, Y. Wang, M. G. Moss, J. Kaufmann, T. L. Brewer, *US Patent* 5,505,093 (1996);

[619] A. Alloui, S. V. Hoa, P. Evesque, J. B. Bai, *Scripta Materialia*, 61 (2009) 628-631;

[620] C. X. Liu, J. W. Choi, *Nanomaterials*, 2 (2012) 329-347;

[621] M. Lillemose, M. Spieser, N. O. Christiansen, A. Christiansen, A. Boisen, *Microelectronic Engineering*, 85 (2008) 969-971;

[622] R. P. McCall, E. M. Scherr, A. G. MacDiarmid, A. J. Epstein, *Physical Review B*, 50 (1994) 5094-5100;

[623] J. N. Pereira, P. Vieira, A. Ferreira, A. J. Paleo, J. G. Rocha, S. Lanceros-Méndez, *Journal of Polymer Research*, 19 (2012) 9815-9821;

[624] http://uk.rs-online.com/web/p/strain-gauges/0632168/;

[625] V. Correia, C. Caparros, C. Casellas, L. Francesch, J. G. Rocha, S. Lanceros-Mendez, *Smart Materials and Structures*, 22/10 (2013) 105028.